DYNAMICS OF FLEXIBLE STRUCTURES PERFORMING LARGE OVERALL MOTIONS: A GEOMETRICALLY-NONLINEAR APPROACH

by

Loc Vu-Quoc

Memorandum No. UCB/ERL M86/36

1 May 1986

DYNAMICS OF FLEXIBLE STRUCTURES PERFORMING LARGE OVERALL MOTIONS: A GEOMETRICALLY-NONLINEAR APPROACH

by

Loc Vu-Quoc

Memorandum No. UCB/ERL M86/36

1 May 1986

ELECTRONICS RESEARCH LABORATORY

College of Engineering
University of California, Berkeley
94720

TITLE PAGE

DYNAMICS OF FLEXIBLE STRUCTURES PERFORMING LARGE OVERALL MOTIONS: A GEOMETRICALLY-NONLINEAR APPROACH

by

Loc Vu-Quoc

Memorandum No. UCB/ERL M86/36

1 May 1986

ELECTRONICS RESEARCH LABORATORY

College of Engineering
University of California, Berkeley
94720

ABSTRACT

This dissertation is concerned with the modeling of flexible structures subjected to large overall motions. Applications span diverse disciplines: from robotics and machine design to aircraft and spacecraft dynamics.

Traditional approaches to this class of problems are based on the assumption of small deformations, thus relying crucially on the use of a floating reference frame. The resulting set of equations of motion is nonlinear and highly coupled in the inertia terms. By contrast, an alternative approach is proposed in which fully nonlinear structural theories, which are properly invariant with respect to superposed rigid body motions, are employed. Owing to this property, the dynamics of motion can be referred directly to the inertial frame, leading to a drastic simplification of the inertia operator (with a structure identical to that found in rigid body mechanics).

Even though the methodology applies to a general class of structural elements, only a one-dimensional type (flexible rod) is considered. Since the rotation field for a rod is represented by orthogonal, generally non-commutative transformations, the deformation map takes values in the nonlinear differentiable manifold $\mathbb{R}^3 \times SO(3)$, instead of the linear space $\mathbb{R}^3$ (for the plane case) usually encountered in nonlinear structural dynamics. Concepts of modern differential geometry and covariant linearization procedures prove useful in the numerical treatment of the nonlinear PDE's governing the motion of the rod.

The dynamics of earth-orbiting flexible satellites is completely described by the same system of equations of motion as for the fully nonlinear rod model. However, to avoid numerical ill-conditioning due to the large difference in magnitude between the distance from the earth to the satellite and the structural deformations, an additive decomposition of the displacement field of the rod

into the far field and the near field is introduced. Follower loading is conveniently accounted for in the formulation. Applications of the proposed methodology to the dynamics of flexible multibody systems (rigid bodies with flexible appendages, all flexible chain systems, flexible closed-loop chains) are also considered.

ACKNOWLEDGEMENTS

Each of the following persons has contributed equally to my education, albeit in different ways. They all have played important role and provided inestimable support.

I am indebted to Professor J.C. Simo of Stanford University for his technical guidance and constant enthusiasm throughout the course of this research. His contribution to my understanding of the subject through several stimulating discussions has proved invaluable.

I am grateful to Professors K.S. Pister, E. Polak, and R.L. Taylor for their support and encouragement, and for their numerous advices during my studies at Berkeley. The opportunity they have given me to introduce myself to new and exciting horizons is gratefully appreciated.

To the many friends who have made my stay at Berkeley one of the most memorable periods of my life, I thank them for the uncountable enjoyable discussions as well as for the encouragement and support I received from them. In particular, I owe a special word of thanks to S.L. Barnes.

I am forever indebted to my parents, sisters, and brothers for their unsparing love and sacrifice; to them, I dedicate my effort.

This work was performed under the auspices of the Air Force Office of Scientific Research, Grant no. AFOSR-83-0361. I gratefully acknowledge this support as well as the University of California Regents Fellowship, which has made possible my graduate studies at Berkeley.

Table of Contents

CHAPTER 1

INTRODUCTION AND OVERVIEW

Scope and fundamental aspects. In recent years, considerable attention has been devoted to the study of dynamic response and control of flexible structures performing large overall motions.† This type of structure is widely used in applications encompassing diverse disciplines such as machine design, robotics, aircraft dynamics and spacecraft dynamics. Elastic linkages, rotating machinery, robot manipulator arms, aircraft propellers, helicopter or turbine rotor blades, flexible satellites and earth-orbiting large space structures furnish some specific examples of these applications.

A common characteristic shared by these structures is their flexibility as one attempts to push the design to the limit of resistance of the material in order to minimize weight. This flexibility often renders inappropriate the assumption of "linearized strains" that has been popularly employed in analysis. The pointing maneuver in many of the above applications is typically an essential phase for these structures to successfully carry out their intended functions. Examples are: a flexible robot arm in high precision welding task to zero-in accurately on a micro spot, a solar array for collecting energy to face the sun, an antenna for data communication to point at control stations, a space-based telescope to focus on a star. It has been proposed to decompose the accurate pointing control of these flexible structures into two stages. In the first stage, an open-loop controller is assigned the task of quickly slewing the referential axis of these structures to a desired direction. As the maneuver nears the end of this stage, structural deformations must be considerably reduced, and the

† See for example the proceedings of the *26th Structures, Structural Dynamics and Material Conference* sponsored by the AIAA, ASME, ASCE, AHS, at Orlando, Florida, April 15-17, 1985.

referential axis must fall within a "cone" of pointing error tolerance. In the second stage, the control is transferred to a closed-loop controller, which may be assigned several tasks: vibration reduction, disturbance suppression, pointing error refinement.

In the design process and in the synthesis of optimal controls for flexible structures undergoing large motions, accurate mathematical modeling and effective simulation of the motion of the structure play a crucial role. These tasks involve: (i) formulation of a physically relevant mathematical model which in turn often includes modeling of effects such as large strains, inelastic constitutive behavior and appropriate, possibly nonlinear, damping mechanisms; and (ii) numerical solution of the resulting initial boundary value problem governing the evolution of the system. For flexible structures, nonlinear effects are particularly important in the first stage of the pointing control. Here, the fast slewing maneuver induces non-negligible transient loading resulting from the effects of Coriolis and centrifugal forces, as well as the inertia effect due to rotation. Moreover, large deformations in the structure relative to its rigid body local equilibrium configuration may occur during this stage. Finally, an integrated design approach should account for worst case designs, for example the possibility of catastrophic failure of the control system, so that an analyst could detect weaknesses in the structure for further reinforcements in the cycle of design-analysis-redesign. These cases may lead to bifurcation and instability, with subsequent large structural displacements, or may even result in structural damage. A unified treatment of these effects can only be accomplished through the use of finite-strain structural theories capable of accommodating general constitutive behavior in the general three-dimensional setting.

Traditional approaches. The dynamics of a flexible structure undergoing large overall motions is typically formulated relative to a coordinate system that

follows the deformed structure. This coordinate system is often referred to as the floating frame (Canavin & Likins [1977]). The introduction of a floating frame, relative to which the strains in the structure are measured, is motivated by the assumption of small strains (e.g., Ashley [1967], de Veubeke [1976], Canavin & Likins [1977], Kane & Levinson [1981]). With the assumption of small strains, the use of a floating frame allows a simple expression for the total potential energy of the structure. By contrast, the expression of the kinetic energy of the system takes a rather cumbersome form. The resulting equations of motion, although restricted to small strains, are nonlinear and *highly coupled in the inertia terms* due to the presence of Coriolis and centrifugal effects as well as inertia due to rotation of the floating frame.

Galerkin discretization of the equations of motion in the space variables leads to a system of implicit, coupled nonlinear differential equations in time of the form $\tilde{\mathbf{g}}(\dot{\mathbf{y}}, \mathbf{y}, t) = 0$, referred to as differential-algebraic equations (DAE). An essential characteristic of this system is that it cannot be transformed to a standard explicit form $\dot{\mathbf{y}} = \mathbf{g}(\mathbf{y}, t)$, without appending an algebraic constraint.† The structural mode shapes, obtained from solving the vibration eigenvalue problem at the reference configuration, may be employed as a Galerkin basis (e.g., Likins [1974]). But unlike the case of linear structural systems, the resulting semi-discrete system of equations remains extensively coupled.

The solution of DAE's requires the use of a special class of numerical integration algorithms first initiated by Gear [1971b]. Recently, follow-up work by many researchers has emerged in the literature (Brenan [1983], Lotstedt [1983,84], Petzold [1982,84]). DAE's are difficult to treat because they are

† One can always set $\dot{\mathbf{y}} = \mathbf{z}$, and append the *algebraic constraint* $\mathbf{g}(\mathbf{z}, \mathbf{y}, t) = 0$. This is a DAE system, and not a standard ODE system (Petzold [1982]).

usually stiff differential equations. Ill-conditioning may arise when the time step size is decreased to zero. The design of numerically robust algorithms to solve DAE's, as well as the assessment of their stability and accuracy characteristics, is one of the areas of current active research in numerical analysis.

The complex nature of these equations has often led to simplifying assumptions based on linear superposition theory, in which the elastic deformations are analyzed assuming known rigid body motion. These deformations are then superposed onto the rigid body motion to obtain the overall motion (e.g., Grotte *et al* [1971]). Selective truncation of nonlinear terms to render the equations of motion linear is another avenue often taken in the past. Such truncation reduces considerably the complexity of the problem; the design of controller based on linear partial differential equations (PDE's) is thus more tractable using established analytical tools in the realm of linear theory (Burns [1985]). For a review of several approaches in the dynamic analysis of mechanisms and machines, we refer to Erdman & Sandor [1972] and to Song & Haug [1980].

A new approach. We propose a methodology which represents a complete departure from traditional approaches where the use of a floating frame is necessary because of the *ab-initio* assumption of small deformations. The philosophy adopted here is opposite to that outlined above: The kinetic energy of the system is reduced to a quadratic uncoupled form simply by referring the motion of the system to the *inertial frame*. This results in a drastic simplification of the inertia operator, which now becomes *linear and uncoupled*, while the stiffness operator emanating from the potential energy functional becomes nonlinear. Conceptually, the essential step needed in developing this alternative approach is the use of *finite-deformation* structural theories — rods, plates, shells, three-dimensional continua —whose appropriate strain measures possess the required property of invariance with respect to superposed isometries (rigid

body motions).

From a computational standpoint, the substantial advantage of the proposed approach over traditional approaches lies in a much simpler structure of the resulting equations. By introducing a Galerkin semi-discretization in the space variables, one obtains, for the plane formulation, the standard nonlinear system of ordinary differential equations (ODE's) that typically arises in nonlinear structural dynamics. The Newmark implicit algorithm is widely used to discretize the time variable of this semi-discrete system of ODE's, and leads to a nonlinear algebraic system of equations whose solution may be obtained by employing the Newton-Raphson iterative procedure. Stability considerations often dictate the choice of an implicit over an explicit algorithm due to severe restriction on the time step size associated with the explicit schemes. There have been extensive investigations in error analysis and stability of integration algorithms for structural dynamics. In the linear case, we refer, for example, to Goudreau & Taylor [1973] and Hilber [1976,78]; the analysis for the nonlinear case —when the deformation map takes value in a linear space —is contained in, e.g., Hughes [1976] (see also Belytchsko & Hughes [1983] and references therein).

The role of nonlinear structural theories. So far, we have mentioned two aspects that render the use of a finite-strain formulation attractive: (i) First, we are able to account for the state of large deformation in flexible structures, a feature clearly desirable for analysis of safe designs; (ii) Second, the mathematical structure of the equations of motion, when the dynamics is referred to the inertial frame, is much simpler as compared to the equations resulting from the small deformation assumption and the use of a floating frame. For cases where infinitesimal deformation in the structure is insured by physical considerations, such as the case of a stiff beam undergoing a rotating motion, it seems obvious

that linear theories should be sufficient to model the behavior of the structure. Surprisingly enough, however this is not the case: It can be shown that the use of linear theory leads to an unphysical destabilizing effect characterized by the loss of stiffness, which is quadratic with the angular velocity of revolution. Such a phenomenon arises precisely because of a partial transfer of the centrifugal force to the equation governing the bending of the beam. On the other hand, higher order structural theories provide a remedy to this situation since they allow a correct transfer of the action of centrifugal force. Recently, Kane, Ryan & Banerjee [1985] have been able to account for such stiffening effect using their discrete approach together with a particular parametrization of the beam. It should be noted that their approach only applies to the case of a flexible beam attached to a rigid body with prescribed motions. Since the dynamics of the beam must be referred to a frame locally attached to the rigid body, the resulting equations of motion, in the general case where the base motion is not known, are nonlinear and highly coupled in the inertia term. Hence, within the context of the proposed finite-strain approach, there is little to be gained by introducing at the outset the additional small strain assumption.

A three-dimensional finite-strain rod model. When the motion of the rod is restricted to a plane, the deformation map, for the model considered herein, take values in the linear space $\mathbb{R}^3$. In three-dimensional motions, appropriate treatment of the rotation field in the rod — with shear deformation accounted for in the model — plays an important role. Nordgren [1974] considers a restricted nonlinear model whereby the cross section is assumed to possess equal principal moments of inertia. Since shear deformation is not accounted for, the deformation map of the rod is entirely described in terms of displacements, and thus takes values in $\mathbb{R}^3$. The model considered by Argyris and co-workers [1979,81,82], on the other hand, does include shear deformation. However,

motivated mainly for a desire for a symmetric stiffness operator, these authors employ the notion of ***semi-tangential rotation*** introduced by Ziegler [1977] to treat the rotation field in the rod. This concept of rotation possesses a property crucial to their approach: ***commutativity*** of two successive semi-tangential rotations, a characteristic not shared by the standard notion of finite rotations with direct physical interpretation. While the derivation of finite element matrices in Argyris *et al* [1979] is based on the concept of "natural formulation," the beam element by Bathe & Bolourchi [1979] is obtained, within the framework of the "total and updated lagrangian" formulation, from employing Hermitian interpolation of the displacements — as in the linear Bernoulli-Euler beam theory — expressed in convected coordinates. The range of application of such an element is restricted to motions that involve large rotations but only small strains. Rigorous error analysis of the spatial discretization requires that the equations of motion be described by PDE's — see Strang & Fix [1973] and Ciarlet [1978] for the analysis of the finite element method in the general context, and Arnold [1981] on the error estimate for the plane beam. In the previously cited work, only Nordgren formulates a model based on PDE's.

The models proposed by Antman [1974] and Simo [1985], as in the classical Kirchoff-Love model in Love [1944], employ a standard notion of rotations — which are elements of the special orthogonal group SO(3), a ***non-commutative*** Lie group. Computationally, we propose a parametrization based on quaternion parameters that avoids the use of Euler angles (Love [1944], Antman [1974]) and their associated singularity (e.g., Goldstein [1980], Kane *et al* [1983]); this parametrization plays a basic role in the algorithmic implementation. The configuration maps of the rod thus take values on the nonlinear differentiable manifold $\mathbb{R}^3 \times SO(3)$, which no longer has the structure of a linear space. The dynamics of rotation of a rigid body furnishes another example of a classical

dynamical system with a nonlinear differentiable manifold (essentially SO(3)) as configuration space (Arnold [1980]).

We have developed an extension of the Newmark time-stepping algorithm of the classical structural dynamics formulation (where the deformation map takes value in the linear space $\mathbb{R}^3 \times \mathbb{R}^3$) to the present case where the deformation map takes values in the nonlinear differentiable manifold $\mathbb{R}^3 \times SO(3)$. This extended Newmark algorithm furnishes a discretization of the time variable, and leads to the temporally discrete dynamic weak form of the equations of motion. Upon linearizing this semi-discrete dynamic weak form with respect to the space variable, numerical solutions are constructed by projection of the tangent space at each configuration onto a finite dimensional subspace. This linearization procedure is a basic step in iterative solution methods of the Newton type. Concepts of modern differential geometry (Spivak [1978]), and covariant linearization procedures (Marsden & Hughes [1983]) prove to be particularly useful in our algorithmic treatment. As an example, the configuration update in the iterative solution process becomes the algorithmic counterpart of the exponential map.

The organization of the dissertation is as follows. Chapter 2 will focus on the dynamics of planar motions of flexible rods to set the stage for the proposed methodology in dealing with flexible structures undergoing large overall motions. Chapter 3 reinforces the role of nonlinear theories in the dynamic analysis of flexible structures. The algorithmic treatment of the stiffness operator of a three-dimensional rod model constitutes the objective of Chapter 4, while its dynamic treatment is the focus of Chapter 5. Finally, in the concluding Chapter 6, we present two important applications of the present approach; namely the dynamics of flexible earth-orbiting satellites and multibody systems.

CHAPTER 2

DYNAMICS OF FLEXIBLE STRUCTURES PERFORMING LARGE MOTIONS

2.1. Introduction

To establish the methodology, we shall focus on the dynamics of a flexible beam subject to large planar motions. The essential ingredient in the proposed approach is the use of the finite-strain beam theory formulated independently by Reissner [1972] and Simo *et al* [1985]. This beam model can accommodate finite deformation in stretch-shear-bending, as well as account for large rotations in the cross section. For small deformations, the model reduces to the well-known Timoshenko beam theory. Moreover, the strain measures satisfy the requirement of invariance with respect to superposed isometries. The floating frame that follows the deformed beam performing large overall motions is sometimes referred to as the *shadow beam* (Laskin *et al* [1983]). The reason for the restriction to plane formulation to expound the essence of the proposed methodology lies in the simpler structure of the partial differential equations in plane motion as compared to the three-dimensional motion: the deformation map here takes values in the linear space $\mathbf{R}^3$ instead of the differentiable manifold $\mathbf{R}^3 \times SO(3)$ (Simo & Vu-Quoc [1985a]). In subsequent chapters, we shall address the three-dimensional motion of flexible rods whose formulation follows essentially the same basic steps set forth in this chapter. The appropriate treatment of the three-dimensional finite rotation field is, however, non-trivial.

As a basis for our discussion, we choose a specific problem to introduce the formulation: the dynamics of a flexible robot arm. This model problem consists of a flexible beam with one end at the origin E of the inertial frame $\{E;\mathbf{e}_1, \mathbf{e}_2, \mathbf{e}_3\}$ as shown in Figure 2.2.1. The robot arm is allowed to rotate about the axis $\mathbf{e}_3$, but the motion of the arm is restrained to the plane $\{\mathbf{e}_1, \mathbf{e}_2\}$. It will become

clear, however, that our formulation can be applied to a more general setting of flexible plane beams subject to large overall motions.

In section 2.2, we review the traditional approach based on the assumption of small strains and the use of a floating frame. The equations of motion here are nonlinear and extensively coupled, and result in a system of differential-algebraic equations upon introducing a Galerkin discretization in the space variables. A novel approach is presented in section 2.3, based on a finite-strain rod model in which the dynamics of motion is referred directly to the inertial frame. This approach leads to equations of motion with a linear uncoupled inertia term. The inherent nonlinearity of the problem, on the other hand, appears in the stiffness operator. Section 2.4 will focus on the temporal discretization of the weak form based on the Newmark implicit algorithm and the Galerkin finite element discretization, in the space variable, of the consistently linearized weak form. For the plane formulation of the rod model considered herein, the structure of the resulting discrete equations is typical of nonlinear structural dynamics. Section 2.5 gives some numerical examples to demonstrate the applicability of our formulation.

2.2. Classical approach based on small strains: Floating frame

In this section, we summarize the equations of motion for a rotating flexible beam using the shadow beam approach and assuming small strains superposed onto large rigid body rotations. Our purpose is to exhibit the main drawback of this approach. The basic kinematic assumption is reviewed in section 2.2.1, followed by the expressions of the potential energy in section 2.2.2 and the kinetic energy in section 2.2.3. Use of the floating frame, although allowing a simple expression for the potential energy, leads to a cumbersome expression for the kinetic energy of the system. The equations of motion, obtained via Hamilton's

principle, are given in section 2.2.4. From a computational standpoint, the numerical integration of these equations is a non-trivial task.

2.2.1. Basic kinematic assumption

Consider the rotating beam shown in Figure 2.2.1. Let $\{O;\, \mathbf{e}_1,\, \mathbf{e}_2\}$ be the inertial frame with base point $O \in \mathbb{R}^2$ and orthonormal basis vectors $(\mathbf{e}_1, \mathbf{e}_2)$. Let (X_1, X_2) denote the coordinates along $\mathbf{e}_1$ and $\mathbf{e}_2$. The domain of the undeformed beam with length L and depth d is $B := [0,\, L]\times[-\frac{d}{2},\, \frac{d}{2}] \subset \mathbb{R}^2$. A material point $X \in B$, in the *undeformed* (reference) configuration, initially located at $\mathbf{X} = X_1\mathbf{e}_1 + X_2\mathbf{e}_2$ is mapped into the point $x = \phi(X) \in \mathbb{R}^2$ by the deformation map ϕ: $B \to \mathbb{R}^2$. $\mathbf{X}$ designates the position vector of point X relative to the base point O. Similarly, the position vector of x relative to the base point O is denoted by $\mathbf{x}$† In addition, we introduce a floating frame $\{O;\mathbf{a}_1, \mathbf{a}_2\}$ that follows the rigid body motion of the beam, i.e., the shadow beam. In the literature, this type of floating frame, which is attached to a point within the deformable body, is often called the *locally attached frame* (Canavin & Likins [1977]). Components of vectors relative to this floating frame will be denoted by a superposed tilde. The basic kinematic assumption is that plane sections remain plane after deformation. Accordingly, we set

$$\mathbf{x} = \mathbf{x}_o + X_2\mathbf{t}_2 \tag{2.1a}$$

where

$$\mathbf{x}_o = \tilde{\boldsymbol{\phi}}_o(X_1, t) := [X_1 + \tilde{u}_1(X_1, t)]\,\mathbf{a}_1(t) + \tilde{u}_2(X_1, t)\,\mathbf{a}_2(t)\,,$$

$$\mathbf{t}_1(X_1, t) := \cos\tilde{\alpha}(X_1, t)\,\mathbf{a}_1(t) + \sin\tilde{\alpha}(X_1, t)\,\mathbf{a}_2(t)\,, \tag{2.1b}$$

† Light face letters denote *points*. Bold face letters denote *position vectors* of the corresponding points.

$$\mathbf{t}_2(X_1,t) := -\sin\tilde{\alpha}(X_1,t)\,\mathbf{a}_1(t) + \cos\tilde{\alpha}(X_1,t)\,\mathbf{a}_2(t)\,.$$

For notational simplicity, explicit indication of the arguments X_1, X_2 and t will often be omitted. Since the motion is planar, $\mathbf{e}_3 = \mathbf{t}_3 = \mathbf{a}_3$. Note that $\{\mathbf{t}_1, \mathbf{t}_2\}$ defines a moving frame that follows the deformation of the beam with $\mathbf{t}_2$ always contained in the deformed cross section and $\mathbf{t}_1$ perpendicular to the cross section. Using matrix notation, relations $(2.1b)_{2,3}$ may be expressed as

$$\begin{Bmatrix}\mathbf{t}_1\\ \mathbf{t}_2\end{Bmatrix} = \tilde{\mathbf{A}}^T\begin{Bmatrix}\mathbf{a}_1\\ \mathbf{a}_2\end{Bmatrix}, \quad \text{where} \quad \tilde{\mathbf{A}} := \begin{bmatrix}\cos\tilde{\alpha} & -\sin\tilde{\alpha}\\ \sin\tilde{\alpha} & \cos\tilde{\alpha}\end{bmatrix}. \tag{2.2}$$

Although it is possible to develop the formulation without introducing any restriction on the size of the strain field, the assumption of small strains is typically introduced *ab-initio*, as discussed below.

2.2.2. Motivation: Total potential energy

By introducing the floating frame $\{\mathbf{a}_1, \mathbf{a}_2\}$ one can enforce at the outset the following infinitesimal strains assumption:

$$\tilde{\alpha} \ \text{small} \ (\leq 10^\circ) \iff \tilde{\mathbf{A}} \cong \begin{bmatrix}1 & -\tilde{\alpha}\\ \tilde{\alpha} & 1\end{bmatrix},$$

$$\text{with} \quad \tilde{u}_1 \quad \text{and} \quad \tilde{u}_2 \quad \text{small}\,. \tag{2.3}$$

The strains $\tilde{\gamma}$ and the curvature $\tilde{\kappa}$ relative to the floating frame $\{\mathbf{a}_1, \mathbf{a}_2\}$ are then defined as

$$\tilde{\gamma} := \tilde{\phi}_o{}' - \mathbf{t}_1, \qquad \kappa := \tilde{\alpha}'\,\mathbf{t}_3, \tag{2.4a}$$

where $(\,\cdot\,)' := d(\,\cdot\,)/dX_1$. In component form, $\tilde{\gamma}$ is expressed as

$$\tilde{\gamma} = \tilde{\gamma}_1\,\mathbf{a}_1 + \tilde{\gamma}_2\,\mathbf{a}_2\,, \tag{2.4b}$$

where

$$\tilde{\gamma}_1 = \tilde{u}_1', \quad \tilde{\gamma}_2 = \tilde{u}_2' - \tilde{\alpha}. \tag{2.4c}$$

One refers to $\tilde{\gamma}_1$ and $\tilde{\gamma}_2$ as the *axial* strain and the *shearing* strain, respectively. Denoting by EA, GA_s and EI the axial, shear and flexural stiffnesses of the beam, the potential energy is expressed as

$$\Pi := \frac{1}{2}\int_{[0,L]} [EA\tilde{\gamma}_1^2 + GA_s\tilde{\gamma}_2^2 + EI(\tilde{\alpha}')^2]\,dS - \Pi_{EXT} - T(t)\psi(t) \tag{2.5}$$

where Π_{EXT} is the potential energy of the external loading acting on the beam and $T(t)\,\mathbf{e}_3$ is an applied torque at the axis of rotation $\mathbf{e}_3$ of the robot arm.

2.2.3. Kinetic energy

The kinetic energy of the system takes a rather cumbersome form compared with the simplicity of (2.5). To obtain the appropriate expression, we introduce the time derivative relative to an observer attached to the floating frame. Accordingly, we define

$$\overset{\nabla}{\mathbf{x}} := \left.\frac{\partial \tilde{\boldsymbol{\varphi}}_0}{\partial t}\right|_{\mathbf{a}_i = \text{fixed}}. \tag{2.6}$$

The following expression for the material time derivative, denoted by a superposed "dot", is standard in rigid body mechanics (Goldstein [1980])

$$\dot{\mathbf{x}} = \overset{\nabla}{\mathbf{x}} + \mathbf{w}\times\mathbf{x} \tag{2.7}$$

where $\mathbf{w}$ is the angular velocity of the floating frame. For the plane case under consideration, the angular velocity $\mathbf{w}$ is given as

$$\mathbf{w} = \frac{d\psi}{dt}\mathbf{a}_3 = \dot{\psi}\,\mathbf{a}_3 \tag{2.8}$$

where $\mathbf{a}_3 := \mathbf{a}_1 \times \mathbf{a}_2 \equiv \mathbf{e}_3$ is *fixed*. Since the time derivative of the floating basis is

$$\dot{\mathbf{a}}_1 = \dot{\psi}\,\mathbf{a}_2, \quad \dot{\mathbf{a}}_2 = -\dot{\psi}\,\mathbf{a}_1, \tag{2.9}$$

it follows from expressions (2.1b) that

$$\dot{\mathbf{t}}_1 = (\dot{\tilde{\alpha}} + \dot{\tilde{\psi}})\,\mathbf{t}_2, \qquad \dot{\mathbf{t}}_2 = -(\dot{\tilde{\alpha}} + \dot{\tilde{\psi}})\,\mathbf{t}_1 \tag{2.10}$$

Thus, we arrive at the following expression for the time derivative of the position vector $\mathbf{x}$

$$\dot{\mathbf{x}} = (\dot{\tilde{u}}_1 - \dot{\tilde{\psi}}\tilde{u}_2)\,\mathbf{a}_1 + [\dot{\tilde{u}}_2 + \dot{\tilde{\psi}}(X_1 + \tilde{u}_1)]\,\mathbf{a}_2 - X_2(\dot{\tilde{\alpha}} + \dot{\tilde{\psi}})\,\mathbf{t}_1 \tag{2.11}$$

The kinetic energy of the system is obtained from the expression

$$K := \tfrac{1}{2}\int_B \rho(X_1, X_2)\,\|\dot{\mathbf{x}}\|^2\,dX_1\,dX_2 \tag{2.12}$$

where $\rho(X_1, X_2)$ is the mass density of the beam material. By substituting (2.11) into (2.12) we obtain

$$K = \tfrac{1}{2}\int_{[0,L]} A_\rho \{\,[\dot{\tilde{u}}_1 - \dot{\tilde{\psi}}\tilde{u}_2]^2 + [\dot{\tilde{u}}_2 + \dot{\tilde{\psi}}(X_1 + \tilde{u}_1)]^2\,\}\,dX_1$$

$$+ \tfrac{1}{2}\int_{[0,L]} I_\rho[\dot{\tilde{\alpha}} + \dot{\tilde{\psi}}]^2\,dX_1 \tag{2.13}$$

Here, the inertia constants A_ρ and I_ρ are defined as

$$A_\rho := \int_{[-\frac{g}{2}, \frac{g}{2}]} \rho(X_1, X_2)\,dX_2, \qquad I_\rho := \int_{[-\frac{g}{2}, \frac{g}{2}]} \rho(X_1, X_2)\,X_2^2\,dX_2 \tag{2.14}$$

2.2.4. Equations of motion: Coupled inertia terms

The equations of motion may be systematically derived by means of Hamilton's principle. Accordingly, we require that the action

$$L := \int_{[t_1, t_2]} (K - \Pi)\,dt \quad \text{be stationary,} \tag{2.15}$$

for arbitrary paths connecting two points at time t_1 and t_2 in the configuration space. Substituting expressions (2.5) and (2.13) into (2.15) and making use of standard arguments involving integration by parts, we arrive at the following

equations governing the extensional and flexural motion of the beam

$$A_\rho[\ddot{\tilde{u}}_1 - \ddot{\psi}\tilde{u}_2 - 2\dot{\psi}\dot{\tilde{u}}_2 - \dot{\psi}^2(X_1+\tilde{u}_1)] \;-\; EA\,\tilde{u}_1'' \;=\; 0$$

$$A_\rho[\ddot{\tilde{u}}_2 + \ddot{\psi}(X_1+\tilde{u}_1) + 2\dot{\psi}\dot{\tilde{u}}_1 - \dot{\psi}^2\tilde{u}_2] \;-\; GA_s\,(\tilde{u}_2' - \tilde{\alpha})' \;=\; 0 \qquad (2.16)$$

$$I_\rho(\ddot{\tilde{\alpha}} + \ddot{\psi}) \;-\; EI\,\tilde{\alpha}'' - GA_s\,(\tilde{u}_2' - \tilde{\alpha}) \;=\; 0$$

Appropriate boundary conditions automatically follow from the stationarity condition. In addition to equations (2.16), one obtains the following constraint equation expressing the overall balance of angular momentum of the system

$$\ddot{\psi}\int_{[0,L]}\{A_\rho[(X_1+\tilde{u}_1)^2+\tilde{u}_2^2] + I_\rho\}\,dX_1 + 2\dot{\psi}\int_{[0,L]}A_\rho\{(X_1+\tilde{u}_1)\dot{\tilde{u}}_1 + \tilde{u}_2\dot{\tilde{u}}_2\}\,dX_1$$

$$+\int_{[0,L]}A_\rho\{(X_1+\tilde{u}_1)\ddot{\tilde{u}}_2 - \tilde{u}_2\ddot{\tilde{u}}_1\}\,dX_1 + \int_{[0,L]}I_\rho\ddot{\tilde{\alpha}}\,dX_1 \;=\; T(t) \qquad (2.17)$$

The highly nonlinear nature of the coupled system (2.16)-(2.17) involving the variables $\{\tilde{u}_1, \tilde{u}_2, \tilde{\alpha}, \psi\}$ should be noted. A Galerkin discretization in the space variable X_1 of (2.16) and (2.17) leads to a system of implicit differential-algebraic equations in time of the form $\tilde{\mathbf{g}}(\dot{\mathbf{y}}, \mathbf{y}, t) = 0$.

Remark 2.1. The Euler-Bernoulli formulation is obtained from the above equations by assuming that shear deformation is negligible. Accordingly, we let $(\tilde{u}_2' - \tilde{\alpha}) \to 0$, and $GA_s \to \infty$ so that $GA_s\,(\tilde{u}_2' - \tilde{\alpha}) \to V$ where V is the shear force acting on the cross section of the beam. Equations $(2.16)_{2,3}$ governing the transverse and flexural vibrations of the beam may be combined, to obtain

$$A_\rho\ddot{\tilde{u}}_2 + EI\,\tilde{u}_2'''' - I_\rho\ddot{\tilde{u}}_2'' + A_\rho[\ddot{\psi}(X_1+\tilde{u}_1) + 2\dot{\psi}\dot{\tilde{u}}_1 - \dot{\psi}^2\tilde{u}_2)] \;=\; 0 \qquad (2.18)$$

The first two terms in (2.18) correspond to the standard linear Euler-Bernoulli beam theory. This equation is, however, attributed to Rayleigh who accounted for the contribution of section rotary inertia to the transverse vibration of the

beam. This contribution is represented by the third term, and is often neglected in structural applications. The last three terms within brackets arise as a result of coupling between deformation and rigid body motion. These terms represent the inertia due to rotation of the shadow beam, the Coriolis and the centrifugal effects, respectively. We shall further discuss in Chapter 3 the effect of the centrifugal term $\dot{\psi}^2 \tilde{u}_2$ appeared in (2.18). ■

2.3. Proposed approach based on finite strains: Inertial frame

By contrast with the formulation outlined above, we propose an alternative approach in which the structure of the inertia operator becomes *linear and uncoupled*. This is achieved by referring the basic equations of motion to the *inertial* frame. As a result, drastic simplification of the inertia (temporal) part is obtained by shifting the nonlinearity of the problem to the stiffness (spatial) part of the equations of motion. Conceptually, the essential step needed to develop this approach is the use of finite-strain rod theories capable of accounting for large rotations. Section 2.3.3 summarizes from a physical standpoint the appropriate finite strain measures. We refer to Reissner [1972] for the plane case, and to Antman [1974] and Simo [1985] for the three-dimensional case. An essential characteristic of these strain measures is their invariance under superposed isometries.

From a computational perspective, the substantial advantage of the proposed approach over the shadow beam approach discussed in section 2.2.2 lies in a much simpler structure of the resulting equations. This structure corresponds to the standard nonlinear system of ODE's that typically arises in structural dynamics. In addition, we automatically account for large strains.

2.3.1. Basic kinematic assumption

As in section 2.2.1, the basic kinematic assumption is the condition that plane sections normal to the axis of the beam in the undeformed configuration remain plane; i.e.,

$$\mathbf{x} = \mathbf{x}_o + X_2 \mathbf{t}_2 \tag{2.1a}$$

The difference from the previous approach based on the use of the floating frame is that the position vector $\mathbf{x}_o$ and the basis vectors $\{\mathbf{t}_1, \mathbf{t}_2\}$ now have their components expressed relative to the *inertial frame* $\{\mathbf{e}_1, \mathbf{e}_2\}$. Accordingly, we set

$$\begin{aligned} \mathbf{x}_o = \boldsymbol{\phi}_o(X_1, t) &:= [X_1 + u_1(X_1, t)]\mathbf{e}_1 + u_2(X_1, t)\mathbf{e}_2 \\ \mathbf{t}_1(X_1, t) &:= \cos\vartheta(X_1, t)\mathbf{e}_1 + \sin\vartheta(X_1, t)\mathbf{e}_2 \\ \mathbf{t}_2(X_1, t) &:= -\sin\vartheta(X_1, t)\mathbf{e}_1 + \cos\vartheta(X_1, t)\mathbf{e}_2 \end{aligned} \tag{2.19}$$

As in (2.2), we shall use matrix notation and express relations $(2.19)_{2,3}$ as

$$\begin{Bmatrix} \mathbf{t}_1 \\ \mathbf{t}_2 \end{Bmatrix} = \mathbf{A}^T \begin{Bmatrix} \mathbf{e}_1 \\ \mathbf{e}_2 \end{Bmatrix}, \quad \text{where} \quad \mathbf{A} := \begin{bmatrix} \cos\vartheta & -\sin\vartheta \\ \sin\vartheta & \cos\vartheta \end{bmatrix} \tag{2.20}$$

Note that the floating basis $\{\mathbf{a}_1, \mathbf{a}_2\}$ plays no role in the present formulation.

2.3.2. Motivation: Kinetic energy

The kinetic energy of the system relative to the inertial basis reduces to the standard quadratic uncoupled form. To see this, note that from (2.20) the rate of change of the basis vectors $\{\mathbf{t}_1, \mathbf{t}_2\}$ is given by

$$\dot{\mathbf{t}}_1 = \dot{\vartheta}\mathbf{t}_2, \qquad \dot{\mathbf{t}}_2 = -\dot{\vartheta}\mathbf{t}_1 \tag{2.21}$$

Hence, the time derivative of the position vector $\mathbf{x}$ is obtained as

$$\dot{\mathbf{x}} = \dot{\boldsymbol{\phi}}_o - X_2\dot{\vartheta}\mathbf{t}_1, \qquad \dot{\boldsymbol{\phi}}_o = \dot{u}_1\mathbf{e}_1 + \dot{u}_2\mathbf{e}_2 \tag{2.22}$$

It follows from (2.22) that $\|\dot{\mathbf{x}}\|^2$ has the expression

$$\|\dot{\mathbf{x}}\|^2 = [\dot{u}_1^2 + \dot{u}_2^2] + X_2^2\dot{\vartheta}^2 - 2\dot{\vartheta}X_2[\cos\vartheta\dot{u}_1 + \sin\vartheta\dot{u}_2] \tag{2.23}$$

Upon integrating $\rho(X_1, X_2)\|\dot{\mathbf{x}}\|^2$ over the body $B = [0, L]\times[-\frac{d}{2}, \frac{d}{2}]$, we arrive at the following expression for the kinetic energy of the system

$$K = \frac{1}{2}\int_{[0,L]}[A_\rho(\dot{u}_1^2 + \dot{u}_2^2) + I_\rho\dot{\vartheta}^2]\,dX_1 \tag{2.24}$$

Here, as in (2.13), the inertia coefficients A_ρ and I_ρ are given by (2.14).

Remark 2.1. It is noted that expression (2.13) for the kinetic energy in the shadow beam approach may be exactly recovered from (2.24) simple by employing the coordinate transformation

$$\begin{Bmatrix} X_1+u_1 \\ u_2 \end{Bmatrix} = \begin{bmatrix} \cos\psi & -\sin\psi \\ \sin\psi & \cos\psi \end{bmatrix}\begin{Bmatrix} X_1+\tilde{u}_1 \\ \tilde{u}_2 \end{Bmatrix} \tag{2.25a}$$

That is, the expression for the kinetic energy of the system is independent of any particular assumption on the magnitude of the strain field. In fact, the time derivative of (2.25a),

$$\begin{Bmatrix} \dot{u}_1 \\ \dot{u}_2 \end{Bmatrix} = \begin{bmatrix} \cos\psi & -\sin\psi \\ \sin\psi & \cos\psi \end{bmatrix}\begin{Bmatrix} \dot{\tilde{u}}_1 - \dot{\psi}\tilde{u}_2 \\ \dot{\tilde{u}}_2 + \dot{\psi}(X_1+\tilde{u}_1) \end{Bmatrix}, \tag{2.25b}$$

simply expresses the transformation of the components of $\dot{\mathbf{x}}_o$ relative to the floating basis $\{\mathbf{a}_1, \mathbf{a}_2\}$ back to the inertial basis $\{\mathbf{e}_1, \mathbf{e}_2\}$:

$$\dot{\mathbf{x}}_o = \dot{u}_1\mathbf{e}_1 + \dot{u}_2\mathbf{e}_2 = [\dot{\tilde{u}}_1 - \dot{\psi}\tilde{u}_2]\mathbf{a}_1 + [\dot{\tilde{u}}_2 + \dot{\psi}(X_1+\tilde{u}_1)]\mathbf{a}_2 \tag{2.25c}$$

This remark would become evident if we express the kinetic energy using coordinate-free notation

$$K = \int_B \rho\|\dot{\mathbf{x}}\|^2\,dX_1 = \int_B \rho\|\dot{\mathbf{x}}_o - X_2\dot{\vartheta}\mathbf{t}_1\|^2\,dX_1 = \int_{[0,L]}\{A_\rho\|\dot{\mathbf{x}}_o\|^2 + I_\rho\dot{\vartheta}^2\}\,dX_1 \tag{2.25d}$$

2.3.3. Potential energy and invariance of strain measures

Potential energy. Within the context of large strains, a definition of the strain field in the beam is provided by

$$\boldsymbol{\gamma} := \boldsymbol{\phi}_o{}' - \mathbf{t}_1 , \qquad \boldsymbol{\kappa} := \vartheta' \mathbf{t}_3 \tag{2.26a}$$

The physical interpretation of $\boldsymbol{\gamma}$ is clear as shown in Figure 2.3.1. $\boldsymbol{\gamma}$ measures the difference between the slope of the deformed axis of the beam and the normal to the cross section defined by $\mathbf{t}_1$, and $\boldsymbol{\kappa}$ is the rate of rotation of the cross section along the undeformed length of the beam. In component form, relative to the inertial frame we have from (2.19) the following expression for $\boldsymbol{\gamma}$

$$\boldsymbol{\gamma} = \gamma_1 \mathbf{e}_1 + \gamma_2 \mathbf{e}_2 = [(1 + u_1{}') - \cos\vartheta]\mathbf{e}_1 + [u_2{}' - \sin\vartheta]\mathbf{e}_2 \tag{2.26b}$$

Alternatively, relative to the basis vectors $\{\mathbf{t}_1, \mathbf{t}_2\}$, from relation (2.20) we have the following expression

$$\boldsymbol{\gamma} = \Gamma_1 \mathbf{t}_1 + \Gamma_2 \mathbf{t}_2 \tag{2.27a}$$

where

$$\begin{Bmatrix} \Gamma_1 \\ \Gamma_2 \end{Bmatrix} = \mathbf{A}^T \begin{Bmatrix} 1 + u_1{}' - \cos\vartheta \\ u_2{}' - \sin\vartheta \end{Bmatrix} = \mathbf{A}^T \begin{Bmatrix} 1 + u_1{}' \\ u_2{}' \end{Bmatrix} - \begin{Bmatrix} 1 \\ 0 \end{Bmatrix} \tag{2.27b}$$

The analogy between expressions (2.4a,b,c) and (2.26a)-(2.26b) should be noted. We now assume the same expression for the potential energy, relative to the moving frame$\{\mathbf{t}_1, \mathbf{t}_2\}$, as the one considered in the small strain shadow beam approach discussed in section 2.2. Accordingly, we set

$$\Pi := \frac{1}{2} \int_{[0,L]} [EA\,\Gamma_1^2 + GA_s\,\Gamma_2^2 + EI\,(\vartheta')^2]\,dS - \Pi_{EXT} - T(t)\vartheta(0,t) \tag{2.28}$$

Invariant strain measures. The components of the strain $\boldsymbol{\gamma}$ in the basis $\{\mathbf{t}_1, \mathbf{t}_2\}$ denoted by (Γ_1, Γ_2) are invariant under superposed isometries on the beam. One can see this by considering the isometry composed of a superposed translation $\mathbf{c}(t)$, and a superposed rotation $\beta(t)$ represented by the orthogonal transformation matrix

$$\mathbf{Q}(t) := \begin{bmatrix} \cos\beta & -\sin\beta \\ \sin\beta & \cos\beta \end{bmatrix} \tag{2.29}$$

The transformed quantities in the expression of Γ_i in (2.27) above are as follows

$$\boldsymbol{\phi}_o^+(X_1, t) = \mathbf{c}(t) + \mathbf{Q}(t)\,\boldsymbol{\phi}_o(X_1, t)\,; \quad \boldsymbol{\phi}_o^{+\prime} = \phi_{o1}^{+\prime}\,\mathbf{e}_1 + \phi_{o2}^{+\prime}\,\mathbf{e}_2 = \mathbf{Q}\boldsymbol{\phi}_o'\,. \tag{2.30a}$$

$$\text{i.e.,} \quad \begin{Bmatrix} \phi_{o1}^{+\prime} \\ \phi_{o2}^{+\prime} \end{Bmatrix} = \mathbf{Q} \begin{Bmatrix} 1 + u_1' \\ u_2' \end{Bmatrix}. \tag{2.30b}$$

$$\mathbf{A}^+ = \mathbf{Q}\mathbf{A} \tag{2.30c}$$

Since $\mathbf{t}_1^+ = \cos(\beta+\vartheta)\,\mathbf{e}_1 + \sin(\beta+\vartheta)\,\mathbf{e}_2$, it follows that

$$\boldsymbol{\gamma}^+ = \Gamma_1^+ \mathbf{t}_1^+ + \Gamma_2^+ \mathbf{t}_2^+ = \boldsymbol{\phi}_o^{+\prime} - \mathbf{t}_1^+ \tag{2.31a}$$

where

$$\begin{Bmatrix} \Gamma_1^+ \\ \Gamma_2^+ \end{Bmatrix} = \mathbf{A}^{+T} \left[\begin{Bmatrix} \phi_{o1}^{+\prime} \\ \phi_{o2}^{+\prime} \end{Bmatrix} - \begin{Bmatrix} \cos(\beta+\vartheta) \\ \sin(\beta+\vartheta) \end{Bmatrix} \right] = \begin{Bmatrix} \Gamma_1 \\ \Gamma_2 \end{Bmatrix} \tag{2.31b}$$

The invariance under superposed isometries of the *curvature* κ follows at once in the plane case from expression (2.26a). This property of invariance of the strain measures is essential for the success of the proposed approach.

Remark 2.2. It can be shown that definition (2.26a) and expressions (2.26b), (2.27) follow from a rigorous argument based on the equivalence of the stress power for the general three dimensional theory with the reduced stress

power of the finite-strain beam theory (Simo [1985]). ■

Remark 2.3. In this chapter, we shall be concerned only with spatially fixed loads, which do not depend on the deformed configuration, as opposed to follower loads that are configuration dependent. A treatment of follower loads in the general context of the three-dimensional finite-strain beam will be given in chapter 3. Accordingly, the potential of the distributed loading is given by

$$\Pi_{EXT} = \int_{[0,L]} [\bar{\mathbf{m}} \cdot \vartheta \mathbf{e}_3 + \bar{\mathbf{n}} \cdot \boldsymbol{\phi}_0] \, dX_1 \tag{2.32a}$$

where

$$\bar{\mathbf{n}}(X_1, t) := \bar{n}_1(X_1, t)\,\mathbf{e}_1 + \bar{n}_2(X_1, t)\,\mathbf{e}_2\,, \qquad \bar{\mathbf{m}}(X_1, t) := \bar{m}(X_1, t)\,\mathbf{e}_3 \tag{2.32b}$$

are the external force and torque per unit of reference length acting on the beam. ■

2.3.4. Equations of motion: Uncoupled inertia terms

We introduce the following notation

$$\begin{Bmatrix} n_1 \\ n_2 \end{Bmatrix} := \mathbf{\Lambda} \begin{bmatrix} EA & 0 \\ 0 & GA_s \end{bmatrix} \mathbf{\Lambda}^T \begin{Bmatrix} 1 + u'_1 - \cos\vartheta \\ u'_2 - \sin\vartheta \end{Bmatrix}, \qquad m := EI\,\vartheta' \tag{2.33}$$

Here, $\mathbf{n}(X_1, t) = n_1(X_1, t)\,\mathbf{e}_1 + n_2(X_1, t)\,\mathbf{e}_2$ and $\mathbf{m}(X_1, t) = m(X_1, t)\,\mathbf{e}_3$ represent the internal force and internal moment acting on a deformed cross section of the beam.

As in section 2.2, the equations of motion governing the evolution of the system may be systematically obtained from Hamilton's principle. Standard manipulations yield the final result

$$\begin{bmatrix} A_\rho & & \\ & A_\rho & \\ & & I_\rho \end{bmatrix} \begin{Bmatrix} \ddot{u}_1 \\ \ddot{u}_2 \\ \ddot{\vartheta} \end{Bmatrix} - \begin{Bmatrix} n_1' \\ n_2' \\ m' + (1 + u_1')n_2 - u_2' n_1 \end{Bmatrix} - \begin{Bmatrix} \bar{n}_1 \\ \bar{n}_2 \\ \bar{m} \end{Bmatrix} = \mathbf{0} \tag{2.34}$$

Equations (2.34) represents the system of nonlinear partial differential equations governing the response of the system. Note that these equations are linear in the term involving time derivative.

For the robot arm in Figure 2.2.1 we have the following natural boundary conditions

$$\mathbf{m}(0,t) = T(t)\mathbf{e}_3, \quad \mathbf{m}(L,t) = \mathbf{n}(L,t) = \mathbf{0} \tag{2.35}$$

These boundary conditions follow automatically from Hamilton's principle and the appropriate expression for Π_{EXT}.

2.3.5. Conservation of global momenta

Within the proposed approach *global* linear and angular momenta are automatically satisfied, and do not provide any additional constraint. This is in contrast with the shadow beam approach in which the basic equations of motion (2.16) must be supplemented by the global angular momentum condition (2.17) for the evolution of the system to be completely determined. To verify conservation of global linear and angular momenta, we rewrite (2.34) with the aid of (2.33) as

$$\dot{\mathbf{L}} - \mathbf{n}' - \bar{\mathbf{n}} = \mathbf{0}, \quad \dot{\mathbf{H}} - \mathbf{m}' - \boldsymbol{\phi}_o{}' \times \mathbf{n} - \bar{\mathbf{m}} = \mathbf{0} \tag{2.36a}$$

Here $\mathbf{L}(X_1,t)$ denotes the linear momentum per unit length, and $\mathbf{H}(X_1,t)$ the angular momentum per unit length relative to the centroid of the deformed cross section. Using (2.19) we have

$$\mathbf{L} := \int_{[-\frac{d}{2},\frac{d}{2}]} \rho \dot{\mathbf{x}}\, dX_2 = A_\rho \dot{\boldsymbol{\phi}}_o, \quad \mathbf{H} := \int_{[-\frac{d}{2},\frac{d}{2}]} \rho [\mathbf{x} - \mathbf{x}_o] \times \dot{\mathbf{x}}\, dX_2 = I_\rho \dot{\boldsymbol{\vartheta}} \tag{2.36b}$$

The global linear and angular momentum of the system denoted by $\mathbf{L}(t)$ and $\mathbf{H}(t)$, respectively, are defined as

$$\mathbf{L}(t) := \int_B \rho\, \dot{\mathbf{x}}\, dX_1 dX_2\,, \qquad \mathbf{H}(t) := \int_B \rho\, \mathbf{x}\times\dot{\mathbf{x}}\, dX_1 dX_2 \tag{2.37}$$

Making use of the identity $\mathbf{x}\times\dot{\mathbf{x}} = (\mathbf{x}-\mathbf{x}_0)\times\dot{\mathbf{x}} + \mathbf{x}_0\times\dot{\mathbf{x}}$, the global angular momentum is expressed as

$$\mathbf{H}(t) = \int_{[0,L]} [\mathbf{H} + \boldsymbol{\phi}_0 \times \mathbf{L}]\, dX_1 \tag{2.38}$$

where $\mathbf{L}(X_1, t)$ and $\mathbf{H}(X_1, t)$ are given in (2.36b). Differentiating (2.38) and using (2.36a), we obtain the following condition involving the applied load and boundary conditions

$$\dot{\mathbf{H}} = [\mathbf{m} + \boldsymbol{\phi}_0 \times \mathbf{n}]\Big|_{X_1=0}^{X_1=L} + \int_{[0,L]} [\bar{\mathbf{m}} + \boldsymbol{\phi}_0 \times \bar{\mathbf{n}}]\, dX_1 \tag{2.39}$$

Condition (2.39) states that the resultant torque of the applied loading equals the rate of change of the total angular momentum. Similarly, for the global linear momentum we obtain

$$\dot{\mathbf{L}} = \mathbf{n}\Big|_{X_1=0}^{X_1=L} + \int_{[0,L]} \bar{\mathbf{n}}\, dX_1 \tag{2.40}$$

which states that the resultant force of the applied loads equals the rate of change of the global linear momentum. Equations of motion (2.36a) along with definitions (2.36b) are general, and remain valid in the three dimensional theory. Thus, the foregoing discussion leading to expressions (2.39) and (2.40) is not restricted to the plane case.

2.4. Numerical approximation: Galerkin finite-element method

In this section, we discuss the numerical treatment of the nonlinear partial differential equations developed in Section 2.3. The basic strategy is to perform the temporal discretization employing standard implicit time-stepping algorithms and a Galerkin discretization of the space variable. The finite element

method provides an established technique for constructing the (spatial) basis functions necessary to perform the Galerkin discretization. This procedure will lead to a discrete system of nonlinear algebraic equations characteristic of nonlinear structural dynamics. Expressions for the matrices resulting from the application of this procedure are given in detail.

2.4.1. Temporal discretization of weak form

Weak form. Define the following quantities

$$\mathbf{I} := Diag[A_\rho, A_\rho, I_\rho]$$
$$\boldsymbol{\phi}(X_1,t) := \begin{Bmatrix} X_1+u_1(X_1,t) \\ u_2(X_1,t) \\ \vartheta(X_1,t) \end{Bmatrix}, \qquad \mathbf{f}(X_1,t) := \begin{Bmatrix} \overline{n}_1(X_1,t) \\ \overline{n}_2(X_1,t) \\ \overline{m}(X_1,t) \end{Bmatrix} \tag{2.41}$$

The weak form of the equations of motion (2.34) is obtained as the scalar product of (2.34) with an arbitrary weighting function $\boldsymbol{\eta} = \eta_i \mathbf{e}_i$

$$G_{dyn}(\boldsymbol{\phi},\boldsymbol{\eta}) := \int_{[0,L]} \boldsymbol{\eta}\cdot\mathbf{I}\,\ddot{\boldsymbol{\phi}}\,dX_1 + G(\boldsymbol{\phi},\boldsymbol{\eta}) = 0, \quad \forall\,\boldsymbol{\eta} \tag{2.42}$$

where $G(\boldsymbol{\phi},\boldsymbol{\eta})$ denotes the weak form of the PDE's when inertia effects are not taken into account

$$G(\boldsymbol{\phi},\boldsymbol{\eta}) := -\int_{[0,L]} \boldsymbol{\eta}\cdot\begin{Bmatrix} n_1' \\ n_2' \\ m' + (1+u_1')n_2 - u_2' n_1 \end{Bmatrix} dX_1 - \int_{[0,L]} \boldsymbol{\eta}\cdot\mathbf{f}\,dX_1 \tag{2.43}$$

Recall that equation (2.34) is linear in the term involving the time derivative, i.e., the acceleration $\ddot{\boldsymbol{\phi}}$. The inherent nonlinearity of the problem, which results from the coupling between large overall motions and (possibly finite) deformations in the beam, is contained in the second term and included in the weak form (2.43). For simplicity of exposition, let $\boldsymbol{\eta}$ be a member of the function

space

$$V := \{ \eta \in (H^1(0,L))^3 \mid \eta(0) = \eta(L) = 0 \},\dagger \tag{2.44}$$

and integrating by parts the first term in (2.43) with respect to the spatial derivative, we obtain

$$G(\phi,\eta) = \int_{[0,L]} \Xi(\phi)\eta \cdot \begin{Bmatrix} n_1 \\ n_2 \\ m \end{Bmatrix} dX_1 - \int_{[0,L]} \eta \cdot \mathbf{f}\, dX_1 \tag{2.45}$$

where $\Xi(\phi)$ denotes the differential operator defined by

$$\Xi(\phi) := \begin{bmatrix} \frac{d}{dX_1} & 0 & u_2' \\ 0 & \frac{d}{dX_1} & -(1+u_1') \\ 0 & 0 & \frac{d}{dX_1} \end{bmatrix} \tag{2.46}$$

Note that in (2.45), we made use of the identity $\eta(0) = \eta(L) = 0$. Strictly speaking, the function space V in (2.44) represents the space of admissible variations corresponding to zero displacement boundary conditions for the PDE's (2.34), i.e., a beam with clamped ends. The choice of the boundary conditions for the space of admissible variations should account for the essential boundary conditions for the PDE's. In general, the following condition $\eta \cdot \{n_1, n_2, m\}^T \Big|_{X_1=0}^{X_1=L} = 0$ determines the choice of boundary conditions for the admissible variations.

Time-stepping scheme. A standard system of nonlinear ODE's, $\dot{\mathbf{y}} = \mathbf{g}(\mathbf{y}, t)$ can be integrated by employing a variety of time-stepping algorithms. It is desirable to use algorithms that prove to be *consistent* with the ODE's and *stable*

† $H^1(0,L)$ denotes the Hilbert space of functions defined on the interval $(0,L)$ whose elements and their first derivatives are square integrable, i.e., elements of the function space L^2. The inner product of a pair $(f,g) \in H^1(0,L)$ is given by $\int_{[0,L]} (fg + f'g')dx$.

for some range of the time step size. We refer to standard textbooks such as Richtmyer & Morton [1967] and Gear [1971] for precise definitions of these concepts. Two basic strategies in devising time-stepping algorithms may be adopted:

(a) *Explicit schemes*: Typically, high accuracy may be achieved by employing high order methods. A classical example is furnished by the family of Runge-Kutta methods. The main drawback of explicit schemes is the severe limitation on the time step size imposed by their restrictive stability characteristics.

(b) *Implicit schemes*: These typically possess very robust stability characteristics. Classical examples are the trapezoidal rule, which is the highest order (second order) A-stable implicit multistep method with smallest truncation error (Dahlquist [1963], Park [1975]), the stiffly stable methods of Gear [1971], and the family of algorithms devised by Newmark [1959] which are widely used in nonlinear structural dynamics (see, e.g., Belytschko & Hughes [1980]).

Here, motivated by stability considerations, attention is focused on the Newmark family of algorithms, which includes the trapezoidal rule as a special case. The error analysis and the stability characteristics of the Newmark algorithm applied to *linear* problems is well established; we refer to the work of Goudreau & Taylor [1973] and Hilber [1976,78].

Let $\boldsymbol{\phi}_n(X_1)$ denote the approximate solution to $\boldsymbol{\phi}(X_1, t_n)$ at time t_n. Similarly, $\mathbf{v}_n(X_1) \cong \dot{\boldsymbol{\phi}}(X_1, t_n)$ and $\mathbf{a}_n(X_1) \cong \ddot{\boldsymbol{\phi}}(X_1, t_n)$ represent respectively the approximate velocity and acceleration at time t_n. Assume that $(\boldsymbol{\phi}_n, \mathbf{v}_n, \mathbf{a}_n)$ completely satisfy the temporally discrete version of the weak form (2.42) at time t_n

$$G_{dyn}(\boldsymbol{\phi}_n, \boldsymbol{\eta}) = \int_{[0,L]} \boldsymbol{\eta} \cdot \mathbf{I} \mathbf{a}_n \, dX_1 + G(\boldsymbol{\phi}_n, \boldsymbol{\eta}) = 0, \quad \forall \boldsymbol{\eta} \tag{2.47}$$

We search for the solution $(\boldsymbol{\phi}_{n+1}, \mathbf{v}_{n+1}, \mathbf{a}_{n+1})$ at time t_{n+1} such that

$$G_{dyn}(\boldsymbol{\phi}_{n+1}, \boldsymbol{\eta}) = \int_{[0,L]} \boldsymbol{\eta} \cdot \mathbf{I} \mathbf{a}_{n+1} dX_1 + G(\boldsymbol{\phi}_{n+1}, \boldsymbol{\eta}) = 0, \quad \forall \boldsymbol{\eta} \tag{2.48}$$

The Newmark time-stepping scheme defines the relationship between $(\boldsymbol{\phi}_n, \mathbf{v}_n, \mathbf{a}_n)$ and $(\boldsymbol{\phi}_{n+1}, \mathbf{v}_{n+1}, \mathbf{a}_{n+1})$ according to

$$\mathbf{a}_{n+1} = \frac{\boldsymbol{\phi}_{n+1} - \boldsymbol{\phi}_n}{h^2 \beta} - \frac{\mathbf{v}_n}{h\beta} - \frac{\frac{1}{2} - \beta}{\beta} \mathbf{a}_n \tag{2.49a}$$

$$\mathbf{v}_{n+1} = \mathbf{v}_n + h[(1-\tau)\mathbf{a}_n + \tau \mathbf{a}_{n+1}], \tag{2.49b}$$

where $h := t_{n+1} - t_n$ denotes the time step size, and (β, τ) are the parameters of the Newmark algorithm. We note that $\beta = 0.25$ and $\tau = 0.5$ correspond to the trapezoidal rule; this choice of the parameters β and τ renders the algorithm unconditionally stable (in the sense of continuity with respect to initial conditions) and second order accurate (Hughes [1976]).

The notion of stability in general corresponds to the well-posedness of the temporally discrete system. In nonlinear structural dynamics, with the presence of certain constants of the motion, a stronger concept of stability is desirable. We refer to Gear [1971], Chorin *et al* [1978], and Belytschko & Hughes [1983] for several notions of stability that have been proposed, such as A-stability, spectral stability, stability in the energy sense, stiffly-stable methods, etc.... The appropriate concept of stability for integration algorithms in nonlinear structural dynamics remains, however, unsettled.

Substitution of (2.49a) into (2.48) yields a temporally discrete nonlinear system in the unknown $\boldsymbol{\phi}_{n+1}(X_1)$. One may employ the classical Newton iterative scheme to solve this system by first obtaining its linearization with respect to the space variable X_1.

2.4.2. Consistent linearization. Tangent operators

Let $\Delta\boldsymbol{\phi} := (\Delta u_1, \Delta u_2, \Delta\vartheta)$ denote the incremental displacement field. Consider a known configuration $\boldsymbol{\phi}_{n+1}^{(i)}(X_1) \in \mathbf{R}^3$, and let $\boldsymbol{\phi}_{n+1,\varepsilon}^{(i)}(X_1) \in \mathbf{R}^3$ represents the curve of perturbed configuration in the direction of $\Delta\boldsymbol{\phi}_{n+1}^{(i)}$ defined as follows

$$\boldsymbol{\phi}_{n+1,\varepsilon}^{(i)} = \boldsymbol{\phi}_{n+1}^{(i)} + \varepsilon\,\Delta\boldsymbol{\phi}_{n+1}^{(i)} \tag{2.50}$$

The superscript (i) designates the ith iteration in the Newton iterative solution process to search for the unknown configuration $\boldsymbol{\phi}_{n+1}$. The linearization of the weak form $G_{dyn}(\boldsymbol{\phi}, \boldsymbol{\eta})$ about the configuration $\boldsymbol{\phi} = \boldsymbol{\phi}_{n+1}^{(i)}$ can be put in the following form

$$L[G_{dyn}(\boldsymbol{\phi}_{n+1}^{(i)}, \boldsymbol{\eta})] = G_{dyn}(\boldsymbol{\phi}_{n+1}^{(i)}, \boldsymbol{\eta}) + DG_{dyn}(\boldsymbol{\phi}_{n+1}^{(i)}, \boldsymbol{\eta}) \cdot \Delta\boldsymbol{\phi}_{n+1}^{(i)} = 0\,, \tag{2.51a}$$

for all $\boldsymbol{\eta} \in V$. $G_{dyn}(\boldsymbol{\phi}_{n+1}^{(i)}, \boldsymbol{\eta})$ represents the dynamic residual at configuration $\boldsymbol{\phi}_{n+1}^{(i)}$. The linear operator $DG_{dyn}(\boldsymbol{\phi}_{n+1}^{(i)}, \boldsymbol{\eta})$ can be obtained by taking the directional derivative of $G_{dyn}(\boldsymbol{\phi}, \boldsymbol{\eta})$ about $\boldsymbol{\phi} = \boldsymbol{\phi}_{n+1}^{(i)}$ and in the direction $\Delta\boldsymbol{\phi}_{n+1}^{(i)}$,

$$DG_{dyn}(\boldsymbol{\phi}_{n+1}^{(i)}, \boldsymbol{\eta}) \cdot \Delta\boldsymbol{\phi}_{n+1}^{(i)} = \left.\frac{d}{d\varepsilon}\right|_{\varepsilon=0} G_{dyn}(\boldsymbol{\phi}_{n+1,\varepsilon}^{(i)}, \boldsymbol{\eta}) \tag{2.51b}$$

We shall proceed to give the linearization of each term in the weak form G_{dyn} given in (2.48) and (2.45).

Tangent inertia operator. Consider the first term in (2.48), which involves the acceleration $\mathbf{a}_{n+1}(X_1)$. Its linearized form is easily obtained from the Newmark algorithm (2.49a) and the perturbed configuration (2.50) as

$$D_{\mathbf{M}} G_{dyn}(\boldsymbol{\phi}_{n+1}^{(i)}, \boldsymbol{\eta}) \cdot \Delta\boldsymbol{\phi}_{n+1}^{(i)} = \frac{1}{h^2\beta} \int_{[0,L]} \boldsymbol{\eta} \cdot \Delta\boldsymbol{\phi}_{n+1}^{(i)}\, dX_1 \tag{2.52}$$

We now introduce some quantities and their linearized forms that prove to be convenient for the linearization of (2.45). Rewrite the *spatial* internal forces defined in (2.33) as

$$\begin{Bmatrix} n_1(\phi) \\ n_2(\phi) \\ m(\phi) \end{Bmatrix} = \mathbf{\Lambda}(\vartheta) \begin{Bmatrix} N_1(\phi) \\ N_2(\phi) \\ M(\phi) \end{Bmatrix}. \tag{2.53}$$

where $\{N_1, N_2, M\}$ represent the *material* internal forces defined by

$$\begin{Bmatrix} N_1(\phi) \\ N_2(\phi) \\ M(\phi) \end{Bmatrix} := \mathbf{C} \left[\mathbf{\Lambda}^T(\vartheta) \begin{Bmatrix} 1+u_1' \\ u_2' \\ \vartheta' \end{Bmatrix} - \begin{Bmatrix} 1 \\ 0 \\ 0 \end{Bmatrix} \right] \tag{2.54a}$$

with

$$\mathbf{C} := Diag[EA, GA_s, EI], \quad \mathbf{\Lambda}(\vartheta) := \begin{bmatrix} \cos\vartheta & -\sin\vartheta & 0 \\ \sin\vartheta & \cos\vartheta & 0 \\ 0 & 0 & 1 \end{bmatrix} \tag{2.54b}$$

The following linearized quantities are needed:

$$D\mathbf{\Lambda}(\hat{\vartheta}) \cdot \Delta\vartheta = \frac{d}{d\varepsilon}\Big|_{\varepsilon=0} \mathbf{\Lambda}(\hat{\vartheta} + \varepsilon\Delta\vartheta) = \begin{bmatrix} 0 & -\Delta\vartheta & 0 \\ \Delta\vartheta & 0 & 0 \\ 0 & 0 & 0 \end{bmatrix} \mathbf{\Lambda}(\hat{\vartheta}), \tag{2.55a}$$

$$D\begin{Bmatrix} N_1 \\ N_2 \\ M \end{Bmatrix}(\hat{\phi}) \cdot \Delta\phi = \frac{d}{d\varepsilon}\Big|_{\varepsilon=0} \begin{Bmatrix} N_1 \\ N_2 \\ M \end{Bmatrix}(\hat{\phi} + \varepsilon\Delta\phi) = \mathbf{C}\mathbf{\Lambda}(\hat{\phi})\,\Xi(\hat{\phi})\,\Delta\phi, \tag{2.55b}$$

$$\frac{d}{d\varepsilon}\Big|_{\varepsilon=0} \Xi(\hat{\phi} + \varepsilon\Delta\phi)\eta = \begin{bmatrix} 0 & 0 & \Delta u_2' \\ 0 & 0 & -\Delta u_1' \\ 0 & 0 & 0 \end{bmatrix} \eta. \tag{2.55c}$$

Recall that the differential operator Ξ has been defined in (2.46). Using the above relations, we obtain the linear part of weak form $G(\phi_{n+1}^{(i)}, \eta)$ in (2.45) as the sum of the tangent material stiffness operator and the tangent geometric stiffness operator given below.

Tangent material stiffness operator. It follows from the definition of the material internal force (2.54a) and its linearized form (2.55b) that one part of

the linearization of (2.45) is given by

$$D_S G_{dyn}(\phi_{n+1}^{(i)}, \eta) \cdot \Delta\phi_{n+1}^{(i)} = \int_{[0,L]} \Xi(\phi_{n+1}^{(i)})\eta \cdot \mathbf{A}(\vartheta_{n+1}^{(i)})\mathbf{C}\mathbf{A}^T(\vartheta_{n+1}^{(i)})\Xi(\phi_{n+1}^{(i)})\Delta\phi_{n+1}^{(i)}\, dX_1 \tag{2.56}$$

Tangent geometric stiffness operator. The remainder of the linearization of (2.45) corresponds to the linearization of Ξ and $\mathbf{A}$ keeping the material internal force fixed, and constitutes the tangent geometric stiffness operator. Making use of (2.55a) and (2.55c) with some rearrangement, we arrive at the expression

$$D_G G_{dyn}(\phi_{n+1}^{(i)}, \eta) \cdot \Delta\phi_{n+1}^{(i)} := \int_{[0,L]} \mathbf{T}\eta \cdot \mathbf{B}(\phi_{n+1}^{(i)})\mathbf{T}\Delta\phi_{n+1}^{(i)}\, dX_1 \tag{2.57a}$$

where $\mathbf{T}$ and $\mathbf{B}$ are defined as follows

$$\mathbf{T} := \begin{bmatrix} \frac{d}{dX_1} & 0 & 0 \\ 0 & \frac{d}{dX_1} & 0 \\ 0 & 0 & 1 \end{bmatrix} \tag{2.57b}$$

$$\mathbf{B}(\hat{\phi}) := \begin{bmatrix} 0 & 0 & -n_2(\hat{\phi}) \\ 0 & 0 & n_1(\hat{\phi}) \\ -n_2(\hat{\phi}) & n_1(\hat{\phi}) & -[(1+\hat{u}_1')n_1(\hat{\phi}) + \hat{u}_2' n_2(\hat{\phi})] \end{bmatrix} \tag{2.57c}$$

Finally, the linear part of G_{dyn} at $\phi = \phi_{n+1}^{(i)}$ is the sum of the above operators

$$DG_{dyn}(\phi_{n+1}^{(i)}, \eta) \cdot \Delta\phi_{n+1}^{(i)} = [D_M + D_S + D_G] G_{dyn}(\phi_{n+1}^{(i)}, \eta) \cdot \Delta\phi_{n+1}^{(i)} \tag{2.58}$$

Upon discretization of the space variable X_1, the tangent inertia operator (2.52) leads to the typical mass matrix in linear structural dynamics. The tangent stiffness operators (2.56) and (2.57) were first obtained by Simo *et al* [1985]; the derivation given above is, however, more amenable to an extension to the three-dimensional formulation. In fact, it will be seen that the three-dimensional

finite-strain beam in Chapter 4 reduces exactly to the above plane formulation.

Starting values for Newton scheme. There are various ways to select the starting values as an "initial guess" for the Newton solution procedure by letting $\mathbf{a}_{n+1}^{(0)} = \mathbf{a}_n$, or $\mathbf{v}_{n+1}^{(0)} = \mathbf{v}_n$, or $\boldsymbol{\phi}_{n+1}^{(0)} = \boldsymbol{\phi}_n$. Numerical experiments indicate the last choice of the above three starting schemes to be the best in avoiding spurious behavior in the results (Taylor [1985]). Accordingly, the starting values are set to be

$$\boldsymbol{\phi}_{n+1}^{(0)} = \boldsymbol{\phi}_n \tag{2.59a}$$

$$\mathbf{a}_{n+1}^{(0)} = -\left[\frac{\mathbf{v}_n}{h\beta} + \frac{\frac{1}{2}-\beta}{\beta}\mathbf{a}_n\right] \tag{2.59b}$$

$$\mathbf{v}_{n+1}^{(0)} = \mathbf{v}_n + h\left[(1-\tau)\,\mathbf{a}_n + \tau\,\mathbf{a}_{n+1}^{(0)}\right] \tag{2.59c}$$

where (2.59b) and (2.59c) follow from the choice (2.59a) and the Newmark scheme (2.49).

Other types of starting schemes has been suggested, such as using the explicit central difference scheme (Newmark with $\beta = 0$) as initial guess (or predictor stage). However, as reported in Sander *et al* [1979], this starting scheme yields computational effort comparable to the one in (2.59a-c), but with a smaller time step size for stability consideration. Hence, the starting scheme given in (2.59a-c) seems to be the most suitable one.

Update procedure. Once the incremental displacement field $\Delta\boldsymbol{\phi}_{n+1}^{(i)}$ is known, the updated configuration $\boldsymbol{\phi}_{n+1}^{(i+1)}$, velocity $\mathbf{v}_{n+1}^{(i+1)}$ and acceleration $\mathbf{a}_{n+1}^{(i+1)}$ are obtained from

$$\boldsymbol{\phi}_{n+1}^{(i+1)} = \boldsymbol{\phi}_{n+1}^{(i)} + \Delta\boldsymbol{\phi}_{n+1}^{(i)} \tag{2.60a}$$

$$\mathbf{v}_{n+1}^{(i+1)} = \mathbf{v}_{n+1}^{(i)} + \frac{\tau}{h\beta}\Delta\boldsymbol{\phi}_{n+1}^{(i)} \tag{2.60b}$$

$$\mathbf{a}_{n+1}^{(i+1)} = \mathbf{a}_{n+1}^{(i)} + \frac{1}{h^2\beta}\Delta\boldsymbol{\phi}_{n+1}^{(i)} \tag{2.60c}$$

We shall next consider the spatial discretization of the residual force and tangent operator.

2.4.3. Spatial discretization: finite-element matrices

Following standard finite element discretization, let the interval $[0, L]$ be the union of a finite number of subintervals with N being the total number of nodes, i.e., $[0, L] = \bigcup_{I=1}^{N}[X_1^I, X_1^{I+1}]$ with $X_1^I \in [0, L]$, $\forall\, j = 1,\ldots,N$, and $X_1^I < X_1^{I+1}$. Consider the approximation of the incremental displacement field $\Delta\boldsymbol{\phi}_{n+1}^{(i)}(X_1)$ with respect to the space variable X_1

$$\Delta\boldsymbol{\phi}_{n+1}^{(i)}(X_1) \cong \sum_{I=1}^{N} N_I(X_1)\Delta\boldsymbol{\phi}_{I,n+1}^{(i)}\,, \quad \text{with } \Delta\boldsymbol{\phi}_{I,n+1}^{(i)} \cong \Delta\boldsymbol{\phi}_{n+1}^{(i)}(X_1^I)\,, \tag{2.61a}$$

where $N_I(X_1)$ designates the global interpolating function corresponding to node I. Further, let the weighting function $\boldsymbol{\eta}(X_1)$ be interpolated in the same manner

$$\boldsymbol{\eta}(X_1) \cong \sum_{I=1}^{N} N_I(X_1)\boldsymbol{\eta}_I\,, \quad \text{with } \boldsymbol{\eta}_I \cong \boldsymbol{\eta}(X_1^I)\,. \tag{2.61b}$$

We refer to classical textbooks such as Strang & Fix [1973] and Zienkiewics [1978] for the choice of the appropriate interpolating function. Note that the above discretization employs continuous piecewise polynomial subspaces of equal degree for both the displacement field and the rotation field. This standard procedure is shown to produces quasi-optimal approximation in $H^1[0, L]$ and optimal order of approximation in $L^2[0, L]$ for a given beam thickness d (Arnold [1981]).† It should be noted however that, for the control of distributed

† The rate of convergenge, with respect to the element size, of the displacement $\boldsymbol{\phi}$ in H^1-norm is of the same order as the degree of the interpolating polynomial; it is of higher order when using the L^2-norm.

parameter systems, care must be taken in choosing appropriate basis functions to insure that certain system properties (controllability, observability, stabilizability, detectability,...) are preserved (Burns, Cliff & Powers [1985]).

Introducing the above approximations into the expressions for $G_{dyn}(\boldsymbol{\phi}_{n+1}^{(i)}, \eta)$ and for the tangent operators derived in the previous section, we obtain their spatially discrete counterparts. First recall that from a known configuration $\boldsymbol{\phi}_{n+1}^{(i)}$ at iteration (i) of the Newton solution procedure, we linearize the weak form $G_{dyn}(\boldsymbol{\phi}, \eta)$ about $\boldsymbol{\phi} = \boldsymbol{\phi}_{n+1}^{(i)}$

$$L[G_{dyn}(\boldsymbol{\phi}_{n+1}^{(i)}, \eta)] \cong \sum_{I=1}^{N} \boldsymbol{\eta}_I \cdot [\mathbf{P}_I(\boldsymbol{\phi}_{n+1}^{(i)}) + \sum_{J=1}^{N} \mathbf{K}_{IJ}(\boldsymbol{\phi}_{n+1}^{(i)}) \Delta\boldsymbol{\phi}_{J,n+1}^{(i)}] = 0 , \quad (2.62a)$$

for all $\boldsymbol{\eta}_I$, and solve for the incremental displacement field $\Delta\boldsymbol{\phi}_{n+1}^{(i)}$. In (2.62a), $\mathbf{P}_I(\boldsymbol{\phi}_{n+1}^{(i)})$ denotes the dynamic residual (or out-of-balance) force at iteration (i), and $\mathbf{K}_{IJ}(\boldsymbol{\phi}_{n+1}^{(i)})$ the discrete dynamics tangent operator coupling node I and node J such that

$$\mathbf{K}_{IJ}(\boldsymbol{\phi}_{n+1}^{(i)}) = \mathbf{M}_{IJ} + \mathbf{S}_{IJ}(\boldsymbol{\phi}_{n+1}^{(i)}) + \mathbf{G}_{IJ}(\boldsymbol{\phi}_{n+1}^{(i)}) \quad (2.62b)$$

where $\mathbf{M}_{IJ}$ is the tangent inertia matrix, $\mathbf{S}_{IJ}(\boldsymbol{\phi}_{n+1}^{(i)})$ the tangent material stiffness matrix, and $\mathbf{G}_{IJ}(\boldsymbol{\phi}_{n+1}^{(i)})$ the tangent geometric stiffness matrix.

Dynamic residual force. The expressions (2.42) and (2.45), together with the discretization (2.61a-b), yield

$$\mathbf{P}_I(\boldsymbol{\phi}_{n+1}^{(i)}) = \int_{[0,L]} N_I(X_1)\, \mathbf{I}\mathbf{a}_{n+1}^{(i)}\, dX_1$$

$$+ \int_{[0,L]} \{\Xi(\boldsymbol{\phi}_{n+1}^{(i)})[N_I(X_1)\mathbf{1}_3]\}^T \begin{Bmatrix} n_1(\boldsymbol{\phi}_{n+1}^{(i)}) \\ n_2(\boldsymbol{\phi}_{n+1}^{(i)}) \\ m(\boldsymbol{\phi}_{n+1}^{(i)}) \end{Bmatrix} dX_1 - \int_{[0,L]} N_I(X_1)\mathbf{f}(t_{n+1})\, dX_1 \quad (2.63)$$

where each term corresponds, respectively, to the inertia, material stiffness, and external applied force with Ξ defined in (2.46) and $\mathbf{1}_3 := Diag[1, 1, 1]$.

Tangent inertia matrix. Substituting approximations (2.61a-b) for $\Delta\boldsymbol{\phi}_{n+1}^{(i)}(X_1)$ and $\boldsymbol{\eta}(X_1)$ in the expression of $D_{\mathcal{M}} G_{dyn}$ in (2.52), we obtain

$$\mathbf{M}_{IJ} = \frac{1}{h^2\beta} \int_{[0,L]} \mathbf{I}\, N_I(X_1) N_J(X_1)\, dX_1 \tag{2.64}$$

Note that in the plane formulation $\mathbf{M}_{IJ}$ is symmetric and constant; hence, it need be evaluated only once throughout the computation. However, in a more general setting of three-dimensional motion, it will be shown in chapter 4 that $\mathbf{M}_{IJ}$ actually depends on the current configuration, and is in general unsymmetric.

Tangent material stiffness matrix. It follows from (2.56) and (2.61a-b) that

$$\mathbf{S}_{IJ}(\boldsymbol{\phi}_{n+1}^{(i)}) = \int_{[0,L]} \{\boldsymbol{\Xi}(\boldsymbol{\phi}_{n+1}^{(i)})[N_I(X_1)\mathbf{1}_3]\}^T \mathbf{A}(\vartheta_{n+1}^{(i)})\mathbf{C}\mathbf{A}^T(\vartheta_{n+1}^{(i)})\boldsymbol{\Xi}(\boldsymbol{\phi}_{n+1}^{(i)})[N_J(X_1)\mathbf{1}_3]\, dX_1 \tag{2.65}$$

Tangent geometric stiffness matrix. Substitution of (2.61a-b) into (2.57a) yields

$$\mathbf{G}_{IJ}(\boldsymbol{\phi}_{n+1}^{(i)}) = \int_{[0,L]} \{\mathbf{T}[N_I(X_1)\mathbf{1}_3]\}^T \mathbf{B}(\boldsymbol{\phi}_{n+1}^{(i)})\mathbf{T}[N_J(X_1)\mathbf{1}_3]\, dX_1 \tag{2.66}$$

with $\mathbf{T}$ being the differential operator defined in (2.57b) and $\mathbf{B}(\boldsymbol{\phi})$ is as defined in (2.57c). Note that both the tangent material stiffness and the tangent geometric stiffness matrices in the plane formulation are *symmetric*. For the three-dimensional rod formulation, the tangent geometric stiffness operator will be shown to be unsymmetric due to the non-commutativity of three-dimensional finite rotations.

Numerical integration. It is well known that using the standard discretization (2.60) the order of approximation deteriorates as the thickness of the beam decreases — the rate of convergence is not uniform in the thickness d. This phenomenon, often referred to as shear locking, is remedied by employing a reduced/selective Gauss quadrature rule first proposed by Zienkiewics *et al*

[1971] and Pawsey & Clough [1971]. This procedure consists of lowering uniformly or selectively the order of the integration rule used to evaluate the tangent stiffness matrix to achieve a better order of approximation. In fact, it can be shown that the order of approximation thus obtained is optimal for (2.60) regardless of the beam thickness (Arnold [1981]). The analysis of Arnold is based on the equivalence between the mixed finite element method and the reduced/selective integration shceme first introduced by Malkus & Hughes [1978]; it is this equivalence property that elevates the reduced/selective integration procedure from a mere numerical trick to a legitimate methodology. For a curved planar beam using a mixed finite element method, we refer to Noor & Peters [1981] and Reddy & Singh [1981]. In all computation, we use a uniformly reduced, one-point Gauss quadrature rule to integrate both the tangent stiffness matrix and the residual force. Noor, Peters & Andersen [1984] employed a mixed finite element method to discretize the fully nonlinear plane beam theory of Reissner [1972], and is therefore equivalent to the finite element displacement model with reduced integration used herein.

The mass matrix, however, is integrated exactly with two-point Gauss quadrature to ensure its positive-definiteness, an essential property for the use of implicit time-stepping (2.49). Note that the positive-definiteness of the dynamic tangent stiffness $\mathbf{K}$ in (2.62b) depends on the positive-definiteness of the mass matrix $\mathbf{M}$ since the tangent stiffness matrix $(\mathbf{S}+\mathbf{G})$ is positive semi-definite. When a diagonal mass matrix is desired, care should be taken in choosing a diagonalizing procedure such that the global momenta are preserved. For instance, the usual "row lumping" procedure preserves only the global linear momentum but not the global angular momentum. The Gauss-Lobatto quadrature rule, sometimes referred to as nodal quadrature rule, is recommended for this purpose.

2.5. Numerical examples

In this section, we present a series of numerical simulations that illustrate the formulation and numerical procedure discussed in sections 2.3 and 2.4. Our purpose is to exhibit:

(a) The simplicity of the numerical procedure. Essentially any existing non-linear structural finite element dynamics code could be employed. Here an extended version of the the computer program FEAP developed by R.L. Taylor and documented in chapter 24 of Zienkiewics [1978] is employed.

(b) The capability of the proposed formulation to automatically handle *finite strains* superposed onto large overall rigid body motions. This includes flexible bodies in free flight.

It is emphasized that no simplification is made in the simulations that follow in the sense that Coriolis and centrifugal effects as well as the inertia effect due to rotation are automatically accounted for. The deformed shapes in all figures reported in this chapter are given at the *same* scale as the geometry of the beam, i.e., there is no magnification of the structural deformations.

In all simulations reported herein, the trapezoidal rule — Newmark algorithm with $\tau = 0.5$ and $\beta = 0.25$ — was employed. Numerical operations were performed in double precision on a VAX 11/780 under the Berkeley UNIX 4.2 BSD operating system.

Example 2.5.1. Flexible robot arm. This simulation is concerned with the re-positioning of a flexible beam rotating horizontally about a vertical axis passing through one end. The finite element mesh consists of 10 elements with linear isoparametric interpolation functions for both displacement and rotation. Two cases are considered.

2.5.1.1. Displacement driven. The geometry, material properties, finite element mesh, as well as the time step size used in the integration are given in

Figure 2.5.1.1*a*. The robot arm is first repositioned to an angle of 1.5 *radians* from its initial position. This is achieved by prescribing the rotation angle $\psi(t) = \vartheta(0, t)$ as a linear function of time, as shown in Figure 2.5.1.1*a*; the sequence of motion during this repositioning stage is depicted in Figure 2.5.1.1*b*. Once the rotation angle $\psi(t)$ is fixed at 1.5 *rad* for all time $t \geq 2.5$, the robot arm then undergoes finite vibrations as shown in Figure 2.5.1.1*c*.

2.5.1.2. Force driven. The robot arm is now driven by a prescribed torque $T(t)$ applied at the axis of rotation $\mathbf{e}_3$, as shown in Figure 2.5.1.2*a*. The applied torque is removed at time $t = 2.5$; the robot arm then undergoes a torque-free motion. The simulation is terminated after completion of one revolution, as shown in Figures 2.5.1.2*b* and 2.5.1.2*c*.

Example 2.5.2. Flying flexible rod. A flexible rod with free ends, initially placed in an inclined position, is subject to a force and a torque applied simultaneously at one end, see Figure 2.5.2.1*a*. The applied force and torque are removed at the same time $t = 2.5$, so that the subsequent free flight of the rod exhibits a periodic tumbling pattern. It should be noted here that the boundary conditions (3.19) becomes $\mathbf{m}(0,t) = \mathbf{m}(L,t) = \mathbf{n}(0,t) = \mathbf{n}(L,t) = 0$ during the free flight stage. Two cases are considered.

2.5.2.1. Flexible beam in free flight. The motion of the rod during application of loading is shown in Figure 2.5.2.1*b*. The stiffness of the rod is low enough exhibit finite deformations. A close-up of the first two revolutions is shown in Figure 2.5.1.3*c*, while the entire sequence of motion is depicted in Figure 2.5.2.1*d*.

2.5.2.2. The "flying spaghetti." The bending stiffness EI of the rod is lowered by a factor of 5 relative to the simulation in 2.5.2.1. This dramatic reduction in stiffness results in the in the sequence of motions depicted in Figure 2.5.2.2.

Example 2.5.3. Spin-up maneuver. The flexible robot arm considered in Example 2.5.1.1 is now subject to a "spin-up" maneuver by prescribing the angle $\psi(t) = \vartheta(0,t)$ for $t \in \mathbf{R}_+$ as follows

$$\psi(t) = \begin{cases} \frac{6}{15}\left[\frac{t^2}{2} + \left[\frac{15}{2\pi}\right]^2 (\cos\frac{2\pi t}{15} - 1)\right] rad & 0 \le t \le 15 \quad sec \\ (6t - 45)\, rad & t > 15 \quad sec \end{cases} \tag{2.67}$$

This type of motion was proposed by Kane *et al* [1985] to demonstrate that the "conventional" approach based on linear beam theory may lead to grossly inaccurate results: instability of a physically stable system. As a result, one need to call upon higher order theories to account for effects such as the *centrifugal stiffening* in this example, even if the deformation remains small. This example may also be of practical interest in applications such as helicopter rotor blades or aircraft propellers. The material properties and time history of $\psi(t)$ are shown in Figure 2.5.3*a*. Deflected shapes for several values of t during the first revolution are depicted in Figure 2.5.3*b*. Also shown in this figure are the time histories of the displacements $\tilde{u}_1(L,t)$, $\tilde{u}_2(L,t)$ relative to the shadow beam, and the section rotation $\tilde{\alpha}(L,t)$. The results in Figure 2.5.3*b* clearly exhibit the centrifugal stiffening effect: after an initial deflection during the acceleration phase, $t \in [0, 15]$, the centrifugal force straightens the robot arm in the constant angular velocity phase, $t > 15$. The exact solution for the steady state extension of a pinned-free beam with length L, axial stiffness EA and mass per unit length ρA, spinning with constant angular velocity ω can be easily shown to be

$$\tilde{u}_1(X,t) = L\left[\frac{\tan aL}{aL} - 1\right]; \quad \text{where} \quad a = \omega\sqrt{\frac{\rho A}{EA}} \tag{2.68}$$

For this particular example $\omega = 6\, rad/sec.$, $L = 10$ and $\rho A/EA = \frac{3}{7} \times 10^{-7}$.

Expression (2.68) then leads to a steady state extension at the free end of $\tilde{u}_1(L,t) = 5.14\times10^{-4}$. This result is in complete agreement with the computed solution (see Figure 2.5.3*b*). The small periodic vibration of the beam about the floating frame during this steady state phase is noted.

2.6. Concluding Remarks

We have presented in this chapter a new approach to the dynamics of a plane beam under large overall motions. The essence of this approach is the fully nonlinear plane beam theory that can account for finite rotations as well as finite strains. The appropriate strain measures in the beam theory are invariant under superposed isometries; such invariance is the necessary ingredient to the success of the present approach. The motion of the beam is completely referred to the inertial frame. We thus obtain the expression of the inertia term in the equations of motion simply as mass times acceleration. By contrast, in the shadow beam approach, one obtains a nonlinear and highly coupled inertia operator; hence a special computer code must be devised to solve the resulting system. In our approach, the inherent nonlinear character of the problem is transferred to the stiffness part of the equations of motion; this results in equations of motion that arise typically in nonlinear structural dynamics. Consequently, the dynamics of flexible beams under large overall motions can be analyzed in any existing nonlinear finite element program.

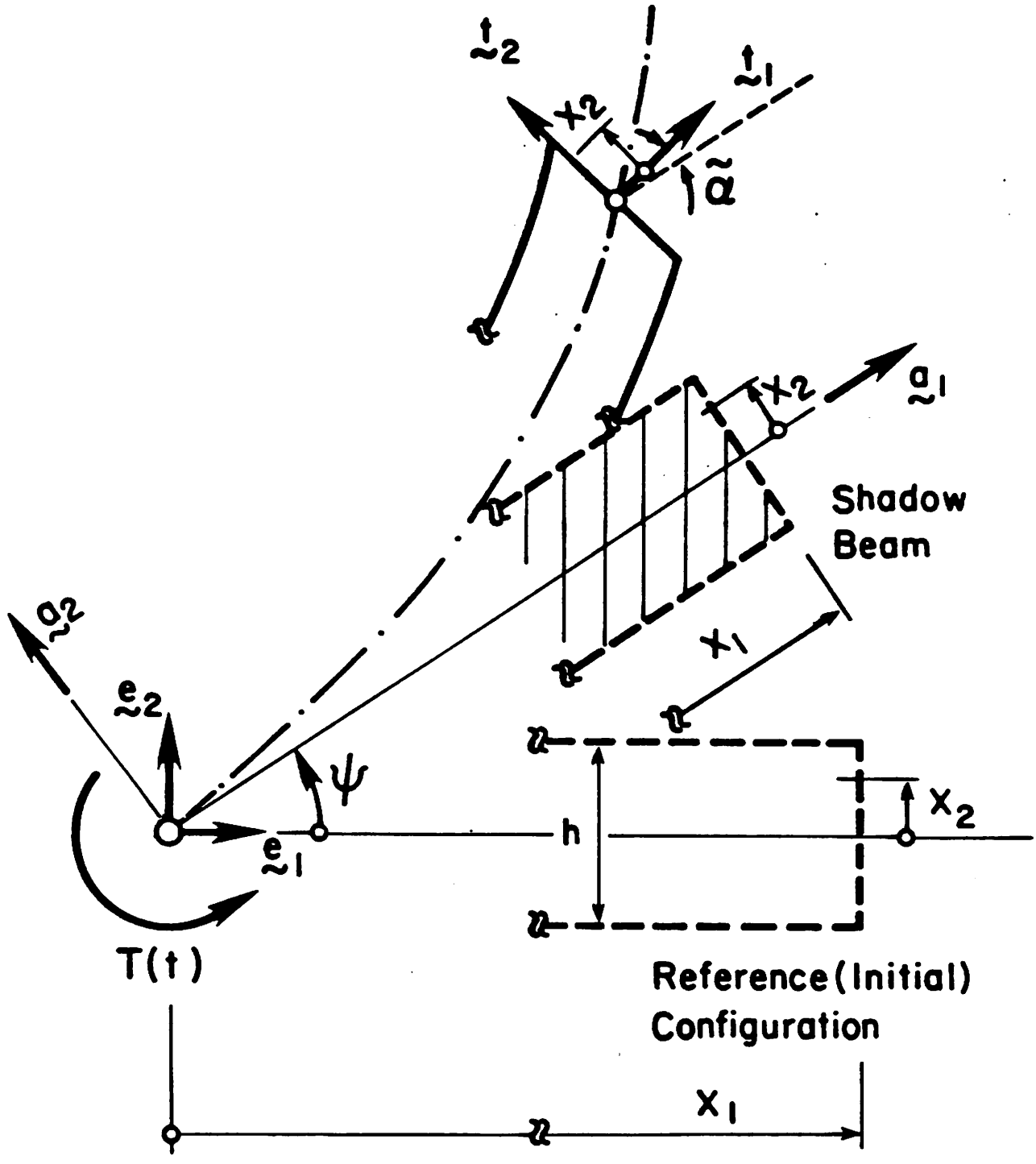

Figure 2.2.1. *Basic kinematics.* Floating and inertial frames.

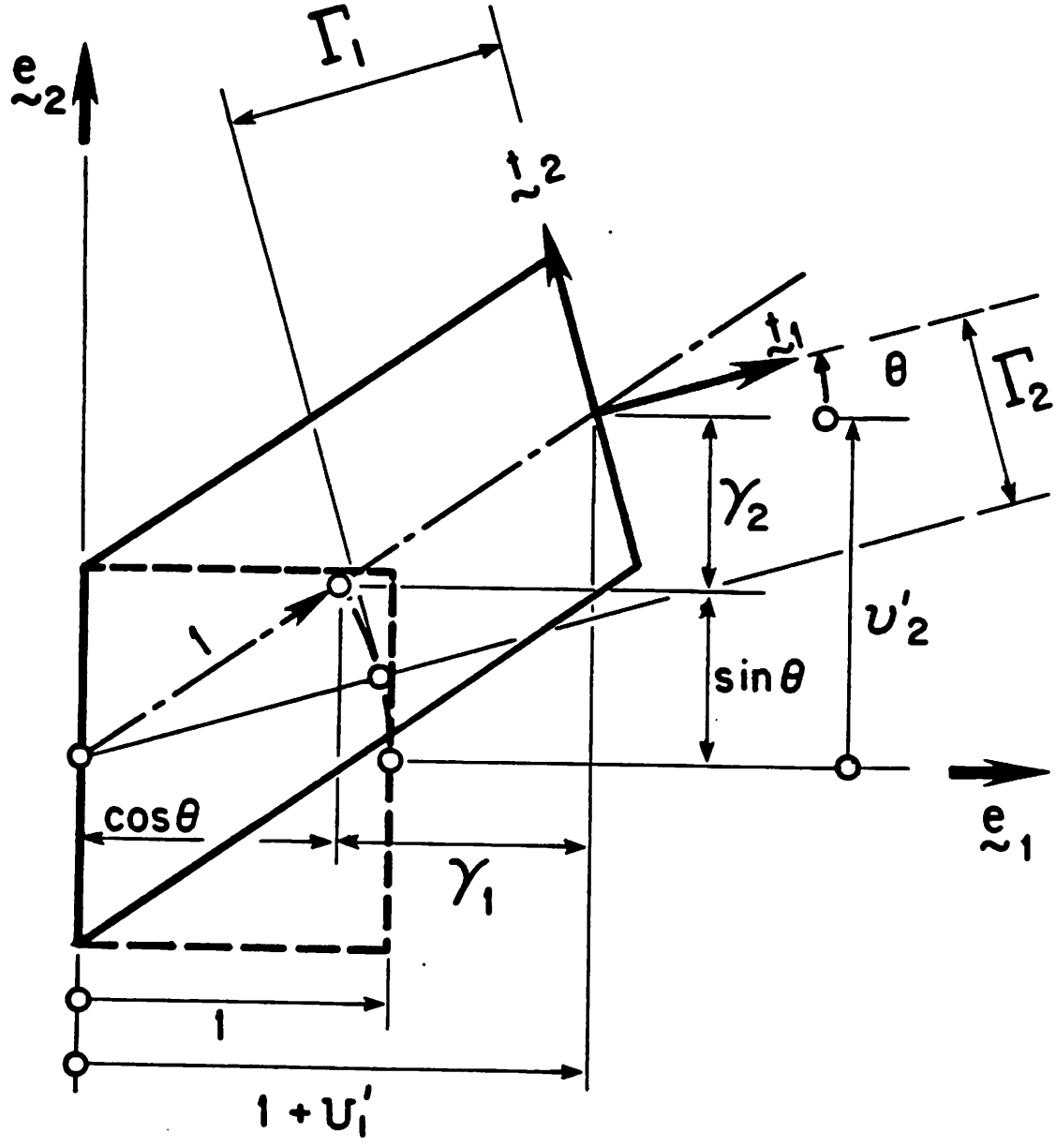

Figure 2.3.1. Physical interpretation of the strain components of a beam in the finite strain case.

Material Properties:

$EA = GA_s = 10{,}000.$

$EI = 1{,}000.$

$A_\rho = 1.$

$I_\rho = 10.$

F.e. Mesh: 10 linear elements

Time history of $\psi(t)$:

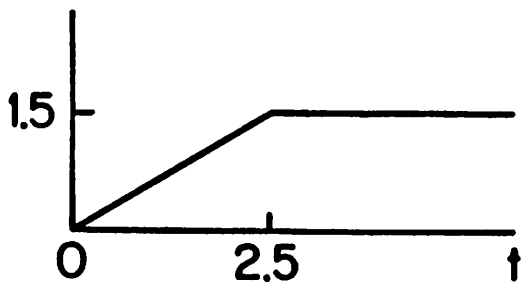

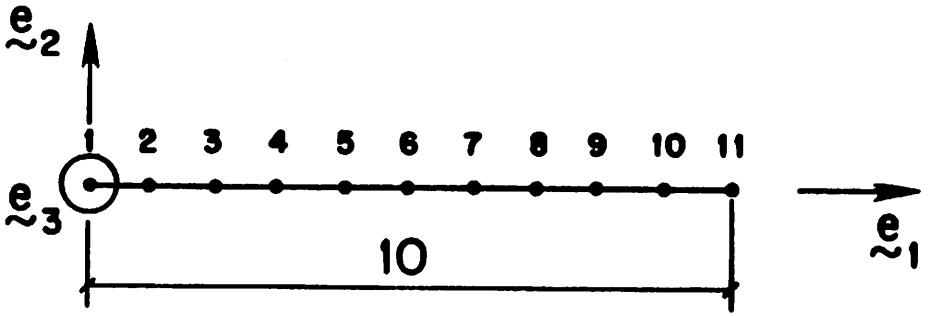

Figure 2.5.1.1a. *Displacement driven flexible robot arm.* Problem data.

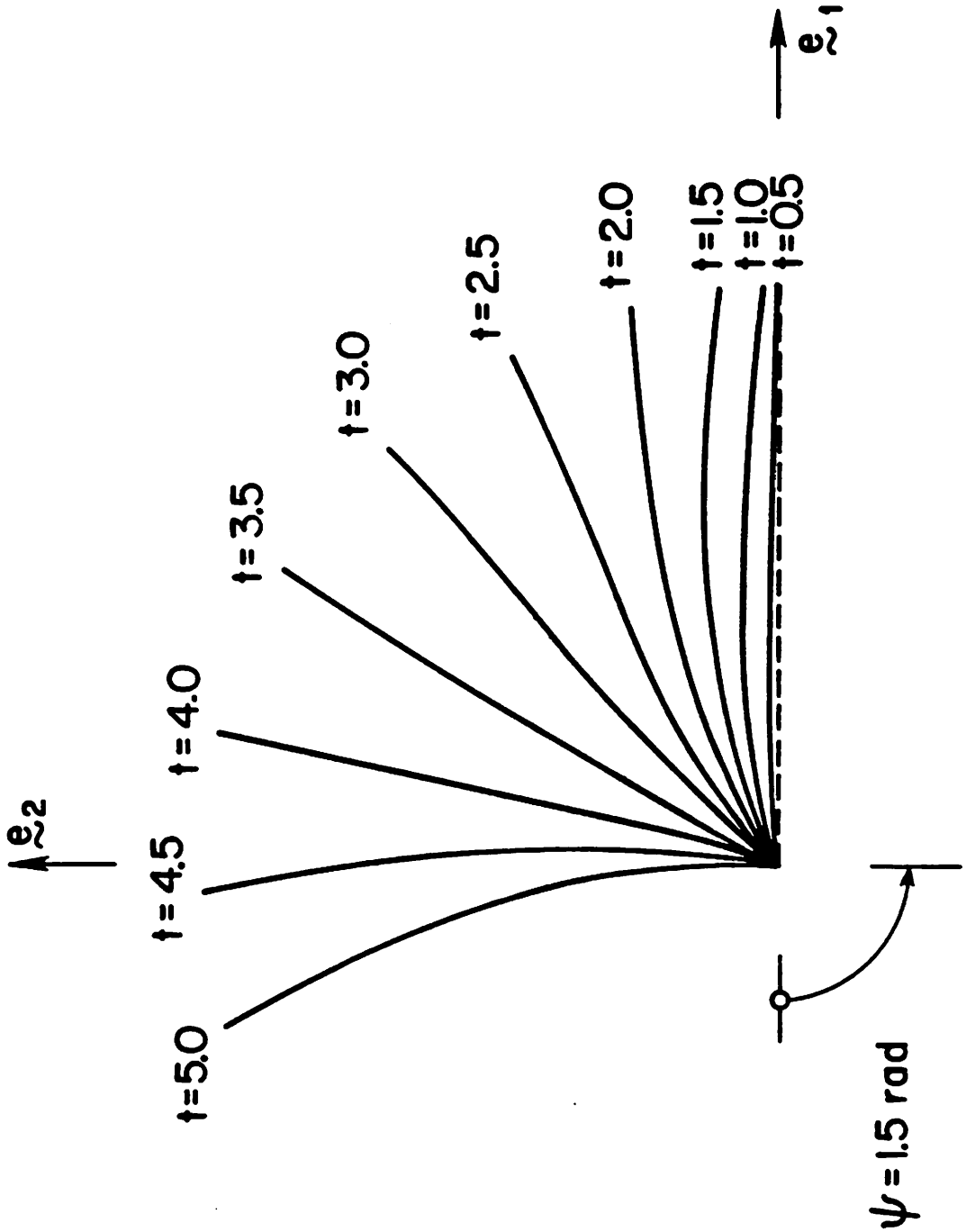

Figure 2.5.1.1b. *Displacement driven flexible robot arm.* Repositioning sequence to stop angle $\psi = 1.5$ *rad.* Time step size $h = 0.5$.

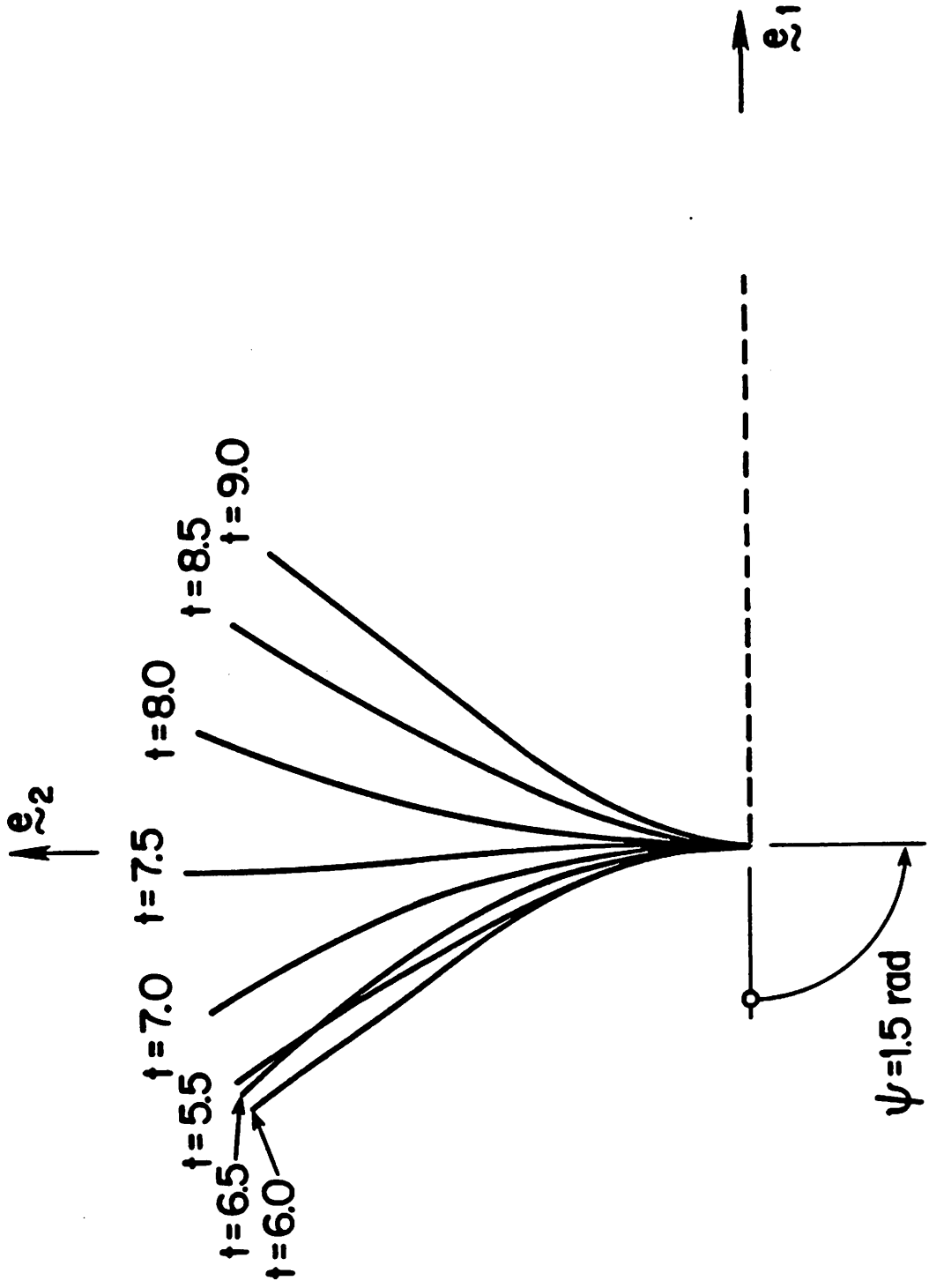

Figure 2.5.1.1c. *Displacement driven flexible robot arm.* Free vibration about $\psi = 1.5$ *rad*. Time step size $h = 0.5$.

Material Properties:

$EA = GA_s = 10{,}000.$

$EI = 1{,}000.$

$A_\rho = 1.$

$I_\rho = 10.$

F.e. Mesh: 10 linear elements.

Time history of T(t):

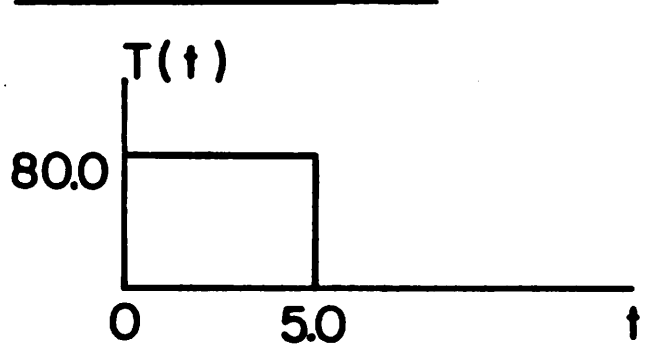

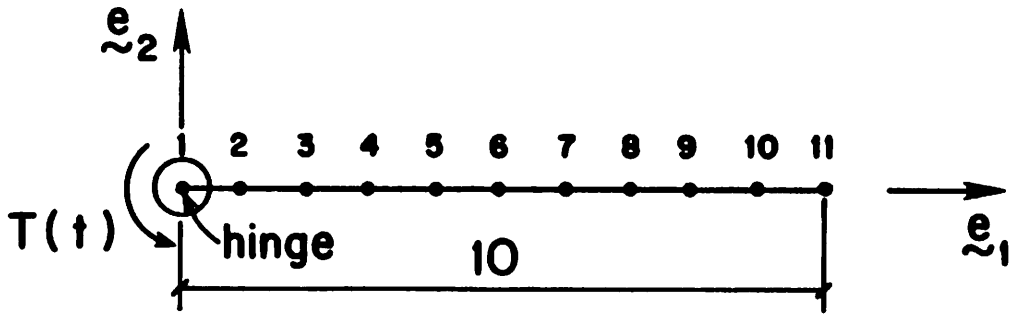

Figure 2.5.1.2a. *Force driven flexible robot arm.* Problem data.

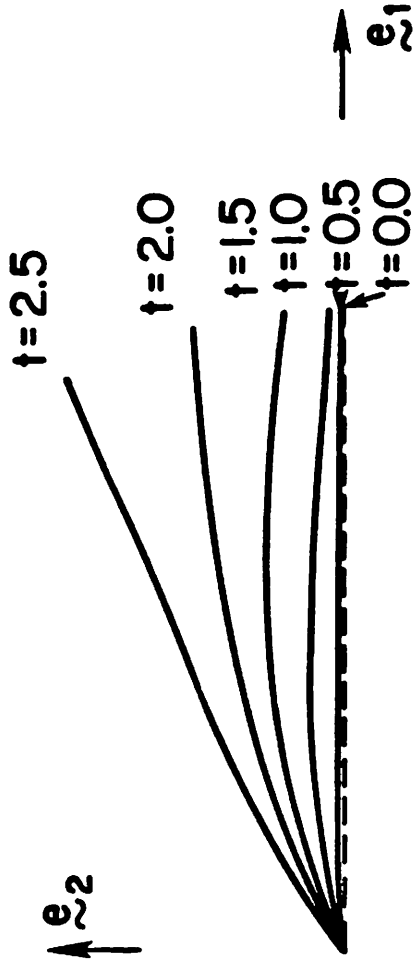

Figure 2.5.1.2b. ***Force driven flexible robot arm.*** Sequence of motion during application of torque. Time step size $h = 0.5$.

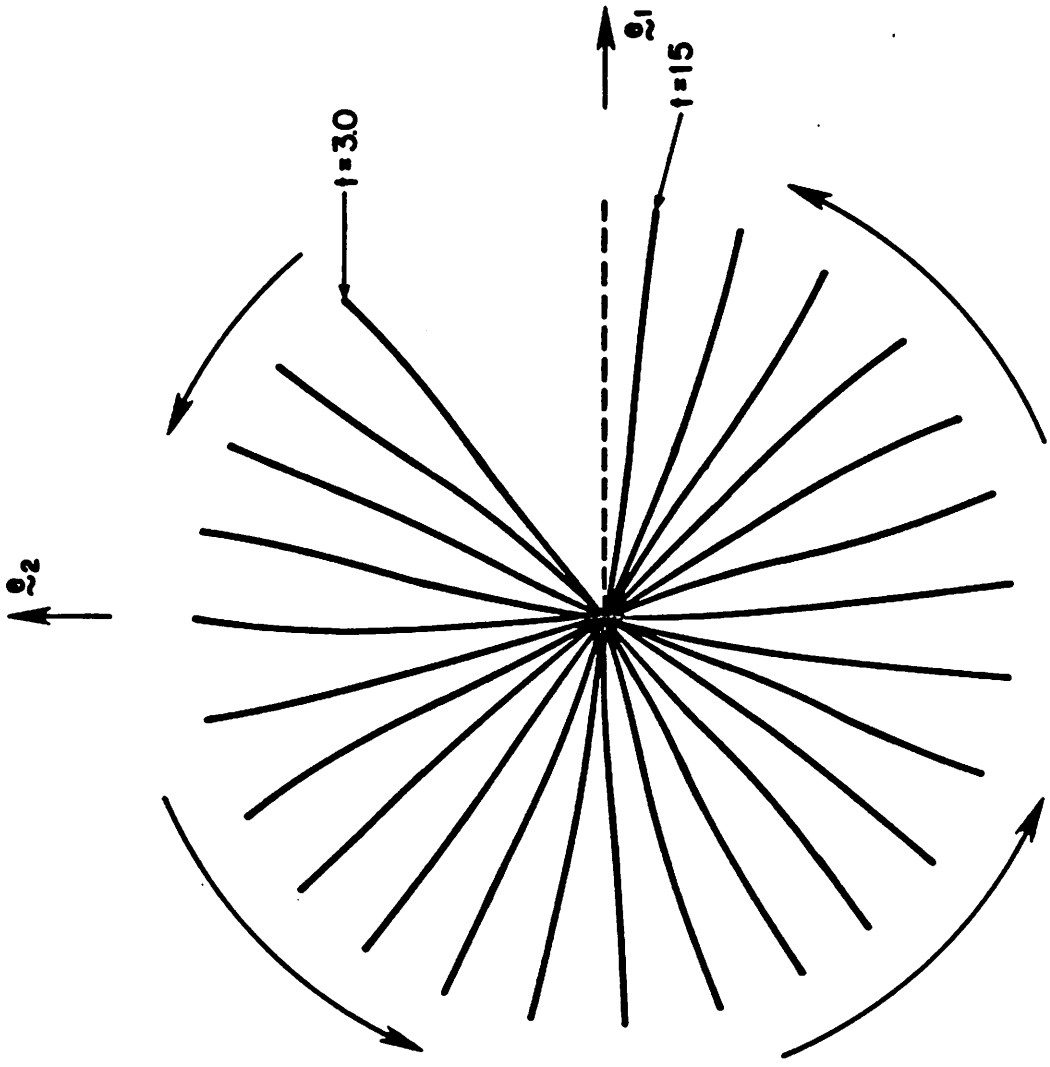

Figure 2.5.1.2c. ***Force driven flexible robot arm.*** Sequence of motion after removal of applied torque —completion of one revolution. Time step size $h = 0.5$.

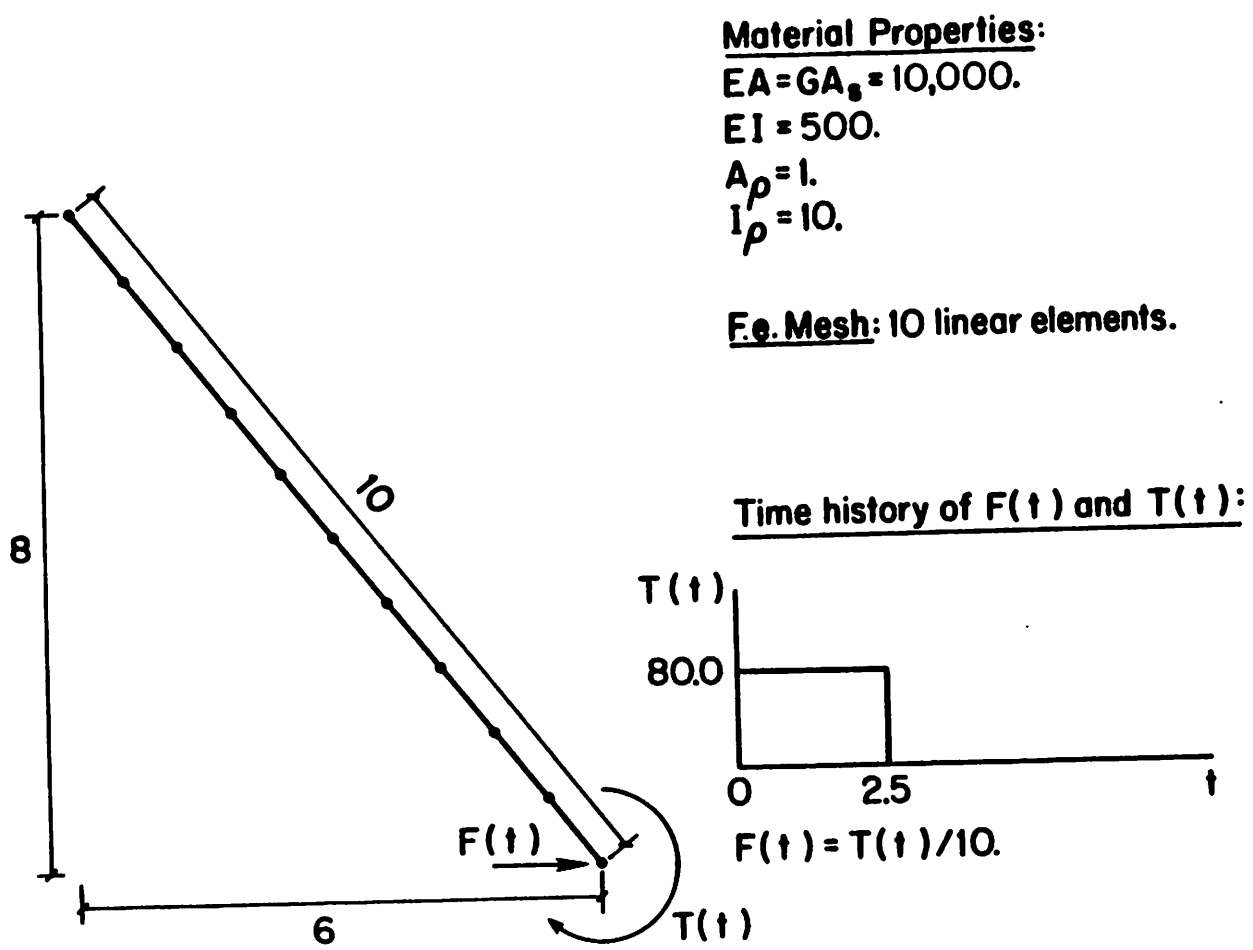

Figure 2.5.2.1a ***Flexible beam in free flight.*** Problem data.

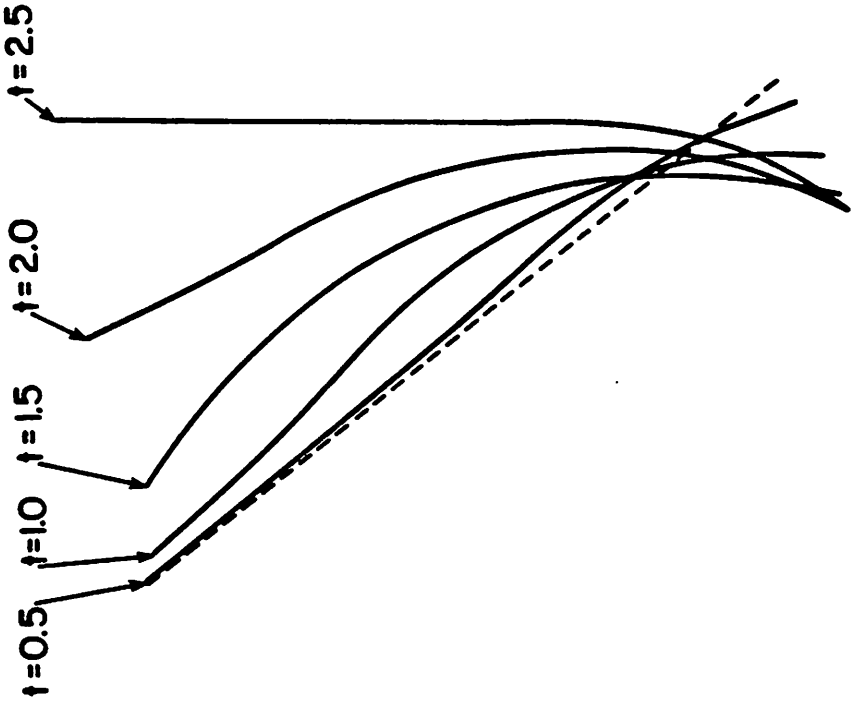

Figure 2.5.2.1b. ***Flexible beam in free flight.*** Sequence of motions during application of loading. Time step size $h = 0.1$, plot after each 5 time increments.

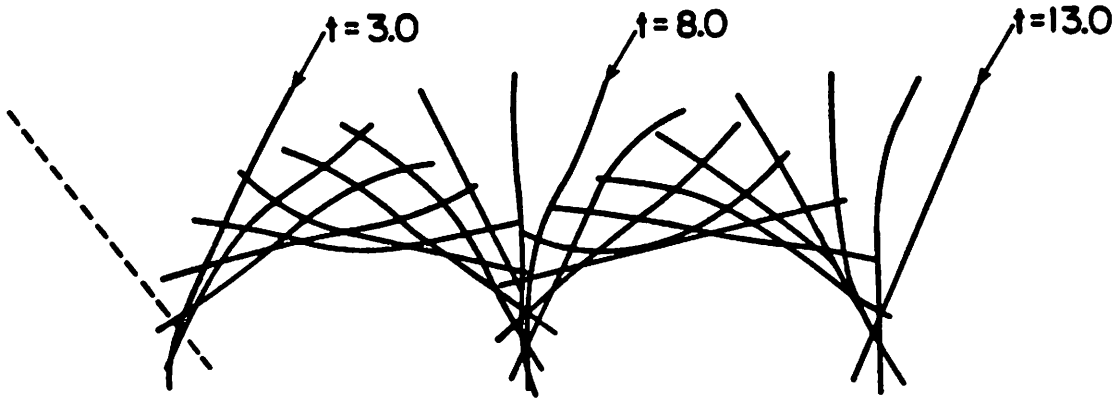

Figure 2.5.2.1c. ***Flexible beam in free flight.*** Free flight of the beam after removal of the loading — close-up on the first 2 revolutions. Time step size $h = 0.1$, plot after each 5 time increments.

Figure 2.5.2.1d. ***Flexible beam in free flight.*** Free flight — entire sequence.

Material Properties:

$EA = GA_s = 10{,}000.$

$EI = 100.$

$A_\rho = 1.$

$I_\rho = 10.$

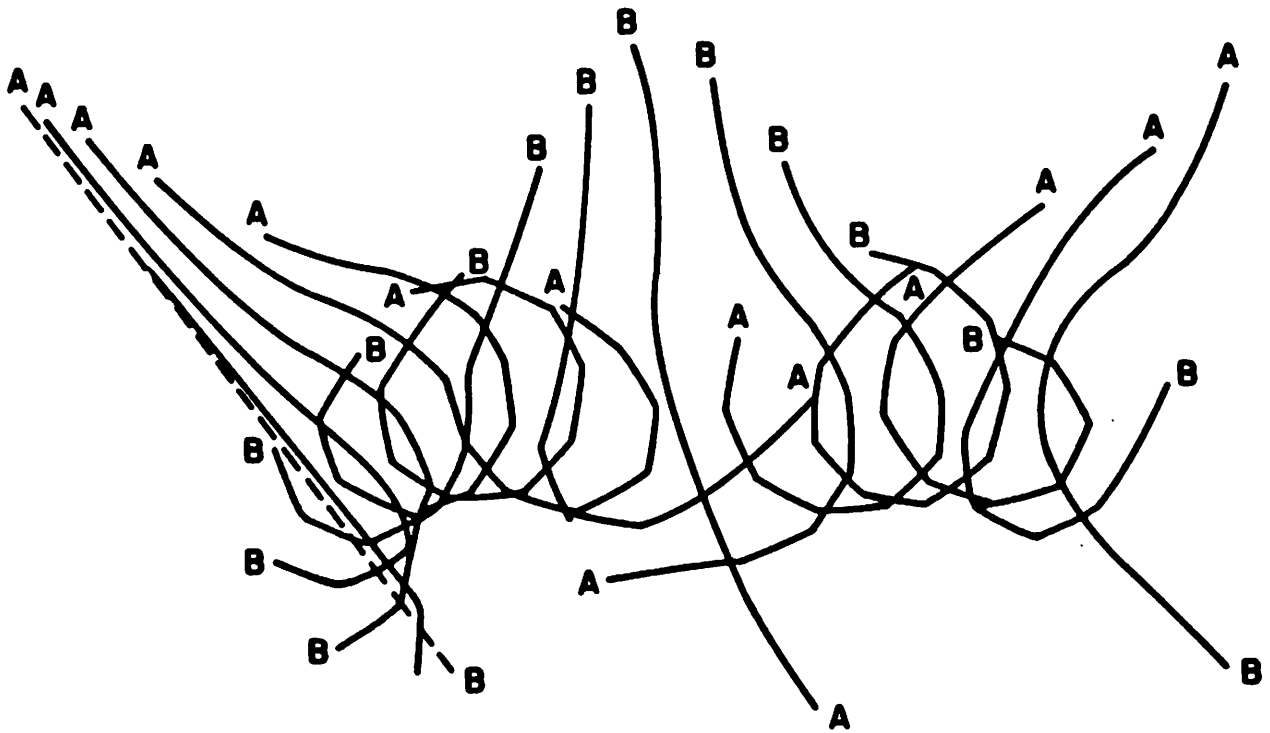

Figure 2.5.2.2. *The "flying spaghetti."* Time step size $h = 0.1$, plot after each 5 time increments.

Material Properties

$EA = 2.8 \times 10^7$

$GA_s = 1 \times 10^7$

$EI = 1.4 \times 10^4$

$A\rho = 1.2$

$I\rho = 6 \times 10^{-4}$

F.E. Mesh: 4 quadratic elements

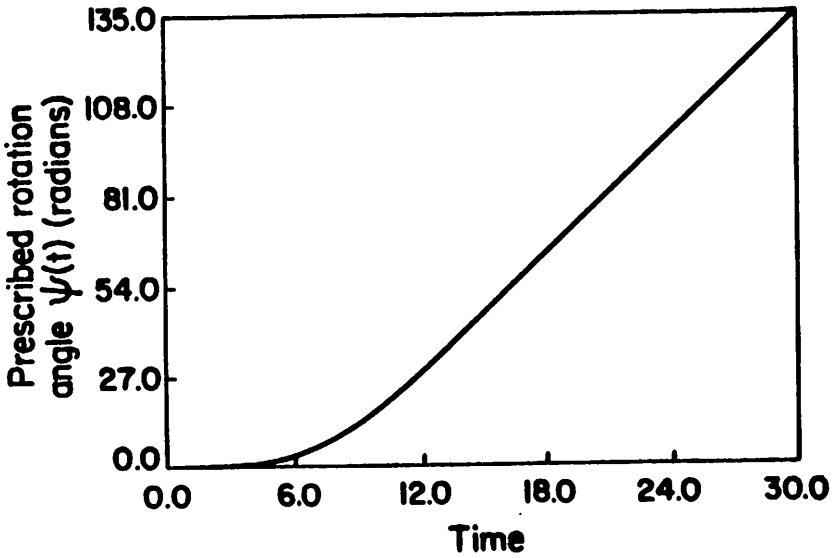

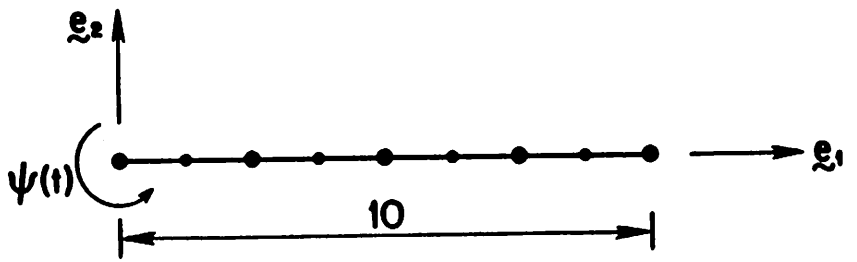

Figure 2.5.3a. ***Spin-up maneuver.*** Problem data.

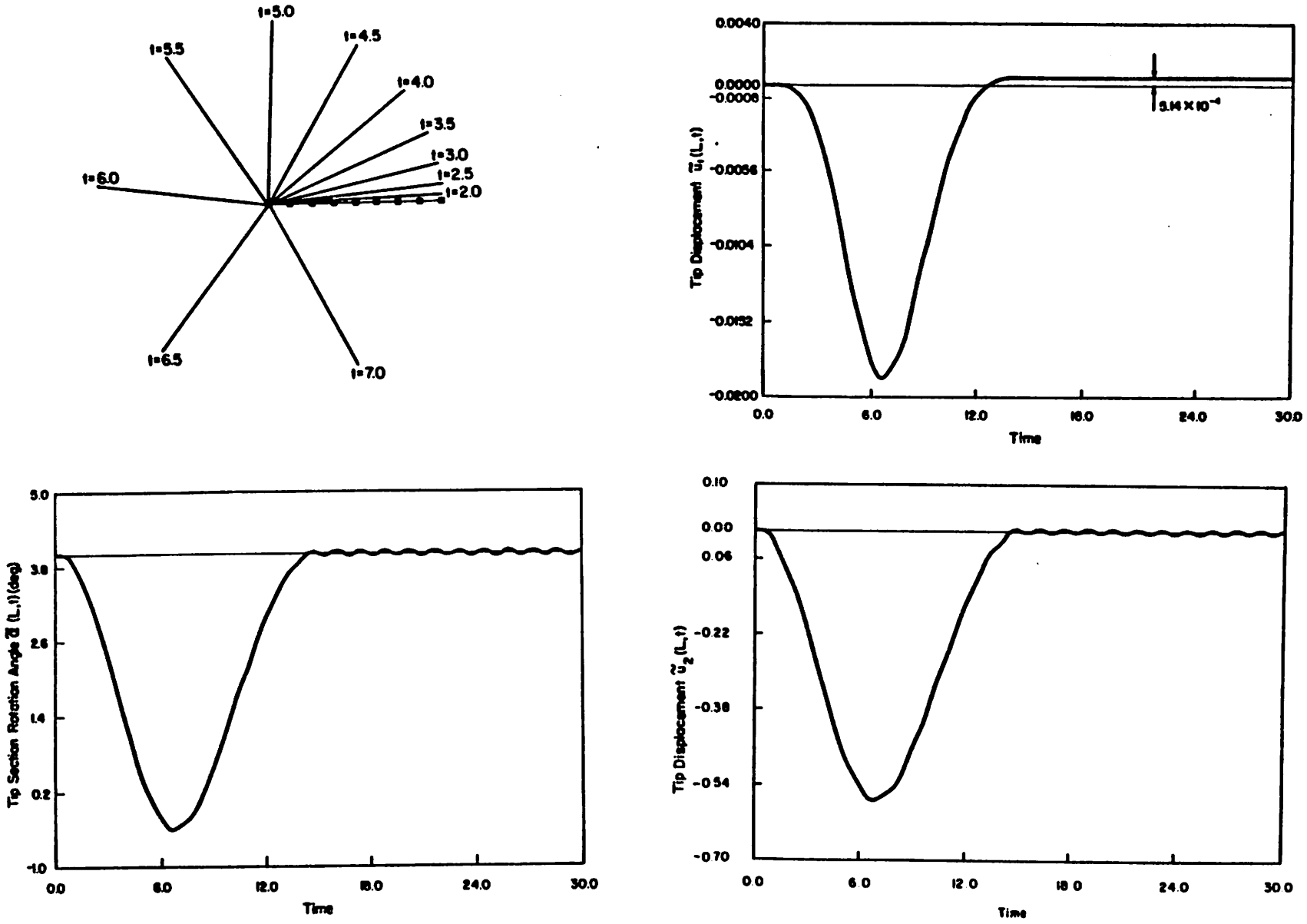

Figure 2.5.3b. *Spin-up maneuver.* Several deflected shapes during first maneuver. Time histories for displacement components and section rotation relative to shadow beam. Time step size $h = 0.005$.

CHAPTER 3

THE ROLE OF NONLINEAR THEORIES IN DYNAMIC ANALYSIS OF ROTATING STRUCTURES

3.1. Introduction

In the previous chapter, we have advocated the use of nonlinear structural theories based essentially on the linearity and uncoupling character of the inertia operator when the dynamics of the structure is referred to the inertial frame. This formulation clearly encompasses a wide class of problems ranging from very stiff to very flexible structures. However, in the case of stiff structures undergoing a rotating motion —such as in the *spin-up maneuver* of example 2.5.3 —where the deformation is expected to remain infinitesimal, does one really need to employ nonlinear structural theories? We shall now attempt to answer this question.

Recently, it has been pointed out by Kane, Ryan & Banerjee [1985] (KRB) that existing approaches to the dynamics of flexible bodies necessitate fundamental modification in order to capture the centrifugal stiffening effect in fast rotating beams. We shall examine this claim, and in fact show that

(i) Accounting for the stiffening effect in fast rotating structures requires a higher order (geometrically nonlinear) theories, hence necessarily *nonlinear* in the strain measures. A hierarchy of beam theories, from the linear to a fully nonlinear formulation, can be systematically developed by successive approximations in terms of a small perturbation parameter.

(ii) Current approaches based on linearized strain measures are not conceived to capture such a stiffening effect, nor to account for any other nonlinear phenomena involving change in stiffness due to axial loading. In fact, use of a geometrically linear beam theory in the modeling of a rapidly rotating beam

leads to a spurious loss of bending stiffness, which is quadratic with the angular velocity. This effect was numerically documented in Kane, Ryan & Banerjee [1985]. Herein, this phenomenon is quantified analytically by providing the relevant partial differential equation of motion for the transverse vibration.

(iii) The KRB approach may be viewed as a reparametrization of a higher order beam theory of the von Karman type, along with a subsequent truncation of nonlinear terms. Specifically, in the case of a beam, the axial displacement field is replaced by the elongation along the line of centroids, with the net result of rendering the stiffness matrix identical to that of a linear Timoshenko beam. This approach, however, ignores the effect of axial forces other than those coming from inertia effects.

(iv) A set of linear partial differential equations of motion is derived as a consistent first order linearization of the nonlinear theory. These linear PDE's capture correctly the action of the centrifugal force on the bending stiffness, and in fact, for the von Karman type model, are the exact counterpart of the KRB discrete approach. However, by contrast with the KRB approach, the Galerkin spatial discretization of these PDE's is straightforward. In addition, explicit expressions of the linear semi-discrete equations of motion in the present context are given.

(v) In cases where modeling of the above nonlinear geometric effects is desired, the use of a fully nonlinear beam or plate theory does not involve more computational effort than the use of a higher order nonlinear theory. In fact, by referring the dynamics of the beam directly to the inertial frame, the inertia operator becomes linear, hence simplifying considerably the task of integrating the equations of motion.

We shall also show that the conclusions obtained from the one-dimensional case of a beam essentially carry over without modification to the more general

case of a plate (Simo & Vu-Quoc [1986a]).

3.2. Consistent higher order theories

For simplicity in the exposition, but without loss of generality, we shall consider the model problem a rotating beam whose motion is restricted to a plane with the same kinematic assumption as in Section 2.2.1. The result obtained, however, can be generalized without difficulty to the three-dimensional motion. Higher order beam theories, including geometrically linear theory, can be systematically obtained by successive approximations of the strain measures characterizing the fully linear theory.

3.2.1. Fully nonlinear theory

Throughout this chapter, the deformation of the beam will be expressed relative to the floating frame $\{O;\mathbf{a}_1, \mathbf{a}_2\}$; the superposed tilde used in Chapter 2 to denote quantities relative to the floating frame will thus be removed to simplify the notation:

$$\mathbf{x} = \mathbf{x}_0 + X_2\, \mathbf{t}_2\,, \tag{3.1a}$$

$$\mathbf{x}_0 := [X_1 + u_1(X_1,t)]\, \mathbf{a}_1(t) + u_2(X_1, t)\, \mathbf{a}_2(t)\,, \tag{3.1b}$$

$$\begin{Bmatrix} \mathbf{t}_1 \\ \mathbf{t}_2 \\ \mathbf{t}_3 \end{Bmatrix} = \mathbf{A}^T \begin{Bmatrix} \mathbf{a}_1 \\ \mathbf{a}_2 \\ \mathbf{a}_3 \end{Bmatrix}, \quad \text{where} \quad \mathbf{A} := \begin{bmatrix} \cos\alpha & -\sin\alpha & 0 \\ \sin\alpha & \cos\alpha & 0 \\ 0 & 0 & 1 \end{bmatrix}. \tag{3.1c}$$

In this model problem, the rotation of the floating frame $\{\mathbf{a}_1, \mathbf{a}_2\}$ relative to the inertial frame $\{\mathbf{e}_1, \mathbf{e}_2\}$ is completely prescribed *a priori*. Recall from Remark 2.1 that the expression of kinetic energy is independent of the magnitude of the strain field. For the planar motion considered herein, the system of partial differential equations (2.34) governing the dynamics of the fully nonlinear beam

can be easily derived using the expression for the kinetic energy (2.13) and for the potential energy (2.28)

$$\begin{Bmatrix} F_1^{inertia} \\ F_2^{inertia} \\ R_3^{inertia} \end{Bmatrix} - \mathbf{A} \begin{Bmatrix} N' - \alpha' V \\ V' + \alpha' N \\ M' + \Gamma_1 V - \Gamma_2 N \end{Bmatrix} = \mathbf{0} \tag{3.2}$$

where A_ρ denotes the mass per unit reference length, and I_ρ the mass moment of inertia of the cross section. The inertia operator is given by

$$\begin{Bmatrix} F_1^{inertia} \\ F_2^{inertia} \\ R_3^{inertia} \end{Bmatrix} := \begin{Bmatrix} A_\rho [\ddot{u}_1 - \ddot{\psi} u_2 - 2\dot{\psi}\dot{u}_2 - \dot{\psi}^2 (X_1 + u_1)] \\ A_\rho [\ddot{u}_2 + \ddot{\psi} (X_1 + u_1) + 2\dot{\psi}\dot{u}_1 - \dot{\psi}^2 u_2] \\ I_\rho (\ddot{\alpha} + \ddot{\psi}) \end{Bmatrix}, \tag{3.3}$$

with $F_1^{inertia}$ and $F_2^{inertia}$ denote the inertia force along axes $\mathbf{a}_1$ and $\mathbf{a}_2$, and $R_3^{inertia}$ the inertia torque about axis $\mathbf{a}_3$. In (3.2), (N, V, M) represent the axial force, shear force, and bending moment relative to the local frame $\{\mathbf{t}_1, \mathbf{t}_2, \mathbf{t}_3\}$, respectively, with $(\Gamma_1, \Gamma_2, \kappa)$ being their respective conjugate strain measures such that

$$\begin{matrix} N = EA\,\Gamma_1 \\ V = GA\,\Gamma_2\,, \\ M = EI\,\kappa \end{matrix} \quad \text{and} \quad \begin{Bmatrix} \Gamma_1 \\ \Gamma_2 \\ \kappa \end{Bmatrix} := \mathbf{A}^T \begin{Bmatrix} 1 + u_1' \\ u_2' \\ \alpha' \end{Bmatrix} - \begin{Bmatrix} 1 \\ 0 \\ 0 \end{Bmatrix} \tag{3.4}$$

where $\mathbf{A}$ is the orthogonal matrix defined earlier in (1b). Recall that, since the function ψ is prescribed, $\dot{\psi}$ and $\ddot{\psi}$ are known functions. We note that the above definition of the strain measures $(\Gamma_1, \Gamma_2, \kappa)$ is unique in the sense that the resulting reduced expended power of the beam is identical to the exact stress power of the three-dimensional continuum theory. Successive approximations to the nonlinear theory (Truesdell & Noll [1965, p. 219]) can be constructed via standard power series expansion in terms of a "small" parameter $\varepsilon > 0$. Such approximations have been employed to obtain consistent higher order plane

beam theories in Simo [1982]. The series expansion of the strain measures defined in (3.4) are given up to second order by

$$\begin{Bmatrix} \Gamma_1 \\ \Gamma_2 \\ \kappa \end{Bmatrix} := \mathbf{A}(\varepsilon\,\alpha)^T \begin{Bmatrix} 1+\varepsilon\,u_1' \\ \varepsilon\,u_2' \\ \varepsilon\alpha' \end{Bmatrix} - \begin{Bmatrix} 1 \\ 0 \\ 0 \end{Bmatrix} = \varepsilon \begin{Bmatrix} u_1' \\ u_2' - \alpha \\ \alpha \end{Bmatrix} + \frac{\varepsilon^2}{2} \begin{Bmatrix} (u_2')^2 - (u_2' - \alpha)^2 \\ -2\alpha\,u_1' \\ 0 \end{Bmatrix} + O(\varepsilon^3)\,. \quad (3.5)$$

In what follows, we denote the first order (ε) approximation to the nonlinear strain measures by $(\bar{\Gamma}_1, \bar{\Gamma}_2, \bar{\kappa})$, and the second order ($\varepsilon^2$) approximation by $(\tilde{\Gamma}_1, \tilde{\Gamma}_2, \tilde{\kappa})$; for example, $\bar{\Gamma}_1 = u_1'$ and $\tilde{\Gamma}_1 = u_1' + [(u_2')^2 - (u_2' - \alpha)^2]/2$. Clearly, $(\bar{\Gamma}_1, \bar{\Gamma}_2, \bar{\kappa})$ are the usual strain measures employed in the linear Timoshenko beam theory.

3.2.2. Linear (first order) beam theory

The equations of motion corresponding to a geometrically linear beam theory in (2.16) are obtained simply by retaining the first order approximation in (3.5):

$$\begin{Bmatrix} F_1^{inertia} \\ F_2^{inertia} \\ R_3^{inertia} \end{Bmatrix} - \begin{Bmatrix} \bar{N}' \\ \bar{V}' \\ \bar{M}' + \bar{V} \end{Bmatrix} = 0 \quad (3.6a)$$

where the first column corresponds to the inertia operator, and the second column to the stiffness operator. In (3.6a), the internal forces (N, V, M) are given by the usual linear constitutive law

$$\begin{aligned} \bar{N} &= EA\,\bar{\Gamma}_1 &&= EA\,u_1' \\ \bar{V} &= GA_s\,\bar{\Gamma}_2 &&= GA_s\,(u_2' - \alpha) \\ \bar{M} &= EI\,\bar{\kappa} &&= EI\,\alpha' \end{aligned} \quad (3.6b)$$

To see the effect of centrifugal force on the bending deformation of the beam, we differentiate $(3.6a)_3$ and make use of $(3.6a)_2$ to obtain the equation of motion for the transverse displacement,

$$A_\rho \ddot{u}_2 + EI\, u_2'''' - A_\rho \dot{\psi}^2 u_2 = -2A_\rho \dot{\psi}\, \dot{u}_1 , \tag{3.7}$$

in which, for simplicity, we have made the assumption of steady state revolution ($\ddot{\psi} = 0$), negligible shear deformation ($u_2' = \alpha + O(\varepsilon)$), as well as negligible section rotary inertia. The destabilizing effect due to the use of linear beam theory mentioned earlier can now be clearly identified: The term $(-A_\rho \dot{\psi}^2 u_2)$ induces a loss of stiffness, which is quadratic in the angular velocity of revolution $\dot{\psi}$. This observation is indeed corroborated by the numerical experiments in Kane *et al* [1985, Figure 8]. Note that only the transverse component along $\mathbf{a}_2$ of the centrifugal force in the shear equation $(3.6)_2$, represented by the term $(-\dot{\psi}\, u_2)$, is transferred to the bending equation $(3.6a)_3$. The contribution of the axial component along $\mathbf{a}_1$ of the centrifugal force, represented by the term $[\dot{\psi}^2 (X_1 + u_1)]$, on the other hand, exerts no influence on the bending. It should be noted here that this term is in fact of order 1, while the term $(-\dot{\psi}\, u_2)$ is of order ε. Thus, from a physical standpoint, the loss of stiffness results precisely from this partial transfer of the action of centrifugal force to the bending equation. Moreover, there is a value of the angular velocity of revolution that renders the stiffness matrix singular.

3.2.3. Second order beam theory

A second order theory can be consistently derived by retaining second order terms in the approximation to the strain measures, according to

$$\begin{Bmatrix} \bar{\Gamma}_1 \\ \bar{\Gamma}_2 \\ \bar{\kappa} \end{Bmatrix} = \begin{Bmatrix} u_1' \\ u_2' - \alpha \\ \alpha \end{Bmatrix} + \begin{Bmatrix} \alpha\, u_2' - \frac{1}{2}\alpha^2 \\ -\alpha\, u_1' \\ 0 \end{Bmatrix} . \tag{3.8}$$

In addition, the second order approximation to the equations of motion (3.2) now takes the form

$$\begin{Bmatrix} F_1^{inertia} \\ F_2^{inertia} \\ R_3^{inertia} \end{Bmatrix} - \begin{Bmatrix} \bar{N}' \\ \bar{V}' \\ \bar{M}' + \bar{V} \end{Bmatrix} + \begin{Bmatrix} (\alpha \bar{V})' \\ -(\alpha \bar{N})' \\ -\bar{\Gamma}_1 \bar{V} + \bar{\Gamma}_2 \bar{N} \end{Bmatrix} = 0, \tag{3.9}$$

where the inertia force components are as given in (3.3), $\bar{N} = EA\,\bar{\Gamma}_1$, $\bar{V} = GA_s\,\bar{\Gamma}_2$ and $\bar{M} = EI\,\alpha'$. To obtain the equation governing the transverse vibration u_2, we proceed as follows: (i) Make use of $(3.9)_1$ to express $\bar{N}'$ in terms of the $\mathbf{a}_1$ component of the inertia force, (ii) Substitute the result into $(3.9)_2$ and solve for $\bar{V}'$, and (iii) Differentiate $(3.9)_3$ and make use the expression for $\bar{V}'$ obtained previously in (ii). Observe that the procedure is analogous to that employed in the first order approximation. The only crucial difference here is that the axial component of the inertia force along the axis $\mathbf{a}_1$ is now transferred to the bending equation due to the presence of the term $(\alpha \bar{N})'$ in $(3.9)_2$. This term accounts for the contribution to the transverse momentum of the axial (along $\mathbf{a}_1$) forces in the beam. Again, as in the previous section, neglecting higher order terms $O(\varepsilon^2)$ in the final equation, considering constant angular velocity of revolution, and assuming for simplicity negligible shear deformation and negligible section rotary inertia, one obtains

$$A_\rho \ddot{u}_2 + EI\,u_2'''' + A_\rho \dot{\psi}^2 (X_1 u_2' - u_2) = -2 A_\rho \dot{\psi} \dot{u}_1 \tag{3.10}$$

Note that equation (3.10), resulting from the foregoing second order approximation, is substantially different from its counterpart equation (3.7), which results from the first order approximation to the nonlinear theory. Now both components of the centrifugal force are completely transferred to the bending

equation: the term $(A_\rho \dot{\psi}^2 X_1 u_2')$ in (3.10) dominates the term $(A_\rho \dot{\psi}^2 u_2)$ — the latter is the only term present in (3.7) — and appropriately accounts for the stiffening effect due to centrifugal force. Conceptually, the transferring of the action of axial load to the bending equation is analogous to the effect of axial force in the linearized buckling analysis (e.g., beam-column equation); the only difference being the dynamic origin of the axial loading.

8.2.4. Consistent linear partial differential equations

We shall obtain the first order partial differential equations governing the motion of the beam by consistent linearization of (3.9). Before truncating the terms of order ε^2, it is crucial to note that the term $(\alpha N')$ in $(3.9)_2$ is actually of first order (ε), and not of second order (ε^2). It follows from the equation for axial vibration $(3.9)_1$ that

$$\alpha N' = -\alpha (A_\rho \dot{\psi} X_1) + O(\varepsilon) \tag{3.11}$$

and therefore must be retained in the first order approximation to the nonlinear equations of motion (3.9). After regrouping terms according to their nature, we obtain the following linear PDE's

$$\begin{bmatrix} A_\rho \ddot{u}_1 \\ A_\rho \ddot{u}_2 \\ I_\rho \ddot{\alpha} \end{bmatrix} + \begin{bmatrix} -2A_\rho \dot{\psi} \dot{u}_2 \\ 2A_\rho \dot{\psi} \dot{u}_1 \\ 0 \end{bmatrix} + \begin{bmatrix} -EA\, u_1'' - A_\rho (\dot{\psi}^2 u_1 + \ddot{\psi} u_2) \\ -GA_s (u_2' - \alpha)' + A_\rho (\ddot{\psi} u_1 - \dot{\psi}^2 u_2 + \dot{\psi}^2 X_1 \alpha) \\ -EI\, \alpha'' - GA_s (u_2' - \alpha) \end{bmatrix} = \begin{bmatrix} A_\rho \dot{\psi}^2 X_1 \\ -A_\rho \ddot{\psi} X_1 \\ -I_\rho \ddot{\psi} \end{bmatrix} \tag{3.12}$$

where the 4 columns correspond respectively to the inertia, gyroscopic, material and geometric stiffness, and inertia force due to revolution effects.

The Galerkin spatial discretization of the linear PDE's (3.12) is standard. For completeness, we shall simply give, without derivation, the expressions of the matrices resulting from applying a Galerkin finite element method. Such a

procedure has been applied to the spatial discretization of a fully nonlinear beam model (Simo & Vu-Quoc [1985,86]). Upon defining the following quantities,

$$\mathbf{d} := (u_1, u_2, \alpha)\,, \qquad \mathbf{I} := Diag[A_\rho, A_\rho, I_\rho]\,, \tag{3.13a}$$

$$\mathbf{g} := 2\,A_\rho\,\dot{\psi}\begin{bmatrix} 0 & -1 & 0 \\ 1 & 0 & 0 \\ 0 & 0 & 0 \end{bmatrix}, \quad \Psi := \begin{bmatrix} \dfrac{d}{dX_1} & 0 & 0 \\ 0 & \dfrac{d}{dX_1} & -1 \\ 0 & 0 & \dfrac{d}{dX_1} \end{bmatrix} \tag{3.13b}$$

$$\mathbf{C} := Diag[EA,\ GA_s,\ EI]\,, \quad \mathbf{B}_1 := A_\rho \begin{bmatrix} -\dot{\psi}^2 & -\ddot{\psi} & 0 \\ \ddot{\psi} & -\dot{\psi}^2 & (\dot{\psi}^2 X_1) \\ 0 & 0 & 0 \end{bmatrix}, \tag{3.13c}$$

and introducing the discretization,

$$\mathbf{d}(X_1,t) \cong \sum_{I=1}^{N} [N_I(X_1)\ \mathbf{1}_3]\ \mathbf{q}_I(t)\,, \quad \text{with } \mathbf{1}_3 := Diag[1, 1, 1] \tag{3.14}$$

the resulting linear semi-discrete equations of motion can be written as

$$\mathbf{M}\,\ddot{\mathbf{q}} + \mathbf{D}\,\dot{\mathbf{q}} + [\mathbf{S} + \mathbf{G}]\,\mathbf{q} = \mathbf{P} \tag{3.15a}$$

where $\mathbf{M}$ designates the mass matrix, $\mathbf{D}$ the gyroscopic matrix, $\mathbf{S}$ the material stiffness matrix, $\mathbf{G}$ the dynamic geometric stiffness matrix, and $\mathbf{P}$ the applied force; $\mathbf{q}$ denotes the vector of all generalized coordinates. It is easy to verify that the following expressions for the (3×3) submatrices coupling the generalized coordinates $\mathbf{q}_I$ to $\mathbf{q}_J$ hold

$$\mathbf{M}_{IJ} = \int_{[0,L]} N_I(X_1)\,N_J(X_1)\,\mathbf{I}\,dX_1\,. \tag{3.15b}$$

$$\mathbf{D}_{IJ} = \int_{[0,L]} N_I(X_1)\,N_J(X_1)\,\mathbf{g}\,dX_1\,. \tag{3.15c}$$

$$\mathbf{S}_{IJ} = \int_{[0,L]} \{\Psi\,[N_I(X_1)\ \mathbf{1}_3]\}^T\,\mathbf{C}\,\Psi\,[N_J(X_1)\ \mathbf{1}_3]\,dX_1\,. \tag{3.15d}$$

$$\mathbf{G}_{IJ} = \int_{[0,L]} N_I(X_1)\, N_J(X_1)\, \mathbf{B}_1\, dX_1 \tag{3.15e}$$

Observe the non-symmetry of the matrices in (3.15), except for the mass matrix **M** and the material stiffness matrix **S**. In addition, we note that the geometric stiffness **G** is of purely dynamic origin.

In what follows, we shall interpret the KRB approach in the context of a similar setting.

3.3. The Kane-Ryan-Banerjee approach

We shall re-examine the discrete approach proposed in Kane, Ryan & Banerjee [1985] and, by deriving the appropriate PDE, show that this approach essentially amounts to a re-parametrization of a nonlinear structural model of the von Karman type. These authors consider a potential energy function

$$\Pi := \int_{[0,L]} [EA(s')^2 + GA_s(u_2' - \alpha)^2 + EI(\alpha')^2]\, dX_1 \tag{3.16a}$$

where s' denotes the partial derivative of the elongation of the center line with respect to X_1, and is given by

$$s(X_1, t) = \int_0^{X_1} \sqrt{J(X_1, t)}\, dX_1 - X_1\,, \quad J(X_1, t) := (1 + u_1')^2 + (u_2')^2\,,$$

$$\text{and} \quad s'(X_1,t) = \sqrt{(1 + u_1')^2 + (u_2')^2} - 1 \tag{3.16b}$$

The essential feature that distinguishes expression (3.16a) from its counterpart in the linearized theory is the use of s' instead of $\Gamma_1 = u_1'$ in the contribution of the axial strain to the potential energy Π of the system. By the change of variable, $\sigma = \bar{\sigma}(X_1) := X_1 + u_1(X_1, t)$, the elongation $s(X_1, t)$ given by (3.16b) can be recast into the form

$$s(X_1, t) = \int_0^{X_1 + u_1(X_1, t)} \left[1 + \left(\frac{\partial u_2(\bar{\sigma}^{-1}(\sigma), t)}{\partial \sigma} \right)^2 \right]^{\frac{1}{2}} d\sigma - X_1 , \qquad (3.17)$$

where we have assumed the boundary condition $u_1(0, t) = 0$. Relation (3.17) is the one essentially used in Kane *et al* [1985] with an additional assumption that $u_2(\bar{\sigma}^{-1}(\sigma), t) = u_2(\sigma, t)$, i.e., these authors consider $\bar{\sigma}$ as an identity map. Such an assumption clearly contradicts the derivation of (3.17). On the other hand, the kinetic energy of the system is given as in (2.13)

$$K = \frac{1}{2} \int_{[0, L]} A_\rho \{ [\dot{u}_1 - \dot{\psi} u_2]^2 + [\dot{u}_2 + \dot{\psi} (X_1 + u_1)]^2 \} \, dX_1$$

$$+ \frac{1}{2} \int_{[0, L]} I_\rho [\dot{\alpha} + \dot{\psi}]^2 \, dX_1 \qquad (3.18)$$

We recall that the same expression for K holds in the nonlinear theory. The Lagrangian of the system is given by $L := K - \Pi$. Note that $\{u_1, u_2, \alpha\}$ are the independent variables in L. However, in place of u_1, Kane *et al* choose to select the *elongation* $s(X_1, t)$ of the line of centroids as independent variable. The basic variables in the KRB approach are thus (s, u_2, α), u_1 being implicitly defined in terms of (s, u_2) using the nonlinear relation $s' = \sqrt{J} - 1$, where J is in turn defined in terms of (u_1, u_2) by (3.16b). An explicit expression of the resulting system of PDE's is difficult to obtain because of the complexity of the inertia operator. These authors proceed numerically and derive linear semi-discrete system of equations, $\mathbf{M}\ddot{\mathbf{q}} + \mathbf{D}\dot{\mathbf{q}} + \mathbf{K}\mathbf{q} = \mathbf{P}$ by first introducing the discretization

$$\begin{aligned} s(X_1, t) &\cong \sum_{I=1}^{N} N_{1I}(X_1) q_{1I}(t) \\ u_2(X_1, t) &\cong \sum_{I=1}^{N} N_{2I}(X_1) q_{2I}(t) . \\ \alpha(X_1, t) &\cong \sum_{I=1}^{N} N_{3I}(X_1) q_{3I}(t) \end{aligned} \qquad (3.19)$$

where $N_{1I}(X_1)$ are prescribed independent basis functions, such as the eigenfunctions of a cantilever beam, and then linearizing the resulting nonlinear inertia operator. Recall that in discretizing (3.17), the additional assumption that $\frac{\partial u_2(\bar{\sigma}^{-1}(\sigma),\, t)}{\partial \sigma} = \sum_{I=1}^{N} N_{2I}{}'(\sigma) q_{2I}(t)$ is made.

To show that the KRB approach outlined above amounts to employing a geometrically nonlinear theory, we obtain below the system of governing PDE's in the variables (u_1, u_2, α). Making use of Hamilton's principle along with the expression (3.16b) for s' in terms of (u_1, u_2) we obtain, after standard manipulation, the system

$$\begin{Bmatrix} F_1^{\text{inertia}} \\ F_2^{\text{inertia}} \\ R_3^{\text{inertia}} \end{Bmatrix} - \begin{Bmatrix} EA\,[(1 - J^{-\frac{1}{2}})\,(1 + u_1{}')]' \\ GA_s\,(u_2{}' - \alpha)' - EA\,[(1 - J^{-\frac{1}{2}})\,u_2{}']' \\ EI\,\alpha'' - GA_s\,(u_2{}' - \alpha) \end{Bmatrix} = 0 \qquad (3.20)$$

where the inertia operator is defined in (3.3). It should be noted that equations (3.20) are *nonlinear* in the stiffness operator, and closely related to the von Karman second order model. Conceptually, by using relation (3.16b), one could recast this system of equations in terms (s, u_2, α). To see this, we introduce the perturbation parameter $\varepsilon > 0$. Assuming that $\{u_1, u_2, \alpha\}$ are of order ε, by expanding $s(X_1, t)$ in powers of ε, we find

$$s_\varepsilon{}' := [(1 + \varepsilon\, u_1{}')^2 + (\varepsilon\, u_2{}')^2]^{\frac{1}{2}} - 1 = \varepsilon\, u_1{}' + \frac{\varepsilon^2}{2}(u_2{}')^2 + O(\varepsilon^3) \qquad (3.21)$$

Thus s' agrees with the consistent second order strain Γ_1 only if shear deformation is of second order, i.e., $u_2{}' = \alpha + O(\varepsilon)$. In addition, we have the following expansions

$$(1 - J_\varepsilon^{-\frac{1}{2}})\,(1 + \varepsilon\, u_1{}') = \varepsilon\, u_1{}' + \frac{\varepsilon^2}{2}(u_2{}')^2 + O(\varepsilon^3) \qquad (3.22a)$$

$$EA\,[(1-J_\varepsilon^{-\frac{1}{2}})\,\varepsilon\,u_2{}']' = \varepsilon^2\,EA\,u_1{}''\,u_2{}' + O(\varepsilon^3) \tag{3.22b}$$

The term (3.22b) is precisely the one responsible for transfer of the axial force acting on the beam to the transverse equilibrium.

Since the direct contribution of the axial component along $\mathbf{a}_1$ of the centrifugal force to the transverse equilibrium given by $(EA\,u_1{}''\,\alpha)$ is absent from the discrete equations in the KRB approach —here $(s,\,u_2,\,\alpha)$ are chosen as independent variables —the question arises as to how centrifugal stiffening is accounted for in this formulation. This is accomplished through the inertia operator by expressing u_1 and $\dot{u}_1$ in terms of $(s,\,u_2)$ and their derivatives with the aid of the nonlinear relation (3.17). Upon introducing the discretization (3.19), the resulting discrete nonlinear inertia operator is then linearized to obtain the linear semi-discrete equations of motion.

Remarkably enough, after some manipulation similar to that described in Section 2.3, we obtain from equations (3.20) exactly the same PDE's for the transverse vibration (3.10). This result shows that the use of the nonlinear von Karman type model can also appropriately account for the action of the centrifugal force on the transverse vibration as manifest in the expression for the first order dynamic geometric stiffness in (3.10). From the expansion (3.22b) of the term $(EA\,[(1-J^{-\frac{1}{2}})\,u_2{}']')$ in $(3.20)_2$, and from the equation for axial vibration $(3.20)_1$, we note that this term is in fact of first order (ε), similar to (3.11), i.e.,

$$EA\,[(1-J_\varepsilon^{-\frac{1}{2}})\,\varepsilon\,u_2{}']' = -\varepsilon\,A_\rho\,\ddot{\psi}\,X_1\,u_2{}' + O(\varepsilon^2)\,. \tag{3.23}$$

Note that instead of α in the consistent approximation from fully nonlinear theory, we obtain $u_2{}'$ in this von Karman type model. This is valid only when shear deformation is of second order, i.e., $u_2{}' = \alpha + O(\varepsilon)$. We then arrive at the

following linear PDE's,

$$\begin{Bmatrix} A_\rho \ddot{u}_1 \\ A_\rho \ddot{u}_2 \\ I_\rho \ddot{\alpha} \end{Bmatrix} + \begin{Bmatrix} -2A_\rho \dot{\psi} \dot{u}_2 \\ 2A_\rho \dot{\psi} \dot{u}_1 \\ 0 \end{Bmatrix} + \begin{Bmatrix} -EA\, u_1'' - A_\rho (\dot{\psi}^2 u_1 + \ddot{\psi} u_2) \\ -GA_s (u_2' - \alpha)' + A_\rho (\ddot{\psi} u_1 - \dot{\psi}^2 u_2 + \dot{\psi}^2 X_1 u_2') \\ -EI\, \alpha'' - GA_s (u_2' - \alpha) \end{Bmatrix} = \begin{Bmatrix} A_\rho \dot{\psi}^2 X_1 \\ -A_\rho \ddot{\psi} X_1 \\ -I_\rho \ddot{\psi} \end{Bmatrix} \tag{3.24}$$

as a first order consistent linearization of (3.20). This system is entirely equivalent to the KRB discrete approach. The only difference, as noted above, is that the dynamic geometric stiffness operator $\mathbf{B}_1$ in (3.13c) must now be redefined as

$$\mathbf{B}_2 := A_\rho \begin{bmatrix} -\dot{\psi}^2 & -\ddot{\psi} & 0 \\ \ddot{\psi} & [-\dot{\psi}^2 + \dot{\psi}^2 X_1 \frac{d}{dX_1}] & 0 \\ 0 & 0 & 0 \end{bmatrix}. \tag{3.25}$$

and hence a slight change in the dynamic geometric stiffness matrix **G** in (3.15e). The other matrices —mass, gyroscopic, material stiffness —remain the same as obtained in Section 2.4. One can easily verify the correspondence of the terms in the discrete equations of motion resulting from the linear PDE's (3.24) to those given in Kane *et al* [1985]. In addition, when there are no dynamic effects, the linear model governed by the PDE's (3.24) reduces exactly to the Timoshenko beam theory. It should be pointed out, however, that the choice of s' and $(u_2' - \alpha)$ as axial and shear strain measures does not agree with the consistent second order strain measures $\bar{\Gamma}_1$ and $\bar{\Gamma}_2$ unless $u_2' = \alpha + O(\varepsilon)$ (negligible shear deformation).

3.4. Extension to plate formulation

As a direct application of the foregoing discussion, we shall extend the results to the case of a plate undergoing three-dimensional rotating motion. Again, for clarity, we assume that the axis of revolution of the plate passes through an inertially fixed material point of the plate. The dynamics of this revolution is completely prescribed *a priori*; the orientation of the axis of revolution, however, need not be fixed with respect to the inertial frame.

3.4.1. Model problem and notation

Consider the material frame $\{O; \mathbf{E}_1, \mathbf{E}_2, \mathbf{E}_3\}$ with base point $O \in \mathbb{R}^3$ and an orthonormal basis $\{\mathbf{E}_i\}$. Let the inertial frame be $\{O; \mathbf{e}_1, \mathbf{e}_2, \mathbf{e}_3\}$ such that $\mathbf{e}_k = \mathbf{E}_k$, for $k=1,2,3$. Coordinates with respect to $\{\mathbf{E}_i\}$ are denoted by (X_1, X_2, X_3); coordinates with respect to $\{\mathbf{e}_i\}$ are denoted by (x_1, x_2, x_3). The domain of the undeformed plate is defined to be $B := \Omega \times [\frac{d}{2}, \frac{d}{2}]$ with $O \in B$ and such that a point $X \in B$ has coordinates $(X_1, X_2) \in \Omega \subset \mathbb{R}^2$ and $X_3 \in [\frac{d}{2}, \frac{d}{2}]$. Consider now a floating frame $\{O; \mathbf{a}_1, \mathbf{a}_2, \mathbf{a}_3\}$, attached to the deformed plate, and whose dynamics with respect to the inertial (material) frame $\{\mathbf{E}_i\}$ is completely prescribed by an orthogonal matrix $\mathbf{Q}(t)$ such that $\mathbf{a}_i(t) = \mathbf{Q}(t)\,\mathbf{E}_i$. The map $t \to \mathbf{Q}(t)$ in fact describes the rigid body rotation of the (undeformed) plate about the origin O. The deformation of the plate relative to the floating frame $\{\mathbf{a}_i\}$ is then given by

$$\mathbf{x} = \mathbf{x}_0 + X_3\,\mathbf{t}_3 \tag{3.26a}$$

$$\mathbf{x}_0 := \sum_{\gamma=1,2} [X_\gamma + u_\gamma(X_1, X_2, t)]\,\mathbf{a}_\gamma + u_3(X_1, X_2, t)\,\mathbf{a}_3\,, \ddagger \tag{3.26b}$$

$$\mathbf{t}_3(X_1, X_2, t) = \mathbf{A}(X_1, X_2, t)\,\mathbf{a}_3(t)\,. \tag{3.26c}$$

where (u_1, u_2, u_3) are the displacement components of a point $X \in B$; $\mathbf{t}_3$ designates the normal to the deformed plate, and $\mathbf{\Lambda}$ an orthogonal transformation.

8.4.2. Second order equations of motion

Consistent second order strain measures. It can be shown that, up to second order, the two-dimensional counterpart of the one-dimensional strain measures in (3.8) is given by

$$\bar{\Gamma}_{\gamma\beta} = u_{[\gamma,\beta]} + \tfrac{1}{2} u_{3,\gamma}\, u_{3,\beta} - \tfrac{1}{2}(u_{3,\gamma} - \alpha_\gamma)\,(u_{3,\beta} - \alpha_\beta)\,, \tag{3.27a}$$

$$\bar{\Gamma}_{3\beta} = (u_{3,\beta} - \alpha_\beta) - u_{\gamma,\beta}\,\alpha_\gamma\,, \tag{3.27b}$$

$$\bar{K}_{\gamma\beta} = \alpha_{[\gamma,\beta]}\,, \tag{3.27c}$$

for $\gamma, \beta = 1,2$, where we have used the notation $u_{[\gamma,\beta]} := \frac{1}{2}(u_{\gamma,\beta} + u_{\beta,\gamma})$, and $u_{\gamma,\beta} := \dfrac{\partial u_\gamma}{\partial X_\beta}$. Note that the strain measures in (3.27a) reduce exactly to the in-plane strain measures of the von Karman plate model,

$$\bar{\Gamma}_{\gamma\beta} = u_{[\gamma,\beta]} + \tfrac{1}{2} u_{3,\gamma}\, u_{3,\beta}\,, \tag{3.28}$$

with the assumption of negligible shear deformation, $u_{3,\beta} = \alpha_\beta + O(\varepsilon)$. This is entirely analogous to the one-dimensional case of the beam considered in previous sections. Further, we recall that the first order strain measures are $\bar{\Gamma}_{\gamma\beta} = u_{[\gamma,\beta]}$, $\bar{\Gamma}_{3\beta} = u_{3,\beta} - \alpha_\beta$, and $\bar{\kappa}_{\gamma\beta} \equiv \bar{K}_{\gamma\beta}$.

Constitutive laws. The elastic material internal forces $\bar{N}_{\gamma\beta}$, $\bar{V}_\gamma$, and moments $\bar{M}_{\gamma\beta}$ are related to the strain measures (3.27) by a functional relation analogous to that of classical small deformation plate theory. That is, one assumes

§ In what follows, subscripts in greek letters take values in {1,2}, while subscripts in roman letters take values in {1,2,3}.

$$\bar{N}_{\gamma\beta} = \frac{Ed}{1-\nu^2}[\nu\,\bar{\Gamma}_{\rho\rho}\,\delta_{\gamma\beta} + (1-\nu)\,\bar{\Gamma}_{\gamma\beta}] \tag{3.29a}$$

$$\bar{V}_\gamma = GA_s\,\bar{\Gamma}_{3\gamma} \tag{3.29b}$$

$$\bar{M}_{\gamma\beta} = \frac{Ed^3}{12\,(1-\nu^2)}[\nu\,\bar{\Gamma}_{\rho\rho}\,\delta_{\gamma\beta} + (1-\nu)\,\bar{\kappa}_{\gamma\beta}] \tag{3.29c}$$

Here, E represents the Young's modulus, ν the Poisson's ratio, G the shear modulus, and A_s may be taken to be $\frac{5}{6}d$. The same relationship holds for the first order internal forces $\bar{N}_{\gamma\beta}$, $\bar{V}_\gamma$, and internal moments $\bar{M}_{\gamma\beta}$ in terms of the first order strain measures $(\bar{\Gamma}_{\gamma\beta}, \bar{\Gamma}_{3\gamma}, \bar{\kappa}_{\gamma\beta})$.

Equations of motion. One can show that following system of partial differential equations, analogous to (3.9), furnishes the consistent second order approximation to the fully nonlinear equations of motion

$$\begin{Bmatrix} F_\beta^{inertia} \\ F_3^{inertia} \\ T_3^{inertia} \end{Bmatrix} - \begin{Bmatrix} \bar{N}_{\beta\gamma,\gamma} \\ \bar{V}_{\beta,\beta} \\ \bar{M}_{\beta\gamma,\gamma} + \bar{V}_\beta \end{Bmatrix} + \begin{Bmatrix} (\alpha_\gamma\,\bar{V}_\gamma)_{,\beta} \\ -(\alpha_\gamma\,\bar{N}_{\beta\gamma})_{,\beta} \\ -\bar{\Gamma}_{\beta\gamma}\,\bar{V}_\gamma + \bar{\Gamma}_{3\gamma}\,\bar{N}_{\beta\gamma} \end{Bmatrix} = \mathbf{0} \tag{3.30}$$

where $\mathbf{F}^{inertia} := F_i^{inertia}\,\mathbf{a}_i$ denotes the inertia operator for the translational part of the equations of motion, and $\mathbf{T}^{inertia} := T_i^{inertia}\,\mathbf{a}_i$ the inertia operator for the rotational part. A similar stiffness operator can be found in Simo [1982 , p. 112]. To evaluate $\mathbf{F}^{inertia}$ and $\mathbf{T}^{inertia}$, one proceed as follows. Let $\mathbf{u} := u_i\,\mathbf{a}_i$, thus $\mathbf{x}_0 := X_\gamma\,\mathbf{a}_\gamma + \mathbf{u}$, and define the angular velocity of the floating frame $\{\mathbf{a}_i\}$ relative to the inertial frame as

$$\mathbf{w} := w_i\,\mathbf{a}_i\,, \quad \text{such that } \dot{\mathbf{Q}} = \mathbf{Q}\,\overset{\blacktriangledown}{\mathbf{w}}, \tag{3.31a}$$

where $\overset{\blacktriangledown}{\mathbf{w}}$ is a skew-symmetric tensor with components relative to $\{\mathbf{a}_i\}$ given by

$$\overset{\blacktriangledown}{\mathbf{w}} = \overset{\blacktriangledown}{w}_{ij}\,\mathbf{a}_i \otimes \mathbf{a}_j\,, \quad \text{and } [\overset{\blacktriangledown}{w}_{ij}] = \begin{bmatrix} 0 & -w_3 & w_2 \\ w_3 & 0 & -w_1 \\ -w_2 & w_1 & 0 \end{bmatrix} \tag{3.31b}$$

Let $\mathbf{L}$ be the linear momentum per unit of mid-surface area. Using the kinematic assumption (3.26) it follows that

$$\mathbf{L} := \int_{[-\frac{d}{2}, \frac{d}{2}]} [\dot{\mathbf{x}}_o + X_3 \dot{\mathbf{t}}_3] \, dX_3 = A_\rho [\overset{\nabla}{\mathbf{u}} + \mathbf{w} \times \mathbf{x}_o] \tag{3.32a}$$

where A_ρ now denotes the plate mass per unit of undeformed area, and a superposed "∇" represents time differentiation keeping fixed the floating frame $\{\mathbf{a}_i\}$. The inertia force $\mathbf{F}^{inertia}$ is then given by

$$\mathbf{F}^{inertia} = \dot{\mathbf{L}} = A_\rho [\overset{\nabla\nabla}{\mathbf{u}} + \dot{\mathbf{w}} \times \mathbf{x}_o + 2\mathbf{w} \times \overset{\nabla}{\mathbf{u}} + \mathbf{w} \times (\mathbf{w} \times \mathbf{x}_o)] . \tag{3.32b}$$

Similarly, the couple $\mathbf{T}^{inertia}$ is obtained from the angular momentum per unit of mid-surface $\mathbf{H} := \int_{[-\frac{d}{2}, \frac{d}{2}]} (\mathbf{x} - \mathbf{x}_o) \times \dot{\mathbf{x}} \, dX_3$ as $\mathbf{T}^{inertia} = \dot{\mathbf{H}}$. The expression for $\mathbf{T}^{inertia}$ is conveniently expressed in terms of the vector $\boldsymbol{\alpha} := \alpha_\gamma \mathbf{a}_\gamma$ that defines the infinitesimal rotation of the normal $\mathbf{t}_3$ of the plate. Note that $\alpha_3 = 0$, i.e., there is no rotational degree of freedom along the axis $\mathbf{a}_3$ as in the classical Mindlin-Reissner plate theory. In addition, let $\mathbf{J}_\rho$ denote the inertia dyadic of a transverse (undeformed) fiber of the plate: $\mathbf{r} := X_3 \mathbf{a}_3$, where $X_3 \in [-\frac{d}{2}, \frac{d}{2}]$. By definition, we have

$$\mathbf{J}_\rho := \int_{[-\frac{d}{2}, \frac{d}{2}]} [\|\mathbf{r}\|^2 \mathbf{1}_3 - \mathbf{r} \otimes \mathbf{r}] \, dX_3 = \frac{\rho d^3}{12} [\mathbf{1}_3 - \mathbf{a}_3 \otimes \mathbf{a}_3] . \tag{3.33b}$$

It can be shown that the rate of angular momentum $\dot{\mathbf{H}}$ takes the form

$$\mathbf{T}^{inertia} = \dot{\mathbf{H}} = [\mathbf{J}_\rho (\overset{\nabla\nabla}{\boldsymbol{\alpha}} + \mathbf{w} \times \overset{\nabla}{\boldsymbol{\alpha}} + \dot{\mathbf{w}}) + (\overset{\nabla}{\boldsymbol{\alpha}} + \mathbf{w}) \times \mathbf{J}_\rho (\overset{\nabla}{\boldsymbol{\alpha}} + \mathbf{w})] . \tag{3.33a}$$

The second order equations of motion for the plate are now completely defined.

3.4.3. Consistent linear partial differential equations

Next, we derive the counterpart of equation (3.10) that governs, to first order approximation, the transverse vibration of the plate. This approximation is systematically obtained exactly as in Section 2.3. We first note that the term $(\alpha_\gamma \bar{N}_{\beta\gamma,\beta})$ in the shear equations $(3.30)_2$ is of first order as a result of the centrifugal terms in the equations for in-plane forces $(3.30)_1$. We recall that this term allows an appropriate account for the action of the centrifugal force on the bending of the plate. For steady state revolution and negligible shear, the transverse vibration of the plate is governed, up to first order, by the linear PDE

$$A_\rho \ddot{u}_3 + D\,\Delta^2 u_3 - [X_\gamma w_\gamma w_\beta - \|\mathbf{w}\|^2 X_\beta]\, u_{3,\beta}$$

$$- A_\rho (w_1^2 + w_2^2)\, u_3 = -w_\gamma (\mathbf{x}_o \cdot \mathbf{a}_\gamma)\, w_3 - 2(w_1 \dot{u}_2 - w_2 \dot{u}_1)\,, \qquad (3.34a)$$

$$D := \frac{Ed^3}{12(1-\nu^2)}, \qquad (3.34b)$$

with Δ denoting the Laplacian operator. A complete analogy with equation (3.10) should be observed: The term $[A_\rho (w_1^2 + w_2^2)\, u_3]$ gives rise to an unphysical loss of stiffness, quadratic with the angular velocity, when linear plate theory is used; a complete account for the action of the centrifugal force is realized up to the first order with the additional term $[X_\gamma w_\gamma w_\beta - \|\mathbf{w}\|^2 X_\beta]\, u_{3,\beta}$ when second order plate theory is employed. These two terms form the dynamic geometric stiffness operator for the fast rotating plate.

The counterpart of equation (3.12) can be obtained in a straightforward manner. The resulting equation is, however, lengthy and will not be given here. The second order theory governed by (3.27),(3.29) and (3.30), with $\mathbf{F}^{inertia}$ and $\mathbf{T}^{inertia}$ given by (3.32) and (3.33) respectively, can be treated numerically by standard finite element procedures. From a computational standpoint the main issue concerns development of the appropriate spatial discretization.

3.5. Concluding remarks

This chapter demonstrates the limited range of application, and even inadequacy, of linear structural theories to model certain physically relevant situations. Our discussion shows that even for extremely stiff beams for which linear theories are expected to be valid, a sufficiently high angular velocity of revolution will predict a physically inadmissible destabilization effect. Fully nonlinear models, on the other hand, are able to account for situations more general than that discussed herein. Efficient computational procedures based on the use of such theories have been developed in Chapter 2.

Conceptually, the approach proposed in Chapter 2 readily carries over to the case of a flexible beam subject to three-dimensional motions. This extension relies on a proper treatment of the finite rotation field, which is in general non-commutative. Chapter 4 will address the formulation and computational aspects of the fully nonlinear three-dimensional rod model without inertia effects. The dynamic treatment of flexible rods undergoing three-dimensional large overall motions of the type presented in this chapter will be postponed until chapter 5.

CHAPTER 4

ALGORITHMIC TREATMENT OF A 3-D FINITE-STRAIN ROD MODEL

4.1. Introduction

In this chapter, we shall be concerned with the variational formulation and numerical implementation in the context of the finite element method of the three-dimensional finite-strain rod model proposed by Simo [1985]. Only static response of the rod will be considered here; the treatment of dynamic response is deferred until the next chapter. We recall that this model is essentially a re-parametrization of an extension to the classical Kirchhoff-Love model, developed by Antman [1974,75] in a different context, which includes finite extension and shearing of the rod. These formulations reduce to the classical Kirchhoff-Love model for vanishing shearing and small axial strains. Other formulations of three-dimensional finite-strain rod restricted primarily to static analysis may be found in Reissner [1973,81] and Parker [1979]. The parametrization of the deformed cross section employed here is based on the use of quaternion parameters to describe orthogonal transformations in $\mathbb{R}^3$. From a computational standpoint, an implementation based on the use of quaternion parameters proves to be the optimal choice, avoiding the singularity of Euler angles and minimizing storage requirements (Simo & Vu-Quoc [1985b]). In the context of aircraft dynamics, issues concerning alternative parametrizations have been addressed in de Veubeke [1976] and Kane *et al* [1983].

In the model considered herein, as in the classical Kirchoff-Love model, rotations have the traditional meaning of orthogonal transformations in Euclidean space. We recall that orthogonal transformations constitute a *non-commutative* (Lie) group referred to as the special orthogonal group SO(3). This approach is at variance with Argyris and co-workers [1979,81,82] in which the

standard notion of rotations is replaced by *semi-tangential* rotations. Thus, the deformation map for this model takes values in the (nonlinear) differentiable manifold $\mathbb{R}^3 \times SO(3)$, instead of a linear space $\mathbb{R}^3$ as for the plane formulation.

The finite element procedure, discussed in Section 3.4, is based on a variational formulation of the partial differential equations of motion summarized in Section 3.2. Consistent linearization (Marsden & Hughes [1983]) is employed to obtain the linearized weak form of momentum balance. The resulting global tangent operator is characterized by possessing a *non-symmetric geometric stiffness*. This lack of symmetry arises from the non-commutativity of the special rotation group SO(3). Argyris and co-workers [1979,82] pointed out that this lack of symmetry inevitably arises at the element (local) level, although it is stated that symmetry is recovered upon assembly at the global level. Such a result is attributed by these authors to a deficiency in the classical definitions of moment and rotation, and it motivated to a large extent their adoption of a numerical formulation based on the concept of semi-tangential rotation introduced by Ziegler [1977]. On the other hand, in the context of a classical formulation of rotations, it is shown in Section 3.5 that

(i) The *global geometric stiffness* arising for the (consistently) linearized weak form is *non symmetric*, even for conservative loading, at a *non-equilibrium* configuration.

(ii) At an *equilibrium* configuration the linearized tangent operator is *always symmetric* provided the loading is conservative. A condition for this then follows, with a structure similar to that discussed by Schweizerhof & Ramm [1984] and Bufler [1984] for pressure loading.

(iii) Upon discretization, from (ii) it follows that both the global and the local (element) geometric stiffness matrices are *symmetric* at an *equilibrium* configuration.

Emphasis is placed throughout the formulation on a geometric approach that enables one to formulate efficient algorithms. A configuration of the rod is described by a vector field giving the position of the current centroidal line and an orthogonal "moving" frame representing the orientation of the cross section. The configuration update procedure for the rotation field becomes the algorithmic counterpart of the exponential map from $so(3)$, the algebra of skew-symmetric tensors, to $SO(3)$. This procedure relies crucially on the closed-form formula for the exponential of a skew-symmetric matrix, often ascribed to Rodrigues (Goldstein [1980], p. 165). In addition, it is possible to obtain a simple closed-form expression for the derivative of the exponential map, which plays a crucial role in the evaluation of the curvatures of the rod. A detailed discussion of the finite element formulation and the configuration update procedure is presented in Section 4.6.

The effectiveness and generality of formulation discussed in this chapter is illustrated in section 4.7 through a set of numerical simulations including plane and three dimensional problems, and both conservative and non-conservative loading. Results are compared with those in the existing literature, as in Argyris [1981,82], and Bathe [1979].

4.2. A finite-strain rod model: Summary and notation

Kinematic description. (See Figure 4.2.1) Consider a (fixed) material coordinate frame $\{O;\mathbf{E}_1,\mathbf{E}_2,\mathbf{E}_3\}$ with base point $O \in \mathbb{R}^3$ and a set of orthonormal basis vectors $\{\mathbf{E}_1,\mathbf{E}_2,\mathbf{E}_3\}$. Coordinates along those vectors are denoted respectively by (X_1,X_2,S). A beam of length L and cross section $\Omega \subset \mathbb{R}^2$ occupies in its undeformed configuration the domain $B := \Omega\times[0,L] \subset \mathbb{R}^3$ such that a point $X \in B$ has coordinates (X_1,X_2,S) with $(X_1,X_2) \in \Omega$ and $S \in [0,L]$ parametrizes the length of the beam. For simplicity, we assume that the beam is prismatic and initially

straight such that point O is the centroid of the cross section at $S = 0$; $(\mathbf{E}_1, \mathbf{E}_2)$ coincide with the principal axes of inertia of the cross section, and $\mathbf{E}_3$ coincides with the undeformed centroidal line. Let $\{O;\mathbf{e}_1, \mathbf{e}_2, \mathbf{e}_3\}$ denote the fixed spatial frame such that $\mathbf{e}_k = \mathbf{E}_k$, for $k=1,2,3$. Consider the deformation map $\phi: B \to \mathbb{R}^3$ which maps a point $X \in B$ with coordinates (X_1, X_2, S) into a point $x = \phi(X) \in \mathbb{R}^3$. Let X_o denote a material point on the undeformed centroidal line with coordinates $(0, 0, S)$ and x_o its image by ϕ.

Let $\{\mathbf{t}_I(S,t)\}_{\{I=1,2,3\}}$ represent the orthonormal basis vector of a moving frame attached to a typical cross section with $t \in \mathbb{R}_+$ being a time parameter. The origin of the moving frame is fixed at the centroid x_o of the cross-section. The basis vector $\mathbf{t}_3$ remains normal to the section at all times. Further, initially at $t = 0$, let $\mathbf{t}_I(S,0) = \mathbf{E}_I$ for $I = 1,2,3$. The basic kinematic assumption is based on the following relation for the position vector of x, denoted by $\mathbf{x}$,

$$\mathbf{x} = \mathbf{x}_o + X_I \mathbf{t}_I \tag{4.1a}$$

with $\mathbf{x}_o$ denotes the position vector of point x_o. Let us introduce the map $\phi_o: [0, L] \to \mathbb{R}^3$ and the orthogonal transformation map $\mathbf{\Lambda}: \mathbb{R}^3 \to \mathbb{R}^3$† with the following definition. A material frame $\{X_o; \mathbf{E}_1, \mathbf{E}_2, \mathbf{E}_3\}$ is mapped into the frame $\{x_o; \mathbf{t}_1, \mathbf{t}_2, \mathbf{t}_3\}$ such that

$$\mathbf{x}_o := \phi_o(S,t) = \phi_{oi}(S,t)\,\mathbf{e}_i\,, \tag{4.1b}$$

$$\mathbf{t}_I(S,t) = \mathbf{\Lambda}(S,t)\,\mathbf{E}_I = \Lambda_{iI}(S,t)\,\mathbf{e}_i\,, \quad (I = 1,2,3)\,, \tag{4.1c}$$

where Λ_{iI} are components of $\mathbf{\Lambda}$ viewed as a two-point tensor

$$\mathbf{\Lambda}(S,t) = \Lambda_{iI}(S,t)\,\mathbf{e}_i \otimes \mathbf{E}_I\,. \tag{4.1d}$$

† $\mathbf{\Lambda}(S,t)$ can be regarded as a linear map from the tangent space $T_{X_o}\mathbb{R}^3$, with basis vectors $\{\mathbf{E}_I\}$, to the tangent space $T_{x_o}\mathbb{R}^3$, with basis vectors $\{\mathbf{t}_I\}$. Recall that both of these tangent spaces are isomorphic to $\mathbb{R}^3$, i.e., they are "copies" of $\mathbb{R}^3$.

Accordingly, the set C of all possible configurations of the rod is defined by

$$C := \{ \boldsymbol{\phi} = (\boldsymbol{\phi}_o, \mathbf{A}) \;\Big|\; \boldsymbol{\phi}_o : [0, L] \to \mathbb{R}^3,\ \mathbf{A} : [0, L] \to SO(3) \} \tag{4.1e}$$

Thus the deformation map $\boldsymbol{\phi}$ takes values in the nonlinear differentiable manifold $\mathbb{R}^3 \times SO(3)$, where $SO(3)$ is the special orthogonal (Lie) group. Before summarizing the rod model formulated by Simo [1985], we shall introduce some notation concerning the manifold $SO(3)$ that will be extensively used later, and recall the relevant properties of exponential map and parallel transport in $SO(3)$. Detailed treatment of this subject may be found in a number of standard textbooks such as Misner, Thorne & Wheeler [1973], Spivak [1979], Bishop & Goldberg [1980], or Karger & Novak [1985].

Notation for $SO(3)$. Following standard usage, the Lie group of proper orthogonal transformations is defined by

$$SO(3) := \{ \mathbf{A} : \mathbb{R}^3 \to \mathbb{R}^3 \;\mid\; \mathbf{A} \text{ linear},\ \mathbf{A}^T \mathbf{A} = \mathbf{1}_3,\ \text{and } \det \mathbf{A} = 1 \} \tag{4.2}$$

Physically, each orthogonal transformation $\mathbf{A} \in SO(3)$ defines a *finite rotation* about the eigenvector $\boldsymbol{\vartheta}$ associated with the only real eigenvalue 1 : $\mathbf{A}\boldsymbol{\vartheta} = \boldsymbol{\vartheta}$.‡ The magnitude of the rotation angle is $\|\boldsymbol{\vartheta}\|$. Euler angles or quaternion parameters can be used as coordinate charts covering $SO(3)$.††

Let $so(3) := \{ \overset{\vee}{\boldsymbol{\vartheta}} : \mathbb{R}^3 \to \mathbb{R}^3 \;\mid\; \overset{\vee}{\boldsymbol{\vartheta}} \text{ linear},\ \overset{\vee}{\boldsymbol{\vartheta}} + \overset{\vee}{\boldsymbol{\vartheta}}^T = \mathbf{0} \}$ be the set of all *skew-symmetric* tensors with either a single eigenvalue equal to zero or all three eigenvalues each equal to zero (Chadwick [1976]). Eliminating the trivial case where all three eigenvalues are zero, then physically, any $\overset{\vee}{\boldsymbol{\vartheta}} \in so(3)$ represents an *infinitesimal rotation* about the eigenvector $\boldsymbol{\vartheta} \in \mathbb{R}^3$ associated with the only

‡ $\mathbf{A}$ has only one eigenvalue, which is equal to 1, if we eliminate the trivial case where $\mathbf{A}$ is the identity, i.e., $\mathbf{A} = \mathbf{1}_3$.

†† Due to the singularity associated with Euler angles, one needs two coordinate chart, defined by two different sets of Euler angles, to cover $SO(3)$.

zero eigenvalue such that $\overset{\vee}{\boldsymbol{\vartheta}}\,\boldsymbol{\vartheta} = 0$. In coordinates, relative to a basis $\{\mathbf{e}_i\}$ in $\mathbb{R}^3$, we have $\overset{\vee}{\boldsymbol{\vartheta}} = \overset{\vee}{\vartheta}_{ij}\,\mathbf{e}_i \otimes \mathbf{e}_j$ and $\boldsymbol{\vartheta} = \vartheta_i\,\mathbf{e}_i$ such that

$$[\overset{\vee}{\vartheta}_{ij}] = \begin{bmatrix} 0 & -\vartheta_3 & \vartheta_2 \\ \vartheta_3 & 0 & -\vartheta_3 \\ -\vartheta_2 & \vartheta_1 & 0 \end{bmatrix}, \quad \{\vartheta_i\} = \begin{Bmatrix} \vartheta_1 \\ \vartheta_2 \\ \vartheta_3 \end{Bmatrix} \tag{4.3}$$

In fact, (4.3) defines the isomorphism between $so(3)$ and $\mathbb{R}^3$. Further, in relation with the cross product, we recall that $\overset{\vee}{\boldsymbol{\vartheta}}\,\mathbf{h} = \boldsymbol{\vartheta} \times \mathbf{h}$, for any $\mathbf{h} \in \mathbb{R}^3$. We shall often use the notation $\overset{\vee}{\boldsymbol{\vartheta}} = [\boldsymbol{\vartheta}\,\times]$ where $\boldsymbol{\vartheta} \in \mathbb{R}^3$ is called the *axial vector* (Chadwick [1976, p. 29]) of $\overset{\vee}{\boldsymbol{\vartheta}} \in so(3)$.

Exponential map. Infinitesimal rotations are *linearized* finite rotations about the identity. Mathematically, one says the $so(3)$ is the tangent space of $SO(3)$ at the identity $\mathbf{1}_3 \in SO(3)$, and employs the notation $T_{\mathbf{1}_3}SO(3) = so(3)$.† Given any $\boldsymbol{\Lambda} \in SO(3)$, and any $\overset{\vee}{\boldsymbol{\vartheta}} \in so(3)$ one says that $\overset{\vee}{\boldsymbol{\vartheta}}\,\boldsymbol{\Lambda}$ is an infinitesimal rotation superposed onto a finite rotation. The set of all superposed infinitesimal rotations

$$T_{\boldsymbol{\Lambda}}SO(3) := \{\, \overset{\vee}{\boldsymbol{\vartheta}}\,\boldsymbol{\Lambda} \;\mid\; \overset{\vee}{\boldsymbol{\vartheta}} \in so(3) \,\}, \tag{4.4}$$

is referred to as the tangent space to $SO(3)$ at $\boldsymbol{\Lambda}$. Consider next the straight line $\varepsilon \to \varepsilon\,\overset{\vee}{\boldsymbol{\vartheta}}\,\boldsymbol{\Lambda} \in T_{\boldsymbol{\Lambda}}SO(3)$, for $\varepsilon > 0$. This line is mapped by the *exponential map* onto the curve $\varepsilon \to \boldsymbol{\Lambda}_\varepsilon \in SO(3)$ according to

$$\begin{aligned} \boldsymbol{\Lambda}_\varepsilon &= \exp[\varepsilon\,\overset{\vee}{\boldsymbol{\vartheta}}]\,\boldsymbol{\Lambda} = \sum_{k\geq 0}\Big[\frac{\varepsilon^k}{k!}\overset{\vee}{\boldsymbol{\vartheta}}^k\Big]\boldsymbol{\Lambda} \\ &= \Big[\mathbf{1}_3 + \varepsilon\,\overset{\vee}{\boldsymbol{\vartheta}} + \frac{\varepsilon^2}{2!}\overset{\vee}{\boldsymbol{\vartheta}}^2 + \frac{\varepsilon^3}{3!}\overset{\vee}{\boldsymbol{\vartheta}}^3 + \cdots\Big]\boldsymbol{\Lambda} \end{aligned} \tag{4.5a}$$

† The Lie group of skew-symmetric tensors $so(3)$, equipped with the Lie bracket $[\overset{\vee}{\boldsymbol{\vartheta}}, \overset{\vee}{\boldsymbol{\psi}}] := \overset{\vee}{\boldsymbol{\vartheta}}\overset{\vee}{\boldsymbol{\psi}} - \overset{\vee}{\boldsymbol{\psi}}\overset{\vee}{\boldsymbol{\vartheta}}$, for $\overset{\vee}{\boldsymbol{\vartheta}}, \overset{\vee}{\boldsymbol{\psi}} \in so(3)$, forms the Lie algebra of the Lie group of orthogonal transformations $SO(3)$.

Thus the exponential map, $\exp : so(3) \to SO(3)$, maps straight lines in $so(3)$ onto one-parameter subgroups of $SO(3)$. It can be shown that these one parameter subgroups are *geodesic* curves in $SO(3)$ relative to an appropriate connection. We say that $\mathbf{\Lambda}$ is left-translated to $\mathbf{\Lambda}_\varepsilon$ by $\exp[\varepsilon \overset{\mathrm{v}}{\boldsymbol{\vartheta}}]$, with the *left-translation* being defined in (4.5a). On the other hand, the *right-tranlation* in $SO(3)$ is defined by $\mathbf{\Lambda}_\varepsilon = \mathbf{\Lambda} \exp[\varepsilon \overset{\mathrm{v}}{\boldsymbol{\Theta}}]$, with $\boldsymbol{\Theta} = \mathbf{\Lambda}^T \boldsymbol{\vartheta}$. We finally recall the following explicit formula to compute the exponential of a skew-symmetric tensor in $so(3)$ (e.g., Argyris [1982])

$$\exp[\overset{\mathrm{v}}{\boldsymbol{\vartheta}}] = \mathbf{1}_3 + \frac{\sin\|\boldsymbol{\vartheta}\|}{\|\boldsymbol{\vartheta}\|} \overset{\mathrm{v}}{\boldsymbol{\vartheta}} + \frac{1}{2} \frac{\sin^2(\|\boldsymbol{\vartheta}\|/2)}{(\|\boldsymbol{\vartheta}\|/2)^2} \overset{\mathrm{v}}{\boldsymbol{\vartheta}}^2 \tag{4.5b}$$

which, in vector form, is often credited to Rodrigues (Goldstein [1980], p. 165). Another formula for the exponential map often found useful in the derivation is given in Argyris [1982]

$$\exp[\overset{\mathrm{v}}{\boldsymbol{\vartheta}}] = \mathbf{1}_3 + \frac{2}{1+\|\bar{\boldsymbol{\vartheta}}\|^2} [\overset{\mathrm{v}}{\bar{\boldsymbol{\vartheta}}} + \overset{\mathrm{v}}{\bar{\boldsymbol{\vartheta}}}^2] \tag{4.5c}$$

where $\bar{\boldsymbol{\vartheta}}$ is defined as follows

$$\bar{\boldsymbol{\vartheta}} := \tan(\|\boldsymbol{\vartheta}\|/2) \frac{\boldsymbol{\vartheta}}{\|\boldsymbol{\vartheta}\|} \tag{4.5d}$$

$\boldsymbol{\vartheta}$ and $\bar{\boldsymbol{\vartheta}}$ are sometimes referred to as rotation vector† and pseudo rotation vector, respectively. An alternative representation of an orthogonal transformation $\mathbf{\Lambda} \in SO(3)$ can be found in Chadwick [1976, p. 32]. A geometric interpretation of the exponential map is given in Figure 4.2.2.

Parallel transport. Consider $\mathbf{\Lambda}^{(1)}$, $\mathbf{\Lambda}^{(2)} \in SO(3)$. Then an element $\overset{\mathrm{v}}{\boldsymbol{\vartheta}}^{(1)} \mathbf{\Lambda}^{(1)} \in T_{\mathbf{\Lambda}^{(1)}} SO(3)$ is parallelly transported along the geodesic connecting $\mathbf{\Lambda}^{(1)}$

† Note that the word *vector* is used here to denote an object with a direction and a magnitude associated with it, and does not carry the meaning of an element of a linear (or vector) space.

and $\mathbf{A}^{(2)}$ to an element $\overset{\vee}{\boldsymbol{\vartheta}}{}^{(2)}\mathbf{A}^{(2)} \in T_{\mathbf{A}^{(2)}}SO(3)$ if and only if

$$\overset{\vee}{\boldsymbol{\vartheta}}{}^{(2)} = \mathbf{A}^{(2)}\mathbf{A}^{(1)T}\overset{\vee}{\boldsymbol{\vartheta}}{}^{(1)}\mathbf{A}^{(1)}\mathbf{A}^{(2)T} \tag{4.6}$$

Note that since in component form we have $\mathbf{A} = \Lambda_{iJ}\,\mathbf{e}_i\otimes\mathbf{E}_J$ and $\overset{\vee}{\boldsymbol{\vartheta}} = \overset{\vee}{\vartheta}_{ij}\,\mathbf{e}_i\otimes\mathbf{e}_j$, $\overset{\vee}{\boldsymbol{\Theta}} := \mathbf{A}^T\overset{\vee}{\boldsymbol{\vartheta}}\mathbf{A}$ belongs to the tangent space $T_{\mathbf{1}_3}SO(3) \cong so(3)$ and has its components with respect to the material basis vector $\{\mathbf{E}_I\}$

$$\begin{aligned}\overset{\vee}{\boldsymbol{\Theta}} &= (\Lambda_{iJ}\,\mathbf{E}_I\otimes\mathbf{e}_i)\,(\overset{\vee}{\vartheta}_{kl}\,\mathbf{e}_k\otimes\mathbf{e}_l)\,(\Lambda_{jJ}\,\mathbf{e}_j\otimes\mathbf{E}_J)\\ &= \Lambda_{iJ}\overset{\vee}{\vartheta}_{ij}\Lambda_{jJ}\,\mathbf{E}_I\otimes\mathbf{E}_J =: \overset{\vee}{\Theta}_{IJ}\,\mathbf{E}_I\otimes\mathbf{E}_J\end{aligned} \tag{4.7}$$

Also from the relation $\mathbf{t}_i = \mathbf{A}\mathbf{E}_i$, it can be seen that the components of $\overset{\vee}{\boldsymbol{\vartheta}}$ relative to the basis $\mathbf{t}_i\otimes\mathbf{t}_j$ are actually identical to $\overset{\vee}{\Theta}_{IJ}$. This result follows easily from the fact that $\overset{\vee}{\boldsymbol{\vartheta}} = \mathbf{A}\overset{\vee}{\boldsymbol{\Theta}}\mathbf{A}^T$ and the identity $\mathbf{A}(\mathbf{E}_I\otimes\mathbf{E}_J)\mathbf{A}^T = (\mathbf{A}\mathbf{E}_I)\otimes(\mathbf{A}\mathbf{E}_J) = \mathbf{t}_i\otimes\mathbf{t}_j$. Thus,

$$\overset{\vee}{\boldsymbol{\vartheta}} = \overset{\vee}{\vartheta}_{ij}\,\mathbf{e}_i\otimes\mathbf{e}_j = \overset{\vee}{\Theta}_{IJ}\,\mathbf{t}_i\otimes\mathbf{t}_j \tag{4.8}$$

To further elaborate, let $\boldsymbol{\Theta}^{(1)}\mathbf{A}^{(1)} \in T_{\mathbf{A}^{(1)}}SO(3)$ and $\boldsymbol{\Theta}^{(2)}\mathbf{A}^{(2)} \in T_{\mathbf{A}^{(2)}}SO(3)$. Relative to the moving bases $\{\mathbf{t}_i^{(1)}\}$ and $\{\mathbf{t}_i^{(2)}\}$ one has the coordinate representations $\overset{\vee}{\boldsymbol{\vartheta}}{}^{(1)} = \overset{\vee}{\Theta}{}^{(1)}_{ij}\,\mathbf{t}_i^{(1)}\otimes\mathbf{t}_j^{(1)}$ and $\overset{\vee}{\boldsymbol{\vartheta}}{}^{(2)} = \overset{\vee}{\Theta}{}^{(2)}_{ij}\,\mathbf{t}_i^{(2)}\otimes\mathbf{t}_j^{(2)}$. According to (4.6), $\overset{\vee}{\boldsymbol{\vartheta}}{}^{(1)}\mathbf{A}^{(1)}$ is parallelly transported to $\overset{\vee}{\boldsymbol{\vartheta}}{}^{(2)}\mathbf{A}^{(2)}$ if and only if $\overset{\vee}{\boldsymbol{\vartheta}}{}^{(2)} = \mathbf{A}^{(2)}\mathbf{A}^{(1)T}\overset{\vee}{\boldsymbol{\vartheta}}{}^{(1)}\mathbf{A}^{(1)}\mathbf{A}^{(2)T}$. In terms of coordinates relative to the moving frames $\{\mathbf{t}_i^{(1)}\}$ and $\{\mathbf{t}_i^{(2)}\}$, since $\mathbf{t}_i^{(2)} = \mathbf{A}^{(2)}\mathbf{A}^{(1)T}\mathbf{t}_i^{(1)}$, it follows that $\overset{\vee}{\Theta}{}^{(2)}_{ij} = \overset{\vee}{\Theta}{}^{(1)}_{ij}$. In conclusion, $\overset{\vee}{\boldsymbol{\vartheta}} \in so(3)$ is parallelly transported by holding fixed its coordinates $\overset{\vee}{\Theta}_{IJ}$ relative to the moving frame $\{\mathbf{t}_i\}$.

Finally, we note that the same conclusion applies to the axial vector. Since $\boldsymbol{\vartheta} = \vartheta_i\,\mathbf{e}_i$ and $\boldsymbol{\Theta} = \Theta_I\,\mathbf{E}_I$ are respectively the axial vectors of $\overset{\vee}{\boldsymbol{\vartheta}}$ and of $\overset{\vee}{\boldsymbol{\Theta}} := \mathbf{A}^T\overset{\vee}{\boldsymbol{\vartheta}}\mathbf{A}$, and since $\mathbf{A}(\mathbf{a}\times\mathbf{b}) = \mathbf{A}\mathbf{a}\times\mathbf{A}\mathbf{b}$, for all $\mathbf{a}, \mathbf{b} \in \mathbb{R}^3$, we obtain

$$\overset{\vee}{\boldsymbol{\Theta}}\mathbf{h} = \boldsymbol{\Theta}\times\mathbf{h} = \mathbf{A}^T\overset{\vee}{\boldsymbol{\vartheta}}\mathbf{A}\,\mathbf{h} = (\mathbf{A}^T\boldsymbol{\vartheta})\times\mathbf{h} \tag{4.9}$$

Thus the axial vector of $\mathbf{A}^T \overset{\mathrm{v}}{\boldsymbol{\vartheta}} \mathbf{A}$ is $\mathbf{A}^T \boldsymbol{\vartheta}$, i.e., $\boldsymbol{\Theta} = \mathbf{A}^T \boldsymbol{\vartheta}$ or $\boldsymbol{\vartheta} = \mathbf{A}\boldsymbol{\Theta}$. It follows that the components of $\boldsymbol{\vartheta}$ with respect to the moving frame $\{\mathbf{t}_i\}$ are identical to those of $\boldsymbol{\Theta}$ with respect to the material basis $\{\mathbf{E}_I\}$:

$$\boldsymbol{\vartheta} = \vartheta_i \, \mathbf{e}_i = \Theta_I \, \mathbf{t}_I \,. \tag{4.10}$$

Partial derivatives of A. The alternative expressions in the *spatial* and *material* descriptions, of the derivatives of the *orthogonal* transformation $(S,t) \to \mathbf{A}(S,t)$ are summarized Box 4.1.

BOX 4.1. *Derivatives of* $\mathbf{A}(S,t)$

Spatial	**Material**
$\dfrac{\partial \mathbf{A}(S,t)}{\partial S} = \overset{\mathrm{v}}{\boldsymbol{\omega}}(S,t)\,\mathbf{A}(S,t)$	$\dfrac{\partial \mathbf{A}(S,t)}{\partial S} = \mathbf{A}(S,t)\,\overset{\mathrm{v}}{\boldsymbol{\Omega}}(S,t)$
$[\overset{\mathrm{v}}{\omega}_{ij}] = \begin{bmatrix} 0 & -\omega_3 & \omega_2 \\ \omega_3 & 0 & -\omega_1 \\ -\omega_2 & \omega_1 & 0 \end{bmatrix}$	$[\overset{\mathrm{v}}{\Omega}_{IJ}] = \begin{bmatrix} 0 & -\Omega_3 & \Omega_2 \\ \Omega_3 & 0 & -\Omega_1 \\ -\Omega_2 & \Omega_1 & 0 \end{bmatrix}$
$\boldsymbol{\omega} := \omega_1 \mathbf{e}_1 + \omega_2 \mathbf{e}_2 + \omega_3 \mathbf{e}_3$ $= \Omega_1 \mathbf{t}_1 + \Omega_2 \mathbf{t}_2 + \Omega_3 \mathbf{t}_3$	$\boldsymbol{\Omega} := \Omega_1 \mathbf{E}_1 + \Omega_2 \mathbf{E}_2 + \Omega_3 \mathbf{E}_3$
$\dfrac{\partial \mathbf{A}(S,t)}{\partial t} = \overset{\mathrm{v}}{\mathbf{w}}(S,t)\,\mathbf{A}(S,t)$	$\dfrac{\partial \mathbf{A}(S,t)}{\partial t} = \mathbf{A}(S,t)\,\overset{\mathrm{v}}{\mathbf{W}}(S,t)$
$\mathbf{w} := w_1 \mathbf{e}_1 + w_2 \mathbf{e}_2 + w_3 \mathbf{e}_3$ $= W_1 \mathbf{t}_1 + W_2 \mathbf{t}_2 + W_3 \mathbf{t}_3$	$\mathbf{W} := W_1 \mathbf{E}_1 + W_2 \mathbf{E}_2 + W_3 \mathbf{E}_3$

Internal force and moment. Denoting by $\mathbf{P} := \mathbf{T}_I \otimes \mathbf{E}_I$ the non-symmetric (first) Piola-Kirchhoff stress tensor, the *spatial* internal force, $\mathbf{n} = n_i \, \mathbf{e}_i$, and the *spatial* internal moment, $\mathbf{m} = m_i \, \mathbf{e}_i$, acting on the cross section $\Omega \subset \mathbb{R}^2$ in its *current* configuration, are defined as

$$\mathbf{n} := \int_\Omega \mathbf{T}_3 \, d\Omega \,, \qquad \mathbf{m} := \int_\Omega [\mathbf{x} - \mathbf{x}_o] \times \mathbf{T}_3 \, d\Omega \tag{4.11}$$

The *material* internal force, $\mathbf{N} = N_I \mathbf{E}_I$ and moment, $\mathbf{M} = M_I \mathbf{E}_I$, are obtained by transforming $\mathbf{n}$ and $\mathbf{m}$ to the reference configuration (see previous section on parallel transport)

$$\mathbf{n} = \Lambda \mathbf{N}, \qquad \mathbf{m} = \Lambda \mathbf{M}. \tag{4.12}$$

Note that, by virtue of (4.10), the components of $\mathbf{n}$ and $\mathbf{m}$ in the moving frame $\{\mathbf{t}_I\}$ are identically the same as the components in the basis $\{\mathbf{E}_I\}$ of $\mathbf{N}$ and $\mathbf{M}$, respectively; i.e., $\mathbf{n} = N_I \mathbf{t}_I$ and $\mathbf{m} = M_I \mathbf{t}_I$. Similarly, the components of $\boldsymbol{\omega}$ in the moving frame equal those of $\boldsymbol{\Omega}$ in the material frame, as shown in Box 4.1.

Conjugate strain measures. Appropriate strain measures conjugate to the corresponding stress resultant and stress couple are obtained through the stress power equivalence

$$\int_B \mathbf{P} : \dot{\mathbf{F}} d\Omega dS = \int_{[0,L]} [\mathbf{n} \cdot \overset{\nabla}{\boldsymbol{\gamma}} + \mathbf{m} \cdot \overset{\nabla}{\boldsymbol{\omega}}] dS = \int_{[0,L]} [\mathbf{N} \cdot \dot{\boldsymbol{\Gamma}} + \mathbf{M} \cdot \dot{\boldsymbol{\Omega}}] dS \tag{4.13}$$

where $\mathbf{F}$ is the deformation gradient, and a superposed "dot" denotes time differentiation (Simo [1985]). Here, $\overset{\nabla}{(\cdot)} := \frac{\partial}{\partial t}(\cdot) - \mathbf{w} \times (\cdot)$ denotes the *co-rotated* rate; that is, the rate measured by an observer attached to the moving frame. The expressions of the spatial and material conjugate strains are summarized in Box 4.2 below.

BOX 4.2. *Strain measures*

spatial	material
$\boldsymbol{\gamma} = \dfrac{\partial \boldsymbol{\phi}_o(S,t)}{\partial S} - \mathbf{t}_3$	$\boldsymbol{\Gamma} = \boldsymbol{\Lambda}^T \dfrac{\partial \boldsymbol{\phi}_o(S,t)}{\partial S} - \mathbf{E}_3$
$\boldsymbol{\omega}$	$\boldsymbol{\Omega} = \boldsymbol{\Lambda}^T \boldsymbol{\omega}$

Equations of motion. The *spatial* form of the local balance laws is given by

$$\frac{\partial \mathbf{n}}{\partial S} + \bar{\mathbf{n}} = A_\rho \ddot{\boldsymbol{\phi}}_o. \tag{4.14a}$$

$$\frac{\partial \mathbf{m}}{\partial S} + \frac{\partial \boldsymbol{\phi}_o}{\partial S} \times \mathbf{n} + \bar{\mathbf{m}} = \mathbb{I}_\rho \dot{\mathbf{w}} + \mathbf{w} \times \mathbb{I}_\rho \mathbf{w}, \tag{4.14b}$$

where A_ρ denotes the mass per unit reference length and $\mathbb{I}_\rho$ the mass inertia tensor of a typical cross section. In this chapter, we shall ignore the inertia effects and focus on obtaining the solution for the left hand side of (4.14a) and (4.14b).

Constitutive laws. the constitutive equations expressed in the *spatial* descriptions take the form

$$\mathbf{n} = \frac{\partial \psi(S,\boldsymbol{\gamma},\boldsymbol{\omega})}{\partial \boldsymbol{\gamma}} \quad \text{and} \quad \mathbf{m} = \frac{\partial \psi(S,\boldsymbol{\gamma},\boldsymbol{\omega})}{\partial \boldsymbol{\omega}}. \tag{4.15}$$

Alternatively, in the *material* description one has the expressions

$$\mathbf{N} = \frac{\partial \Psi(S,\boldsymbol{\Gamma},\boldsymbol{\Omega})}{\partial \boldsymbol{\Gamma}} \quad \text{and} \quad \mathbf{M} = \frac{\partial \Psi(S,\boldsymbol{\Gamma},\boldsymbol{\Omega})}{\partial \boldsymbol{\Omega}}. \tag{4.16}$$

The functions ψ and Ψ are subjected to the invariance requirements under superposed isometries (Naghdi [1972], Antman [1972]). Finally, one defines the *material* elasticity tensor according to the expression

$$\mathbf{C}(S,\boldsymbol{\Gamma},\boldsymbol{\Omega}) = \begin{bmatrix} \dfrac{\partial \Psi}{\partial \boldsymbol{\Gamma}\, \partial \boldsymbol{\Gamma}} & \dfrac{\partial \Psi}{\partial \boldsymbol{\Gamma}\, \partial \boldsymbol{\Omega}} \\ \dfrac{\partial \Psi}{\partial \boldsymbol{\Gamma}\, \partial \boldsymbol{\Omega}} & \dfrac{\partial \Psi}{\partial \boldsymbol{\Omega}\, \partial \boldsymbol{\Omega}} \end{bmatrix} \tag{4.17}$$

The *spatial* form of the elasticity tensor can be also defined. In the development that follows, $\mathbf{C}$ is often assumed constant and diagonal; hence given by

$$\mathbf{C} = Diag\,[GA_1, GA_2, EA, EI_1, EI_2, GJ], \tag{4.18a}$$

and the material internal force $\mathbf{N}$ and moment $\mathbf{M}$ are chosen to be linear with respect to the strain measures

$$\begin{Bmatrix} \mathbf{N} \\ \mathbf{M} \end{Bmatrix} = \mathbf{C} \begin{Bmatrix} \boldsymbol{\Gamma} \\ \boldsymbol{\Omega} \end{Bmatrix}. \tag{4.18b}$$

Here, GA_1 and GA_2 denote the shear stiffness along $\mathbf{t}_1$ and $\mathbf{t}_2$, EA is the axial stiffness, EI_1 and EI_2 are the principal bending stiffnesses relative to $\mathbf{t}_1$ and $\mathbf{t}_2$, and GJ is the torsional stiffness of the rod.

This completes our summary of the rod model. The numerical treatment developed in the next section hinges on the the variational form of the equations summarized above, and considered in Section 3.4.

4.3. Admissible variations. Linearization of strain measures

A distinct characteristic of the model problem summarized above is that the deformation map belonging to the configuration space C defined in (4.1e) takes values in the nonlinear differentiable manifold $\mathbb{R}^3 \times SO(3)$ and not in a linear space. In this section we first consider the appropriate definition of admissible variations which play an essential role in the variational formulation of the governing equations. The consistent linearization of the strain measures about an arbitrary configuration summarized in Box 4.2 is considered next. These results are essential for the linearization of the variational equations discussed later in Section 4.4.

4.3.1. Admissible variations

Consider an arbitrary configuration of the rod specified by the position of its line of centroids and the orientation of the moving frame $\{\mathbf{t}_I\}_{\{I=1,2,3\}}$, that is,

$$\boldsymbol{\phi}(S) = (\boldsymbol{\phi}_o(S), \boldsymbol{\Lambda}(S)) \in C \tag{4.19}$$

We construct the perturbed configuration relative to $\boldsymbol{\phi}(S)$, denoted by $\boldsymbol{\phi}_\varepsilon(S) = (\boldsymbol{\phi}_{o\varepsilon}, \boldsymbol{\Lambda}_\varepsilon)$, as follows. Let $\boldsymbol{\eta}_o(S)$ be a vector field interpreted, for $\varepsilon > 0$, as a superposed infinitesimal displacement onto the line of centroids defined by $\boldsymbol{\phi}_o(S)$. In addition, let $\boldsymbol{\psi}(S) \in so(3)$ be a *skew-symmetric* tensor field

interpreted, for $\varepsilon > 0$, as a superposed infinitesimal rotation onto the moving frame defined by $\mathbf{\Lambda}(S)$, with an axial vector $\varepsilon\boldsymbol{\psi}(S)$. In components we have

$$\boldsymbol{\eta}_o(S) = \eta_{oi}\,\mathbf{e}_i\,, \qquad \overset{\vee}{\boldsymbol{\psi}}(S) = \overset{\vee}{\psi}_{ij}(S)\,\mathbf{e}_i \otimes \mathbf{e}_j \tag{4.20}$$

The curve of perturbed configuration $\varepsilon \to \boldsymbol{\phi}_\varepsilon(S) = (\boldsymbol{\phi}_{o\varepsilon}(S), \mathbf{\Lambda}_\varepsilon(S)) \in C$ is then obtained by setting

$$\boldsymbol{\phi}_{o\varepsilon}(S) = \boldsymbol{\phi}_o(S) + \varepsilon\,\boldsymbol{\eta}_o(S), \qquad \mathbf{\Lambda}_\varepsilon(S) = \exp[\varepsilon\,\overset{\vee}{\boldsymbol{\psi}}(S)]\,\mathbf{\Lambda}(S) \tag{4.21}$$

Recall that finite rotations are defined by orthogonal transformations (elements of $SO(3)$), whereas infinitesimal rotations are obtained through skew-symmetric transformations (elements of $so(3) = T_{\mathbf{1}_3}SO(3)$). A finite rotation of amplitude $\|\boldsymbol{\psi}\|$ about the axis of vector $\boldsymbol{\psi}$ is represented by an orthogonal transformation obtained via exponentiation of $\overset{\vee}{\boldsymbol{\psi}}$. Thus, $(4.21)_2$ is constructed so that $\mathbf{\Lambda}_\varepsilon$ *remains orthogonal* and thus defines a possible orientation of the moving frame. Hence, by construction, $\boldsymbol{\phi}_\varepsilon \in C$, for all $\varepsilon \in \mathbb{R}$.

For simplicity, in what follows attention is focused on the boundary value problem in which displacements and rotations are the prescribed boundary data. Accordingly, the set of kinematically admissible variations about the configuration $\boldsymbol{\phi} = (\boldsymbol{\phi}_o, \mathbf{\Lambda})$ is the tangent space to the configuration space C at the "base point" $\boldsymbol{\phi} \in C$ defined by

$$T_{\boldsymbol{\phi}}C := \{\boldsymbol{\eta}(S) = (\boldsymbol{\eta}_o(S), \overset{\vee}{\boldsymbol{\psi}}(S)\,\mathbf{\Lambda}(S)) \in \mathbb{R}^3 \times T_{\mathbf{\Lambda}}SO(3) \;\mid\; \boldsymbol{\eta}_o\big|_{S\in\{0,L\}} = \boldsymbol{\psi}\big|_{S\in\{0,L\}} = 0\} \tag{4.22}$$

A pair $\boldsymbol{\eta}(S) = (\boldsymbol{\eta}_o(S), \boldsymbol{\psi}(S)) \in \mathbb{R}^3 \times \mathbb{R}^3$ is referred to as an admissible variation.

4.3.2. Linearization of strain measures

We now consider the linearization of the strain measures summarized in Box 4.2. The basic set-up is as above: Given a configuration $\boldsymbol{\phi} = (\boldsymbol{\phi}_o, \mathbf{\Lambda}) \in C$, we consider an admissible variation $\boldsymbol{\eta} = (\boldsymbol{\eta}_o, \boldsymbol{\psi})$ and the corresponding perturbed configuration $\boldsymbol{\phi}_\varepsilon \in C$ defined in (4.21). First, note that by taking the directional derivative one has

$$\begin{aligned} D\boldsymbol{\phi}_o \cdot \boldsymbol{\eta}_o &:= \left.\frac{d}{d\varepsilon}\right|_{\varepsilon=0} \boldsymbol{\phi}_{o\varepsilon}(S) = \boldsymbol{\eta}_o(S) \\ D\mathbf{\Lambda} \cdot \overset{\vee}{\boldsymbol{\psi}} &:= \left.\frac{d}{d\varepsilon}\right|_{\varepsilon=0} \mathbf{\Lambda}_\varepsilon(S) = \overset{\vee}{\boldsymbol{\psi}}(S)\, \mathbf{\Lambda}(S) \end{aligned} \tag{4.23}$$

where we made use of the definition of the exponential map in (4.5a). It is not surprising to note that the above linearized quantities lie in the tangent space of C at $\boldsymbol{\phi}$. Next, we proceed to linearize the strain measures in Box 4.2 about the configuration $\boldsymbol{\phi} \in C$.

Linearization of curvature tensors. Making use of the definition of $\overset{\vee}{\boldsymbol{\omega}}$ in Box 4.1, we have

$$\overset{\vee}{\boldsymbol{\omega}}_\varepsilon = \frac{d\mathbf{\Lambda}_\varepsilon}{dS}\mathbf{\Lambda}_\varepsilon^T = \left(\frac{d\exp[\varepsilon\overset{\vee}{\boldsymbol{\psi}}]}{dS}\right)\exp[-\varepsilon\overset{\vee}{\boldsymbol{\psi}}] + \exp[\varepsilon\overset{\vee}{\boldsymbol{\psi}}]\overset{\vee}{\boldsymbol{\omega}}\exp[-\varepsilon\overset{\vee}{\boldsymbol{\psi}}] \tag{4.24}$$

Making use of the definition of the exponential map (4.5a), it can be easily seen that

$$\left.\frac{d}{d\varepsilon}\right|_{\varepsilon=0} \left(\frac{d\exp[\varepsilon\overset{\vee}{\boldsymbol{\psi}}]}{dS}\right)\exp[-\varepsilon\overset{\vee}{\boldsymbol{\psi}}] = \frac{d\overset{\vee}{\boldsymbol{\psi}}}{dS} \tag{4.25}$$

Therefore, with the aid of (4.25), the linearized spatial curvature tensor may be expressed as

$$D\overset{\vee}{\boldsymbol{\omega}} \cdot \boldsymbol{\psi} = \left.\frac{d}{d\varepsilon}\right|_{\varepsilon=0} \overset{\vee}{\boldsymbol{\omega}}_\varepsilon = \frac{d\overset{\vee}{\boldsymbol{\psi}}}{dS} + \overset{\vee}{\boldsymbol{\psi}}\overset{\vee}{\boldsymbol{\omega}} - \overset{\vee}{\boldsymbol{\omega}}\overset{\vee}{\boldsymbol{\psi}} \tag{4.26}$$

Similarly for the material curvature tensor $\overset{\mathbf{v}}{\boldsymbol{\Omega}}$, since $\overset{\mathbf{v}}{\boldsymbol{\Omega}}_\varepsilon = \boldsymbol{\Lambda}_\varepsilon^T \frac{\partial \boldsymbol{\Lambda}_\varepsilon}{\partial S}$, an analogous calculation shows that

$$D\overset{\mathbf{v}}{\boldsymbol{\Omega}}\cdot\boldsymbol{\psi} := \left.\frac{d}{d\varepsilon}\right|_{\varepsilon=0} \overset{\mathbf{v}}{\boldsymbol{\Omega}}_\varepsilon = \boldsymbol{\Lambda}^T \frac{d\overset{\mathbf{v}}{\boldsymbol{\psi}}}{dS}\boldsymbol{\Lambda} \tag{4.27}$$

Linearization of curvature axial vectors. In order to obtain the linearization of $\boldsymbol{\omega}(S)$, one simply needs to express (4.26) in terms of axial vectors. For this purpose, recall that the commutator (Lie bracket) of two skew-symmetric matrices may be expressed as

$$[\overset{\mathbf{v}}{\boldsymbol{\psi}}, \overset{\mathbf{v}}{\boldsymbol{\omega}}]\mathbf{h} := (\overset{\mathbf{v}}{\boldsymbol{\psi}}\overset{\mathbf{v}}{\boldsymbol{\omega}} - \overset{\mathbf{v}}{\boldsymbol{\omega}}\overset{\mathbf{v}}{\boldsymbol{\psi}})\mathbf{h} = (\boldsymbol{\psi}\times\boldsymbol{\omega})\times\mathbf{h}, \quad \forall\ \mathbf{h}\in\mathbb{R}^3. \tag{4.28}$$

Therefore, the linearized spatial curvature tensor in (4.26) can be written as

$$(D\overset{\mathbf{v}}{\boldsymbol{\omega}}\cdot\overset{\mathbf{v}}{\boldsymbol{\psi}})\mathbf{h} = (\frac{d\boldsymbol{\psi}}{dS} + \boldsymbol{\psi}\times\boldsymbol{\omega})\times\mathbf{h}, \quad \forall\ \mathbf{h}\in\mathbb{R}^3, \tag{4.29a}$$

from which follows the linearized spatial curvature vector

$$D\boldsymbol{\omega}\cdot\boldsymbol{\psi} = \frac{d\boldsymbol{\psi}}{dS} + \boldsymbol{\psi}\times\boldsymbol{\omega} \tag{4.29b}$$

The axial vector of the linearized material curvature tensor in (4.27) provides directly the linearization of the material curvature vector $\boldsymbol{\Omega}$

$$D\boldsymbol{\Omega}\cdot\boldsymbol{\psi} = \boldsymbol{\Lambda}^T \frac{d\boldsymbol{\psi}}{dS} \tag{4.30}$$

This follows from the relationship noted in (4.9) on parallel transport. Note that the same result would be obtained from the definition $\boldsymbol{\Omega}_\varepsilon = \boldsymbol{\Lambda}_\varepsilon^T\boldsymbol{\omega}_\varepsilon$ and using $(4.23)_2$ together with (4.29b).

Linearization of strain measure $\boldsymbol{\Gamma}$. Applying the directional derivative to the expression of $\boldsymbol{\Gamma}$ given in Box 4.2, we obtain

$$\begin{aligned} D\boldsymbol{\Gamma}\cdot\boldsymbol{\eta} := \left.\frac{d}{d\varepsilon}\right|_{\varepsilon=0} \boldsymbol{\Gamma}_\varepsilon &= \left.\frac{d}{d\varepsilon}\right|_{\varepsilon=0} (\boldsymbol{\Lambda}_\varepsilon^T\boldsymbol{\phi}_{o\varepsilon}' - \mathbf{E}_3) \\ &= \boldsymbol{\Lambda}^T(\frac{d\boldsymbol{\eta}_o}{dS} - \boldsymbol{\psi}\times\frac{d\boldsymbol{\phi}_o}{dS}) \end{aligned} \tag{4.31}$$

Remark 4.1. The linearized material curvature vector $D\Omega\cdot\psi$ and the linearized material strain $D\Gamma\cdot\eta$ are material objects and have their components expressed relative to the material basis $\{\mathbf{E}_i\}$, even though $\eta = (\eta_o, \psi)$ are spatial objects. Their spatial counterparts can be obtained by parallel transport using the orthogonal transformation $\mathbf{\Lambda}$, i.e.,

$$\mathbf{\Lambda} D\Omega\cdot\psi = \frac{d\psi}{dS}, \qquad \mathbf{\Lambda} D\Gamma\cdot\eta = \frac{d\eta_o}{dS} - \psi\times\frac{d\phi_o}{dS}. \tag{4.32}$$

The above procedure can be viewed as taking the Lie derivative: *pull-back* a spatial object along the flow to the material setting, take the derivative, then *push-forward* the differentiated object along the flow to the current position. ■

For convenience, the linearization of the strain measures in the spatial and material descriptions is summarized in Box 4.3, where a superposed "prime" designates the spatial derivative d/dS.

BOX 4.3. *Linearized strain measures* $(\eta := (\eta_o, \psi)\in T_\phi C)$

spatial	material
$\eta_o' - \psi\times\phi_o'$	$D\Gamma\cdot\eta = \mathbf{\Lambda}^T[\eta_o' - \psi\times\phi_o']$
ψ'	$D\Omega\cdot\psi = \mathbf{\Lambda}^T\psi'$

4.4. Tangent operator and symmetry condition

Weak form. Consider again any arbitrary admissible variation $\eta(S) = (\eta_o(S), \psi(S))\in T_\phi C$. Recall that in this chapter, we focus our attention on the static response of the rod; i.e., we shall consider only the left hand sides of equations (4.14a-b), referred to as balance equations, and ignore the inertia effects of the right hand side. Multiplying these balance equations by the

admissible variation η and integrating over the interval $[0, L]$, we obtain the weak form

$$G(\phi,\eta) := \int_{[0,L]} [(\frac{d\mathbf{n}}{dS} + \bar{\mathbf{n}}) \cdot \eta_o + (\frac{d\mathbf{m}}{dS} + \frac{d\phi_o}{dS} \times \mathbf{n} + \bar{\mathbf{m}}) \cdot \psi] dS = 0 \quad (4.33)$$

Integrating by parts (4.33) and making use of the boundary conditions $\eta(S)\big|_{S \in \{0,L\}} = 0$, we obtain the spatial weak form of the balance equations expressed as

$$G(\phi,\eta) = \int_{[0,L]} \{ \mathbf{n} \cdot [\frac{d\eta_o}{dS} - \psi \times \frac{d\phi_o}{dS}] + \mathbf{m} \cdot \frac{d\psi}{dS} \} dS$$

$$- \int_{[0,L]} (\bar{\mathbf{n}} \cdot \eta_o + \bar{\mathbf{m}} \cdot \psi) dS = 0, \quad \forall \eta \in T_\phi C. \quad (4.34)$$

Concerned mainly with the development of a displacement type finite element formulation, we shall assume that constitutive equations (4.15-16) hold strongly, or point-wise.

To perform the linearization of the weak form of momentum balance, it is convenient to rephrase (4.34) in material form. Making use of relations (4.12) we obtain the following alternative (material) expression of (4.34)

$$G(\phi,\eta) = \int_{[0,L]} \left\{ \mathbf{N} \cdot \Lambda^T [\frac{d\eta_o}{dS} - \psi \times \frac{d\phi_o}{dS}] + \mathbf{M} \cdot \Lambda^T \frac{d\psi}{dS} \right\} dS$$

$$- \int_{[0,L]} (\bar{\mathbf{n}} \cdot \eta_o + \bar{\mathbf{m}} \cdot \psi) dS, \quad \forall \eta \in T_\phi C. \quad (4.35)$$

4.4.1. Consistent Linearization of weak form

A complete account of linearization procedures relevant to the problem at hand is given in Marsden & Hughes [1983, Chap. 4]. Here, we proceed in the context discussed in Section 4.3. Denote by $L[G(\hat{\phi},\eta)]$ the linear part of the functional $G(\phi,\eta)$ at the configuration $\phi = \hat{\phi} = (\hat{\phi}_o, \hat{\Lambda})$. By definition, we have

$$L[G(\hat{\boldsymbol{\phi}},\boldsymbol{\eta})] = G(\hat{\boldsymbol{\phi}},\boldsymbol{\eta}) + DG(\hat{\boldsymbol{\phi}},\boldsymbol{\eta})\cdot\Delta\boldsymbol{\phi}\,. \tag{4.36a}$$

where $\Delta\boldsymbol{\phi} := (\Delta\mathbf{u}, \Delta\boldsymbol{\vartheta}) \in T_{\boldsymbol{\phi}}C$ designates incremental displacements, and the (Frechet) differential $DG(\hat{\boldsymbol{\phi}},\boldsymbol{\eta})$, linear in $\Delta\boldsymbol{\phi}$, is obtained through the directional derivative formula

$$DG(\hat{\boldsymbol{\phi}},\boldsymbol{\eta})\cdot\Delta\boldsymbol{\phi} = \left.\frac{d}{d\varepsilon}\right|_{\varepsilon=0} G(\boldsymbol{\phi}_\varepsilon,\boldsymbol{\eta}) \tag{4.36b}$$

where $\boldsymbol{\phi}_\varepsilon$ denotes the curve of perturbed configuration about $\hat{\boldsymbol{\phi}}$ as given in (4.21). Away from the equilibrium configuration, the term $G(\hat{\boldsymbol{\phi}},\boldsymbol{\eta})$ in (4.36a) supplies the residual (or unbalanced) force at the configuration $\hat{\boldsymbol{\phi}}\in C$ and the term $DG(\hat{\boldsymbol{\phi}},\boldsymbol{\eta})$, a linear operator, is referred to as the tangent stiffness operator. Searching for the equilibrium configuration $\boldsymbol{\phi} \in C$, i.e., the weak solution to the balance equations characterized by $G(\boldsymbol{\phi},\boldsymbol{\eta}) = 0$, $\forall\, \boldsymbol{\eta} \in T_{\boldsymbol{\phi}}C$, the classical Newton iterative solution procedure may be employed such that at iteration (i) we solve for the incremental displacement $\Delta\boldsymbol{\phi}^{(i)}$ by setting

$$L[G(\boldsymbol{\phi}^{(i)},\boldsymbol{\eta})] = G(\boldsymbol{\phi}^{(i)},\boldsymbol{\eta}) + DG(\boldsymbol{\phi}^{(i)},\boldsymbol{\eta})\cdot\Delta\boldsymbol{\phi}^{(i)} = 0\,,\quad \forall\ \boldsymbol{\eta} \in T_{\boldsymbol{\phi}^{(i)}}C \tag{4.36c}$$

where $\boldsymbol{\phi}^{(i)} \in C$ is known. We then proceed to update the configuration $\boldsymbol{\phi}^{(i)}$ to a new configuration $\boldsymbol{\phi}^{(i+1)}$ using the incremental displacement $\Delta\boldsymbol{\phi}^{(i)}$, solution of (4.36c). One of the salient features of the present formulation rests on an update procedure that forces the iterated solutions $\boldsymbol{\phi}^{(k)}$ to remain in the configuration manifold C, for all k. In fact, this update procedure is the discrete counterpart of the curves of perturbed configuration defined in (4.21). We shall now proceed to obtain the expression for the tangent stiffness operator.

The weak form (4.35) may be rephrased in a more compact form by introducing the following notation. Define *material* and *spatial* vectors of resultant stresses and stress couples, $\mathbf{R}$ and $\mathbf{r}$, by setting

$$\mathbf{R} := \begin{Bmatrix} \mathbf{N} \\ \mathbf{M} \end{Bmatrix}, \quad \mathbf{r} := \begin{Bmatrix} \mathbf{n} \\ \mathbf{m} \end{Bmatrix} = \Pi \mathbf{R}, \quad \text{where} \quad \Pi := \begin{bmatrix} \Lambda & \mathbf{0} \\ \mathbf{0} & \Lambda \end{bmatrix} \tag{4.37}$$

In addition, introduce a matrix differential operator Ξ, similar to (2.46), defined as

$$\Xi(\phi_o) := \begin{bmatrix} \frac{d}{dS}\mathbf{1}_3 & [\phi_o{}' \times] \\ \mathbf{0} & \frac{d}{dS}\mathbf{1}_3 \end{bmatrix} \tag{4.38a}$$

where a superposed prime, $(\cdot)'$, denotes differentiation with respect to S, and recall that $\mathbf{1}_3 := Diag\,[1, 1, 1]$ is the identity matrix. In addition, $[\phi_o{}' \times] \equiv \overset{\mathbf{v}}{\phi}_o{}'$ is the skew-symmetric matrix associated with the axial vector $\phi_o{}' = \phi_{oi}{}' \mathbf{e}_i$, and $\frac{d}{dS}\mathbf{1}_3$ is the block diagonal operator defined below,

$$[\phi_o{}' \times] := \begin{bmatrix} 0 & -\phi_{o3}{}' & \phi_{o2}{}' \\ \phi_{o3}{}' & 0 & -\phi_{o1}{}' \\ -\phi_{o2}{}' & \phi_{o1}{}' & 0 \end{bmatrix}, \quad \frac{d}{dS}\mathbf{1}_3 := Diag\,[\tfrac{d}{dS}, \tfrac{d}{dS}, \tfrac{d}{dS}] \tag{4.38b}$$

With this notation at hand, equation (4.35) may then be recast as

$$G(\phi, \eta) = \int_{[0,L]} [(\Xi\eta) \cdot (\Pi \mathbf{R}) - \eta \cdot \bar{\mathbf{r}}]\, dS \tag{4.39}$$

where $\bar{\mathbf{r}}^T := [\bar{\mathbf{n}}, \bar{\mathbf{m}}]^T$. To obtain the linear part (4.36) of (4.39) we need to obtain the expression for the linearized constitutive equations. First, note that with the aid of Ξ defined by (4.38a), the results in Box 2 may be expressed as

$$\begin{Bmatrix} D\mathbf{r}(\hat{\phi}) \cdot \Delta\mathbf{u} \\ D\Omega(\hat{\phi}) \cdot \Delta\vartheta \end{Bmatrix} = \Pi^T(\hat{\mathbf{A}})\, \Xi(\hat{\phi}) \begin{Bmatrix} \Delta\mathbf{u} \\ \Delta\vartheta \end{Bmatrix} = \Pi^T(\hat{\mathbf{A}})\, \Xi(\hat{\phi})\, \Delta\phi\,. \tag{4.40}$$

Thus, on account of (4.16-17), the linearized internal force is given by

$$D\mathbf{R}(\hat{\phi}) \cdot \Delta\phi = \mathbf{C}(\hat{\phi}) \begin{Bmatrix} D\mathbf{r}(\hat{\phi}) \cdot \Delta\mathbf{u} \\ D\Omega(\hat{\phi}) \cdot \Delta\vartheta \end{Bmatrix} = \mathbf{C}(\hat{\phi})\, \Pi(\hat{\mathbf{A}})\, \Xi^T(\hat{\phi})\, \Delta\phi\,. \tag{4.41}$$

where $\mathbf{C}(\hat{\boldsymbol{\phi}})$ is the material tangent elasticity tensor given by (4.17). Linearization of (4.39) leads to :

$$DG(\hat{\boldsymbol{\phi}},\boldsymbol{\eta})\cdot\Delta\boldsymbol{\phi} \;=\; D_S G(\hat{\boldsymbol{\phi}},\boldsymbol{\eta})\cdot\Delta\boldsymbol{\phi} + D_C G(\hat{\boldsymbol{\phi}},\boldsymbol{\eta})\cdot\Delta\boldsymbol{\phi} \tag{4.42}$$

where the term $D_S G(\hat{\boldsymbol{\phi}},\boldsymbol{\eta})$ results from the linearization of the internal force $\mathbf{R}$, and corresponds to the *material* part of the tangent stiffness operator,

$$D_S G(\hat{\boldsymbol{\phi}},\boldsymbol{\eta})\cdot\Delta\boldsymbol{\phi} \;=\; \int_{[0,L]} [\boldsymbol{\Xi}(\hat{\boldsymbol{\phi}})\boldsymbol{\eta}]\cdot[\boldsymbol{\Pi}(\hat{\mathbf{A}})\,\mathbf{C}\boldsymbol{\Pi}^T(\hat{\mathbf{A}})\,\boldsymbol{\Xi}(\hat{\boldsymbol{\phi}})\,\Delta\boldsymbol{\phi}]\,dS\,. \tag{4.43}$$

The second term, $D_C G(\hat{\boldsymbol{\phi}},\boldsymbol{\eta})$ is referred to as the tangent *geometric* stiffness operator, and results from the linearization of the operator $[\boldsymbol{\Xi}\,\boldsymbol{\Pi}]$ defined in (4.37-38),

$$D_C G(\hat{\boldsymbol{\phi}},\boldsymbol{\eta})\;\cdot\;\Delta\boldsymbol{\phi} \;=\; \int_{[0,L]} [\mathbf{T}\,\boldsymbol{\eta}]\cdot[\mathbf{B}(\hat{\boldsymbol{\phi}})\,\mathbf{T}\,\Delta\boldsymbol{\phi}]\,dS\,, \tag{4.44}$$

where, $\mathbf{T}$ is a matrix differential operator,

$$\mathbf{T}^T := \begin{bmatrix} \dfrac{d}{dS}\mathbf{1}_3 & \mathbf{0} & \mathbf{0} \\ \mathbf{0} & \dfrac{d}{dS}\mathbf{1}_3 & \mathbf{1}_3 \end{bmatrix}, \tag{4.45}$$

and $\mathbf{B}$ a matrix of the form

$$\mathbf{B}(\boldsymbol{\phi}) \;:=\; \begin{bmatrix} \mathbf{0} & \mathbf{0} & [-\mathbf{n}\times] \\ \mathbf{0} & \mathbf{0} & [-\mathbf{m}\times] \\ [\mathbf{n}\times] & \mathbf{0} & [\mathbf{n}\otimes\boldsymbol{\phi}_o{}' - (\mathbf{n}\cdot\boldsymbol{\phi}_o{}')\mathbf{1}_3] \end{bmatrix}. \tag{4.46}$$

Recall that $[(\,\cdot\,)\times]$ denotes the skew-symmetric matrix whose axial vector is given by $(\,\cdot\,)$. Inspection of (4.46) reveals that the geometric stiffness $\mathbf{B}$ is generally non-symmetric. Hence, it appears that the geometric tangent operator given by (4.44) is *non-symmetric*. We show next that this is indeed the case only if the configuration $\hat{\boldsymbol{\phi}}\in C$ is not an equilibrium configuration.

4.4.2. Existence condition for potential: Symmetry of tangent operator

To examine the nature of the lack in symmetry of the tangent $DG(\hat{\boldsymbol{\phi}},\eta)\cdot\Delta\boldsymbol{\phi}$ we consider the skew-symmetric part given by

$$[DG(\hat{\boldsymbol{\phi}},\eta)\cdot\Delta\boldsymbol{\phi}]^A := D_2G(\hat{\boldsymbol{\phi}},\eta)\cdot\Delta\boldsymbol{\phi} - D_2G(\hat{\boldsymbol{\phi}},\Delta\boldsymbol{\phi})\cdot\eta$$

$$= \int_{[0,L]} [\mathbf{T}\eta]\cdot[\mathbf{B}^A(\hat{\boldsymbol{\phi}})\,\mathbf{T}\,\Delta\boldsymbol{\phi}]\,dS \tag{4.47}$$

where $\mathbf{B}^A := \frac{1}{2}[\mathbf{B}-\mathbf{B}^T]$. We have

$$[DG(\hat{\boldsymbol{\phi}},\eta)\cdot\Delta\boldsymbol{\phi}]^A = \int_{[0,L]} \{\mathbf{m}\cdot[\boldsymbol{\psi}\times\Delta\boldsymbol{\vartheta}' - \Delta\boldsymbol{\vartheta}\times\boldsymbol{\psi}'] + \mathbf{n}\cdot[\Delta\boldsymbol{\vartheta}\times(\boldsymbol{\psi}\times\hat{\boldsymbol{\phi}}_o') - \boldsymbol{\psi}\times(\Delta\boldsymbol{\vartheta}\times\hat{\boldsymbol{\phi}}_o')]\}\,dS$$

$$= \int_{[0,L]} \{\mathbf{m}\cdot(\boldsymbol{\psi}\times\Delta\boldsymbol{\vartheta})' + \mathbf{n}\cdot[(\Delta\boldsymbol{\vartheta}\cdot\hat{\boldsymbol{\phi}}_o')\boldsymbol{\psi} - (\boldsymbol{\psi}\cdot\hat{\boldsymbol{\phi}}_o')\Delta\boldsymbol{\vartheta}]\}\,dS$$

$$= \int_{[0,L]} \{\mathbf{m}\cdot(\boldsymbol{\psi}\times\Delta\boldsymbol{\vartheta})' - \mathbf{n}\cdot[(\boldsymbol{\psi}\times\Delta\boldsymbol{\vartheta})\times\hat{\boldsymbol{\phi}}_o']\}\,dS \tag{4.48}$$

Integration by parts of (4.48) finally yields

$$[DG(\hat{\boldsymbol{\phi}},\eta)\cdot\Delta\boldsymbol{\phi}]^A = -\int_{[0,L]} [\mathbf{m}' + \hat{\boldsymbol{\phi}}_o'\times\mathbf{n} + \bar{\mathbf{m}}]\cdot(\boldsymbol{\psi}\times\Delta\boldsymbol{\vartheta})\,dS$$

$$+ \int_{[0,L]} \bar{\mathbf{m}}\cdot(\boldsymbol{\psi}\times\Delta\boldsymbol{\vartheta})\,dS + [\mathbf{m}\cdot(\boldsymbol{\psi}\times\Delta\boldsymbol{\vartheta})]\Big|_{S=0}^{S=L} \tag{4.49}$$

It follows that for our choice of $T_{\boldsymbol{\phi}}C$ given by (4.22) $\mathbf{m}\cdot(\boldsymbol{\psi}\times\Delta\boldsymbol{\vartheta})\Big|_{S=0}^{S=L} = 0$. In addition, the first term in (4.49) is simply the weighted form of the the static version of the local balance of angular momentum equation (4.14b). Accordingly, this term vanishes at an equilibrium configuration. Thus, (4.49) vanishes identically provided that $\bar{\mathbf{m}} = 0$ and the configuration $\hat{\boldsymbol{\phi}}$ is in equilibrium.

Remark 4.1. The condition of no distributed moment $\bar{\mathbf{m}} = 0$, appears to be in agreement with the fact pointed out by Ziegler [1977] and elaborated upon by Argyris and co-workers [1978,1980,1982], that loading by "moments with fixed axes" is non-conservative. The *boundary* term $\mathbf{m}\cdot(\boldsymbol{\psi}\times\Delta\boldsymbol{\vartheta})\Big|_{S=0}^{S=L} = 0$ in (4.49)

vanishes identically for most boundary conditions of practical interest, such as simply supported, clamped, or free end. Other boundary conditions which result in cancellation of this boundary term are possible. However, this term does *not* vanish for the case of an *applied end moment with "fixed spatial axis,"* and thus this type of loading is non-conservative (see, e.g., Argyris and co-workers [1978]). The condition of conservative loading expressed by

$$\int_{[0,L]} \overline{\mathbf{m}} \cdot (\boldsymbol{\psi} \times \Delta\boldsymbol{\vartheta})\, dS + [\mathbf{m} \cdot (\boldsymbol{\psi} \times \Delta\boldsymbol{\vartheta})]\Big|_{S=0}^{S=L} = 0 \tag{4.50}$$

is analogous in structure to that arising in pressure dependent loading (Bufler [1984], Schweizerhof & Ramm [1984]). ■

In view of expression (4.49) the following conclusion can be stated :

(i) At an *equilibrium* configuration, the symmetry of the tangent stiffness depends solely upon external loading and boundary conditions; e.g., depends on whether the loading is conservative. The possible lack of symmetry at an equilibrium configuration is not related in any way to the presence of the classical rotation group SO(3) in the configuration space. The fact that a potential exists if (4.49) vanishes is the result of a well-known theorem due to Vainberg (see Marsden & Hughes [1983, Sec. 1.7] for a discussion in the general context of manifolds).

(ii) At a *non-equilibrated* configuration, the tangent operator is *non-symmetric* in general, even for conservative loading. The reason for this is again found in the fact that the configuration space C is a *nonlinear manifold*.

4.5. Treatment of follower force

Several practical applications require the ability to account for the action of a follower force, which depends on the current configuration, in the formulation. Such a loading condition can be accommodated easily within the present context. Consider, for instance, the case of a distributed load characterized by

$$\bar{\mathbf{n}}^{nc} := N_I^{nc}\,\mathbf{t}_I, \qquad \text{where} \qquad N_I^{nc} = CONST., \tag{4.51}$$

which follows the deformation of the cross section determined by the frame $\{\mathbf{t}_I\}$, and thus has constant components relative to this frame. The non-conservative loading in (4.51) in fact falls into the category of follower load of the circulatory type —that is, loading which is not derivable from a potential and not explicitly dependent on time. By virtue of (4.1c), the loading $\bar{\mathbf{n}}^{nc}$ can be expressed in terms of the spatial basis $\{\mathbf{e}_i\}$ as

$$\bar{\mathbf{n}}^{nc}(\Lambda) = \Lambda_{iI}\, N_I^{nc}\, \mathbf{e}_i\,, \tag{4.52}$$

expliciting its dependence on the configuration (specifically, the rotation field).

The contribution of $\bar{\mathbf{n}}^{nc}$ to the weak form of momentum balance is then given in the standard manner as

$$G^{nc}(\boldsymbol{\phi}, \boldsymbol{\eta}) = -\int_{[0,L]} \boldsymbol{\eta}_0 \cdot \bar{\mathbf{n}}^{nc}(\Lambda)\, dS \tag{4.53}$$

Previously, in the linearization of the weak form $G(\boldsymbol{\phi}, \boldsymbol{\eta})$, we have assumed that the external load is spatially fixed, and hence no contribution of the loading term to the tangent stiffness operator results. Here, with the configuration dependent loading defined above, such contribution to the tangent stiffness operator can easily be computed by noting that, for any variation $\Delta\boldsymbol{\phi} := (\Delta\mathbf{u}, \Delta\boldsymbol{\vartheta}) \in T_{\boldsymbol{\phi}}C$, the moving frame $\{\mathbf{t}_I\}_{I=1,2,3}$ is "perturbed" according to

$$D\mathbf{t}_I \cdot \Delta\boldsymbol{\phi} = \Delta\boldsymbol{\vartheta} \times \mathbf{t}_I, \qquad (I = 1,2,3) \tag{4.54}$$

Consequently, since $N^{nc} = CONST.$, it follows that $D\bar{\mathbf{n}}^{nc} \cdot \Delta\boldsymbol{\phi} = \Delta\boldsymbol{\vartheta} \times \bar{\mathbf{n}}^{nc}$, so that the contribution to the tangent stiffness, referred to as the tangent load stiffness, becomes

$$D_L G(\hat{\boldsymbol{\phi}}, \boldsymbol{\eta}) \cdot \Delta\boldsymbol{\phi} := DG^{nc}(\hat{\boldsymbol{\phi}}, \boldsymbol{\eta}) \cdot \Delta\boldsymbol{\phi}$$

$$= -\int_{[0,L]} \boldsymbol{\eta}_o \cdot [\Delta\boldsymbol{\vartheta} \times \bar{\mathbf{n}}^{nc}(\hat{\mathbf{A}})]\, dS = \int_{[0,L]} \boldsymbol{\eta}_o \cdot [\bar{\mathbf{n}}^{nc}(\hat{\mathbf{A}})\times]\, \Delta\boldsymbol{\vartheta}\, dS \tag{4.55}$$

where we recall that $[(\,\cdot\,)\times]$ denotes the skew-symmetric matrix whose axial vector is $(\,\cdot\,)$. The tangent stiffness operator in (4.42) now has an additional term,

$$DG(\hat{\boldsymbol{\phi}}, \boldsymbol{\eta}) \cdot \Delta\boldsymbol{\phi} = [\, D_S + D_G + D_L \,]\, G(\hat{\boldsymbol{\phi}}, \boldsymbol{\eta}) \cdot \Delta\boldsymbol{\phi}\,. \tag{4.56}$$

Remark 4.2. The case of pressure loading, characterized by the condition that an applied distributed load remains *normal to the line of centroids* in all configurations, often arises in applications. This type of loading condition may be easily characterized by introducing a second moving frame $\{\mathbf{a}_1, \mathbf{a}_2, \mathbf{a}_3\}$ such that $\mathbf{a}_3$ is tangent to the deformed line of centroids. Accordingly, we may set

$$\mathbf{a}_3 := \frac{\boldsymbol{\phi}'_o}{\|\boldsymbol{\phi}'_o\|}, \quad \mathbf{a}_2 := \frac{[1_3 - \mathbf{a}_3 \otimes \mathbf{a}_3]\, \mathbf{t}_2}{\|[1_3 - \mathbf{a}_3 \otimes \mathbf{a}_3]\, \mathbf{t}_2\|}, \quad \mathbf{a}_1 := \mathbf{a}_2 \times \mathbf{a}_3 \tag{4.57}$$

Recall that $[1_3 - \mathbf{a}_3 \otimes \mathbf{a}_3]$ simply represents the projection operator onto a plane with normal $\mathbf{a}_3$. The pressure loading may then be expressed as $\bar{\mathbf{n}} = p\,\mathbf{a}_1 + q\,\mathbf{a}_2$. The contribution to the tangent stiffness may be computed with the aid of the directional derivative; the derivation is straightforward but lengthy, and will not be pursued further. ■

4.6. Spatial discretization and update procedure

We now consider the (spatial) discretization of the tangent stiffness operator obtained in Section 4.4. The Galerkin discretization procedure follows steps identical to those outlined in Section 2.4.3 for the plane case. However, from a known configuration $\boldsymbol{\phi}^{(i)} \in C$ together with a given incremental displacement $\Delta\boldsymbol{\phi}^{(i)}$, the basic problem is how to obtain an updated configuration that remains in the configuration space, i.e., $\boldsymbol{\phi}^{(i+1)} \in C$. In addition, it is essential that the spatial curvature vector $\boldsymbol{\omega}$ be updated in a consistent manner with the update of the orthogonal transformation $\mathbf{A}$, which defines the orientation of the cross section.

We shall first obtain the spatial dicretization of the tangent operator, then discuss in detail the update procedure in its conceptual form as well as the practical consideration for its implementation.

4.6.1. Discrete tangent operator: Galerkin finite element method

Let the interval $[0, L]$ be subdivided into subintervals with a total number of nodes N, that is, $[0, L] = \bigcup_{k=1}^{N-1} [S_k, S_{k+1}]$ with $S_j \in [0, L]$, $\forall\, j=1,\ldots,N$ such that $S_j < S_{j+1}$. Consider the following standard finite element discretization of the incremental displacement $\Delta\boldsymbol{\phi} := (\Delta\mathbf{u}, \Delta\boldsymbol{\vartheta}) \in T_{\boldsymbol{\phi}}C$ from a known configuration $\boldsymbol{\phi} \in C$,

$$\Delta\mathbf{u}(S) = \Delta u_i(S)\,\mathbf{e}_i \in \mathbb{R}^3, \quad \Delta\boldsymbol{\vartheta}(S) = \Delta\vartheta_i(S)\,\mathbf{e}_i \in \mathbb{R}^3, \tag{4.58a}$$

$$\Delta\mathbf{u}(S) \cong \sum_{I=1}^{N} [N_I(S)\mathbf{1}_3]\Delta\mathbf{u}_I, \quad \Delta\boldsymbol{\vartheta}(S) \cong \sum_{I=1}^{N} [N_I(S)\mathbf{1}_3]\Delta\boldsymbol{\vartheta}_I, \tag{4.58b}$$

where $N_I(S)$ denotes the global finite element shape functions, $\mathbf{1}_k := Diag[1,\ldots,1]$ the unit $k\times k$ matrix, $\Delta\mathbf{u}_I \cong \Delta\mathbf{u}(S_I)$, and $\Delta\boldsymbol{\vartheta}_I \cong \Delta\boldsymbol{\vartheta}(S_I)$. We recall that $T_{\boldsymbol{\phi}}C$ is isomorphic to $\mathbb{R}^3\times\mathbb{R}^3$; this linear space is approximated by a

finite dimensional subspace defined by the discretization (4.58b). Further, let the admissible variations (weighting functions) $\boldsymbol{\eta} := (\boldsymbol{\eta}_o, \boldsymbol{\psi}) \in T_{\boldsymbol{\phi}} C$ be discretized in the same manner

$$\boldsymbol{\eta}_o(S) \cong \sum_{I=1}^{N} [N_I(S)\mathbf{1}_3]\boldsymbol{\eta}_{oI} , \quad \boldsymbol{\psi}(S) \cong \sum_{I=1}^{N} [N_I(S)\mathbf{1}_3]\boldsymbol{\psi}_I . \tag{4.58c}$$

with $\boldsymbol{\eta}_{o_I} := \boldsymbol{\eta}_o(S_I)$ and $\boldsymbol{\psi}_I := \boldsymbol{\psi}(S_I)$. The linear part of the weak form about a configuration $\hat{\boldsymbol{\phi}} \in C$ as given in (4.36c) can then be written in the discretized form

$$L[G(\hat{\boldsymbol{\phi}}, \boldsymbol{\eta})] \cong \sum_{I=1}^{N} \boldsymbol{\eta}_I \{ \mathbf{P}_I(\hat{\boldsymbol{\phi}}) + \sum_{J=1}^{N} [\mathbf{S}_{IJ}(\hat{\boldsymbol{\phi}}) + \mathbf{G}_{IJ}(\hat{\boldsymbol{\phi}}) + \mathbf{L}_{IJ}(\hat{\boldsymbol{\Lambda}})] \Delta\boldsymbol{\phi}_J \} = 0 \tag{4.59a}$$

$\forall\, \boldsymbol{\eta}_I$, where $\Delta\boldsymbol{\phi}_J := (\Delta\mathbf{u}_J, \Delta\boldsymbol{\vartheta}_J)$. In (4.59a), $\mathbf{P}_I$ is the residual force at configuration $\boldsymbol{\phi} = \hat{\boldsymbol{\phi}}$, the discrete counterpart of $G(\hat{\boldsymbol{\phi}}, \boldsymbol{\eta})$; $\mathbf{S}_{IJ}$ and $\mathbf{G}_{IJ}$ denote respectively the tangent material stiffness matrix and the tangent geometric stiffness matrix, the discrete version of the tangent operator $DG(\hat{\boldsymbol{\phi}}, \boldsymbol{\eta})$; the tangent load stiffness $\mathbf{L}_{IJ}$ is only included in the case of follower loading of the type given in (4.51). It follows from (4.59a) that the incremental displacement is computed by solving the system of linear equations

$$\mathbf{P}_I(\hat{\boldsymbol{\phi}}) + \sum_{J=1}^{N} [\, \mathbf{S}_{IJ}(\hat{\boldsymbol{\phi}}) + \mathbf{G}_{IJ}(\hat{\boldsymbol{\phi}}) + \mathbf{L}_{IJ}(\hat{\boldsymbol{\Lambda}}) \,] \Delta\boldsymbol{\phi}_J = 0 , \quad \text{for } I=1,\ldots,N \tag{4.59b}$$

The expressions for the relevant matrices in (4.59b) are obtained as follows.

Residual force. Substitution of the discretization (4.58b-c) into the expression for $G(\hat{\boldsymbol{\phi}}, \boldsymbol{\eta})$ yields

$$\mathbf{P}_I(\hat{\boldsymbol{\phi}}) = \int_{[0,L]} \Big[\{ \boldsymbol{\Xi}(\hat{\boldsymbol{\phi}}_o)[N(S)\mathbf{1}_6] \}^T \mathbf{r}(\hat{\boldsymbol{\phi}}) - [N(S)\mathbf{1}_6]\bar{\mathbf{r}} \} \Big] dS \tag{4.60}$$

Tangent material stiffness matrix. It follows from the expression for the tangent material stiffness operator $D_S G(\hat{\boldsymbol{\phi}}, \boldsymbol{\eta})$ in (4.43), upon introducing the

approximation (4.58b-c), that

$$\mathbf{S}_{IJ}(\hat{\boldsymbol{\phi}}) = \int_{[0,L]} \{\Xi(\hat{\boldsymbol{\phi}}_o)[N_I(S)\mathbf{1}_6]\}^T \{\Pi(\hat{\mathbf{\Lambda}})\,\mathbf{C}\Pi^T(\hat{\mathbf{\Lambda}})\,\Xi(\hat{\boldsymbol{\phi}}_o)[N_J(S)\mathbf{1}_6]\}\,dS \quad (4.61)$$

Tangent geometric stiffness matrix. The discrete version of the tangent geometric stiffness operator $D_G(\hat{\boldsymbol{\phi}}, \boldsymbol{\eta})$ in (4.44) is given by

$$\mathbf{G}_{IJ}(\hat{\boldsymbol{\phi}}) = \int_{[0,L]} \{\mathbf{T}[N_I(S)\mathbf{1}_6]\}^T \{\mathbf{B}(\hat{\boldsymbol{\phi}})\,\mathbf{T}[N_J(S)\mathbf{1}_6]\}\,dS \quad (4.62)$$

Tangent load stiffness matrix. In the case where follower loading of the type given in (4.51) is applied, the discrete counterpart of the tangent load stiffness operator in (4.55) is given by

$$\mathbf{L}_{IJ}(\hat{\mathbf{\Lambda}}) = \int_{[0,L]} \begin{bmatrix} \mathbf{0} & N_I(S)\,N_J(S)\,[\bar{\mathbf{n}}^{nc}(\hat{\mathbf{\Lambda}})\times] \\ \mathbf{0} & \mathbf{0} \end{bmatrix} dS \quad (4.63)$$

We recall that the components of $\bar{\mathbf{n}}^{nc}(\hat{\mathbf{\Lambda}})$ relative to the spatial frame $\{\mathbf{e}_i\}$ is given in (4.52).

Computationally, the above integrals are evaluated using a uniformly reduced Gauss quadrature rule to avoid shear locking as mentioned in Section 2.4. The following approximation of the map $\boldsymbol{\phi}_o(S)$ and its spatial derivative $\boldsymbol{\phi}_o'(S)$,

$$\boldsymbol{\phi}_o(S) \cong \sum_{I=1}^{N} [N_I(S)\mathbf{1}_3]\boldsymbol{\phi}_{oI} \quad \text{and} \quad \boldsymbol{\phi}_o'(S) \cong \sum_{I=1}^{N} [N_I'(S)\mathbf{1}_3]\boldsymbol{\phi}_{oI}\,, \quad (4.64a)$$

are introduced to interpolate the values of $\boldsymbol{\phi}_o$ and of $\boldsymbol{\phi}_o'$ at the Gauss points from the nodal values $\boldsymbol{\phi}_{oI} := \boldsymbol{\phi}_o(S_I)$. On the other hand, there are two ways to obtain the values of $\mathbf{\Lambda}$ at the Gauss points: (i) either allocate memories for the components the $\mathbf{\Lambda}$'s at the Gauss points, and update these after each iteration, or (ii) interpolate the rotation vectors associated with the $\mathbf{\Lambda}$'s at the nodal points, then exponentiate to obtain the value of $\mathbf{\Lambda}$ at Gauss points as follows. At

the nodal points, we have $\mathbf{\Lambda}_I := \mathbf{\Lambda}(S_I)$, and let $\overset{\blacktriangledown}{\boldsymbol{\chi}}_I$ denote the nodal rotation vector associated with $\mathbf{\Lambda}_I$ such that $\mathbf{\Lambda}_I = \exp[\overset{\blacktriangledown}{\boldsymbol{\chi}}_I]$. Then we can use the following interpolation to compute the value of $\mathbf{\Lambda}$ at Gauss points

$$\mathbf{\Lambda}(S) = \exp\Big(\sum_{I=1}^{N} [N_I(S)\mathbf{1}_3]\overset{\blacktriangledown}{\boldsymbol{\chi}}_I\Big) . \tag{4.64b}$$

We shall next address the central issue concerning the update procedure for $(\boldsymbol{\phi}_o, \mathbf{\Lambda})$ and for the curvature vector $\boldsymbol{\omega}$.

4.6.2. Configuration and stress update algorithm

In principle, the configuration update procedure has been addressed earlier in Section 4.3.1 under the guise of the curves of perturbed configuration, which play a crucial role in the linearization process. In fact, as mentioned earlier, the configuration update is the discrete counterpart of the curves of perturbed configuration. It is well known that quadratic rate of convergence, characteristic of the Newton iterative solution, can only be achieved by a linearization that is consistent with respect to the update procedure.

Configuration update. Recall that at iteration (i), with known configuration $\boldsymbol{\phi}^{(i)} := (\boldsymbol{\phi}_o^{(i)}, \mathbf{\Lambda}^{(i)}) \in C$, we compute the incremental displacement $\Delta\boldsymbol{\phi}^{(i)} := (\Delta\mathbf{u}^{(i)}, \Delta\boldsymbol{\vartheta}^{(i)})$ by solving (4.59b). The updated configuration $\boldsymbol{\phi}^{(i+1)} := (\boldsymbol{\phi}_o^{(i+1)}, \mathbf{\Lambda}^{(i+1)}) \in C$ is then obtained from (4.21) by

$$\boldsymbol{\phi}_o^{(i+1)} = \boldsymbol{\phi}_o^{(i)} + \Delta\mathbf{u}^{(i)} , \quad \mathbf{\Lambda}^{(i+1)} = \exp[\Delta\overset{\blacktriangledown}{\boldsymbol{\vartheta}}^{(i)}]\, \mathbf{\Lambda}^{(i)} . \tag{4.65}$$

Next, the updated internal force $\mathbf{N}(\boldsymbol{\phi}^{(i+1)})$ and moment $\mathbf{M}(\boldsymbol{\phi}^{(i+1)})$ are required to evaluate the tangent geometric stiffness matrix $\mathbf{G}(\boldsymbol{\phi}^{(i+1)})$ for the next iteration. But before the internal force and moment can be updated, we need to address the

Strain update. The strain measure $\Gamma^{(i+1)}$ can be easily obtained from its expression in Box 4.2 and the updated configuration $(4.65)_1$ as

$$\Gamma^{(i+1)} = \mathbf{A}^{(i+1)T} \frac{d\boldsymbol{\phi}_0^{(i+1)}}{dS} - \mathbf{E}_3 \tag{4.66}$$

where $\dfrac{d\boldsymbol{\phi}_0^{(i+1)}}{dS}$ can be evaluated as in $(4.64a)_2$. On the other hand, the updated spatial curvature tensor $\overset{\mathbf{v}}{\boldsymbol{\omega}}{}^{(i+1)}$, as given in Box 4.1,

$$\overset{\mathbf{v}}{\boldsymbol{\omega}}{}^{(i+1)} = \frac{d\mathbf{A}^{(i+1)}}{dS}\mathbf{A}^{(i+1)T}, \tag{4.67a}$$

requires the spatial derivative of $\mathbf{A}^{(i+1)}$. It follows from $(4.65)_2$, and since $\overset{\mathbf{v}}{\boldsymbol{\omega}}{}^{(i)} = \dfrac{d\mathbf{A}^{(i)}}{dS}\mathbf{A}^{(i)T}$, that

$$\overset{\mathbf{v}}{\boldsymbol{\omega}}{}^{(i+1)} = \frac{d\exp[\Delta\overset{\mathbf{v}}{\boldsymbol{\vartheta}}{}^{(i)}]}{dS}\exp[-\Delta\overset{\mathbf{v}}{\boldsymbol{\vartheta}}{}^{(i)}] + \exp[\Delta\overset{\mathbf{v}}{\boldsymbol{\vartheta}}{}^{(i)}]\,\overset{\mathbf{v}}{\boldsymbol{\omega}}{}^{(i)}\exp[-\Delta\overset{\mathbf{v}}{\boldsymbol{\vartheta}}{}^{(i)}] \tag{4.67b}$$

In fact, (4.67b) can be obtained directly from the curve of perturbed curvature $\varepsilon \to \overset{\mathbf{v}}{\boldsymbol{\omega}}_\varepsilon$ given in (4.24). The geometric interpretation of (4.67b) is as follows: (i) The point $\mathbf{A}^{(i)} \in SO(3)$ is left-translated to the point $\mathbf{A}^{(i+1)} \in SO(3)$ by the action of the exponential map $\exp[\Delta\overset{\mathbf{v}}{\boldsymbol{\vartheta}}{}^{(i)}]$ as given in $(4.65)_2$;† (ii) This map parallelly transports the skew-symmetric curvature tensor $\overset{\mathbf{v}}{\boldsymbol{\omega}}{}^{(i)} \in T_{\mathbf{A}^{(i)}}SO(3)$ to the tangent space $T_{\mathbf{A}^{(i+1)}}SO(3)$ as expressed in the second term of (4.67b); (iii) The first term in (4.67b) actually represents the incremental curvature, expressed in the tangent space $T_{\mathbf{A}^{(i+1)}}SO(3)$, as a consequence of the incremental rotation field $\Delta\overset{\mathbf{v}}{\boldsymbol{\vartheta}}{}^{(i)}$ (the addition operation here makes sense since both the curvature tensor and its increment are in the same tangent space).

† Equivalently, $\mathbf{A}^{(i)}$ is right-tranlated to $\mathbf{A}^{(i+1)}$ by $\exp[\Delta\overset{\mathbf{v}}{\boldsymbol{\Theta}}{}^{(i)}]$, where $\Delta\overset{\mathbf{v}}{\boldsymbol{\Theta}}{}^{(i)} = \mathbf{A}^{(i)T}\Delta\overset{\mathbf{v}}{\boldsymbol{\vartheta}}{}^{(i)}$, such that $\mathbf{A}^{(i+1)} = \mathbf{A}^{(i)}\exp[\Delta\boldsymbol{\Theta}^{(i)}]$.

To proceed further, we need the following results.

Lemma 4.1. Derivative of the exponential map. *Let* $\hat{\boldsymbol{\vartheta}}(S) \in so(3)$, $\forall S$, *such that* $\boldsymbol{\vartheta}:[0,L]\to\mathbb{R}^3$ *is continuously differentiable, then the axial vector of* $\hat{\boldsymbol{\psi}} := \frac{d\exp[\hat{\boldsymbol{\vartheta}}(S)]}{dS}\exp[-\hat{\boldsymbol{\vartheta}}(S)] \in so(3)$ *is given by*

$$\boldsymbol{\psi} = \frac{2}{1+\|\bar{\boldsymbol{\vartheta}}\|^2}[\,\bar{\boldsymbol{\vartheta}}' + (\bar{\boldsymbol{\vartheta}}\times\bar{\boldsymbol{\vartheta}}')\,], \tag{4.68}$$

where $\bar{\boldsymbol{\vartheta}}(S) := \tan(\|\boldsymbol{\vartheta}\|/2)\,\frac{\boldsymbol{\vartheta}}{\|\boldsymbol{\vartheta}\|}$.

Proof. Using the closed form formula for the exponential map (4.5c-d), and taking the derivative with respect to S, we obtain

$$\frac{d\exp[\hat{\boldsymbol{\vartheta}}(S)]}{dS} = \frac{2}{1+\|\bar{\boldsymbol{\vartheta}}\|^2}\left[\hat{\boldsymbol{\vartheta}}' + \hat{\boldsymbol{\vartheta}}'\hat{\boldsymbol{\vartheta}} + \hat{\boldsymbol{\vartheta}}\hat{\boldsymbol{\vartheta}}' - \frac{2\bar{\boldsymbol{\vartheta}}\cdot\bar{\boldsymbol{\vartheta}}'(\hat{\boldsymbol{\vartheta}}+\hat{\boldsymbol{\vartheta}}^2)}{1+\|\bar{\boldsymbol{\vartheta}}\|^2}\right]. \tag{4.69a}$$

Next, upon noting the identity $\hat{\boldsymbol{\vartheta}}^3 = -\|\bar{\boldsymbol{\vartheta}}\|^2\hat{\boldsymbol{\vartheta}}$, a lengthy but straightforward manipulation yields the result

$$\hat{\boldsymbol{\psi}} = \frac{d\exp[\hat{\boldsymbol{\vartheta}}(S)]}{dS}\exp[-\hat{\boldsymbol{\vartheta}}(S)] = \frac{2}{1+\|\bar{\boldsymbol{\vartheta}}\|^2}[\,\hat{\boldsymbol{\vartheta}}' + \hat{\boldsymbol{\vartheta}}\hat{\boldsymbol{\vartheta}}' - \hat{\boldsymbol{\vartheta}}'\hat{\boldsymbol{\vartheta}} + \mathbf{A}\,] \tag{4.69b}$$

where $\mathbf{A}$ is given by

$$\mathbf{A} = -\bar{\boldsymbol{\vartheta}}\cdot\bar{\boldsymbol{\vartheta}}'[\hat{\boldsymbol{\vartheta}} - \hat{\boldsymbol{\vartheta}}^2] - \hat{\boldsymbol{\vartheta}}\hat{\boldsymbol{\vartheta}}'\hat{\boldsymbol{\vartheta}} + \hat{\boldsymbol{\vartheta}}\hat{\boldsymbol{\vartheta}}'\hat{\boldsymbol{\vartheta}}^2. \tag{4.69c}$$

It follows at once from the identities

$$\hat{\boldsymbol{\vartheta}}\hat{\boldsymbol{\vartheta}}'\hat{\boldsymbol{\vartheta}} = -(\bar{\boldsymbol{\vartheta}}\cdot\bar{\boldsymbol{\vartheta}}')\hat{\boldsymbol{\vartheta}}, \qquad \hat{\boldsymbol{\vartheta}}\hat{\boldsymbol{\vartheta}}'\hat{\boldsymbol{\vartheta}}^2 = -(\bar{\boldsymbol{\vartheta}}\cdot\bar{\boldsymbol{\vartheta}}')\hat{\boldsymbol{\vartheta}}^2 \tag{4.69d}$$

that in fact $\mathbf{A} = 0$. In addition, as noted in (4.28), the axial vector of $(\hat{\boldsymbol{\vartheta}}\hat{\boldsymbol{\vartheta}}' - \hat{\boldsymbol{\vartheta}}'\hat{\boldsymbol{\vartheta}})$ is given by $(\bar{\boldsymbol{\vartheta}}\times\bar{\boldsymbol{\vartheta}}')$. Hence, we obtain the expression for the axial vector $\boldsymbol{\psi}$ given in (4.68). ∎

It proves computationally more convenient to express $\boldsymbol{\psi}$ in (4.68) in terms of the rotation vector $\boldsymbol{\vartheta}$ rather than in terms of the pseudo rotation vector $\bar{\boldsymbol{\vartheta}}$. This can be found in

Lemma 4.2. *The axial vector $\boldsymbol{\psi}$ of the skew-symmetric tensor $\overset{\times}{\boldsymbol{\psi}} = \frac{d\exp[\overset{\times}{\boldsymbol{\vartheta}}]}{dS}\exp[-\overset{\times}{\boldsymbol{\vartheta}}]$ can be obtained as follows*

$$\boldsymbol{\psi} = \frac{\sin\|\boldsymbol{\vartheta}\|}{\|\boldsymbol{\vartheta}\|}\boldsymbol{\vartheta}' + \left[1 - \frac{\sin\|\boldsymbol{\vartheta}\|}{\|\boldsymbol{\vartheta}\|}\right]\left[\frac{\boldsymbol{\vartheta}\cdot\boldsymbol{\vartheta}'}{\|\boldsymbol{\vartheta}\|}\right]\frac{\boldsymbol{\vartheta}}{\|\boldsymbol{\vartheta}\|} + \frac{1}{2}\left[\frac{\sin(\|\boldsymbol{\vartheta}\|/2)}{\|\boldsymbol{\vartheta}\|/2}\right]^2\boldsymbol{\vartheta}\times\boldsymbol{\vartheta}' . \quad (4.70)$$

Proof. This follows from (4.68) and the definition of the pseudo rotation vector $\bar{\boldsymbol{\vartheta}}$. The same result is obtained by using formula (4.5b) for the exponential map instead of (4.5c) in the proof of Lemma 4.1. ∎

Remark 4.3. Recall that $\frac{\sin\|\boldsymbol{\vartheta}\|}{\|\boldsymbol{\vartheta}\|} \to 1$ as $\|\boldsymbol{\vartheta}\| \to 0$. Hence, for $\|\boldsymbol{\vartheta}\|$ small, we obtain $\boldsymbol{\vartheta}'$ as the first order approximation of $\boldsymbol{\psi}$, from (4.70). This remark is in fact confirmed by relation (4.25). ∎

Lemma 4.3. *The following expression gives the updated spatial curvature vector $\boldsymbol{\omega}^{(i+1)}$ in terms of the incremental rotation $\Delta\boldsymbol{\vartheta}^{(i)}$*

$$\boldsymbol{\omega}^{(i+1)} = \frac{\sin\|\Delta\boldsymbol{\vartheta}^{(i)}\|}{\|\Delta\boldsymbol{\vartheta}^{(i)}\|}\Delta\boldsymbol{\vartheta}^{(i)\prime} + \left[1 - \frac{\sin\|\Delta\boldsymbol{\vartheta}^{(i)}\|}{\|\Delta\boldsymbol{\vartheta}^{(i)}\|}\right]\left[\frac{\Delta\boldsymbol{\vartheta}^{(i)}\cdot\Delta\boldsymbol{\vartheta}^{(i)\prime}}{\|\Delta\boldsymbol{\vartheta}^{(i)}\|}\right]\frac{\Delta\boldsymbol{\vartheta}^{(i)}}{\|\Delta\boldsymbol{\vartheta}^{(i)}\|} \quad (4.71)$$

$$+ \frac{1}{2}\left[\frac{\sin(\|\Delta\boldsymbol{\vartheta}^{(i)}\|/2)}{\|\Delta\boldsymbol{\vartheta}^{(i)}\|/2}\right]^2\Delta\boldsymbol{\vartheta}^{(i)}\times\Delta\boldsymbol{\vartheta}^{(i)\prime} + \exp[\Delta\overset{\times}{\boldsymbol{\vartheta}}^{(i)}]\,\boldsymbol{\omega}^{(i)} .$$

Proof. Using Lemma 4.2, and by noting that the axial vector of the second term in (4.67b) is $\exp[\Delta\overset{\times}{\boldsymbol{\vartheta}}^{(i)}]\,\boldsymbol{\omega}^{(i)}$ by virtue of (4.9), we obtain (4.71). ∎

Finally, the updated material curvature vector is simply $\boldsymbol{\Omega}^{(i+1)} = \boldsymbol{\Lambda}^{(i+1)T}\boldsymbol{\omega}^{(i+1)}$. The next step is to obtain the updated internal force and moment needed to compute the tangent geometric stiffness matrix for iteration

$(i+1)$ in the solution procedure.

Stress update. By assuming that the constitutive laws (4.15) and (4.16) hold pointwise, we have

$$\mathbf{n}^{(i+1)} = \frac{\partial \psi(S,\boldsymbol{\gamma}^{(i+1)},\boldsymbol{\omega}^{(i+1)})}{\partial \boldsymbol{\gamma}} \quad \text{and} \quad \mathbf{m}^{(i+1)} = \frac{\partial \psi(S,\boldsymbol{\gamma}^{(i+1)},\boldsymbol{\omega}^{(i+1)})}{\partial \boldsymbol{\omega}}. \tag{4.72}$$

$$\mathbf{N}^{(i+1)} = \frac{\partial \Psi(S,\boldsymbol{\Gamma}^{(i+1)},\boldsymbol{\Omega}^{(i+1)})}{\partial \boldsymbol{\Gamma}} \quad \text{and} \quad \mathbf{M}^{(i+1)} = \frac{\partial \Psi(S,\boldsymbol{\Gamma}^{(i+1)},\boldsymbol{\Omega}^{(i+1)})}{\partial \boldsymbol{\Omega}}. \tag{4.73}$$

In all numerical examples, we assume that relations (4.18a-b) hold pointwise, thus

$$\begin{Bmatrix} \mathbf{N}^{(i+1)} \\ \mathbf{M}^{(i+1)} \end{Bmatrix} = \mathbf{C} \begin{Bmatrix} \boldsymbol{\Gamma}^{(i+1)} \\ \boldsymbol{\Omega}^{(i+1)} \end{Bmatrix}. \tag{4.74}$$

The update procedure thus far explored is summarized in its implementable version in Box 4.4.

Remark 4.4. On the Hughes-Winget update formula. By applying the generalized mid-point rule to the differential equation $\dot{\mathbf{A}} = \overset{\mathrm{v}}{\boldsymbol{\omega}}\mathbf{A}$, for $\mathbf{A} \in SO(3)$, Hughes & Winget [1980] derive an update formula which is essentially a second order approximation to the formula (4.65) used herein:

$$\mathbf{A}^{(i+1)} - \mathbf{A}^{(i)} = \frac{h}{2}\overset{\mathrm{v}}{\boldsymbol{\omega}}^{(i+\frac{1}{2})} [\, \mathbf{A}^{(i+1)} + \mathbf{A}^{(i)} \,] \tag{4.75a}$$

hence

$$\mathbf{A}^{(i+1)} = \mathbf{Q}\,\mathbf{A}^{(i)}, \tag{4.75b}$$

$$\mathbf{Q} := [\, 1 - \frac{h}{2}\overset{\mathrm{v}}{\boldsymbol{\omega}}^{(i+\frac{1}{2})} \,]^{-1} [\, 1 + \frac{h}{2}\overset{\mathrm{v}}{\boldsymbol{\omega}}^{(i+\frac{1}{2})} \,] \in SO(3) \tag{4.75c}$$

Define $\boldsymbol{\vartheta} := \frac{h}{2}\boldsymbol{\omega}^{(i+\frac{1}{2})}$, then $\mathbf{Q}$ in the Hughes-Winget formula is the counterpart of the exponential map $\exp[\overset{\mathrm{v}}{\boldsymbol{\vartheta}}]$ in (4.65). To see that the Hughes-Winget formula

BOX 4.4 *Configuration and stress update: Implementable algorithm*

- Data

$$\boldsymbol{\phi}^{(i)} := (\boldsymbol{\phi}_0^{(i)}, \mathbf{A}^{(i)}) \in C\,,$$

$$\Delta\boldsymbol{\phi}^{(i)} := (\Delta\mathbf{u}^{(i)}, \Delta\boldsymbol{\vartheta}^{(i)}) \in \mathbb{R}^3 \times \mathbb{R}^3\,.$$

- Update configuration

$$\boldsymbol{\phi}^{(i+1)} := (\boldsymbol{\phi}_0^{(i+1)}, \mathbf{A}^{(i+1)}) \in C \quad \text{such that}$$

$$\boldsymbol{\phi}_0^{(i+1)} = \boldsymbol{\phi}_0^{(i)} + \Delta\mathbf{u}^{(i)}\,, \quad \mathbf{A}^{(i+1)} = \exp[\Delta\hat{\boldsymbol{\vartheta}}^{(i)}]\,\mathbf{A}^{(i)}\,.$$

- Update strain measures

$$\boldsymbol{\Gamma}^{(i+1)} = \mathbf{A}^{(i+1)T}\,\boldsymbol{\phi}_0^{(i+1)\prime} - \mathbf{E}_3\,.$$

$$\boldsymbol{\omega}^{(i+1)} = \frac{\sin\|\Delta\boldsymbol{\vartheta}^{(i)}\|}{\|\Delta\boldsymbol{\vartheta}^{(i)}\|}\Delta\boldsymbol{\vartheta}^{(i)\prime} + \left[1 - \frac{\sin\|\Delta\boldsymbol{\vartheta}^{(i)}\|}{\|\Delta\boldsymbol{\vartheta}^{(i)}\|}\right]\left[\frac{\Delta\boldsymbol{\vartheta}^{(i)}\cdot\Delta\boldsymbol{\vartheta}^{(i)\prime}}{\|\Delta\boldsymbol{\vartheta}^{(i)}\|}\right]\frac{\Delta\boldsymbol{\vartheta}^{(i)}}{\|\Delta\boldsymbol{\vartheta}^{(i)}\|}$$

$$+ \frac{1}{2}\left[\frac{\sin(\|\Delta\boldsymbol{\vartheta}^{(i)}\|/2)}{\|\Delta\boldsymbol{\vartheta}^{(i)}\|/2}\right]^2 \Delta\boldsymbol{\vartheta}^{(i)}\times\Delta\boldsymbol{\vartheta}^{(i)\prime} + \exp[\Delta\hat{\boldsymbol{\vartheta}}^{(i)}]\,\boldsymbol{\omega}^{(i)}\,.$$

$$\boldsymbol{\Omega}^{(i+1)} = \mathbf{A}^{(i+1)T}\,\boldsymbol{\omega}^{(i+1)}\,.$$

- Update internal force and moment

$$\begin{Bmatrix}\mathbf{N}^{(i+1)}\\ \mathbf{M}^{(i+1)}\end{Bmatrix} = \mathbf{C}\begin{Bmatrix}\boldsymbol{\Gamma}^{(i+1)}\\ \boldsymbol{\Omega}^{(i+1)}\end{Bmatrix}, \quad \begin{Bmatrix}\mathbf{n}^{(i+1)}\\ \mathbf{m}^{(i+1)}\end{Bmatrix} = \begin{Bmatrix}\mathbf{A}^{(i+1)}\mathbf{N}^{(i+1)}\\ \mathbf{A}^{(i+1)}\mathbf{M}^{(i+1)}\end{Bmatrix}$$

(4.75b-c) furnishes only a second order approximation to the update formula (4.65), we first note that, by the Newman series, $[\mathbf{1}_3 - \hat{\boldsymbol{\vartheta}}]^{-1} = \sum_{k=0}^{\infty}\hat{\boldsymbol{\vartheta}}^k$, hence

$$\mathbf{Q} = \mathbf{1}_3 + 2\sum_{k=1}^{\infty}\hat{\boldsymbol{\vartheta}}^k\,. \tag{4.75d}$$

Moreover, from the identity $\hat{\boldsymbol{\vartheta}}^3 = -\|\boldsymbol{\vartheta}\|^2\hat{\boldsymbol{\vartheta}}$, and thus $\hat{\boldsymbol{\vartheta}}^4 = -\|\hat{\boldsymbol{\vartheta}}\|^2\hat{\boldsymbol{\vartheta}}^2$, $\hat{\boldsymbol{\vartheta}}^5 = \|\hat{\boldsymbol{\vartheta}}\|^4\hat{\boldsymbol{\vartheta}}$, ..., one has

$$\mathbf{Q} = \mathbf{1}_3 + 2[\hat{\boldsymbol{\vartheta}} + \hat{\boldsymbol{\vartheta}}^2][\mathbf{1}_3 - \|\boldsymbol{\vartheta}\|^2 + \|\boldsymbol{\vartheta}\|^4 - \|\boldsymbol{\vartheta}\|^6 + \cdots]$$

$$= \mathbf{1}_3 + \frac{2}{1+\|\boldsymbol{\vartheta}\|^2}[\hat{\boldsymbol{\vartheta}} + \hat{\boldsymbol{\vartheta}}^2]\,. \tag{4.75e}$$

The above formula was obtained in Hughes [1984]. On the other hand, define the incremental rotation $\boldsymbol{\psi} := 2\boldsymbol{\vartheta} = h\,\boldsymbol{\omega}^{(i+\frac{1}{2})}$, then by (4.65), we have

$$\mathbf{A}^{(i+1)} = \exp[\overset{\times}{\boldsymbol{\psi}}]\,\mathbf{A}^{(i)} \tag{4.75f}$$

where $\exp[\overset{\times}{\boldsymbol{\psi}}]$ is evaluated by (4.5c-d). It can be seen that since $\frac{\boldsymbol{\psi}}{2} = \boldsymbol{\vartheta}$ approximates $\bar{\boldsymbol{\psi}} := \tan(\|\boldsymbol{\psi}\|/2)\,\frac{\boldsymbol{\psi}}{\|\boldsymbol{\psi}\|}$ up to second order, the Hughes-Winget formula is therefore a second order approximation to (4.65). ■

4.6.3. Practical implementation consideration

We discuss in detail practical considerations concerning the implementation of the update of the components of the orthogonal transformation $\mathbf{A}$, given in $(4.65)_2$, based on the use of quaternion parameters. The update of the deformed centroidal line poses no difficulty. Given an incremental rotation $\Delta\boldsymbol{\vartheta}$, either formula (4.5b) or (4.5c) can be used to evaluate the components of exponential map $\exp[\Delta\overset{\times}{\boldsymbol{\vartheta}}]$. Due to the singularity at $\|\Delta\boldsymbol{\vartheta}\| = (2n+1)\pi$ in the pseudo rotation vector $\Delta\bar{\boldsymbol{\vartheta}}$ in (4.5d), it is preferable not to use (4.5c) in actual computation. Let $\mathbf{A}^{(i)} := \exp[\overset{\times}{\boldsymbol{\vartheta}}^{(i)}]$; then instead of representing $\mathbf{A}^{(i)}$ by its 9 components Λ_{IJ} according to (4.1c), one can represent $\mathbf{A}$ by the rotation vector $\boldsymbol{\vartheta}^{(i)}$. However, an optimal parametrization of three-dimensional rotations that avoids singularities, minimizes storage requirement, and involves the least possible number of operations in the update procedure is the use of four (4) quaternion parameters.† This also provides a third way of evaluating the components of the exponential map.

† Sometimes referred to as Euler parameters, e.g., Goldstein [1980] or Kane, Likins & Levinson [1983].

Recall that quaternions are elements of the hypercomplex space expressed as

$$\hat{\mathbf{q}} = q_o + \mathbf{q}; \qquad \mathbf{q} = q_1\mathbf{e}_1 + q_2\mathbf{e}_2 + q_3\mathbf{e}_3 \tag{4.76}$$

where q_o represents the scalar part, and $\mathbf{q}$ the vector part of $\hat{\mathbf{q}}$. A unit quaternion is defined such that $\sum_{i=0}^{3} q_i^2 = 1$. In the definition (4.76), we have identified the spatial basis $(\mathbf{e}_1, \mathbf{e}_2, \mathbf{e}_3)$ with the imaginary basis of the hypercomplex space. Recall that the (linear) space of quaternions equipped with the quaternion multiplicative operation (composition of orthogonal transformations in $\mathbb{R}^3$) forms an associative but non-commutative algebra. An orthogonal transformation can be represented by the four parameters (q_o, q_1, q_2, q_3) of a unit quaternion instead of the nine components of an orthogonal matrix. Quaternion parameters are therefore kept in the data base to minimize storage requirements. The update procedure for the rotation field is summarized in Box 4.5 below.

BOX 4.5. *Update of quaternion describing section rotation.*

(i) Retrieve $\hat{\mathbf{q}}^{(i)}$, and compute $\mathbf{A}^{(i)}$ from $\hat{\mathbf{q}}^{(i)}$.

(ii) Compute $\hat{\mathbf{q}}$ associated with $\Delta\boldsymbol{\vartheta}^{(i)}$.

(iii) Compute $\exp[\Delta\tilde{\boldsymbol{\vartheta}}^{(i)}]$ from $\hat{\mathbf{q}}$.

(iv) Perform $\mathbf{A}^{(i+1)} = \exp[\Delta\tilde{\boldsymbol{\vartheta}}^{(i)}]\,\mathbf{A}^{(i)}$.

(v) Extract $\hat{\mathbf{q}}^{(i+1)}$ from $\mathbf{A}^{(i+1)}$, and store $\hat{\mathbf{q}}^{(i+1)}$.

The unit quaternion corresponding to an incremental rotation vector $\Delta\boldsymbol{\vartheta}^{(i)} = \Delta\vartheta_i^{(i)}\,\mathbf{e}_i$ (see step (ii) in Box 4.5) can be evaluated by

$$\hat{\mathbf{q}} = \cos\frac{\|\Delta\boldsymbol{\vartheta}^{(i)}\|}{2} + \frac{\Delta\boldsymbol{\vartheta}^{(i)}}{\|\Delta\boldsymbol{\vartheta}^{(i)}\|}\sin\frac{\|\Delta\boldsymbol{\vartheta}^{(i)}\|}{2} \tag{4.77}$$

The pseudo-vector of rotation $\Delta\bar{\theta}^{(i)}$ is then the vector part of a unit quaternion whose scalar part is normalized to one:

$$\frac{\hat{q}}{q_o} = 1 + \frac{q}{q_o} = 1 + \Delta\bar{\theta}^{(i)} \tag{4.78}$$

Clearly, a singularity occurs when $\|\Delta\bar{\theta}^{(i)}\| = (2n+1)\pi$, i.e., when $q_o = \cos(\|\Delta\bar{\theta}^{(i)}\|/2) = 0$.

The components of the exponential map $\exp[\Delta\tilde{\theta}^{(i)}]$ in step (iii) can be evaluated using the quaternion representation of $\Delta\bar{\theta}^{(i)}$ in (4.77) as follows. Let $\mathbf{Q}$ be an orthogonal matrix associated with the unit quaternion $\hat{\mathbf{q}}$, then (Whittaker [1937])

$$\mathbf{Q} = 2\begin{bmatrix} q_o^2 + q_1^2 - \frac{1}{2} & q_1q_2 - q_3q_o & q_1q_3 + q_2q_o \\ q_2q_1 + q_3q_o & q_o^2 + q_2^2 - \frac{1}{2} & q_2q_3 - q_1q_o \\ q_3q_1 - q_2q_o & q_3q_2 + q_1q_o & q_o^2 + q_3^2 - \frac{1}{2} \end{bmatrix} \tag{4.79}$$

The above relation also applies to step (i) in Box 4.5.

Conversely, given an orthogonal matrix $\mathbf{Q}$, the associated quaternion parameters can be obtained from (4.79) by

$$\begin{aligned} q_o &= \pm\tfrac{1}{2}\sqrt{1 + \mathrm{Tr}(\mathbf{Q})} \\ q_1 &= \pm(Q_{32} - Q_{23})/4q_o \\ q_2 &= \pm(Q_{13} - Q_{31})/4q_o \\ q_3 &= \pm(Q_{21} - Q_{12})/4q_o \end{aligned} \tag{4.80}$$

where $\mathrm{Tr}(\mathbf{Q}) = Q_{ii}$. Note that we only need to determine the sign of q_o, as the sign of q_1, q_2, q_3 will follow. Either a positive or negative sign for q_o is possible; to fix the choice, we may choose $q_o \geq 0$. However, relations (4.80) suffer from round-off errors since the numerators and the denominators in q_1, q_2, q_3 are obtained from subtraction of nearly equal quantities in the vicinity of 0^0 and 180^0. Moreover, the computation breaks down when the rotation is exactly 180^0,

e.g., in the case of $\mathbf{Q} = Diag(-1,-1,1)$. There are several proposed algorithms to extract a quaternion from an orthogonal transformation matrix. Among them, the algorithm proposed by Spurrier [1978] has been reported to be the fastest (Lowrie [1979]), and is summarized in Box 4.6.

BOX 4.6. *Spurrier's algorithm for quaternion extraction.*

$M := \max(\mathrm{Tr}(\mathbf{Q}); Q_{11}, Q_{22}, Q_{33})$

If $M = \mathrm{Tr}(\mathbf{Q})$, then:

$$q_o = \frac{1}{2}\sqrt{1 + \mathrm{Tr}(\mathbf{Q})}$$

$$q_i = (Q_{kj} - Q_{jk})/4q_o, \quad \text{for } i=1,2,3$$

Else:

Let i be such that $M = Q_{(ii)}$,

$$q_i = \left[\frac{Q_{(ii)}}{2} + \frac{1 - \mathrm{Tr}(\mathbf{Q})}{4}\right]^{\frac{1}{2}}$$

$$q_o = (Q_{kj} - Q_{jk})/4q_i$$

$$q_l = (Q_{ik} + Q_{ki})/4q_i, \quad \text{for } l=j,k$$

There, (i,j,k) represents a cyclic permutation of 1,2,3, and $Q_{(ii)}$ denotes the component (i,i) of matrix $\mathbf{Q}$ (summation convention does not apply here). This extraction algorithm can be used in step (v) of BOX 4.5, and will play a crucial role in our treatment of the dynamics of three-dimensional flexible rods in

Chapter 5.

4.7. Numerical examples

In this section, we consider a series of numerical simulations that illustrates the performance of the formulation described above. These applications show the quadratic rate of convergence obtained, even for very large load steps, in well documented examples. In the first four examples, attention is focused on the plane problem where the rotation field is easily described by means of a single rotation angle (Reissner [1972,82], Simo *et al* [1984]). A basic objective then is to show that the proposed three dimensional parametrization of the rotation field exactly replicates the plane rotation. The last three examples, on the other hand, are concerned with fully three-dimensional deformation, and have been considered in previous work (Bathe [1979], Argyris and co-workers [1979,81]). These examples demonstrate that symmetry of the tangent stiffness does *not* hold in the iteration process but is attained at the converged solution. Throughout all the examples discussed below, the constitutive model defined by (2.10) is considered.

Convergence of the finite element solution is established on the basis of the Euclidean norm of the out-of-balance force. A full Newton-Raphson iterative solution procedure is employed in all the calculations reported herein. Tracing of post-buckling diagrams throughout the simulations is accomplished by a generalized form of the classical arc-length method, (Riks [1972], Wempner [1971]) to include an arbitrary linear combination of degrees of freedom as a constraint condition. The basic implementation of this procedure proceeds in two steps and is due to Schweizerhof; see Simo, Wriggers, Schweizerhof and Taylor [1984]. The first step involves the solution of the linearized problem under a unit load. For the case of a follower load, this unit load must be properly updated. It is

emphasized that no special effort is made to optimize the total number of loading steps for a given calculation.

Example 4.7.1. Pure bending of a cantilever beam. A straight rod of unit length and bending stiffness $EI = 2.$ is subject to a concentrated end moment M. The finite element mesh consists of five elements with linear interpolation shape functions N_I. A one-point (uniformly reduced) quadrature is employed to compute the tangent stiffness matrix and residual. The exact solution to this problem is a circular curve with radius $\rho = EI/M$. An applied end moment, $M = 4\pi$, will force the rod to deform into a full closed circle. In this example a moment *twice* this magnitude, i.e., $M = 8\pi$, is applied in *one load step*, making the rod wind around itself twice. Convergence to the exact solution is attained in *two iterations*. The final shape of the rod is depicted in Figure 4.7.1. It is noted that the same performance, i.e., exact result in two iterations, is obtained for *any* magnitude of the applied end moment. The values of the residual norm throughout the iteration process are summarized in Box 4.7.

BOX 4.7. Example 4.7.1.: *Iteration number vs. residual norm.*

Iteration Number	*Euclidean Norm of Residual*
0	$0.251 \times 10^{+02}$ (8π)
1	$0.425 \times 10^{+02}$
2	0.441×10^{-13}

Example 4.7.2. Cantilever beam subject to follower end load. The material properties for this example, considered by Argyris & Symeonidis [1981], are $EI = 3.5\times10^{7}$ and $GA = 1.61538\times10^{8}$, and the total length is $L = 100$. The finite element mesh consists of *five* elements with quadratic shape functions. Two-point (uniformly reduced) Gauss integration is used to compute all matrices.

For the purpose of tracing the load-deflection curve reported by Argyris & Symeonidis, a loading increment of 1000 was selected. The agreement found with these results is complete (see Figures 4.7.2*a* and 4.7.2*b*). The characteristic quadratic convergence rate observed in a typical iteration of a load step is illustrated in Box 4.8 for the first loading step. An Identical convergence rate was observed in subsequent load steps.

BOX 4.8. Example 4.7.2.: *Iteration number vs. residual norm.*

Iteration Number	*Euclidean Norm of Residual*
0	$0.100 \times 10^{+04}$
1	$0.542 \times 10^{+07}$
2	$0.270 \times 10^{+05}$
3	$0.583 \times 10^{+02}$
4	0.159×10^{-02}
5	0.197×10^{-08}

Example 4.7.3. Clamped-hinged deep circular arch subject to point load. This example has been considered by a number of authors (e.g., Noor & Peters [1981] and Simo *et al* [1984]), and the exact solution based on the Kirchhoff-Love theory is given by DaDeppo and Schmidt [1975]. The solution shown in Figure 4.7.3*a* for various stages of deformation is obtained with 40 *linear isoparametric* elements. The plot of the vertical and horizontal displacements under the applied concentrated load is shown in Figure 4.7.3*b*. Load control is employed in the first eight load steps, each of them of magnitude 100. Subsequently, a combined displacement control/arch length control is employed. The calculation was completed in a total number of 155 load steps. The analysis yields a value for the buckling load of 905.28. The exact value reported by DaDeppo and Schmidt [1975] is 897. A second limit point is found for a *negative value* of the applied load of −77.07. The global computed solution is in complete agreement

with the solution first obtained for the entire post-buckling range in Simo *et al* [1984]. The convergence rate observed during a typical load step is shown in Box 4.9 for the first load increment.

BOX 4.9. Example 4.7.3.: *Iteration number vs. residual norm.*

Iteration Number	*Euclidean Norm of Residual*
0	$0.100 \times 10^{+03}$
1	$0.553 \times 10^{+05}$
2	$0.325 \times 10^{+03}$
3	$0.309 \times 10^{+03}$
4	$0.990 \times 10^{+00}$
5	0.125×10^{-01}
6	0.920×10^{-08}

Example 4.7.4. Snap-through of a hinged right-angle frame under both fixed and follower point load. This example, also considered by Argyris and Symeonidis [1981], is concerned with the loss of stability by divergence (as opposed to flutter) of the right angle frame shown in Figure 4.7.4*a*. The length of each leg is 120. The inertia and area of the cross section are respectively 2 and 6. The value of Young's modulus is 7.2×10^6; the value of Poisson's ratio is 0.3. The vertical point load is applied on the horizontal member at 24 units from its left end. Ten quadratic elements, 5 on each leg, are employed in the calculation. The deformed shapes are shown in Figures 4.7.4*a* and 4.7.4*b*. The load-deflection curves are shown in Figures 4.7.4*c* and 4.7.4*d*. Note that the entire post-buckling range is depicted in these figures, in contrast with the results reported by Argyris & Symeonidis which are limited to the pre-buckling case. It is interesting to observe that the load-deflection curves for both conservative and non-conservative loading cross the zero-load axis at exactly the same values, as shown in Figures 4.7.4*c* and 4.7.4*d*. These curves were traced after 43

load increments for the fixed load case, and 99 load increments for the follower load case. As noted by Argyris & Symeonidis, the follower loading (non-conservative) has a positive effect of stabilizing the system and leads to a value of the buckling load of 35447 in contrast with the value of 18532 obtained for fixed loading (conservative).

Example 4.7.5. Cantilever 45-degree bend subject to fixed and follower end load. This example has been considered by Bathe and Bolourchi [1979] under fixed end load. The bend has a radius of 100 with a unit square cross section. The material properties are $E = 10^7$ and $G = 0.5\times10^7$. These authors performed the analysis for conservative loading only using 8 three-dimensional degenerated beam elements. In the present calculation 8 linear elements are used. For comparison purposes with the results reported in Bathe & Bolourchi the bend is subject to a sequence of *three* load increments of magnitude 300, 150 and 150. The results are summarized in Box 4.10.

BOX 4.10. Example 4.7.5.: *Comparison of results by* Bathe & Bolourchi [1979].

Load level	Number of Iterations	Tip displacement					
		Present			Bathe & Bolourchi [1979]		
		u	v	w	u	v	w
300	13	22.33	58.84	40.08	22.5	59.2	39.5
450	8	18.62	52.32	48.39	—	—	—
600	8	15.79	47.23	53.37	15.9	47.2	53.4

It should be noted that the final load of 600 was achieved in the present simulation in *three* load increments. This accounts for the large number of iterations (13) required to attain convergence. By contrast, the results reported in Bathe & Bolourchi were obtained after *sixty* equal load increments. A perspective view

and a projection view of the deformed bend at various load levels are shown in Figures 4.7.5*a* and 4.7.5*b*. The tip displacement versus applied load curve, shown in Figure 4.7.5*c*, is given up to a load level of 3000.

In addition to the loading discussed above, the bend also is analyzed for a *follower load*. The deformed configurations of the bend at various follower load levels are shown in Figures 4.7.5*d* and 4.7.5*e* — compare these with Figures 4.7.5*a* and 4.7.5*b*. The tip displacement versus applied load curve obtained for this non-conservative loading is shown in Figure 4.7.5*f*. It should be noted from Figures 4.7.5*c* and 4.7.5*f* that the tip displacement increases monotonically with the load for fixed loading, whereas in the case of follower load the tip displacement reaches a maximum and then decreases. This effect is a consequence of the twist experienced by the bend as a result of the follower load.

Finally, a similar simulation is performed with both the consistent (non-symmetric) and the *symmetrized* element tangent stiffness matrices. The total load of 600 is applied in 8 equal load increments of magnitude 75. The purpose of the calculation is to show that *no significant loss* of asymptotic convergence rate results from using the symmetrized tangent matrix. This follows from our discussion in Section 4.4. The residual and energy norms shown in Box 4.11 below correspond to the fifth load increment.

Example 4.7.6. Lateral buckling of a cantilever right-angle frame under end load. This problem also has been analyzed by Argyris *et al* [1979]. The geometric characteristics of the frame are shown in Figure 4.7.6*a*. The value of Young's modulus is 71240; and the value of Poisson's ratio is 0.31. The extreme slenderness of the cross section, $\frac{thickness}{heigth} = \frac{1}{50}$, should be noted. The frame is subject to an in-plane fixed end load as shown in Figure 4.7.6*a*. Further, the frame is driven to the buckling mode by a perturbation load initially applied at

BOX 4.11. Example 4.7.5.: *Performance of symmetrized tangent stiffness.*

Iteration	Non-symmetric	Symmetric	
number	*Residual norm*	*Residual Norm*	*Energy Norm*
0	$0.750 \times 10^{+02}$	$0.750 \times 10^{+02}$	$0.410 \times 10^{+03}$
1	$0.147 \times 10^{+06}$	$0.147 \times 10^{+06}$	$0.228 \times 10^{+05}$
2	$0.426 \times 10^{+03}$	$0.423 \times 10^{+03}$	$0.453 \times 10^{+01}$
3	$0.173 \times 10^{+04}$	$0.140 \times 10^{+04}$	$0.258 \times 10^{+01}$
4	$0.299 \times 10^{+01}$	$0.844 \times 10^{+00}$	0.950×10^{-04}
5	$0.177 \times 10^{+00}$	0.661×10^{-01}	0.269×10^{-08}
6	0.230×10^{-07}	0.190×10^{-04}	0.275×10^{-13}

the free end normal the plane of the frame. This perturbation is removed in a neighborhood of the buckling load, as shown in Figure 4.7.6c. A value of ≈ 1.09 is found for the critical load. The plot of end load versus lateral tip displacement of the frame shown in Figure 4.7.6c is in agreement with the result reported by Argyris *et al* [1979]. The calculation is completed after a total number of 25 loading steps employing displacement control. Perspective and projection views of deformed centroidal line corresponding to the final value of the applied end load are shown in Figures 4.7.6a and 4.7.6b.

Example 4.7.7. Lateral buckling of a hinged right-angle frame subject to fixed end moment. Our final example is concerned with the tracing of the complete post-buckling range of a hinged right-angle frame acted upon by in-plane end moments, as shown in Figure 4.7.7a. The degrees of freedom at the hinged ends are translation along the x direction and rotation about the z direction. The apex of the frame is constrained to lie in the y-z plane. Due to the symmetry of the problem, only half of the frame need be modeled. The problem at hand involves truly large three dimensional rotations and poses a severe test on

the performance of the three dimensional rod model. As the rotation of the hinged end varies from 0° to 360°, the frame rotates out-of-plane about the axis connecting its supports and returns to its initial configuration. During the deformation process the legs of the frame experience significant amounts of twist. This example was first proposed and analyzed by Argyris *et al* [1979] within the framework of a natural formulation based on the notion of *semi-tangential rotation*. Their analysis made use of 10 finite elements with *cubic* interpolation for the displacement field.

The present analysis based on the formulation described above, employs 10 finite elements with *quadratic* isoparametric interpolation for both displacement and rotation fields. Perspective and projection views of deformed configurations of the frame corresponding to various load levels are shown in Figures 4.7.7*b* and 4.7.7*c*. Figure 4.7.7*d* shows the plot of the abscissa of the left hinged end versus the load levels. The results of this analysis differ from those reported by Argyris and co-workers in the following. Upon returning to the initial configuration, the applied end moment must be *identical in magnitude*, but with *reverse sign*, to the critical moment. Hence, the plot of the applied end moment versus lateral displacement of the apex must intersect symmetrically the moment axis. This is clearly the case for the curve shown in Figure 4.7.7.*e*. The analogous curve reported in by Argyris *et al* [1979] violates this condition. The analysis is further pursued past this (negative) critical point and terminated upon completion of a second revolution of the frame about the line connecting its hinged ends. This results in the post-buckling diagram, completely *symmetric* relative to the moment axis, as depicted in Figure 4.7.7*e*. It is emphasized that at the end of the second revolution, the exact *positive critical value* of the applied end moment is recovered. Thus there no difficulty in subjecting the frame to any number of revolutions about the line connecting its

supports. This would lead to the repeated tracing of the bifurcation diagram shown in Figure 4.7.7*e*.

Indeed after completion of the first revolution, the moment vs. lateral apex displacement plot intersects the moment axis at ≈ −626. A value of ≈ +626 for this intersection point is found after completing the second revolution. Initially, a value of only 615.5 is obtained for the maximum moment due to the perturbation load. We recall that this perturbation load is removed subsequently.

The computational effort involved in the calculation for one revolution amounts to 160 loading steps, performed with a combined arc-length and displacement control algorithm. It is noted that the number of loading steps was not optimized.

The basic observation made in Section 4.4 concerning the *lack of symmetry* away from equilibrium, and *recovery of symmetry* at an equilibrium configuration, is numerically illustrated next. The table below shows the row norms of the skew-symmetric part of the global tangent stiffness at an arbitrarily selected load level. These results demonstrate lack of symmetry during the equilibrium iteration process, and confirm symmetry at the equilibrium configuration.

4.8. Concluding remarks

The proposed formulation is developed based on a fully nonlinear rod theory that allows for three dimensional finite rotation, and accounts for finite extension and shearing of the rod. The rotation and moment fields possess the usual physical meaning assigned in classical rod theories, such as the Kirchhoff-Love model; i.e., generally *non-commutative* orthogonal transformations. As a result, it has been shown that the consistent geometric tangent stiffness is *non-symmetric* for any configuration away from equilibrium. This lack of symmetry

BOX 4.12. *Example* 4.7.7.: Recovering of symmetry at equilibrium.

Iteration number	*Skew-symmetric part:* Row-Norm	*Out-of-Balance* Norm
0	1.7×10^{-08}	$0.100 \times 10^{+01}$
1	$1.1 \times 10^{+04}$	$0.784 \times 10^{+04}$
2	$6.9 \times 10^{+02}$	$0.354 \times 10^{+03}$
3	$6.2 \times 10^{+02}$	$0.347 \times 10^{+03}$
4	$1.9 \times 10^{+01}$	$0.108 \times 10^{+02}$
5	$1.6 \times 10^{+00}$	$0.807 \times 10^{+00}$
6	2.5×10^{-03}	0.141×10^{-02}
7	4.6×10^{-08}	0.322×10^{-07}

concerns solely the rotational degrees of freedom, and is absent in the plane problem. It has also been proved that ***full symmetry*** always holds at equilibrium for conservative loading.

The practical implications of the lack of symmetry have been explored in numerical simulations employing a Newton type of iterative solution scheme. Due to the localized character of this non-symmetry, and the full symmetry at equilibrium, it has been demonstrated that use of the symmetrized element tangent stiffness results in *no loss* of asymptotic rate of quadratic convergence.

Based on geometric considerations, an *exact* configuration update procedure has been developed. To avoid the singularity typically associated with parametrizations employing Euler angles or a pseudo-vector of rotation, use has been made of *quaternion* parameters. This choice is optimal in the sense that singularities are avoided and storage requirements are minimized. Particular attention is given to practical aspects involved in the implementation of the update procedure, such as the quaternion extraction from an orthogonal transformation matrix.

In addition, follower loading of the circulatory type is conveniently accounted for in the present formulation as a consequence of the representation of the section rotation by means of a moving orthogonal frame.

A number of numerical simulations have been documented to demonstrate the robustness of the proposed formulation. In particular, the performance of the symmetrized stiffness, the effectiveness of the update procedure, and the excellent rate of convergence have been illustrated throughout these simulations.

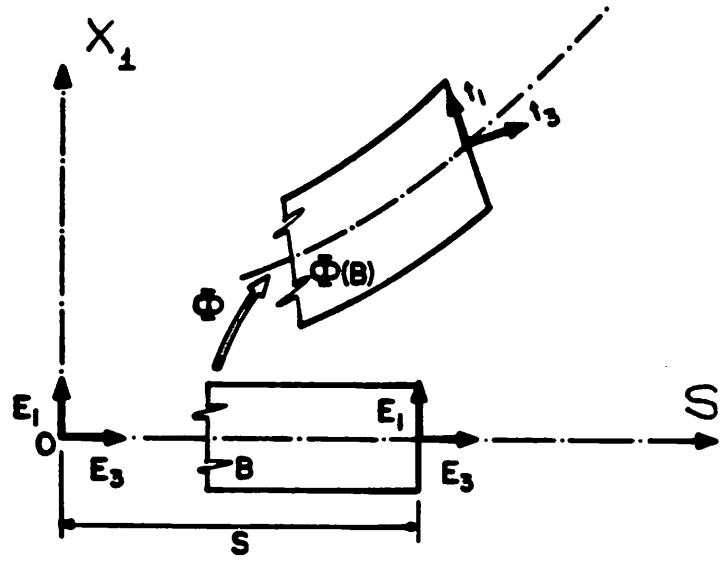

Fig. 4.2.1. Kinematic description of the rod. Definition of various frames.

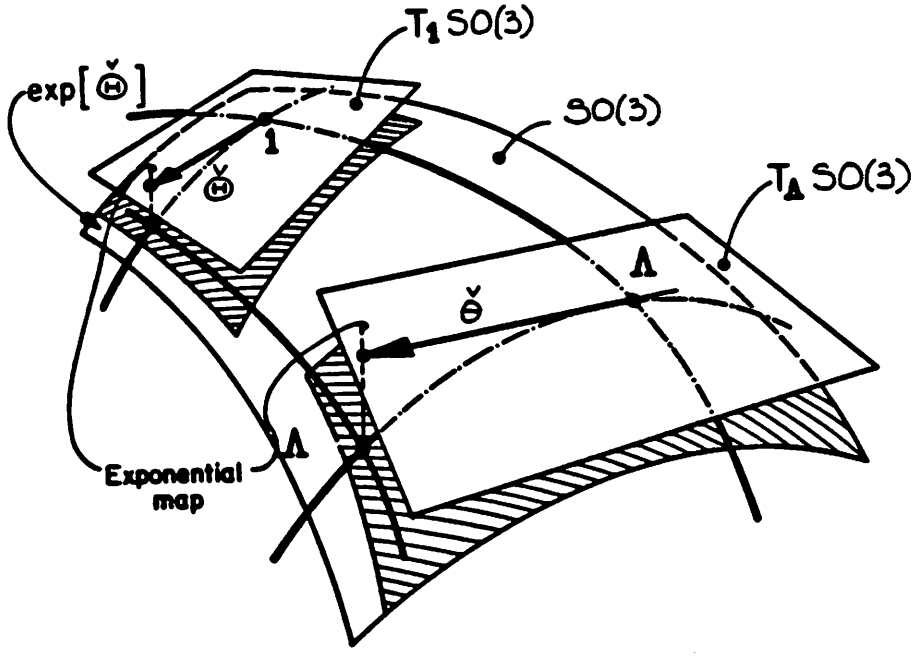

Fig. 4.2.2. Geometric interpretation of the exponential map.

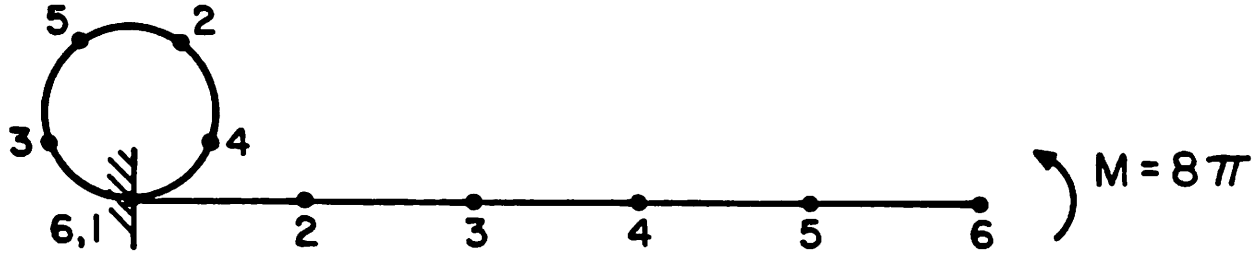

Figure 4.7.1. *Pure bending of a cantilever beam subject to end moment. One* load step. *Two* iterations to convergence.

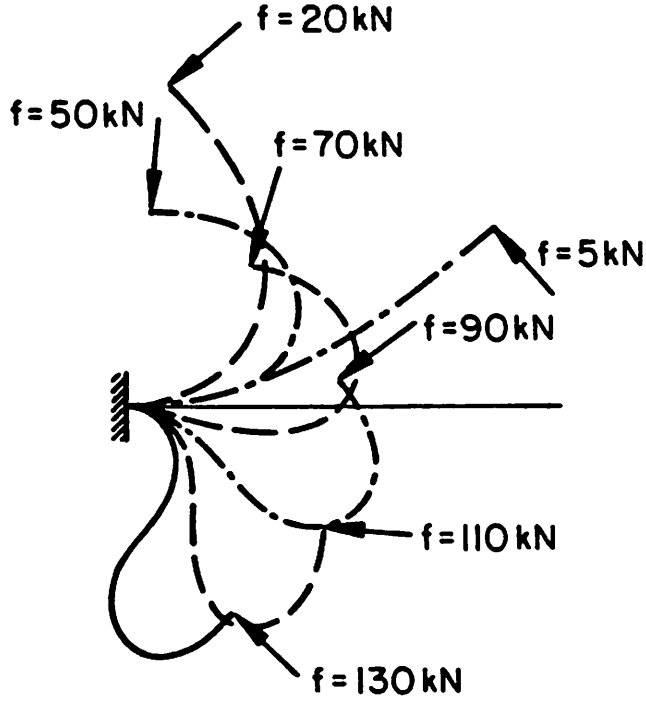

Figure 4.7.2a. *Cantilever beam subject to follower end load.* Deformed shapes.

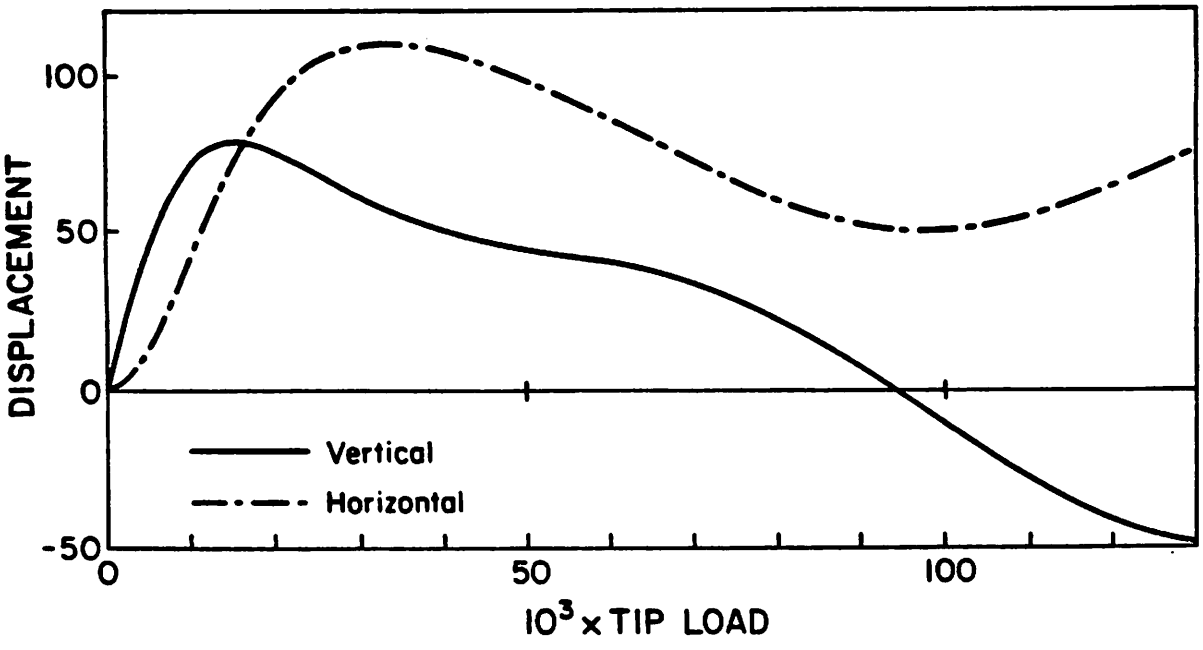

Figure 4.7.2b. *Cantilever beam subject to follower end load.* Vertical and horizontal tip displacement versus applied end load.

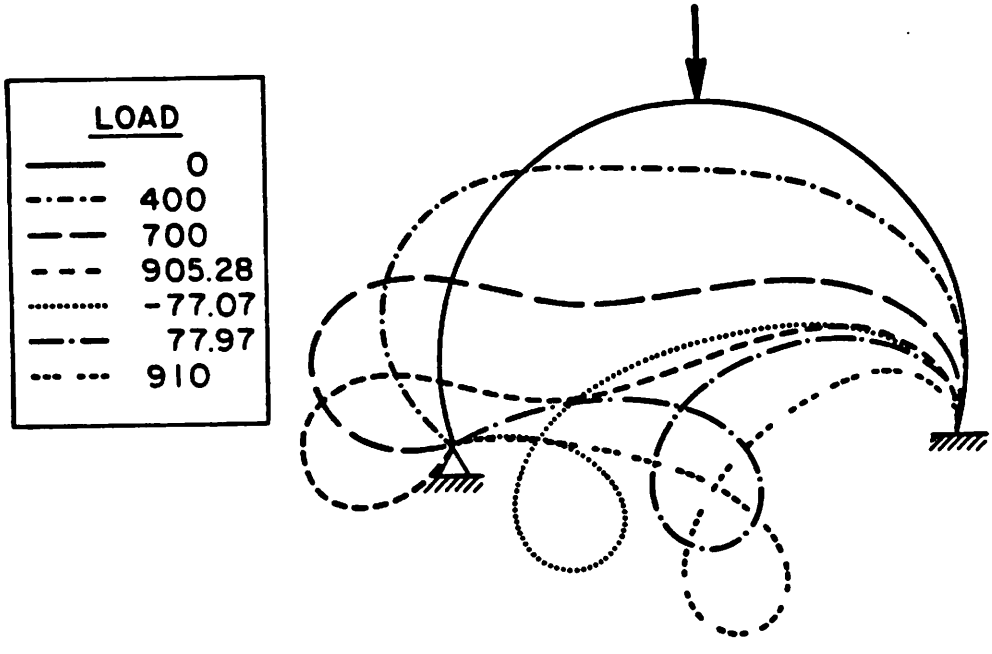

Figure 4.7.3a. *Clamped-hinged deep circular arch subject to point load.* Deformed shapes.

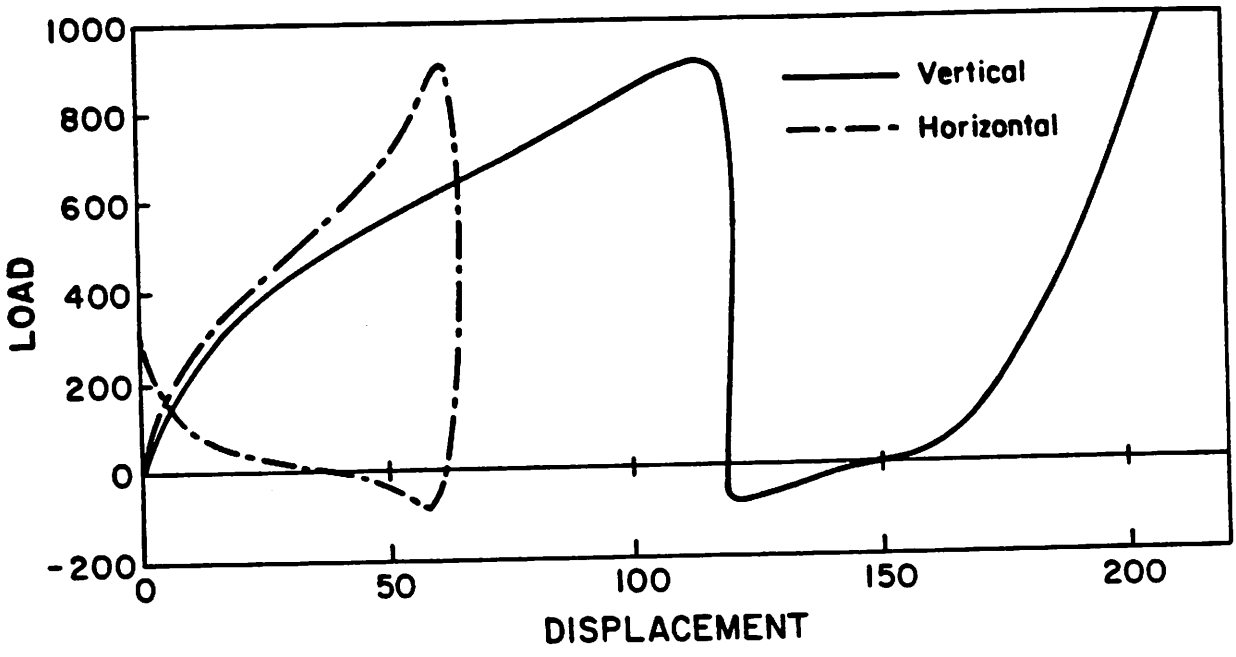

Figure 4.7.3b. *Clamped-hinged deep circular arch subject to point load.* Applied load versus vertical and horizontal displacements of the apex.

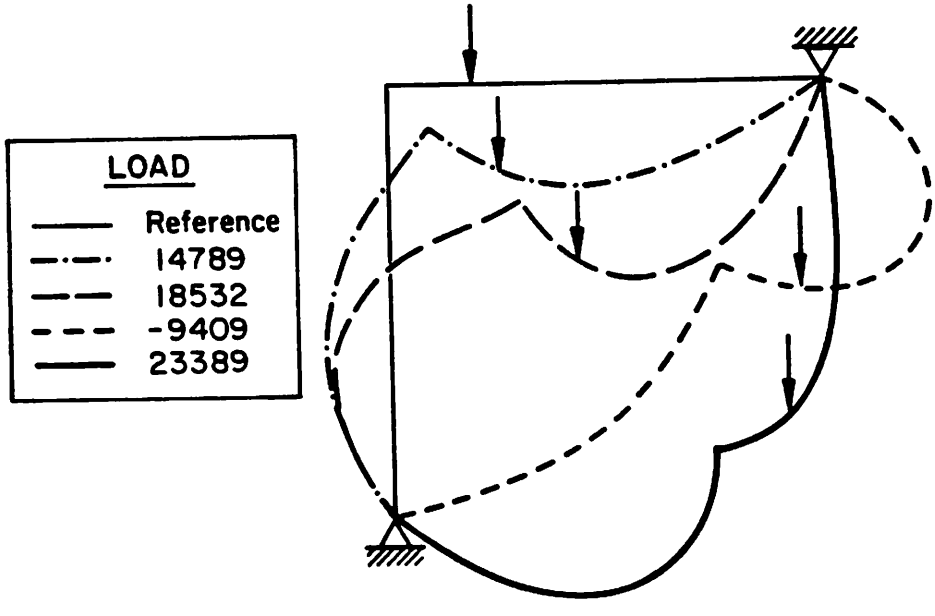

Figure 4.7.4a. *Snap-through of a hinged right-angle frame under fixed point load.* Deformed shapes.

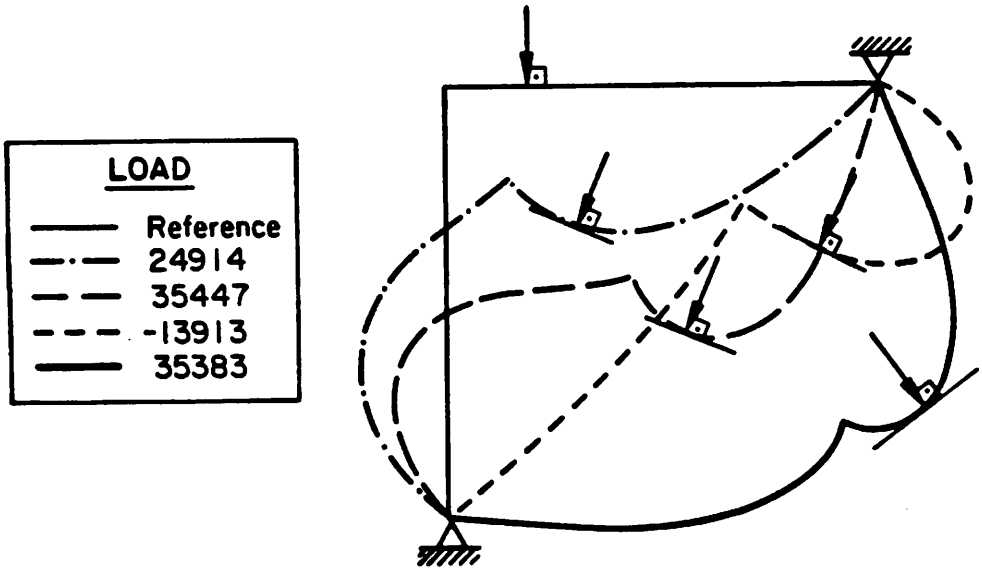

Figure 4.7.4b. *Snap-through of a hinged right-angle frame under follower point load.* Deformed shapes.

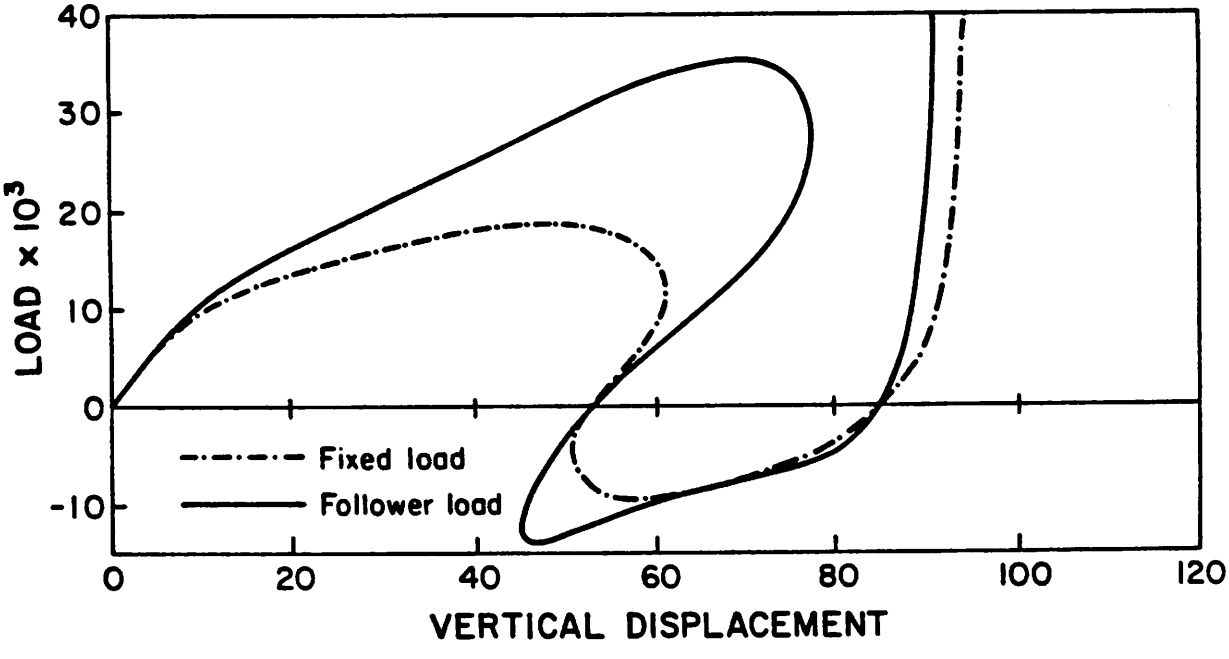

Figure 4.7.4c. *Snap-through of a hinged right-angle frame under fixed and follower load.* Load versus vertical displacement under applied load.

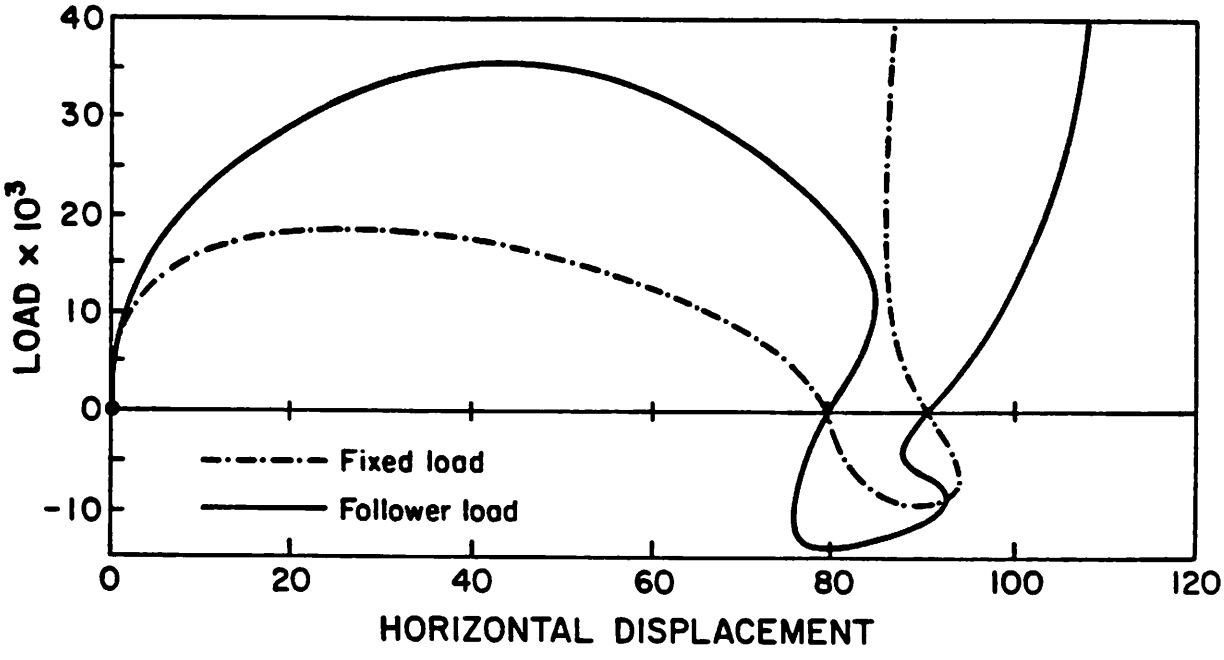

Figure 4.7.4d. *Snap-through of a hinged right-angle frame under fixed and follower load.* Load versus horizontal displacement under applied load.

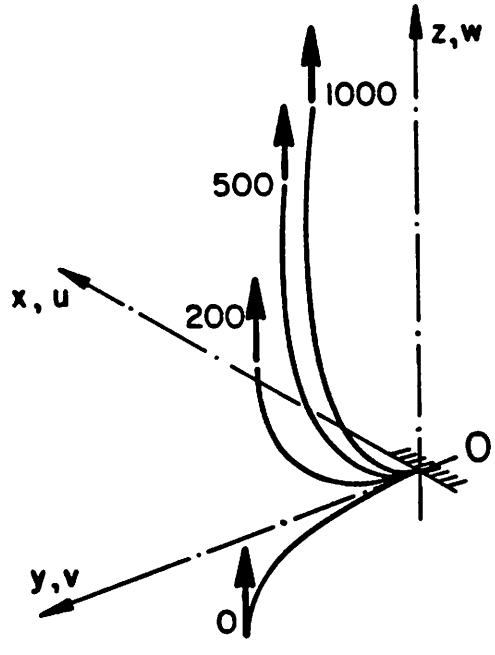

Figure 4.7.5a. *Cantilever* 45° bend subject to fixed end load. Perspective view of deformed shapes.

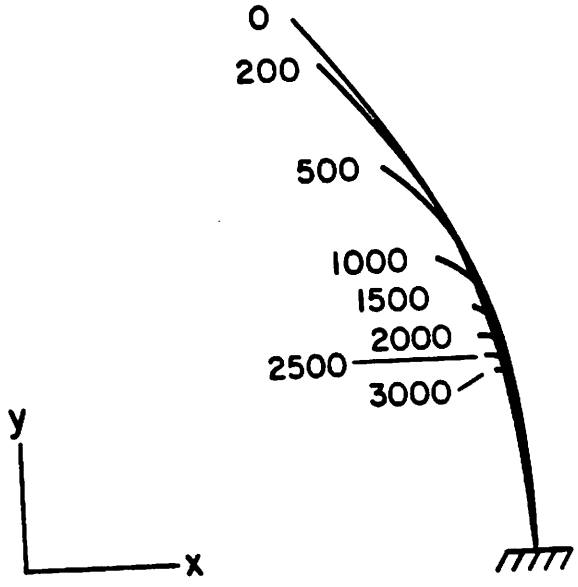

Figure 4.7.5b. *Cantilever* 45° bend subject to fixed end load. Projection of deformed shapes onto the x-y plane.

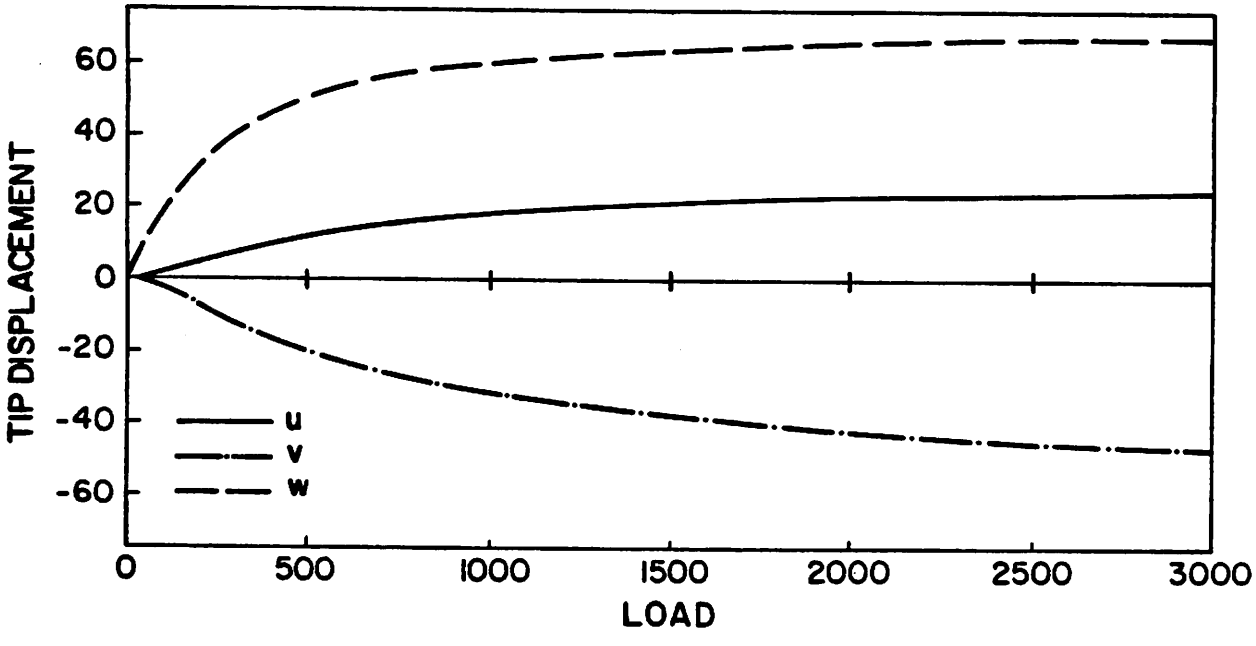

Figure 4.7.5c. *Cantilever* 45° bend subject to fixed end load. Components of tip displacement versus applied load.

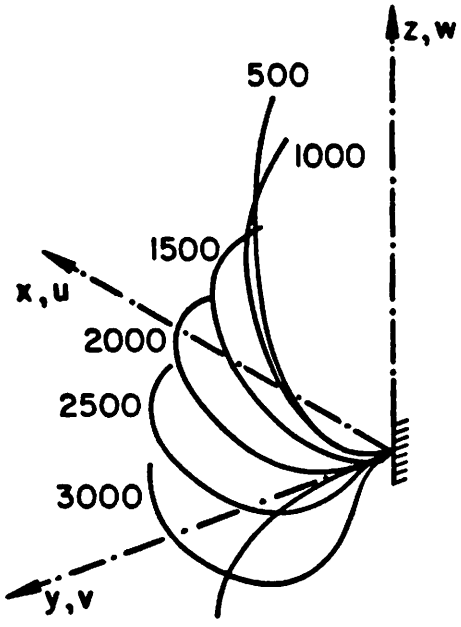

Figure 4.7.5d. *Cantilever* 45° bend subject to follower end load. Perspective view of deformed shapes.

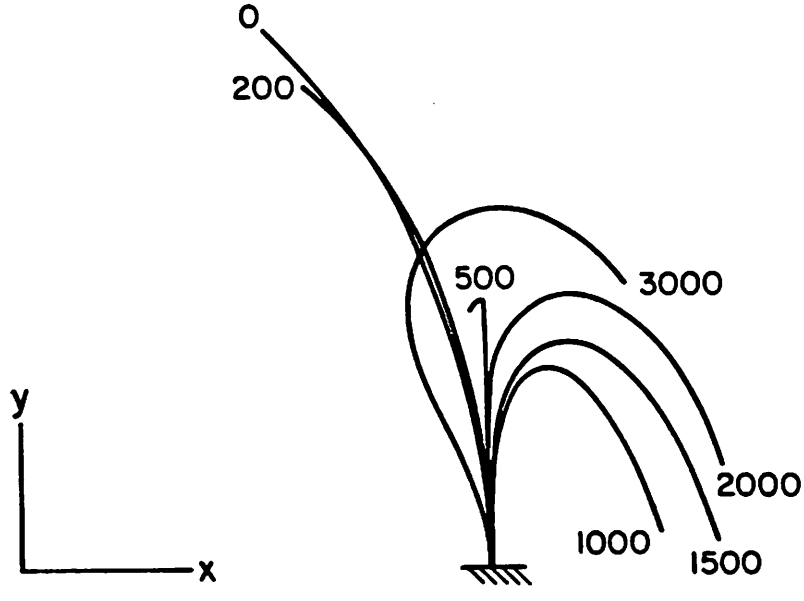

Figure 4.7.5e. *Cantilever* 45° bend subject to follower end load. Projection of deformed shapes onto the x-y plane.

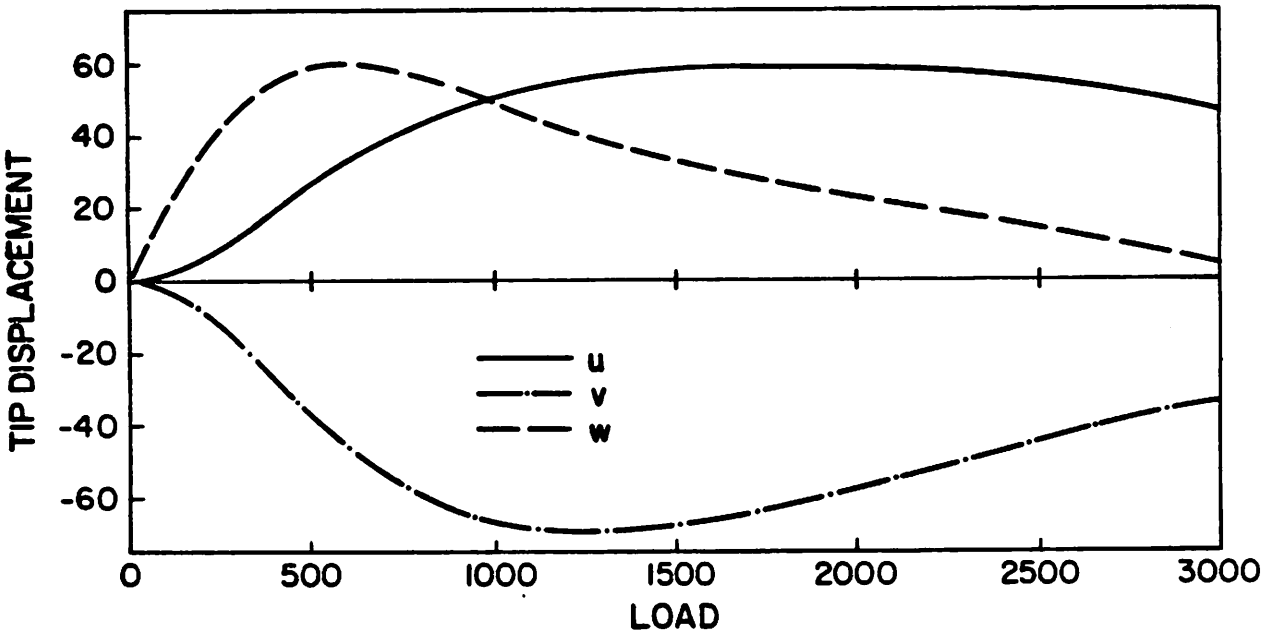

Figure 4.7.5f. *Cantilever* 45° bend subject to follower end load. Components of tip displacement versus applied load.

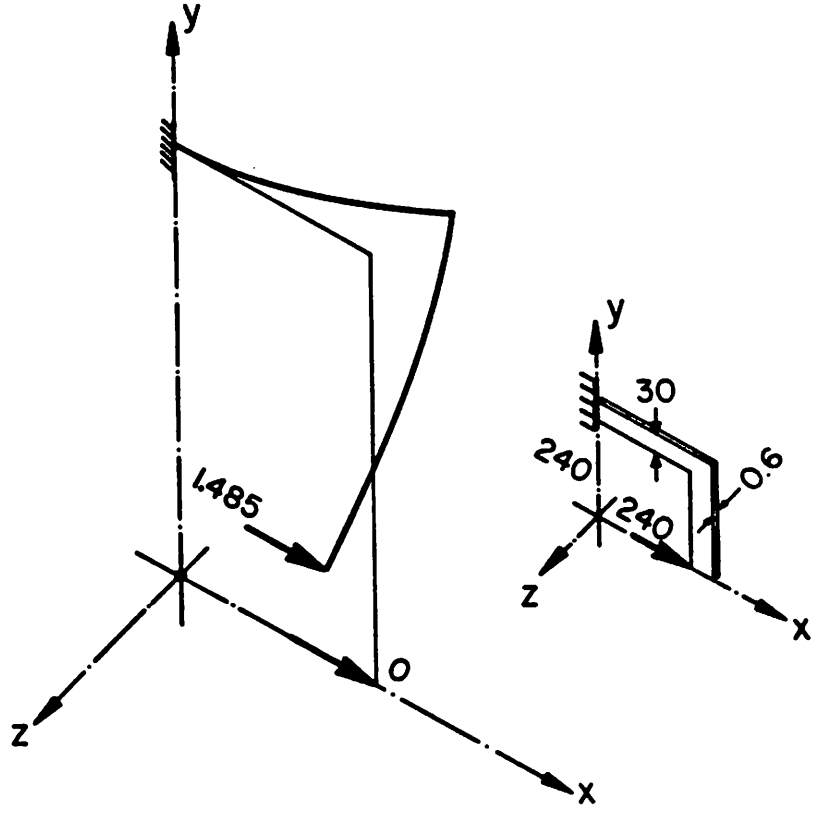

Figure 4.7.6a. *Lateral buckling of a cantilever right-angle frame under end load.* Geometry and perspective view of final deformed shape.

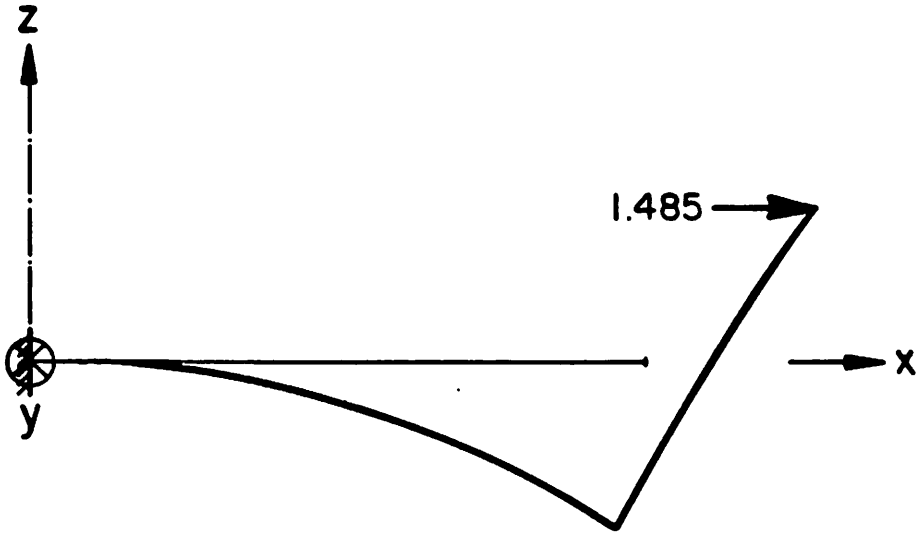

Figure 4.7.6b. ***Lateral buckling of a cantilever right-angle frame under end load.*** Projection of final deformed shape onto the x-z plane.

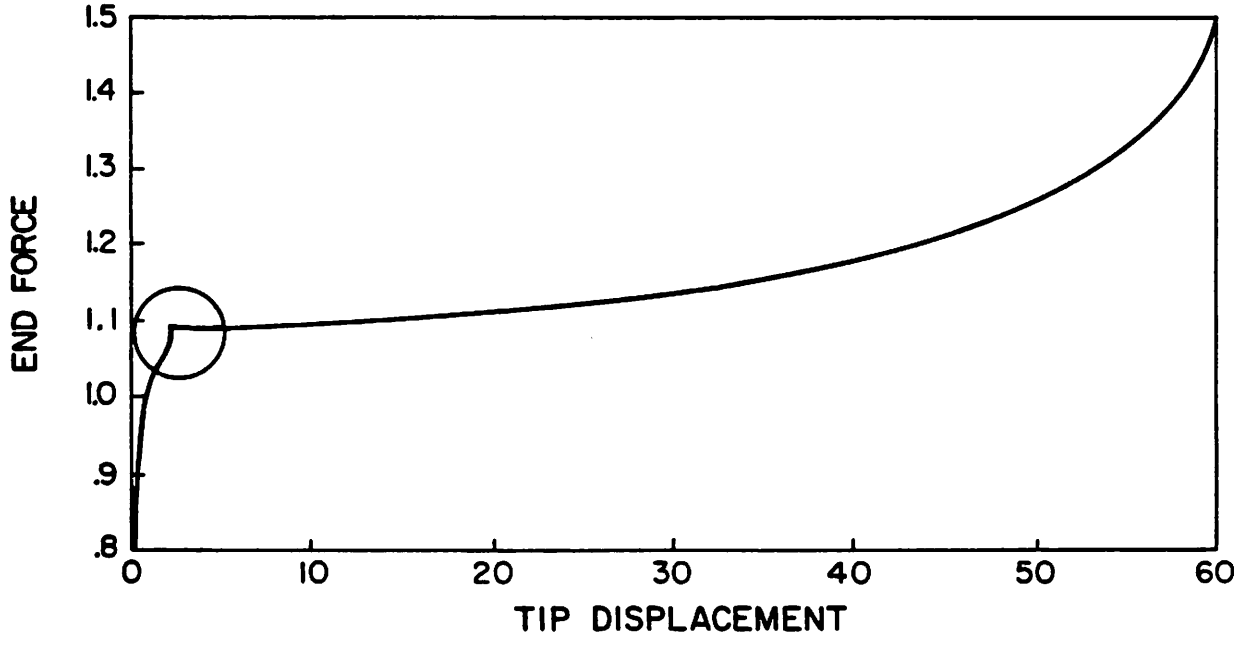

Figure 4.7.6c. ***Lateral buckling of a cantilever right-angle frame under end load.*** Applied load versus lateral tip displacement of the free end.

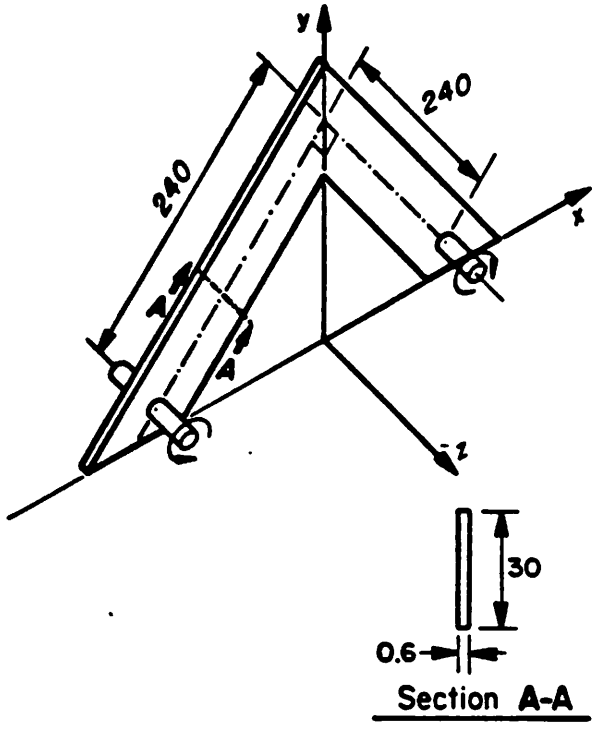

Figure 4.7.7a. ***Lateral buckling of a hinged right-angle frame subject to fixed end moment.*** Geometric characteristics.

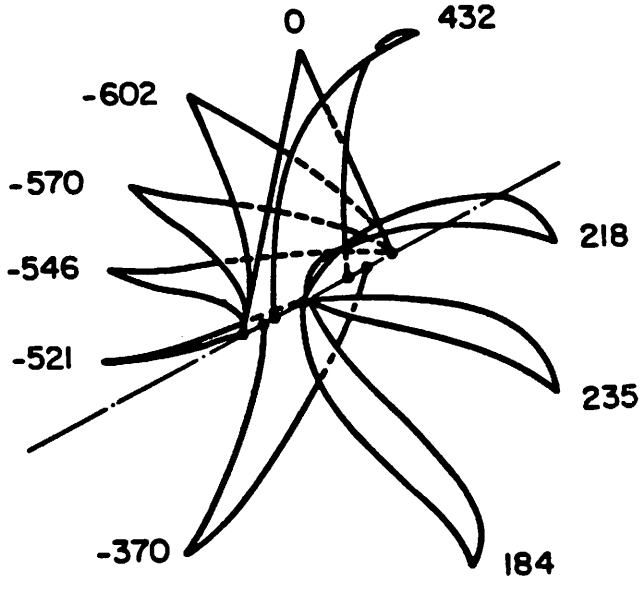

Figure 4.7.7b. ***Lateral buckling of a hinged right-angle frame subject to fixed end moment.*** First revolution: perspective view of deformed shapes at various load level.

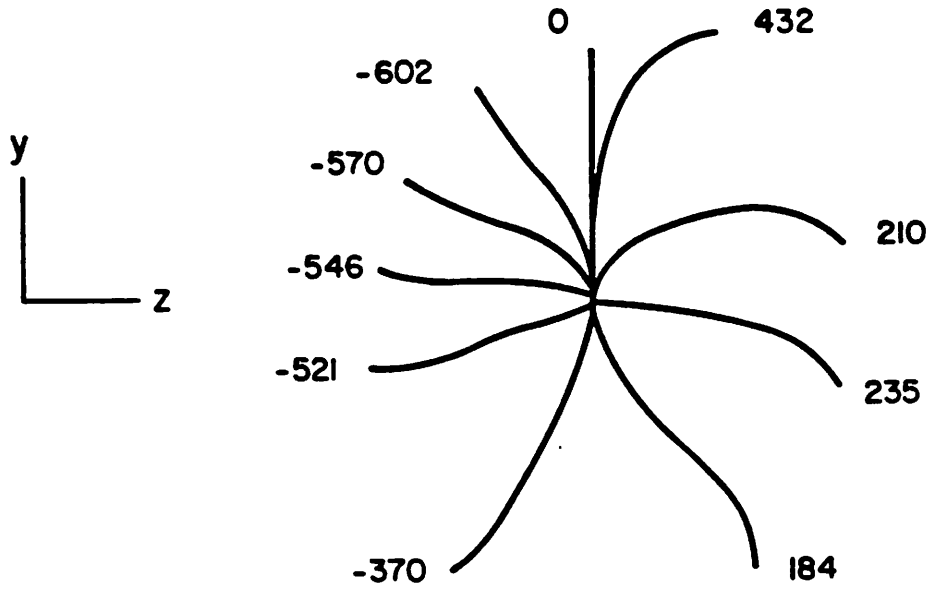

Figure 4.7.7c. *Lateral buckling of a hinged right-angle frame subject to fixed end moment.* First revolution: projection of deformed shapes onto the y-z plane.

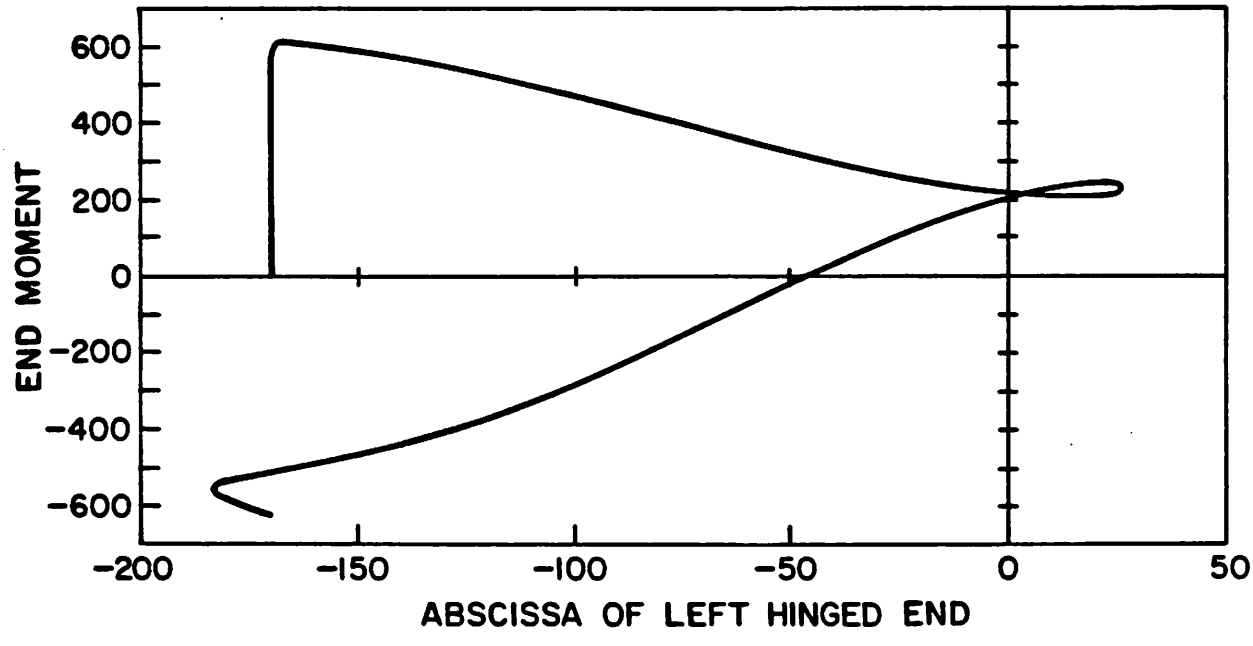

Figure 4.7.7d. *Lateral buckling of a hinged right-angle frame subject to fixed end moment.* First revolution: applied end moment versus abscissa of left hinged end.

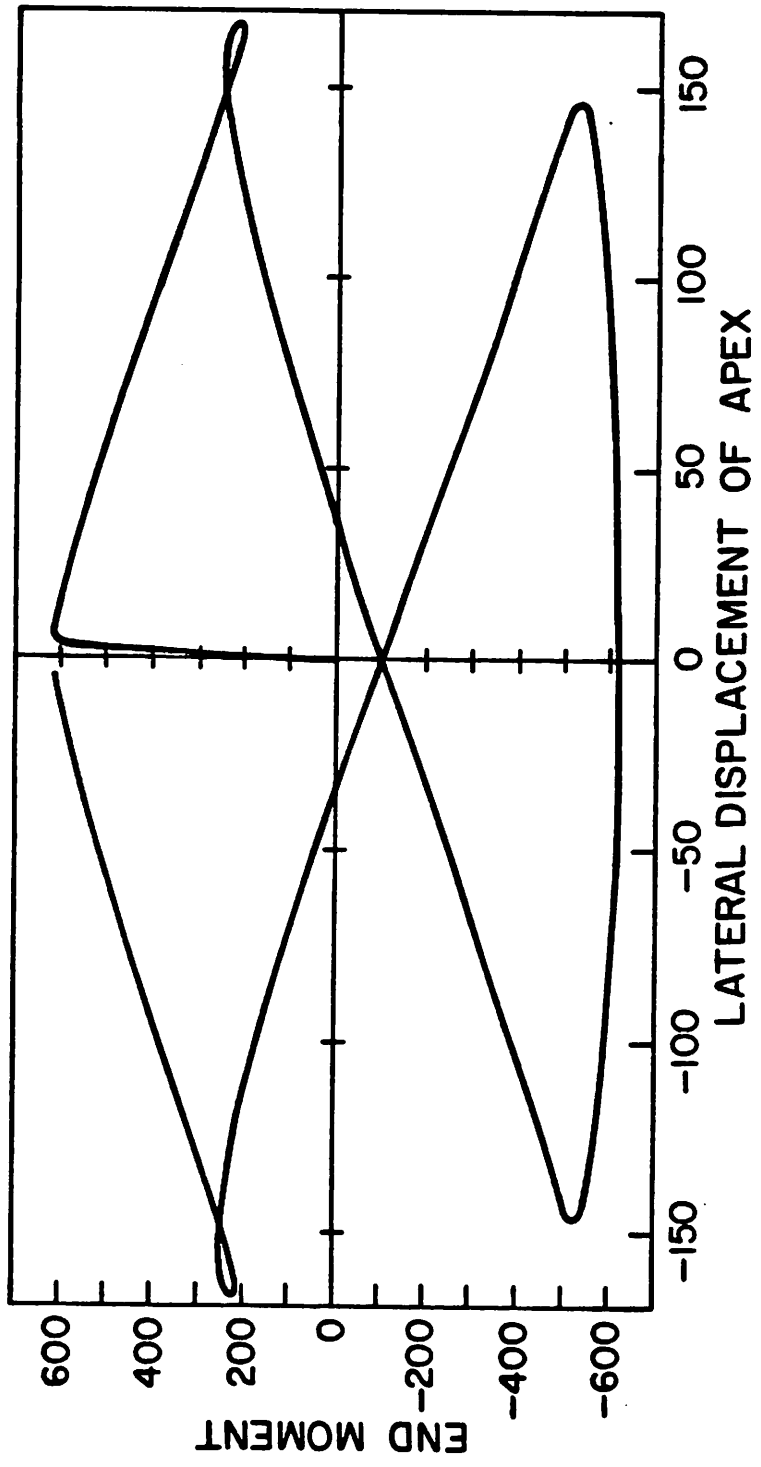

Figure 4.7.7e. ***Lateral buckling of a hinged right-angle frame subject to fixed end moment.*** First and second revolution: applied end moment versus lateral displacement of the apex.

CHAPTER 5

THE DYNAMICS OF THREE-DIMENSIONAL FINITE-STRAIN RODS

5.1. Introduction

The dynamics of a fully nonlinear rod model capable of undergoing finite bending, shearing and extension, whose governing set of nonlinear partial differential equations was given in (4.14), is considered in detail in this chapter. The numerical treatment of the left hand side of these equations, i.e., the static problem, has been considered in the previous chapter. We note that the structure of the inertia operator associated with the rotation field of this rod model is identical to the one that typically arises in rigid body mechanics. Previously developed finite-strain rod models by Reissner [1972,73,81,82] and Parker [1979] in a classical context, and by Antman [1974,75] in the context of a director type of formulation, have been restricted to the static problem. Moreover, the appropriate parametrization of the configuration space, a fundamental question for computational significance, has not been addressed previously.

We recall that, from a computational standpoint, the central issue concerns the treatment of the rotation field which, in the present formulation, has the same physical meaning as in the classical Kirchhoff-Love model; that is, a one parameter family of orthogonal transformations $\mathbf{A}:[0,L] \to SO(3)$ of the rotation group $SO(3)$. The basic difficulty lies in the nature of $SO(3)$, a non-commutative Lie group and not a linear vector space. This difficulty is by-passed in the numerical treatment of the dynamic rod model by Nordgren [1974] by restricting the formulation to cross sections with equal principal moment of inertia and by ignoring the effects of the section rotary inertia. The treatment advocated by Argyris and co-workers [1979,81a-c,82] relies on an alternative characterization of the rotation field employing the notion of semi-tangential rotations.

The numerical integration of the rotation field proposed in this chapter employs an implicit transient algorithm that furnishes the canonical extension of the Newmark formulae, classically stated in the linear space $\mathbf{R}^3 \times \mathbf{R}^3$, to the nonlinear differential manifold $\mathbf{R}^3 \times SO(3)$. In this extension, notions of differential geometry, such as exponential mapping and parallel transport, play a crucial role (Simo & Vu-Quoc [1986b]). The associated configuration update procedure is amenable to a geometric interpretation consistent with that found in the static treatment of the previous chapter. Proofs of the convergence and second order accuracy of the algorithm are also given. In addition, *exact* linearization of the proposed algorithm and associated configuration update is obtained in closed form, leading to a *configuration dependent* tangent inertia matrix, which is *non-symmetric* in the rotational degrees of freedom. This exact linearization results in a *quadratic* rate of asymptotic convergence in solution strategies of the Newton type. Finally, the proposed time-stepping procedure exactly reduces to the classical Newmark algorithm for the plane problem, as illustrated in our first numerical example presented in section 5.5.

The spatial version of the proposed rotation update is related to the procedure first proposed by Hughes & Winget [1980], subsequently rephrased in Hughes [1984] (see Remark 4.4), and employed by a number of authors in different contexts, including the recent comprehensive work of Stanley [1985]. Although both procedures are second order accurate, the update of the rotation field set forth by Hughes & Winget [1980] does not reduce exactly to the plane problem. In addition, the linearization of the latter update procedure was not addressed by the authors. From a computational standpoint both approaches involve essentially the same computational effort.

The formulation developed herein encompasses a general class of nonlinear structural dynamics problems that includes elastic instability and non-

conservative loading, such as follower loads of the circulatory type. A fundamental property of the proposed formulation is that the proper requirements of invariance of strain measures under superposed rigid body motions, satisfied by the continuum rod model, are preserved exactly by the integration algorithm and configuration update procedure. In fact, the appropriate invariance of the strain measures along with the inherent conservation of global linear and angular momenta of the formulation are the essential ingredients for the success of the methodology proposed in Chapter 2 on the dynamics of flexible beams undergoing large overall motions. We note that application of the present algorithm is also of interest in bioengineering (e.g., Mital & King [1979]).

5.2. Weak form of the governing equations

We first summarize in Box 5.1 the complete set of partial differential equations governing the motion of the rod. The function $\psi(S, \mathbf{\Gamma}, \mathbf{\Omega})$ corresponds to the constitutive law relating the strain measures $\mathbf{\Gamma}$ and $\mathbf{\Omega}$ to the internal forces $\mathbf{n}$ and $\mathbf{m}$. We often assume in practice

$$\psi(S, \mathbf{\Gamma}, \mathbf{\Omega}) = \frac{1}{2}\begin{Bmatrix}\mathbf{\Gamma}\\ \mathbf{\Omega}\end{Bmatrix}\cdot \mathbf{C}\begin{Bmatrix}\mathbf{\Gamma}\\ \mathbf{\Omega}\end{Bmatrix}, \tag{5.1}$$

with $\mathbf{C}$ defined in (4.18a). The mass per unit reference length of the beam is denoted by $A_\rho := \int_\Omega \rho_0 \, d\Omega$, where ρ_0 represents the mass density. Let $\mathbf{I}_\rho = \mathbb{I}_{IJ}\mathbf{E}_I\otimes\mathbf{E}_J$ be the inertia dyadic (constant with respect to time) of the cross section in the reference configuration given by

$$\mathbf{I}_\rho(S) := \mathbb{I}_{\alpha\beta}(S)\,[\delta_{\alpha\beta}\,\mathbf{1}_3 - \mathbf{E}_\alpha\otimes\mathbf{E}_\beta]\,, \qquad \mathbb{I}_{\alpha\beta}(S) := \int_{\Omega(S)} \rho_0(S)\, X_\alpha\, X_\beta \, d\Omega\dagger \tag{5.2}$$

† Subscripts in greek letters take values in {1,2}, while subscripts in roman letters take values in {1,2,3}.

BOX 5.1. *Partial differential equations of motion*

$$\frac{\partial \mathbf{\Lambda}(S,t)}{\partial S} = \overset{\mathbf{v}}{\boldsymbol{\omega}}(S,t)\,\mathbf{\Lambda}(S,t)\,, \qquad \frac{\partial \mathbf{\Lambda}(S,t)}{\partial t} = \overset{\mathbf{v}}{\mathbf{w}}(S,t)\,\mathbf{\Lambda}(S,t)$$

$$\boldsymbol{\Gamma} = \mathbf{\Lambda}^T \frac{\partial \boldsymbol{\phi}_o(S,t)}{\partial S} - \mathbf{E}_3\,, \qquad \boldsymbol{\Omega} = \mathbf{\Lambda}^T\,\boldsymbol{\omega}$$

$$\mathbf{n} = \mathbf{\Lambda}\,\frac{\partial \psi(S,\boldsymbol{\Gamma},\boldsymbol{\Omega})}{\partial \boldsymbol{\Gamma}}, \qquad \mathbf{m} = \mathbf{\Lambda}\,\frac{\partial \psi(S,\boldsymbol{\Gamma},\boldsymbol{\Omega})}{\partial \boldsymbol{\Omega}}$$

$$\frac{\partial \mathbf{n}}{\partial S} + \bar{\mathbf{n}} = A_\rho\,\ddot{\boldsymbol{\phi}}_o$$

$$\frac{\partial \mathbf{m}}{\partial S} + \frac{\partial \boldsymbol{\phi}_o}{\partial S} \times \mathbf{n} + \bar{\mathbf{m}} = \mathbf{I}_\rho\,\dot{\mathbf{w}} + \mathbf{w} \times [\mathbf{I}_\rho\,\mathbf{w}]$$

Further, we introduce the time dependent spatial tensor $\mathbf{I}_\rho = \mathrm{I}_{\alpha\beta}\mathbf{e}_\alpha \otimes \mathbf{e}_\beta$ such that $\mathbf{I}_\rho(S,t) = \mathbf{\Lambda}(S,t)\,\mathbf{I}_\rho(S)\,\mathbf{\Lambda}^T(S,t)$.

Dynamic weak form. Multiplying the equations of balance laws in spatial local form by an arbitrary admissible variation $\boldsymbol{\eta} := (\boldsymbol{\eta}_o, \boldsymbol{\psi}) \in T_{\boldsymbol{\phi}}C$ defined in (4.22), one obtains the dynamic (spatial) weak form

$$G_{dyn}(\boldsymbol{\phi}, \boldsymbol{\eta}) := \int_{[0,L]} \{A_\rho\,\ddot{\boldsymbol{\phi}}_o \cdot \boldsymbol{\eta}_o + [\mathbf{I}_\rho\,\dot{\mathbf{w}} + \mathbf{w} \times (\mathbf{I}_\rho\,\mathbf{w})] \cdot \boldsymbol{\psi}\}\,dS - G(\boldsymbol{\phi}, \boldsymbol{\eta}) = 0, \quad (5.3a)$$

where $G(\boldsymbol{\phi}, \boldsymbol{\eta})$ is the weak form of the local static equilibrium equations given in spatial form in (4.34) and in material form in (4.35). The rotation part of the inertia part can be rephrased in material form as follows

$$G_{dyn}(\boldsymbol{\phi}, \boldsymbol{\eta}) := \int_{[0,L]} \{A_\rho\,\ddot{\boldsymbol{\phi}}_o \cdot \boldsymbol{\eta}_o + \mathbf{\Lambda}[\mathbf{I}_\rho\,\dot{\mathbf{W}} + \mathbf{W} \times (\mathbf{I}_\rho\,\mathbf{W})] \cdot \boldsymbol{\psi}\}\,dS - G(\boldsymbol{\phi}, \boldsymbol{\eta}) = 0. \quad (5.3b)$$

5.3. Implicit time-stepping algorithms

In this section we develop an implicit time-stepping algorithm for the time integration of the weak form (5.3). The novelty of the proposed approach lies in the treatment of the rotational part, which relies crucially on the use of the discrete counterparts of the *exponential map* and *parallel transport* in the orthogonal group $SO(3)$. The algorithm and associated configuration update may be phrased in either a *spatial* or a *material* setting. In the language of rigid body mechanics, the difference amounts to phrasing the formulation in either spatial or body coordinates. The geometric interpretation of the proposed procedure and its implementation are considered in detail.

5.3.1. Formulation

In line with standard usage, we employ the subscript n to denote the temporal discrete approximate of a time-varying quantity at time t_n; thus for the displacement field $\mathbf{d}_n(S) \cong \boldsymbol{\phi}_o(S,t_n)$, $\mathbf{v}_n(S) \cong \dot{\boldsymbol{\phi}}_o(S,t_n)$, $\mathbf{a}_n(S) \cong \ddot{\boldsymbol{\phi}}_o(S,t_n)$, and for the rotation field $\boldsymbol{\Lambda}_n(S) \cong \boldsymbol{\Lambda}(S,t_n)$, $\mathbf{w}_n(S) \cong \mathbf{w}(S,t_n)$, $\boldsymbol{\alpha}_n(S) \cong \boldsymbol{\alpha}(S,t_n)$. The material version of the spatial angular velocity $\mathbf{w}$ and acceleration $\boldsymbol{\alpha}$ are denoted respectively by $\mathbf{W}$ and $\mathbf{A}$ such that $\mathbf{W} = \boldsymbol{\Lambda}^T\mathbf{w}$ and $\mathbf{A} = \boldsymbol{\Lambda}^T\boldsymbol{\alpha}$. The basic problem concerning the discrete time-stepping update may be formulated as follows. Given a configuration $\boldsymbol{\phi}_n := (\mathbf{d}_n, \boldsymbol{\Lambda}_n) \in C$, its associated linear and angular velocities, $(\mathbf{v}_n, \mathbf{w}_n)$, and linear and angular accelerations $(\mathbf{a}_n, \boldsymbol{\alpha}_n)$, obtain the *updated* configuration $\boldsymbol{\phi}_{n+1} := (\mathbf{d}_{n+1}, \boldsymbol{\Lambda}_{n+1}) \in C$ at time $t_{n+1} = t_n + h$, the associated updated linear and angular velocities $(\mathbf{v}_{n+1}, \mathbf{w}_{n+1})$, and the updated linear and angular acceleration $(\mathbf{a}_{n+1}, \boldsymbol{\alpha}_{n+1})$, in a manner that is (a) *consistent* and (b) *stable* with the weak form (5.3a,b).

To this end, we proposed the algorithm summarized in Box 5.2 below. Note that the algorithm for the translational part of the configuration, that is

$(S, t) \to \boldsymbol{\phi}_o(S, t) \in \mathbb{R}^3$, is the classical Newmark algorithm of nonlinear elastodynamics (see e.g., Belytschko & Hughes [1983]). The proposed algorithm for the rotational part $(S, t) \to \mathbf{A}(S, t) \in SO(3)$, in its material version, furnishes the canonical extension of the Newmark formulas to the orthogonal group $SO(3)$.

BOX 5.2. *Implicit time-stepping algorithm*

Momentum Balance at t_{n+1}

$$\int_{[0,L]} \{A_\rho \, \mathbf{a}_{n+1} \cdot \boldsymbol{\eta}_o + [\mathbf{I}_{\rho n+1} \, \boldsymbol{\alpha}_{n+1} + \mathbf{w}_{n+1} \times (\mathbf{I}_{\rho n+1} \, \mathbf{w}_{n+1})] \cdot \boldsymbol{\psi}\} \, dS + G(\boldsymbol{\phi}_{n+1}, \boldsymbol{\eta}) = 0$$

or

$$\int_{[0,L]} \{A_\rho \, \mathbf{a}_{n+1} \cdot \boldsymbol{\eta}_o + \mathbf{A}_{n+1}[\mathbf{I}_\rho \, \mathbf{A}_{n+1} + \mathbf{W}_{n+1} \times (\mathbf{I}_\rho \, \mathbf{W}_{n+1})] \cdot \boldsymbol{\psi}\} \, dS + G(\boldsymbol{\phi}_{n+1}, \boldsymbol{\eta}) = 0$$

Translational Part (Classical Newmark)

$$\mathbf{d}_{n+1} = \mathbf{d}_n + \mathbf{u}_n$$

$$\mathbf{u}_n = h \, \mathbf{v}_n + h^2 [(\tfrac{1}{2} - \beta) \, \mathbf{a}_n + \beta \, \mathbf{a}_{n+1}]$$

$$\mathbf{v}_{n+1} = \mathbf{v}_n + h \, [(1 - \tau) \, \mathbf{a}_n + \tau \, \mathbf{a}_{n+1}]$$

Rotational Part

Spatial Setting	*Material Setting*
$\mathbf{A}_{n+1} = \exp[\overset{\vee}{\boldsymbol{\vartheta}}_n] \, \mathbf{A}_n$	$\mathbf{A}_{n+1} = \mathbf{A}_n \exp[\overset{\vee}{\boldsymbol{\Theta}}_n]$
$\overset{\vee}{\boldsymbol{\vartheta}}_n = h \, \overset{\vee}{\mathbf{w}}_n + h^2 [(\frac{1}{2} - \beta) \, \overset{\vee}{\boldsymbol{\alpha}}_n + \beta \, \overset{\vee}{\boldsymbol{\alpha}}_{n+1}]$	$\overset{\vee}{\boldsymbol{\Theta}}_n = h \, \overset{\vee}{\mathbf{W}}_n + h^2 [(\frac{1}{2} - \beta) \, \overset{\vee}{\mathbf{A}}_n + \beta \, \overset{\vee}{\mathbf{A}}_{n+1}]$
$\overset{\vee}{\mathbf{w}}_{n+1} = \overset{\vee}{\mathbf{w}}_n + h \, [(1 - \tau) \, \overset{\vee}{\boldsymbol{\alpha}}_n + \tau \, \overset{\vee}{\boldsymbol{\alpha}}_{n+1}]$	$\overset{\vee}{\mathbf{W}}_{n+1} = \overset{\vee}{\mathbf{W}}_n + h \, [(1 - \tau) \, \overset{\vee}{\mathbf{A}}_n + \tau \, \overset{\vee}{\mathbf{A}}_{n+1}]$

β and τ designate the Newmark parameters.

Remark 5.1. Since the inertia dyadic has constant components in the material basis $\{\mathbf{E}_i\}$, it is more advantageous to write the time-stepping algorithm for the rotation part in the material setting, as indicated in Box 5.2. Recall that the update of the rotation field in the spatial setting is given by the left translation in $SO(3)$, while in the material setting it is given by the right translation. The spatial setting of the time-stepping algorithm can be thought of as

emanating from the system of differential equations

$$\begin{aligned} \dot{\mathbf{A}} &= \overset{\mathrm{v}}{\mathbf{w}}\mathbf{A}, \quad \mathbf{A} \in SO(3), \\ \dot{\mathbf{w}} &= \mathbf{a}; \end{aligned} \tag{5.4a}$$

the material setting is, on the other hand, governed by

$$\begin{aligned} \dot{\mathbf{A}} &= \mathbf{A}\overset{\mathrm{v}}{\mathbf{W}}, \quad \mathbf{A} \in SO(3), \\ \dot{\mathbf{W}} &= \mathbf{A}. \end{aligned} \tag{5.4b}$$

A precise consistency argument of the algorithm will be given in Lemma 5.2. ∎

Geometric interpretation. Further insight into the nature of the algorithm summarized in Box 5.2 is gained by examining its geometric interpretation. For the translational part, the time-stepping procedure is the standard Newmark algorithm and takes place in $\mathbb{R}^3$. Hence, the exponential map reduces to the identity, and the parallel transport is simply a shift of the base point. Pictorially, we have the situation depicted in Figure 5.3.1.

For the rotational part, the time-stepping procedure takes place in $SO(3)$. A given configuration $\mathbf{A}_n \in SO(3)$ is updated forward in time by exponentiating the incremental rotation $\overset{\mathrm{v}}{\boldsymbol{\vartheta}}_n \in so(3)$ to obtain $\mathbf{A}_{n+1} = \exp[\overset{\mathrm{v}}{\boldsymbol{\vartheta}}_n]\,\mathbf{A}_n$ (left translation). Since $\overset{\mathrm{v}}{\boldsymbol{\Theta}}_n = \mathbf{A}_n^T \overset{\mathrm{v}}{\boldsymbol{\vartheta}}_n \mathbf{A}_n$ (or in terms of axial vector $\boldsymbol{\Theta}_n = \mathbf{A}_n^T \boldsymbol{\vartheta}_n$), it follows from the properties of the exponential map (see definition (4.5a)) that $\mathbf{A}_{n+1} = \mathbf{A}_n \exp[\overset{\mathrm{v}}{\boldsymbol{\Theta}}_n]$ (right translation), which is the update formula recorded in Box 5.2. Such a procedure ensures that $\mathbf{A}_{n+1}$ remains in $SO(3)$ in the natural way by making use of the translation in $SO(3)$. Note that the step forward in time of the angular velocity and acceleration is performed in the same tangent space $T_1SO(3)$. The result is then parallel transported to $T_{\mathbf{A}_{n+1}}SO(3)$.

5.3.2. Update procedure: Basic setup

The formulae contained in Box 5.2, define the velocity $(\mathbf{v}_{n+1}, \mathbf{w}_{n+1})$ and the acceleration $(\mathbf{a}_{n+1}, \boldsymbol{\alpha}_{n+1})$ in terms of the *incremental field* $\Delta\boldsymbol{\phi}_n := (\mathbf{u}_n, \boldsymbol{\vartheta}_n)$ from the base points $(\mathbf{v}_n, \mathbf{w}_n)$ and $(\mathbf{a}_n, \boldsymbol{\alpha}_n)$, respectively. Thus, the weak form of momentum balance at time t_{n+1}, $G_{dyn}(\boldsymbol{\phi}(S, t_{n+1}), \boldsymbol{\eta}(S)) = 0$, depending on velocity and acceleration becomes, by virtue of the time stepping-algorithm, a nonlinear functional of the configuration $\boldsymbol{\phi}_{n+1}$ denoted by $G_{dyn}(\boldsymbol{\phi}_{n+1}, \boldsymbol{\eta})$. The solution of this nonlinear variational equation is accomplished by an iterative scheme of the Newton type, as follows.

Assume that $\boldsymbol{\phi}_{n+1}^{(i)} := (\mathbf{d}_{n+1}^{(i)}, \mathbf{A}_{n+1}^{(i)})$ is known. By solving the linearized weak form about $\boldsymbol{\phi}_{n+1}^{(i)}$ one obtains an *incremental* field $\Delta\boldsymbol{\phi}_{n+1}^{(i)} := (\Delta\mathbf{u}_{n+1}^{(i)}, \Delta\boldsymbol{\vartheta}_{n+1}^{(i)})$. The basic setup is: Given $\Delta\boldsymbol{\phi}_{n+1}^{(i)} \in T_{\boldsymbol{\phi}_{n+1}^{(i)}} C$, update $\boldsymbol{\phi}_{n+1}^{(i)} \in C$ to $\boldsymbol{\phi}_{n+1}^{(i+1)} \in C$ in a manner consistent with the time-stepping algorithm in Box 5.2. Again the central issue concerns the update of the incremental rotation. First, making use of the exponential, one sets

$$\mathbf{A}_{n+1}^{(i)} = \exp[\hat{\boldsymbol{\vartheta}}_n^{(i)}]\, \mathbf{A}_n \,, \qquad \mathbf{A}_{n+1}^{(i+1)} = \exp[\hat{\boldsymbol{\vartheta}}_n^{(i+1)}]\, \mathbf{A}_n \,. \tag{5.5}$$

Note that (5.5) makes sense since $\boldsymbol{\Theta}_n^{(i)}\, \mathbf{A}_n$ and $\boldsymbol{\Theta}_n^{(i+1)}\, \mathbf{A}_n$ are both in the tangent space at $\mathbf{A}_n$. Next, making use of the incremental exponential map we have

$$\mathbf{A}_{n+1}^{(i+1)} = \exp[\Delta\hat{\boldsymbol{\vartheta}}_{n+1}^{(i)}]\, \mathbf{A}_{n+1}^{(i)} \tag{5.6}$$

Again we note that (5.6) makes geometric sense since $\Delta\hat{\boldsymbol{\vartheta}}_{n+1}^{(i)}\mathbf{A}_{n+1}^{(i)}$ is in the tangent space at $\mathbf{A}_{n+1}^{(i)}$. Combining (5.5) and (5.6) we obtain the update formula in Box 5.3.

Remark 5.2. Initial guess. The update procedure in Box 5.3 applies for $i \geq 1$. As noted in Section 2.4.2 of Chapter 2, the best suitable starting scheme

BOX 5.3. *Update procedure given* $\Delta\boldsymbol{\phi}_{n+1}^{(i)} := (\Delta\mathbf{u}_{n+1}^{(i)}, \Delta\boldsymbol{\vartheta}_{n+1}^{(i)}) \in T_{\boldsymbol{\phi}_{n+1}^{(i)}} C$

Translation	Rotation
$\mathbf{d}_{n+1}^{(i+1)} = \mathbf{d}_{n+1}^{(i)} + \Delta\mathbf{u}_{n+1}^{(i)}$	$\mathbf{A}_{n+1}^{(i+1)} = \exp[\Delta\overset{\vee}{\boldsymbol{\vartheta}}_{n+1}^{(i)}]\,\mathbf{A}_{n+1}^{(i)}$
$\mathbf{v}_{n+1}^{(i+1)} = \mathbf{v}_{n+1}^{(i)} + \frac{\tau}{h\beta}\Delta\mathbf{u}_{n+1}^{(i)}$	$\exp[\overset{\vee}{\boldsymbol{\vartheta}}_{n}^{(i+1)}] = \exp[\Delta\overset{\vee}{\boldsymbol{\vartheta}}_{n+1}^{(i)}]\exp[\overset{\vee}{\boldsymbol{\vartheta}}_{n}^{(i)}]$
$\mathbf{a}_{n+1}^{(i+1)} = \mathbf{a}_{n+1}^{(i)} + \frac{1}{h^2\beta}\Delta\mathbf{u}_{n+1}^{(i)}$	$\mathbf{W}_{n+1}^{(i+1)} = \mathbf{W}_{n+1}^{(i)} + \frac{\tau}{h\beta}[\boldsymbol{\Theta}_{n}^{(i+1)} - \boldsymbol{\Theta}_{n}^{(i)}]$
	$\mathbf{A}_{n+1}^{(i+1)} = \mathbf{A}_{n+1}^{(i)} + \frac{1}{h^2\beta}[\boldsymbol{\Theta}_{n}^{(i+1)} - \boldsymbol{\Theta}_{n}^{(i)}]$

(i.e., for $i = 0$) in the Newton process is to initialize the displacement quantities with the previously converged ones; that is, one sets $\mathbf{d}_{n+1}^{(0)} = \mathbf{d}_n$ and $\mathbf{A}_{n+1}^{(0)} = \mathbf{A}_n$. With this assumption, $(\mathbf{v}_{n+1}^{(0)}, \mathbf{a}_{n+1}^{(0)})$ and $(\mathbf{W}_{n+1}^{(0)}, \mathbf{A}_{n+1}^{(0)})$ are then computed by the Newmark formulae given in Box 5.2,

$$\mathbf{a}_{n+1}^{(0)} = -\frac{h}{\beta}\mathbf{v}_n - \frac{h^2}{\beta}(\tfrac{1}{2} - \beta)\,\mathbf{a}_n\,, \qquad \mathbf{A}_{n+1}^{(0)} = -\frac{h}{\beta}\mathbf{W}_n - \frac{h^2}{\beta}(\tfrac{1}{2} - \beta)\,\mathbf{A}_n\,, \tag{5.7a}$$

$$\begin{aligned} \mathbf{v}_{n+1}^{(0)} &= \mathbf{v}_n + h[\,(1-\tau)\,\mathbf{a}_n + \tau\,\mathbf{a}_{n+1}^{(0)}\,]\,, \\ \mathbf{W}_{n+1}^{(0)} &= \mathbf{W}_n + h[\,(1-\tau)\,\mathbf{A}_n + \tau\,\mathbf{A}_{n+1}^{(0)}\,]\,. \end{aligned} \tag{5.7b}$$

Recall that alternative starting procedures, such as $(\mathbf{a}_{n+1}^{(0)}, \boldsymbol{\alpha}_{n+1}^{(0)}) = (\mathbf{a}_n, \boldsymbol{\alpha}_n)$, often result in spurious behavior. ■

Remark 5.3. Implementation. This remark is intended to discuss certain practical aspects of implementing the update procedure for the rotation field as delineated in Box 5.3. We recall that the exponentiation of a given rotation vector can be obtained following the procedure outlined in Section 4.6.3. Similarly, the extraction of the associated unit quaternion from an orthogonal matrix could be carried out in a accurate manner employing Spurrier's algorithm

summarized in Box 4.6. The issue here is how to compute appropriately the updated rotation vector $\boldsymbol{\vartheta}_n^{(i+1)}$ from from its unit quaternion representation. Recall the relationship between a rotation vector $\boldsymbol{\vartheta} = \vartheta_i \mathbf{e}_i$ and its associated unit quaternion parameters

$$\hat{\mathbf{q}} = q_o + q_1\mathbf{e}_1 + q_2\mathbf{e}_2 + q_3\mathbf{e}_3 = \cos(\frac{\|\boldsymbol{\vartheta}\|}{2}) + \sin(\frac{\|\boldsymbol{\vartheta}\|}{2})\,\frac{\boldsymbol{\vartheta}}{\|\boldsymbol{\vartheta}\|} \tag{5.8a}$$

Thus, given the four quaternion parameters (q_o, q_1, q_2, q_3), the associated rotation vector $\boldsymbol{\vartheta} = \vartheta_i \mathbf{e}_i$ can be theoretically computed by

$$\|\boldsymbol{\vartheta}\| = 2\cos^{-1}(q_o), \quad \boldsymbol{\vartheta} = \|\boldsymbol{\vartheta}\|\,\frac{q_1\mathbf{e}_1 + q_2\mathbf{e}_2 + q_3\mathbf{e}_3}{[\sum_{j=1}^{3}(q_j)^2]^{\frac{1}{2}}} \tag{5.8b}$$

However, the above procedure does not yield accurate numerical results when $\|\boldsymbol{\vartheta}\|$ is small. The reason can be seen from the Taylor series expansions: $\cos\vartheta = (1 - \frac{\vartheta^2}{2} + \cdots)$, $\sin\vartheta = (\vartheta - \frac{\vartheta^3}{3!} + \cdots)$. Since the sine function is more sensitive then the cosine function for $\|\boldsymbol{\vartheta}\|$ small, it is computationally more accurate to evaluate $\|\boldsymbol{\vartheta}\|$ from the given quaternion parameters using

$$\|\boldsymbol{\vartheta}\| = 2\sin^{-1}([q_1^2 + q_2^2 + q_3^2]^{\frac{1}{2}}) \tag{5.8c}$$

to avoid round-off error. To support this observation, consider the following example with a given $\boldsymbol{\vartheta} = 0.2380016\times10^{-7}\mathbf{e}_2$. We first compute the four quaternion parameters using (5.8a) to obtain

$$\begin{aligned} q_o &= 1.0000000 \\ q_1 &= 0.0000000 \\ q_2 &= 0.1190008\times10^{-7} \\ q_3 &= 0.0000000 \end{aligned} \tag{5.8d}$$

Next we compute the rotation vector $\boldsymbol{\vartheta}$ from the quaternion parameters in (5.8d) using $(5.8b)_1$ and (5.8c) respectively

$\vartheta = \vartheta_i \mathbf{e}_i$	
$(5.8b)_1$	(5.8c)
$\vartheta_1 = 0.0000000$ $\vartheta_2 = 0.2356080\times10^{-7}$ $\vartheta_3 = 0.0000000$	$\vartheta_1 = 0.0000000$ $\vartheta_1 = 0.2380016\times10^{-7}$ $\vartheta_3 = 0.0000000$

The result from using $(5.8b)_1$ is only correct up to two digits. This example is in fact taken from the analysis of the closed-loop chain in the next chapter, in which the above round-off error spoiled the desire asymptotic quadratic rate of convergence in the Newton iterative solution. ■

5.3.3. Exact linearization of the algorithm

We consider the linearization of the temporally discrete weak form $G_{dyn}(\boldsymbol{\phi}_{n+1}, \eta)$ about a configuration $\boldsymbol{\phi}_{n+1}^{(i)} = (\mathbf{d}_{n+1}^{(i)}, \boldsymbol{\Lambda}_{n+1}^{(i)}) \in C$ in a manner that is *consistent* with the update procedure summarized in Box 5.3. For this purpose, given an incremental field $\Delta\boldsymbol{\phi}_{n+1}^{(i)} = (\Delta\mathbf{u}_{n+1}^{(i)}, \Delta\boldsymbol{\vartheta}_{n+1}^{(i)})$ in the tangent space at $\boldsymbol{\phi}_{n+1}^{(i)}$, we construct a curve of perturbed configurations in C; that is, a map $\varepsilon \to \boldsymbol{\phi}_{n+1,\varepsilon}^{(i)} = (\mathbf{d}_{n+1,\varepsilon}^{(i)}, \boldsymbol{\Lambda}_{n+1,\varepsilon}^{(i)}) \in C$, by setting

$$\mathbf{d}_{n+1,\varepsilon}^{(i)} = \mathbf{d}_{n+1}^{(i)} + \varepsilon\, \Delta\mathbf{u}_{n+1}^{(i)}\,, \qquad \boldsymbol{\Lambda}_{n+1,\varepsilon}^{(i)} = \exp[\,\varepsilon\, \Delta\tilde{\boldsymbol{\vartheta}}_{n+1}^{(i)}]\, \exp[\tilde{\boldsymbol{\vartheta}}_{n}^{(i)}]\, \boldsymbol{\Lambda}_n \tag{5.9}$$

We then define linearized quantities $(\delta\mathbf{d}_{n+1,\varepsilon}^{(i)}, \delta\boldsymbol{\Lambda}_{n+1,\varepsilon}^{(i)})$ at configuration $\boldsymbol{\phi}_{n+1}^{(i)} \in C$, as objects in the tangent space $T_{\boldsymbol{\phi}_{n+1}^{(i)}} C$ given in terms of the directional derivative formula by the expressions

$$\delta \mathbf{d}_n^{(i)}{}_{+1} := \left.\frac{d}{d\varepsilon}\right|_{\varepsilon=0} \mathbf{d}_{n,\varepsilon}^{(i)}{}_{+1} = \Delta \mathbf{u}_n^{(i)}{}_{+1}$$
$$\delta \mathbf{A}_n^{(i)}{}_{+1} := \left.\frac{d}{d\varepsilon}\right|_{\varepsilon=0} \mathbf{A}_{n,\varepsilon}^{(i)}{}_{+1} = \Delta \overset{\vee}{\boldsymbol{\vartheta}}_n^{(i)}{}_{+1}\, \mathbf{A}_n^{(i)}{}_{+1} \tag{5.10}$$

To proceed further with the linearization of the rotation field, we make use of representations for $\mathbf{A}_{n,\varepsilon}^{(i)}{}_{+1}$ and $\mathbf{A}_n^{(i)}{}_{+1}$ in terms of exponential maps starting at $\mathbf{A}_n$. As in (5.5), we have that

$$\mathbf{A}_{n,\varepsilon}^{(i)}{}_{+1} = \exp[\overset{\vee}{\boldsymbol{\vartheta}}_{n,\varepsilon}^{(i)}]\, \mathbf{A}_n \,. \tag{5.11a}$$

where $\boldsymbol{\vartheta}_{n,\varepsilon}^{(i)}$ and $\boldsymbol{\vartheta}_n^{(i)}$ (or more precisely $\overset{\vee}{\boldsymbol{\vartheta}}_{n,\varepsilon}^{(i)}\mathbf{A}_n$ and $\overset{\vee}{\boldsymbol{\vartheta}}_n^{(i)}\mathbf{A}_n$) are in the tangent space $T_{\mathbf{A}_n}SO(3)$ at $\mathbf{A}_n$. Note that $\Delta\boldsymbol{\vartheta}_n^{(i)}{}_{+1}$ (or more precisely $\Delta\overset{\vee}{\boldsymbol{\vartheta}}_n^{(i)}{}_{+1}\mathbf{A}_n^{(i)}{}_{+1}$) belongs to the tangent space $T_{\mathbf{A}_n^{(i)}{}_{+1}}SO(3)$ at $\mathbf{A}_n^{(i)}{}_{+1}$. Hence, from (5.11a) and $(5.9)_2$, we obtain

$$\exp[\overset{\vee}{\boldsymbol{\vartheta}}_{n,\varepsilon}^{(i)}] = \exp[\varepsilon\, \Delta\overset{\vee}{\boldsymbol{\vartheta}}_n^{(i)}{}_{+1}] \exp[\overset{\vee}{\boldsymbol{\vartheta}}_n^{(i)}] \tag{5.11b}$$

Lemma 5.1. *The Frèchet derivative of* $\mathbf{e} := \boldsymbol{\vartheta}/\|\boldsymbol{\vartheta}\|$, *with* $\boldsymbol{\vartheta} \in \mathbb{R}^3$, *is given by*

$$D\mathbf{e} = \frac{\mathbf{1}_3 - \mathbf{e}\otimes\mathbf{e}}{\|\boldsymbol{\vartheta}\|} \tag{5.12}$$

Proof. By the directional derivative formula

$$\left.\frac{d}{d\varepsilon}\right|_{\varepsilon=0} \|\boldsymbol{\vartheta} + \varepsilon\,\mathbf{h}\| = \frac{1}{2\|\boldsymbol{\vartheta}\|}\left.\frac{d}{d\varepsilon}\right|_{\varepsilon=0} (\boldsymbol{\vartheta} + \varepsilon\,\mathbf{h})\cdot(\boldsymbol{\vartheta} + \varepsilon\,\mathbf{h})$$
$$= \frac{\boldsymbol{\vartheta}\cdot\mathbf{h}}{\|\boldsymbol{\vartheta}\|} = \mathbf{e}\cdot\mathbf{h}\,, \quad \forall\, \mathbf{h}\in\mathbb{R}^3\,. \tag{5.13a}$$

Thus, $D\|\boldsymbol{\vartheta}\| = \boldsymbol{\vartheta}/\|\boldsymbol{\vartheta}\| = \mathbf{e}$. Therefore,

$$D\mathbf{e}\cdot\mathbf{h} \doteq \left.\frac{d}{d\varepsilon}\right|_{\varepsilon=0} \frac{\boldsymbol{\vartheta}+\varepsilon\,\mathbf{h}}{\|\boldsymbol{\vartheta}+\varepsilon\,\mathbf{h}\|} = \frac{\|\boldsymbol{\vartheta}\|\mathbf{h} - (\mathbf{e}\cdot\mathbf{h})\,\boldsymbol{\vartheta}}{\|\boldsymbol{\vartheta}\|^2} = \frac{\mathbf{1}_3 - \mathbf{e}\otimes\mathbf{e}}{\|\boldsymbol{\vartheta}\|}\cdot\mathbf{h} \quad \blacksquare \tag{5.13b}$$

With this relation in mind, we record below the main result needed in the exact linearization of the weak form in Box 5.2. This result is the mathematical

statement of the linearization of the *compound rotation* $\boldsymbol{\vartheta}_{n,\varepsilon}^{(i)}$, which is the axial vector of $\overset{\mathbf{v}}{\boldsymbol{\vartheta}}_{n,\varepsilon}^{(i)}$ in (5.11).

Proposition 5.1. *The linear part of the compound rotation $\boldsymbol{\vartheta}_{n,\varepsilon}$ as given in (5.11) is obtained according to*

$$\delta\boldsymbol{\vartheta}_n^{(i)} = \left.\frac{d}{d\varepsilon}\right|_{\varepsilon=0} \boldsymbol{\vartheta}_{n,\varepsilon}^{(i)} = \mathbf{T}(\boldsymbol{\vartheta}_n^{(i)})\,\Delta\boldsymbol{\vartheta}_{n+1}^{(i)} \tag{5.14a}$$

where the map $\mathbf{T}$: $T_{\mathbf{A}_{n+1}^{(i)}}SO(3) \to T_{\mathbf{A}_n}SO(3)$ *is a linear map defined by*

$$\mathbf{T}(\boldsymbol{\vartheta}) := \mathbf{e}\otimes\mathbf{e} + \frac{\|\boldsymbol{\vartheta}\|/2}{\tan(\|\boldsymbol{\vartheta}\|/2)}[\,\mathbf{1}_3 - \mathbf{e}\otimes\mathbf{e}\,] - \frac{\overset{\mathbf{v}}{\boldsymbol{\vartheta}}}{2} \tag{5.14b}$$

with $\mathbf{e}$ *being the unit vector defined by* $\mathbf{e} := \boldsymbol{\vartheta}/\|\boldsymbol{\vartheta}\|$.

Proof. To simplify the notation, we shall omit the subscript $n+1$ and the superscript (i); the relation (5.11) can then be written as

$$\exp[\overset{\mathbf{v}}{\boldsymbol{\vartheta}}_\varepsilon] = \exp[\varepsilon\,\Delta\overset{\mathbf{v}}{\boldsymbol{\vartheta}}]\exp[\overset{\mathbf{v}}{\boldsymbol{\vartheta}}] \tag{5.15a}$$

We first differentiate this expression with respect to ε, at $\varepsilon = 0$, to obtain

$$\left.\frac{d}{d\varepsilon}\right|_{\varepsilon=0} \exp[\overset{\mathbf{v}}{\boldsymbol{\vartheta}}_\varepsilon] = \frac{2}{1+\|\bar{\boldsymbol{\vartheta}}\|^2}[\delta\overset{\mathbf{v}}{\boldsymbol{\vartheta}} + \delta\overset{\mathbf{v}}{\boldsymbol{\vartheta}}\,\overset{\mathbf{v}}{\boldsymbol{\vartheta}} - \overset{\mathbf{v}}{\boldsymbol{\vartheta}}\,\delta\overset{\mathbf{v}}{\boldsymbol{\vartheta}}]\exp[\overset{\mathbf{v}}{\boldsymbol{\vartheta}}]\,, \tag{5.15b}$$

where $\overset{\mathbf{v}}{\boldsymbol{\vartheta}} = \overset{\mathbf{v}}{\boldsymbol{\vartheta}}_\varepsilon\big|_{\varepsilon=0}$ and $\delta\overset{\mathbf{v}}{\boldsymbol{\vartheta}} := \left.\frac{d}{d\varepsilon}\right|_{\varepsilon=0} \overset{\mathbf{v}}{\boldsymbol{\vartheta}}_\varepsilon$, using the proof of Lemma 4.1. Thus from (4.68), the final result in terms of axial vectors leads to

$$\Delta\boldsymbol{\vartheta} = \frac{2}{1+\|\bar{\boldsymbol{\vartheta}}\|^2}[\delta\bar{\boldsymbol{\vartheta}} + \bar{\boldsymbol{\vartheta}}\times\delta\bar{\boldsymbol{\vartheta}}] \tag{5.15c}$$

Expressed in operator notation, the above equation reads

$$\Delta\boldsymbol{\vartheta} = \mathbf{U}^{-1}(\bar{\boldsymbol{\vartheta}})\,\delta\bar{\boldsymbol{\vartheta}}\,, \quad \text{where} \quad \mathbf{U}^{-1}(\bar{\boldsymbol{\vartheta}}) := \frac{2}{1+\|\bar{\boldsymbol{\vartheta}}\|^2}[\mathbf{1}_3 + \overset{\mathbf{v}}{\bar{\boldsymbol{\vartheta}}}] \tag{5.15d}$$

Inversion of $\mathbf{U}^{-1}(\bar{\boldsymbol{\vartheta}})$ yields

$$\mathbf{U}(\bar{\boldsymbol{\vartheta}}) = \tfrac{1}{2}[(1+\|\bar{\boldsymbol{\vartheta}}\|^2)\,\mathbf{1}_3 - \overset{\mathbf{v}}{\bar{\boldsymbol{\vartheta}}} + \overset{\mathbf{v}}{\bar{\boldsymbol{\vartheta}}}^2] = \tfrac{1}{2}[\mathbf{1}_3 - \overset{\mathbf{v}}{\bar{\boldsymbol{\vartheta}}} + \bar{\boldsymbol{\vartheta}}\otimes\bar{\boldsymbol{\vartheta}}] \tag{5.15e}$$

In addition, by differentiating the expression $\boldsymbol{\vartheta}_\varepsilon = 2\,\dfrac{\tan^{-1}\|\bar{\boldsymbol{\vartheta}}_\varepsilon\|}{\|\bar{\boldsymbol{\vartheta}}_\varepsilon\|}\bar{\boldsymbol{\vartheta}}_\varepsilon$ with respect to ε with the aid of Lemma 5.1, we obtain, at $\varepsilon = 0$,

$$\delta\boldsymbol{\vartheta} = \mathbf{V}(\bar{\boldsymbol{\vartheta}})\,\delta\bar{\boldsymbol{\vartheta}}\,, \tag{5.15f}$$

where $\mathbf{V}(\bar{\boldsymbol{\vartheta}})$ is given by

$$\mathbf{V}(\bar{\boldsymbol{\vartheta}}) = \frac{2}{1+\|\bar{\boldsymbol{\vartheta}}\|^2}\mathbf{e}\otimes\mathbf{e} + \frac{2\tan^{-1}\|\bar{\boldsymbol{\vartheta}}\|}{\|\bar{\boldsymbol{\vartheta}}\|}[\mathbf{1}_3 - \mathbf{e}\otimes\mathbf{e}]\,. \tag{5.15g}$$

Thus, from (5.15d) and (5.15f), it follows that

$$\delta\boldsymbol{\vartheta} = \mathbf{V}(\bar{\boldsymbol{\vartheta}})\,\mathbf{U}(\bar{\boldsymbol{\vartheta}})\,\Delta\boldsymbol{\vartheta} =: \mathbf{T}(\bar{\boldsymbol{\vartheta}})\,\Delta\boldsymbol{\vartheta} \tag{5.15h}$$

Next, using the definition of $\bar{\boldsymbol{\vartheta}} := \dfrac{\tan(\|\boldsymbol{\vartheta}\|/2)}{\|\boldsymbol{\vartheta}\|}\boldsymbol{\vartheta}$ and after some manipulation, we obtain the expression for $\mathbf{T}(\boldsymbol{\vartheta})$ as given in (5.14b). ∎

Remark 5.4. The above proof can also be obtained by first expressing the axial vector $\boldsymbol{\vartheta}^{(i)}_{n,\varepsilon}$ as a compound rotation vector of of $\boldsymbol{\vartheta}_{n+1}$ and $\varepsilon\Delta\boldsymbol{\vartheta}^{(i)}_{n+1}$. Consider two successive finite rotations $\boldsymbol{\psi}^{(1)}$ and $\boldsymbol{\psi}^{(2)}$ with $\hat{\mathbf{q}}^{(1)} = q_o^{(1)} + \mathbf{q}^{(1)}$ and $\hat{\mathbf{q}}^{(2)} = q_o^{(2)} + \mathbf{q}^{(2)}$ denoting their respective unit quaternion representation. Further, let $\boldsymbol{\psi}$ denote the resulting compound rotation, and $\hat{\mathbf{q}} = q_o + \mathbf{q}$ its unit quaternion representation. We have the following relation for the compound quaternion $\hat{\mathbf{q}}$

$$\hat{\mathbf{q}} = \hat{\mathbf{q}}^{(2)}\circ\hat{\mathbf{q}}^{(1)} = q_o^{(1)}q_o^{(2)} - (\mathbf{q}^{(1)}\cdot\mathbf{q}^{(2)}) + q_o^{(2)}\mathbf{q}^{(1)} + q_o^{(1)}\mathbf{q}^{(2)} + \mathbf{q}^{(2)}\times\mathbf{q}^{(1)} \tag{5.16a}$$

where "$\circ$" denotes the quaternion multiplication (e.g., Karger & Novak [1985]). The scalar part of $\hat{\mathbf{q}}$ is thus $q_o = q_o^{(1)}q_o^{(2)} - (\mathbf{q}^{(1)}\cdot\mathbf{q}^{(2)})$. From the relation between rotation pseudo vector and quaternion representation given in (4.78), we obtain

$$\bar{\boldsymbol{\psi}} = \frac{\mathbf{q}}{q_o} = \frac{\dfrac{\mathbf{q}^{(1)}}{q_o^{(1)}} + \dfrac{\mathbf{q}^{(2)}}{q_o^{(2)}} + \dfrac{\mathbf{q}^{(2)}}{q_o^{(2)}}\times\dfrac{\mathbf{q}^{(1)}}{q_o^{(1)}}}{1 - \dfrac{\mathbf{q}^{(1)}\cdot\mathbf{q}^{(2)}}{q_o^{(1)}q_o^{(2)}}} = \frac{\bar{\boldsymbol{\psi}}^{(1)} + \bar{\boldsymbol{\psi}}^{(2)} + \bar{\boldsymbol{\psi}}^{(2)}\times\bar{\boldsymbol{\psi}}^{(1)}}{1 - \bar{\boldsymbol{\psi}}^{(1)}\cdot\bar{\boldsymbol{\psi}}^{(2)}} \tag{5.16b}$$

Now, let $\overline{\psi}^{(1)} = \overline{\vartheta} = \frac{\tan(\|\vartheta\|/2)}{\|\vartheta\|}\vartheta$, $\overline{\psi}^{(2)} = \Delta\overline{\vartheta}_\varepsilon = \frac{\tan(\varepsilon\|\Delta\vartheta\|/2)}{\|\Delta\vartheta\|}\Delta\vartheta$, and the compound rotation $\overline{\psi} = \overline{\vartheta}_\varepsilon$. We obtain from (5.16b)

$$\overline{\vartheta}_\varepsilon = \frac{1}{1-(\overline{\vartheta}\cdot\Delta\overline{\vartheta}_\varepsilon)}[\,\overline{\vartheta} + \Delta\overline{\vartheta}_\varepsilon - \overline{\vartheta}\times\Delta\overline{\vartheta}_\varepsilon\,] \tag{5.16c}$$

The above expression could also be found in Argyris [1982]. First, note that

$$\left.\frac{d}{d\varepsilon}\right|_{\varepsilon=0}\Delta\overline{\vartheta}_\varepsilon = \frac{\Delta\vartheta}{2}. \tag{5.16d}$$

Then by differentiating (5.16d) with respect to ε, at $\varepsilon = 0$, we obtain directly the expression of $\mathbf{U}(\overline{\vartheta})$ given in (5.15e) without the need of matrix inversion. ∎

Tangent inertia operator. From (5.14) and the time-stepping algorithm in Box 5.3, we obtain the linearization of the angular velocity and acceleration about the configuration $\phi_{n+1}^{(i)}$

$$\delta\mathbf{W}_{n+1}^{(i)} = \frac{\tau}{h\beta}\mathbf{A}_n^T\,\mathbf{T}(\vartheta_n^{(i)})\,\Delta\vartheta_{n+1}^{(i)}, \quad \delta\mathbf{A}_{n+1}^{(i)} = \frac{1}{h\beta}\mathbf{A}_n^T\,\mathbf{T}(\vartheta_n^{(i)})\,\Delta\vartheta_{n+1}^{(i)} \tag{5.17}$$

Consider now the linearization of the weak form $G_{dyn}(\phi, \eta)$ about the configuration $\phi = \phi_{n+1}^{(i)}$. By definition, we have

$$L[\,G_{dyn}(\phi_{n+1}^{(i)}, \eta)\,] = G_{dyn}(\phi_{n+1}^{(i)}, \eta) + DG_{dyn}(\phi_{n+1}^{(i)}, \eta)\cdot\Delta\phi_{n+1}^{(i)} \tag{5.18}$$

where $G_{dyn}(\phi_{n+1}^{(i)}, \eta)$ represents the dynamic out-of-balance force, and by using the above results of linearization

$$DG_{dyn}(\phi_{n+1}^{(i)}, \eta)\cdot\Delta\phi_{n+1}^{(i)} = [\,D_M + D_S + D_G + D_L\,]\,G_{dyn}(\phi_{n+1}^{(i)}, \eta)\cdot\Delta\phi_{n+1}^{(i)} \tag{5.19a}$$

where D_M corresponds to the linearization of the inertia operator given by

$$D_M G_{dyn}(\phi_{n+1}^{(i)}, \eta)\cdot\Delta\phi_{n+1}^{(i)} = \frac{1}{h^2\beta}\int_{[0,L]}\eta_0\cdot A_\rho\Delta\mathbf{u}_{n+1}^{(i)}\,dS$$

$$+\int_{[0,L]}\psi\cdot\Big[-[\,\mathbf{A}_{n+1}^{(i)}\{\,\mathbf{I}_\rho\,\mathbf{A}_{n+1}^{(i)} + \mathbf{W}_{n+1}^{(i)}\times\mathbf{I}_\rho\,\mathbf{W}_{n+1}^{(i)}\,\}\times]\Big] \tag{5.19b}$$

$$+ \frac{1}{h^2\beta}\mathbf{\Lambda}_n^{(i)}{}_{+1}\{\mathbf{I}_\rho - h\tau[\mathbf{I}_\rho \mathbf{W}_n^{(i)}{}_{+1}\times] + h\tau[\mathbf{W}_n^{(i)}{}_{+1}\times]\mathbf{I}_\rho\}\Big]\mathbf{\Lambda}_n^T\,\mathbf{T}(\boldsymbol{\vartheta}_n^{(i)}{}_{+1})\,\Delta\boldsymbol{\vartheta}_n^{(i)}{}_{+1}\,dS\,.$$

Expressions for the tangent material stiffness operator $D_S G_{dyn}$, the tangent geometric stiffness operator $D_G G_{dyn}$, and the tangent follower load stiffness $D_L G_{dyn}$ were obtained in Chapter 4 —see equations (4.43), (4.44), and (4.55). The tangent inertia operator $D_M G_{dyn}$, as obtained in (5.19b), possesses an unusual characteristic with respect to standard structural dynamics formulations: It is *non-symmetric* and *configuration dependent*. This lack of symmetry concerns only the rotational degrees of freedom and follows from the fact that the deformation map $\boldsymbol{\phi}$ in the configuration space C takes values in the nonlinear differentiable manifold $\mathbb{R}^3\times SO(3)$ rather than in the linear space $\mathbb{R}^3\times\mathbb{R}^3$. The latter typically arises in standard structural dynamics formulations employing the infinitesimal rotation field.

5.4. Spatial discretization: Galerkin finite element method

In this section, we shall be concerned with the spatial discretization of the temporally discrete version of the dynamic weak form, given in (5.3), and its linear part in (5.17) employing the finite element method. Section 4.1 focuses on obtaining the tangent inertia matrix, which is a basic feature of the present approach to nonlinear structural dynamics. Detailed expressions for the tangent stiffness matrices can be found in Chapter 4. In section 4.2, we establish the convergence property of the proposed time-stepping algorithm.

5.4.1. Tangent inertia matrix

Following the same discretization procedure employed in Section 4.6.1, consider the partition $[0, L] = \bigcup_{k=1}^{N-1}[S_k, S_{k+1}]$ with $0 = S_1 < \cdots < S_N = L$. The incre-

mental field $\Delta\boldsymbol{\phi}_{n+1}^{(i)} := (\Delta\mathbf{u}_{n+1}^{(i)}, \Delta\boldsymbol{\vartheta}_{n+1}^{(i)})$ and the admissible variation $\boldsymbol{\eta} := (\boldsymbol{\eta}_o, \boldsymbol{\psi})$ are approximated according to

$$\Delta\mathbf{u}_{n+1}^{(i)}(S) \cong \sum_{I=1}^{N} N_I(S)\,\Delta\mathbf{u}_{I,n+1}^{(i)}, \qquad \Delta\boldsymbol{\vartheta}_{n+1}^{(i)}(S) \cong \sum_{I=1}^{N} N_I(S)\,\Delta\boldsymbol{\vartheta}_{I,n+1}^{(i)}, \tag{5.20a}$$

$$\boldsymbol{\eta}_o(S) \cong \sum_{I=1}^{N} N_I(S)\,\boldsymbol{\eta}_{oI}, \qquad \boldsymbol{\psi}(S) \cong \sum_{I=1}^{N} N_I(S)\,\boldsymbol{\psi}_I, \tag{5.20b}$$

where $N_I(S)$ denotes the finite element global function corresponding to node I constructed in the standard manner from the element shape function. $(\Delta\mathbf{u}_{I,n+1}^{(i)}, \Delta\boldsymbol{\vartheta}_{I,n+1}^{(i)})$ are the values of $(\Delta\mathbf{u}_{n+1}^{(i)}, \Delta\boldsymbol{\vartheta}_{n+1}^{(i)})$ at node I; similar notation is used concerning the variation $\boldsymbol{\eta}$. Next, we recall that from a known configuration $\boldsymbol{\phi}_n$ at time t_n, a Newton iterative scheme is employed to solve for the configuration $\boldsymbol{\phi}_{n+1}$ at time t_{n+1}. At iteration (i), substitution of the above approximations into the linearized dynamic weak form about the configuration $\boldsymbol{\phi}_{n+1}^{(i)}$ yields the following spatially discrete version of the linearized weak form (5.16)

$$L[G_{dyn}(\boldsymbol{\phi}_{n+1}^{(i)}, \boldsymbol{\eta})] \cong \sum_{I=1}^{N} \boldsymbol{\eta}_I \cdot \left\{ \mathbf{P}_I(\boldsymbol{\phi}_{n+1}^{(i)}) + \sum_{J=1}^{N} \mathbf{K}_{IJ}(\boldsymbol{\Lambda}_n, \boldsymbol{\phi}_{n+1}^{(i)})\,\Delta\boldsymbol{\phi}_{J,n+1}^{(i)} \right\} = 0 \tag{5.21a}$$

for any $\boldsymbol{\eta}_I$, thus

$$\mathbf{P}_I(\boldsymbol{\phi}_{n+1}^{(i)}) + \sum_{J=1}^{N} \mathbf{K}_{IJ}(\boldsymbol{\Lambda}_n, \boldsymbol{\phi}_{n+1}^{(i)})\,\Delta\boldsymbol{\phi}_{J,n+1}^{(i)} = 0 \tag{5.21b}$$

for $I=1,\ldots,N$, where

$$\mathbf{K}_{IJ}(\boldsymbol{\Lambda}_n, \boldsymbol{\phi}_{n+1}^{(i)}) := \mathbf{M}_{IJ}(\boldsymbol{\Lambda}_n, \boldsymbol{\Lambda}_{n+1}^{(i)}) + \mathbf{S}_{IJ}(\boldsymbol{\phi}_{n+1}^{(i)}) + \mathbf{G}_{IJ}(\boldsymbol{\phi}_{n+1}^{(i)}) + \mathbf{L}_{IJ}(\boldsymbol{\Lambda}_{n+1}^{(i)}) \tag{5.21c}$$

In (5.21a), $\mathbf{P}_I(\boldsymbol{\phi}_{n+1}^{(i)})$ represents the residual or out-of-balance force at iteration (i) of the Newton scheme,

$$\mathbf{P}_I(\boldsymbol{\phi}_{n+1}^{(i)}) = \int_{[0,L]} [N_I(S)\mathbf{1}_6] \begin{Bmatrix} A_\rho\,\mathbf{a}_{n+1}^{(i)} \\ \mathbf{I}_{\rho,n+1}^{(i)}\boldsymbol{\alpha}_{n+1}^{(i)} + \mathbf{w}_{n+1}^{(i)} \times [\mathbf{I}_{\rho,n+1}^{(i)}] \end{Bmatrix} dS$$

$$+ \int_{[0,L]} \left[\{\Xi(\phi_{n+1}^{(i)})[N_I(S)1_6]\}^T \begin{Bmatrix} \mathbf{n}_{n+1}^{(i)} \\ \mathbf{m}_{n+1}^{(i)} \end{Bmatrix} - [N_I(S)1_6] \begin{Bmatrix} \bar{\mathbf{n}}(t_{n+1}) \\ \bar{\mathbf{m}}(t_{n+1}) \end{Bmatrix} \right] dS \,. \qquad (5.22)$$

Recall that the differential operator was defined in (4.38). The discrete dynamic tangent operator $\mathbf{K}_{IJ}(\mathbf{A}_n, \phi_{n+1}^{(i)})$ coupling the degrees of freedom of node I and of node J is the sum of (i) the tangent inertia matrix $\mathbf{M}_{IJ}(\mathbf{A}_n, \mathbf{A}_{n+1}^{(i)})$, (ii) the tangent material stiffness $\mathbf{S}_{IJ}(\phi_{n+1}^{(i)})$, (iii) the tangent geometric stiffness $\mathbf{G}_{IJ}(\phi_{n+1}^{(i)})$, and (iv) the tangent load stiffness due to follower load $\mathbf{L}_{IJ}(\mathbf{A}_{n+1}^{(i)})$. The incremental displacement and rotation at node J is denoted by $\Delta\phi_{J,n+1}^{(i)} := (\Delta\mathbf{u}_{J,n+1}^{(i)}, \Delta\boldsymbol{\vartheta}_{J,n+1}^{(i)})$, computed by solving the system of linear equations (5.21b).

From the expression for the tangent inertia operator $D_{\mathbf{u}} G_{dyn}$ in (5.17b), we obtain its discrete form

$$\mathbf{M}_{IJ}(\mathbf{A}_n, \mathbf{A}_{n+1}^{(i)}) = \begin{bmatrix} \mathbf{m}_{IJ}^{(1,1)} & \mathbf{0} \\ \mathbf{0} & \mathbf{m}_{IJ}^{(2,2)}(\mathbf{A}_n, \mathbf{A}_{n+1}^{(i)}) \end{bmatrix} \in \mathbb{R}^{6\times 6} \qquad (5.23a)$$

with

$$\mathbf{m}_{IJ}^{(1,1)} := \frac{1}{h^2\beta} \{ \int_{[0,L]} A_\rho \, N_I(S) \, N_J(S) \, dS \} \, 1_3 \qquad (5.23b)$$

$$\mathbf{m}_{IJ}^{(2,2)}(\mathbf{A}_n, \mathbf{A}_{n+1}^{(i)}) := \int_{[0,L]} \Big[-[\, \mathbf{A}_{n+1}^{(i)} \{ \mathbb{I}_\rho \bar{\boldsymbol{\alpha}}_{n+1}^{(i)} + \bar{\mathbf{w}}_{n+1}^{(i)} \times \mathbb{I}_\rho \bar{\mathbf{w}}_{n+1}^{(i)} \} \times]$$

$$+ \frac{1}{h^2\beta} \mathbf{A}_{n+1}^{(i)} \{ \mathbb{I}_\rho - h\gamma [\mathbb{I}_\rho \bar{\mathbf{w}}_{n+1}^{(i)} \times] + h\gamma [\bar{\mathbf{w}}_{n+1}^{(i)} \times] \mathbb{I}_\rho \} \Big] \mathbf{A}_n^T \mathbf{T}(\boldsymbol{\vartheta}_{n+1}^{(i)}) \, N_I(S) \, N_J(S) \, dS$$

(5.23c)

Both $\mathbf{m}_{IJ}^{(1,1)}$ and $\mathbf{m}_{IJ}^{(2,2)}$ are elements of $\mathbb{R}^{3\times 3}$. As noted in Section 5.3, the tangent inertia matrix is *non-symmetric* and *configuration dependent*. This property concerns only the rotational degrees of freedom as is manifest from the expression for $\mathbf{m}_{IJ}^{(2,2)}(\mathbf{A}_n, \mathbf{A}_{n+1}^{(i)})$. The submatrix $\mathbf{m}_{IJ}^{(1,1)}$ corresponds to the translational degrees of freedom and is constant, as usually found in the expression for the

consistent mass matrix when the deformation map takes values in a linear space. We recall that the identical property, i.e., the localized character of this non-symmetry, was found as well in the tangent geometric stiffness $\mathbf{G}_{JJ}$.

5.4.2. Convergence and accuracy of time-stepping algorithm

The proposed time-stepping algorithm summarized in Box 5.2 can be shown to be convergent with second order accuracy when $\beta = \frac{1}{4}$ and $\tau = \frac{1}{2}$. In the case where the deformation map takes values in a linear space, these values of β and τ correspond to the trapezoidal rule with an established convergence property (Hughes [1976]). We shall first consider the extension of the Newmark algorithm to solve the differential equations in (5.4a-b) whose accuracy is by the following

Lemma 5.2. *Consider the differential equations (5.4b) and assume that* $\mathbf{W}(t)$ *is twice continuously differentiable. Then the algorithm in material setting given Box* 5.2 *is locally at most third order accurate regardless of the values taken by* β, *i.e.*,

$$\mathbf{A}(t+h) = \mathbf{A}(t)\exp[\, h\overset{\blacktriangledown}{\mathbf{W}}(t) + h^2\{(\tfrac{1}{2}-\beta)\overset{\blacktriangledown}{\mathbf{A}}(t) + \beta\overset{\blacktriangledown}{\mathbf{A}}(t+h)\}\,] + O(h^3)\,, \tag{5.24}$$

where $\mathbf{A}(t) := \dot{\mathbf{W}}(t)$.

Proof. Consider the Taylor series expansion of $\mathbf{A}(t+h)$,

$$\mathbf{A}(t+h) = \sum_{k\geq 0}\frac{h^k}{k!}\frac{d^k}{dt^k}\mathbf{A}(t) \tag{5.25a}$$

with

$$\frac{d}{dt}\mathbf{A}(t) = \mathbf{A}\overset{\blacktriangledown}{\mathbf{W}} \tag{5.25b}$$

$$\frac{d^2}{dt^2}\mathbf{A}(t) = \mathbf{A}[\,\overset{\blacktriangledown}{\mathbf{A}} + \overset{\blacktriangledown}{\mathbf{W}}^2\,] \tag{5.25c}$$

$$\frac{d^3}{dt^3}\mathbf{A}(t) = \mathbf{A}[\,\overset{\blacktriangledown}{\mathbf{W}}^3 + 2\overset{\blacktriangledown\blacktriangledown}{\mathbf{W}\mathbf{A}} + \overset{\blacktriangledown\blacktriangledown}{\mathbf{A}\mathbf{W}} + \frac{d}{dt}\overset{\blacktriangledown}{\mathbf{A}}\,]\,. \tag{5.25d}$$

On the other hand, $\mathbf{A}(t+h)$ obtained from the time-stepping algorithm is given by

$$\hat{\mathbf{A}}(h) := \mathbf{A}(t+h) = \mathbf{A}(t)\exp[\, h\overset{\blacktriangledown}{\mathbf{W}}(t) + h^2\{(\tfrac{1}{2}-\beta)\overset{\blacktriangledown}{\mathbf{A}}(t) + \beta\overset{\blacktriangledown}{\mathbf{A}}(t+h)\}\,] \quad (5.25e)$$

The consistency and local third order accuracy of algorithm (5.25e) are ascertained by the following identities

$$\hat{\mathbf{A}}(0) = \mathbf{A}(t) \quad (5.25f)$$

$$\frac{d}{dh}\hat{\mathbf{A}}(0) = \mathbf{A}\overset{\blacktriangledown}{\mathbf{W}} \quad (5.25g)$$

$$\frac{d^2}{dh^2}\hat{\mathbf{A}}(0) = \mathbf{A}[\,\overset{\blacktriangledown}{\mathbf{A}} + \overset{\blacktriangledown}{\mathbf{W}}^2\,] \quad (5.25h)$$

$$\frac{d^3}{dh^3}\hat{\mathbf{A}}(0) = \mathbf{A}[\,\overset{\blacktriangledown}{\mathbf{W}}^3 + \tfrac{3}{2}(\overset{\blacktriangledown}{\mathbf{A}}\overset{\blacktriangledown}{\mathbf{W}} + \overset{\blacktriangledown}{\mathbf{W}}\overset{\blacktriangledown}{\mathbf{A}}) + 2\beta\frac{d}{dt}\overset{\blacktriangledown}{\mathbf{A}}\,] \quad (5.25i)$$

It can be seen that (5.25f-h) are identically the same as (5.25a-c) regardless of the value taken by β. However, there is no value of β that can render (5.25i) identically the same as (5.25d). Hence the algorithm is at most of local third order accuracy. ∎

With the above result, the convergence property of the algorithm with $\beta = \frac{1}{4}$ and $\tau = \frac{1}{2}$ is established by

Proposition 5.2. *Consider the system of differential equations* $\dot{\mathbf{A}} = \mathbf{A}\overset{\blacktriangledown}{\mathbf{W}}$, $\frac{d}{dt}\overset{\blacktriangledown}{\mathbf{W}} = \mathbf{f}(\overset{\blacktriangledown}{\mathbf{W}}, \mathbf{A})$ *with* $\mathbf{A} \in SO(3)$ *and* $\mathbf{W} \in \mathbb{R}^3$. *Assume that* $\mathbf{f}(\overset{\blacktriangledown}{\mathbf{W}}, \mathbf{A})$ *satisfies the Lipschitz condition with respect to* $\overset{\blacktriangledown}{\mathbf{W}} \in so(3)$ *and* $\mathbf{A} \in SO(3)$. *The algorithm*

$$\begin{aligned} \mathbf{A}_{n+1} &= \mathbf{A}_n \exp[\, \tfrac{h}{2}\{\overset{\blacktriangledown}{\mathbf{W}}_{n+1} + \overset{\blacktriangledown}{\mathbf{W}}_n\}\,] \\ \overset{\blacktriangledown}{\mathbf{W}}_{n+1} &= \overset{\blacktriangledown}{\mathbf{W}}_n + \tfrac{h}{2}\{\overset{\blacktriangledown}{\mathbf{A}}_{n+1} + \overset{\blacktriangledown}{\mathbf{A}}_n\} \end{aligned} \quad (5.26)$$

is convergent, i.e., $\mathbf{W}_n \to \mathbf{W}(t_n)$ *and* $\mathbf{A}_n \to \mathbf{A}(t_n)$ *as* $h \to 0$, *and second order accurate, provided both* $\mathbf{W}(t_n)$ *and* $\mathbf{W}_n$ *are bounded.*

Proof. Let the error measures on $\mathbf{A}$ and $\mathbf{W}$ be defined as $\xi_n := \mathbf{A}(t_n) - \mathbf{A}_n$, and $\zeta_n := \overset{\blacktriangledown}{\mathbf{W}}(t_n) - \overset{\blacktriangledown}{\mathbf{W}}_n$. Moreover, the isomorphism between $so(3)$ and $\mathbb{R}^3$ allows the definition $\|\overset{\blacktriangledown}{\mathbf{W}}\| := \|\mathbf{W}\|$. From Lemma 5.2, and the local third order accuracy of the trapezoidal rule with respect to relation $(5.26)_2$, i.e.,

$$\overset{\blacktriangledown}{\mathbf{W}}(t_{n+1}) - \overset{\blacktriangledown}{\mathbf{W}}(t_n) = \frac{h}{2}[\, \mathbf{f}(\overset{\blacktriangledown}{\mathbf{W}}(t_{n+1}), \mathbf{A}(t_{n+1})) + \mathbf{f}(\overset{\blacktriangledown}{\mathbf{W}}(t_n), \mathbf{A}(t_n)) \,] + O(h^3) \quad (5.27a)$$

we obtain the following recurrence relations for ξ_{k+1} and ζ_{k+1}

$$\xi_{k+1} = \xi_k + [\, \mathbf{A}(t_k)(\overset{\blacktriangledown}{\mathbf{R}}_k + \tfrac{1}{2}\overset{\blacktriangledown}{\mathbf{R}}_k^2) - \mathbf{A}_k(\overset{\blacktriangledown}{\mathbf{S}}_k + \tfrac{1}{2}\overset{\blacktriangledown}{\mathbf{S}}_k^2) \,] + O(h^3) \quad (5.27b)$$

$$\zeta_{k+1} = \zeta_k + \frac{h}{2}[\, \overset{\blacktriangledown}{\mathbf{A}}(t_{k+1}) - \overset{\blacktriangledown}{\mathbf{A}}_{k+1} + \overset{\blacktriangledown}{\mathbf{A}}(t_k) - \overset{\blacktriangledown}{\mathbf{A}}_k \,] + O(h^3) \quad (5.27c)$$

where we define $\overset{\blacktriangledown}{\mathbf{R}}_k$ and $\overset{\blacktriangledown}{\mathbf{S}}_k$ to be

$$\overset{\blacktriangledown}{\mathbf{R}}_k := \frac{h}{2}\{\, \overset{\blacktriangledown}{\mathbf{W}}(t_{k+1}) + \overset{\blacktriangledown}{\mathbf{W}}(t_k) \,\} \quad (5.27d)$$

$$\overset{\blacktriangledown}{\mathbf{S}}_k := \frac{h}{2}\{\, \overset{\blacktriangledown}{\mathbf{W}}_{k+1} + \overset{\blacktriangledown}{\mathbf{W}}_k \,\} \quad (5.27e)$$

Note that in (5.27b), we have expanded the exponential $\exp[\overset{\blacktriangledown}{\mathbf{R}}_k]$ and $\exp[\overset{\blacktriangledown}{\mathbf{S}}_k]$ in series and retained terms up to order h^2; higher order terms of the form $\frac{\overset{\blacktriangledown}{\mathbf{R}}_n^k}{k!}$ with bounded norm are lumped together in $O(h^3)$. Next, sum up the relations (5.27b) and (5.27c) for $k = 1,\ldots,n$ to obtain

$$\xi_{n+1} = \sum_{i=0}^{n}[\, \mathbf{A}(t_i)(\overset{\blacktriangledown}{\mathbf{R}}_i + \tfrac{1}{2}\overset{\blacktriangledown}{\mathbf{R}}_i^2) - \mathbf{A}_i(\overset{\blacktriangledown}{\mathbf{S}}_i + \tfrac{1}{2}\overset{\blacktriangledown}{\mathbf{S}}_i^2) \,] + O(h^2) \quad (5.27f)$$

$$\zeta_{n+1} = \frac{h}{2}[\, \overset{\blacktriangledown}{\mathbf{A}}(t_{n+1}) - \overset{\blacktriangledown}{\mathbf{A}}_{n+1} \,] + h\sum_{i=1}^{n}[\, \overset{\blacktriangledown}{\mathbf{A}}(t_n) - \overset{\blacktriangledown}{\mathbf{A}}_n \,] + O(h^2) \quad (5.27g)$$

assuming that there is no initial error, i.e., $\xi_0 = \zeta_0 = 0$. Since $\overset{\blacktriangledown}{\mathbf{A}} = \mathbf{f}(\overset{\blacktriangledown}{\mathbf{W}}, \mathbf{A})$ satisfies the Lipschitz condition with respect to its arguments, taking the norm

of (5.27f,g), we have

$$\|\xi_{n+1}\| \le \sum_{i=1}^{n} \|A(t_i)\,[\,\overset{\vee}{R}_i + \tfrac{1}{2}\overset{\vee}{R}_i^2\,] - A_i\,[\,\overset{\vee}{S}_i + \tfrac{1}{2}\overset{\vee}{S}_i^2\,]\,\| + c_1 h^2 \tag{5.27h}$$

$$\|\zeta_{n+1}\| \le \frac{hL}{2}(\|\zeta_{n+1}\| + \|\xi_{n+1}\|) + hL\sum_{i=1}^{n}(\|\zeta_i\| + \|\xi_i\|) + c_2 h^2 \tag{5.27i}$$

where c_1 and c_2 are constants and L is the Lipschitz constant. Now note that

$$\begin{aligned}\|A(t_i)\overset{\vee}{R}_i - A_i\overset{\vee}{S}_i\| &\le \|A(t_i)\|\,\|\overset{\vee}{R}_i - \overset{\vee}{S}_i + \overset{\vee}{S}_i - A^T(t_i)A_i\overset{\vee}{S}_i\| \\ &\le \|\overset{\vee}{R}_i - \overset{\vee}{S}_i\| + \|1_3 - A^T(t_i)A_i\|\,\|\overset{\vee}{S}_i\| \\ &\le \frac{h}{2}(\|\zeta_{i+1}\| + \|\zeta_i\|) + hK_1\|\xi_i\| \end{aligned} \tag{5.27j}$$

and similarly

$$\begin{aligned}\|A(t_i)\overset{\vee}{R}_i^2 - A_i\overset{\vee}{S}_i^2\| &\le \|\overset{\vee}{R}_i^2 - \overset{\vee}{S}_i^2\| + \|1_3 - A^T(t_i)A_i\|\,\|\overset{\vee}{S}_i^2\| \\ &\le \|\overset{\vee}{R}_i^2 - \overset{\vee}{S}_i^2\| + h^2K_2\|\xi_i\|\,. \end{aligned} \tag{5.27k}$$

where K_1, K_2 are constants. Moreover, we have

$$\begin{aligned}\|\overset{\vee}{R}_i^2 - \overset{\vee}{S}_i^2\| &\le \|\overset{\vee}{R}_i + \overset{\vee}{S}_i\|\,\|\overset{\vee}{R}_i - \overset{\vee}{S}_i\| + \|\overset{\vee}{R}_i\overset{\vee}{S}_i - \overset{\vee}{S}_i\overset{\vee}{R}_i\| \\ &\le hK_3\|\zeta_{i+1} + \zeta_i\| + \|R_i \times S_i\| \\ &\le (hK_3 + \tfrac{1}{2}h^2K_1)\,(\|\zeta_{i+1}\| + \|\zeta_i\|)\,. \end{aligned} \tag{5.27l}$$

which in fact follows from the inequality $\|R_i \times S_i\| \le \|R_i\|\|R_i - S_i\| \le \frac{1}{2}K_1(\|\zeta_{i+1} + \zeta_i\|)$. In the above, we have used the assumption that $\|W(t_n)\|$ and $\|W_n\|$ are bounded: $\|\overset{\vee}{R}_i\| \le K_1$ and $\|\overset{\vee}{R}_i + \overset{\vee}{S}_i\| \le K_3$. There results

$$\|\xi_{n+1}\| + \|\zeta_{n+1}\| \le C_1(h)h^2 + C_2(h)\sum_{i=1}^{n}(\|\xi_i\| + \|\zeta_i\|) \tag{5.27m}$$

in which $C_1(h) = (1 + P(h))^{-1}$ is of order 1 when $h \to 0$, and $P(h)$ and $C_2(h)$ are some polynomials of h. From (5.27m), it follows that

$$\|\xi_{n+1}\| + \|\zeta_{n+1}\| \le h^2 C_1(h) \exp[C_2(h)] \tag{5.27n}$$

Thus, $\mathbf{A}_n \to \mathbf{A}(t_n)$ and $\mathbf{W}_n \to \mathbf{W}(t_n)$ as $h \to 0$ and the rate of convergence is of second order. ∎

Note that this algorithm is a generalization of the trapezoidal rule to treat the rotation field as expressed in (5.26). The proof of proposition 5.2 is readily extended to the time-stepping algorithm for the dynamics of the three-dimensional rod with $\beta = \frac{1}{4}$ and $\tau = \frac{1}{2}$. Let $\mathbf{d}^+$ denote the global vector that contains all the nodal displacement degrees of freedom, and similarly for $\mathbf{v}^+$, $\overline{\mathbf{w}}^+$ concerning the linear and angular velocities. On the other hand, $\mathbf{A}^+$ denotes the block diagonal matrix constituted from the $\mathbf{A}$'s at the nodal points.

Proposition 5.3. *Consider the discrete nonlinear structural dynamics problem recast as follows*

$$\frac{d}{dt}\begin{Bmatrix} \mathbf{d}^+ \\ \mathbf{v}^+ \\ \overline{\mathbf{w}}^+ \end{Bmatrix} = \begin{Bmatrix} \mathbf{v}^+ \\ \mathbf{f}_1(\mathbf{d}^+, \mathbf{A}^+) \\ \mathbf{f}_2(\overline{\mathbf{w}}^+, \mathbf{d}^+, \mathbf{A}^+) \end{Bmatrix} \tag{5.28}$$

$$\dot{\mathbf{A}}^+ = (\mathbf{A}\,\overline{\mathbf{w}})^+$$

Assume that $\mathbf{f}_1$ *and* $\mathbf{f}_2$ *satisfy the Lipschitz condition with respect to the arguments, then* $\mathbf{d}_n^+ \to \mathbf{d}^+(t_n)$, $\mathbf{A}_n^+ \to \mathbf{A}^+(t_n)$, $\mathbf{v}_n^+ \to \mathbf{v}^+(t_n)$, $\mathbf{W}_n^+ \to \mathbf{W}^+(t_n)$ *as* $h \to 0$ *with second order accuracy, where* $\mathbf{d}_n^+$, $\mathbf{A}_n^+$, $\mathbf{v}_n^+$, *and* $\mathbf{W}_n^+$ *are obtained from the time-stepping algorithm described in Box* 5.2.

Proof. The proof is similar to the above and will not be repeated. ∎

5.5. Numerical Examples

In this last section, numerical simulations are presented that involve (i) finite vibration, (ii) fluttering (dynamic instability) due to follower loading, (iii) dynamic snap-through, and (iv) large overall motions of flexible beam structures. Owing to a linearization that is completely consistent with the update procedure, as discussed above, all the numerical simulations exhibit a *quadratic* rate of convergence. The geometric and material properties are selected so that finite deformation occurs during the motion. It is emphasized that the deformed shapes in all figures reported in this paper are given at the same scale as the geometry of the structures, i.e., there is no magnification of the deformation.

Example 5.5.1. Right-angle cantilever beam subject to out-of-plane loading. The right-angle cantilever beam with material properties shown in Figure 5.5.1*a* is subjected to an out-of-plane concentrated load applied at the elbow. The magnitude of this applied load follows the pattern of a hat function, as shown in Figure 5.5.1*a*. The cantilever undergoes finite free vibration with combined bending and torsion after removal of the applied load; the time histories of out-of-plane displacements of the elbow and of the tip are given in Figure 5.5.1*b*. We note that the amplitude of vibration is of the same order of magnitude as the length of each leg of the cantilever. Figure 5.5.1*c* gives the perspective view of a deformed shape. A linear mode shape analysis of the structure about the reference configuration reveals that the second bending mode of the free-end leg appears as the 10th mode of the structure, with period $T_{10} = 1.6$. This period provides a reasonable estimate for the time step size. Throughout the calculation, we employ a time step size of $h = 0.25$, which is about $\frac{1}{6}$th of T_{10}. The results obtained from a discretization of the cantilever using *two* elements with

quadratic interpolation are in good agreement with those obtained from using *ten* elements of the same type.

Example 5.5.2. Fluttering of a 45-degree bend under follower load. The static response of the 45-degree bend depicted in Figure 5.5.2*a* under follower loading was analyzed in Example 4.7.5. In this example, we consider the inertia effects on the response of the bend under follower load that ultimately leads to fluttering (dynamic instability). A follower concentrated force of the circulatory type described in (4.51) is applied at the tip of the bend with steady increase in magnitude at the rate of 100 units of force per unit of time. Throughout the analysis, we use a time step size of $h = 0.1$. Two perspective views of the deformed shapes are given in Figures 5.5.2*b* and 5.5.2*c* to help visualize this complex motion. In Figure 5.5.2*c*, we also give the path of the tip in the static loading for comparison with the response from dynamic loading. The static loading path is obtained by increments of 50 in the magnitude of the follower load up to a magnitude of 3000 (see Example 4.7.5). From Figure 5.5.2*c*, one can see that initially the dynamic response follows closely the static response. The inertia effects become gradually more pronounced, leading to the divergence of the two paths; then subsequently, dynamic instability sets in to cause strong vibrations of the bend with increasing amplitude and velocity.

Example 5.5.3. Out-of-plane dynamic snap-through of a right-angle frame. The right-angle frame depicted in Figure 5.5.3*a* was analyzed statically in Example 4.7.7. Here we provide an analysis of this frame accounting for inertia effects. The degrees of freedom at the hinged end are translation along the x direction and rotation about the z direction. The apex of the frame is constrained to lie in the y-z plane. Due to the symmetry of the problem, only half of the frame is modeled employing 10 elements with quadratic interpolation for both displacement and rotation fields. The value of Young's modulus is 71240,

and the value of Poisson's ratio is 0.31. The magnitude of the applied moment at the hinged end is chosen to have the same value as the time t. As the magnitude of the applied moment increased, a perturbed concentrated force is applied at the apex of the frame to induce a lateral motion of the apex. When the moment reaches the critical value of about 615, the loading is removed and the frame snaps through dynamically to the other side as shown in Figure 5.5.3*b*. Figure 5.5.3c reports the time history of the lateral displacement of the apex. In a static analysis, due to the presence of limit points, it is essential to employ a judicious combination of arc-length and displacement control methods in the numerical solution. In a dynamic analysis, such special techniques (continuation methods) are avoided since the mass matrix, as opposed to the tangent stiffness matrix, remains positive definite throughout the entire analysis. The slenderness of the cross-section of the frame with ratio $\frac{height}{thickness} = 50$ causes large amount of twist during the motion. To provide an estimate for the time step size, an eigenvalue analysis is performed at the reference configuration. The first two modes that involve torsional deformation of the leg are the 8th mode and the 11th mode of the structure with period $T_8 = 0.07$ and $T_{11} = 0.03$ respectively. Note that since the frame is very flexible in the out-of-plane direction, frequency modes below the eighth mode are out-of-plane bending modes. A time step size of $h = 0.005$ was selected in the numerical simulation of the dynamic snap-through of the frame.

Example 5.5.4. Free-free flexible beam undergoing large overall motions. This problem was first analyzed in the plane case in Simo & Vu-Quoc [1985b]. The beam is initially at an inclined position in the plane $(\mathbf{e}_1, \mathbf{e}_2)$ as depicted in Figure 5.5.4*a*. A spatially fixed force along $\mathbf{e}_1$ is applied at the lower end denoted by the letter A. Simultaneously, we apply a spatially fixed torque with

components along $\mathbf{e}_1$ and along $\mathbf{e}_2$ at end A. The time histories of the magnitude of these applied force and torque are given in Figure 5.5.4*a*. The applied force produces the translational motion; the component along $\mathbf{e}_1$ of the applied torque induces the forward tumbling while its component along $\mathbf{e}_2$ causes the out-of-plane motion of the beam. The resulting three-dimensional motion of the beam follows a periodic "kayak-rowing" pattern. Figure 5.5.4*b* shows the motion of the beam during the early tumbling stage; the entire sequence of motion is depicted in Figure 5.5.4*c*. The traces of end A and end B of the beam are shown by dotted lines. A side view of the motion in the plane $(\mathbf{e}_2, \mathbf{e}_3)$ is given in Figure 5.5.4*d*, and a perspective view of the entire sequence of motion in Figure 5.5.4*e*. During the loading stage, finite deformation of the beam is clearly discernible. An eigenvalue analysis at the reference configuration of the free-free beam yields a period of vibration of 1.06 for the second bending mode (the first two torsional modes appear at lower frequencies). A time step size of $h = 0.1$ is subsequently chosen for the entire analysis.

5.6. Concluding Remarks

Within the context of a general nonlinear finite-strain rod model, we have developed an implicit, second order accurate transient algorithm that furnishes a canonical extension of the classical Newmark algorithm to the rotation group $SO(3)$. The exact linearization of the algorithm and associated configuration update has been obtained in closed form, with accuracy and convergence characteristics precisely stated.

We have demonstrated the generality and effectiveness of the present formulation in several numerical examples involving vibration with finite amplitude, dynamic instability due to follower load, dynamic snap-through of a thin right-angle frame, and a free-free flexible beam subject to large overall motions and

undergoing infinitesimal or large deformation. The latter example illustrates the applicability of the proposed formulation to the transient analysis of free-free flexible beam structures undergoing large overall motions. Since the dynamics of the motion is referred directly to the inertial frame, this methodology represents a radical departure from traditional formulations in which small deformation is assumed at the outset, and the use of a floating frame that moves along with the deformed structure is necessary. In the present approach, the dynamic coupling in the inertia terms that appears in the use of the floating frame is exactly accounted for, and nonlinear geometric effects leading to instability are automatically included.

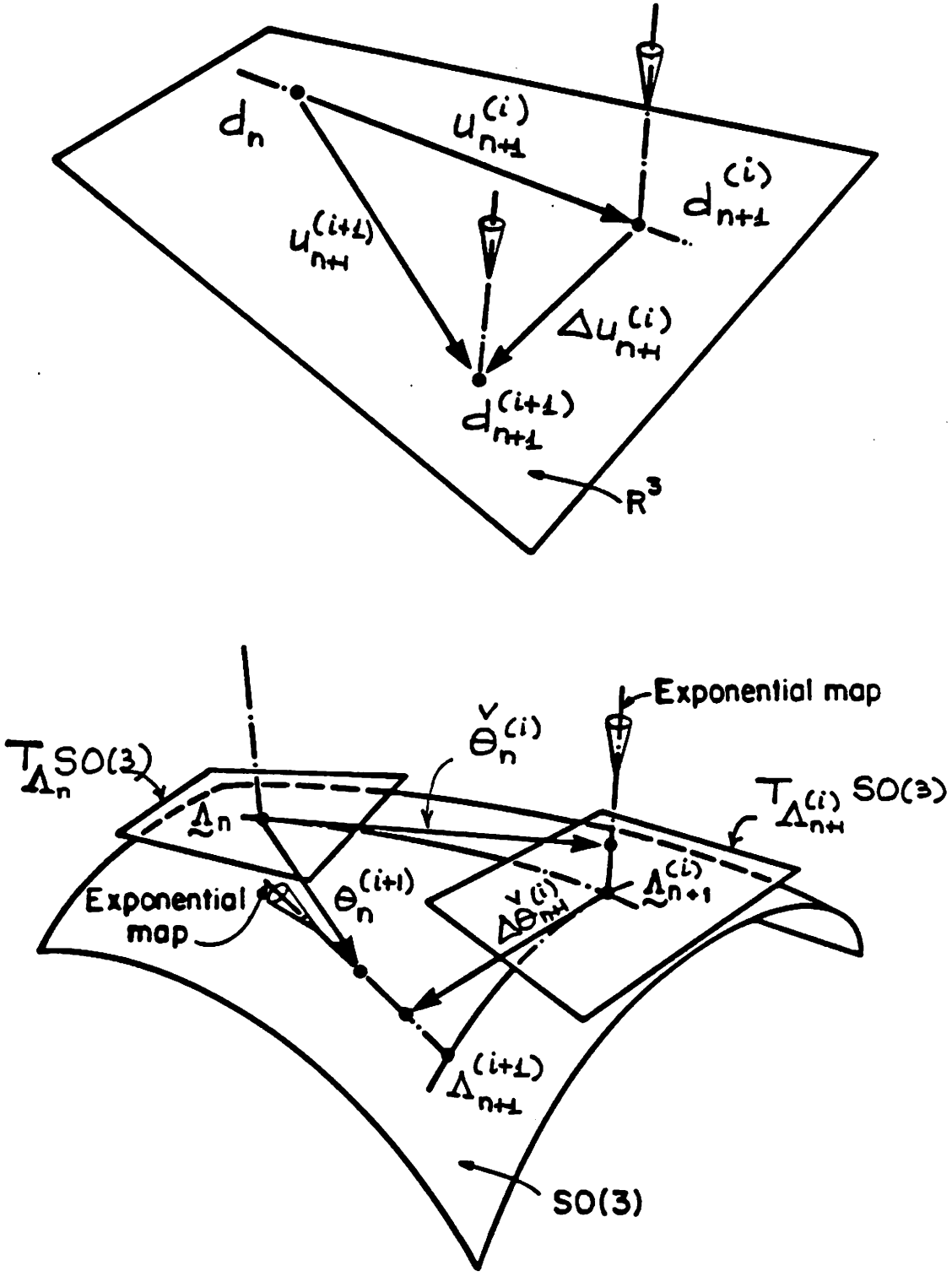

Figure 5.3.1 Geometric interpretation of the time-stepping algorithm. (a) Translational part takes place in $\mathbf{R}^3$. (b) Rotational part takes place in $SO(3)$. Velocity and acceleration update takes place *in the same tangent space*.

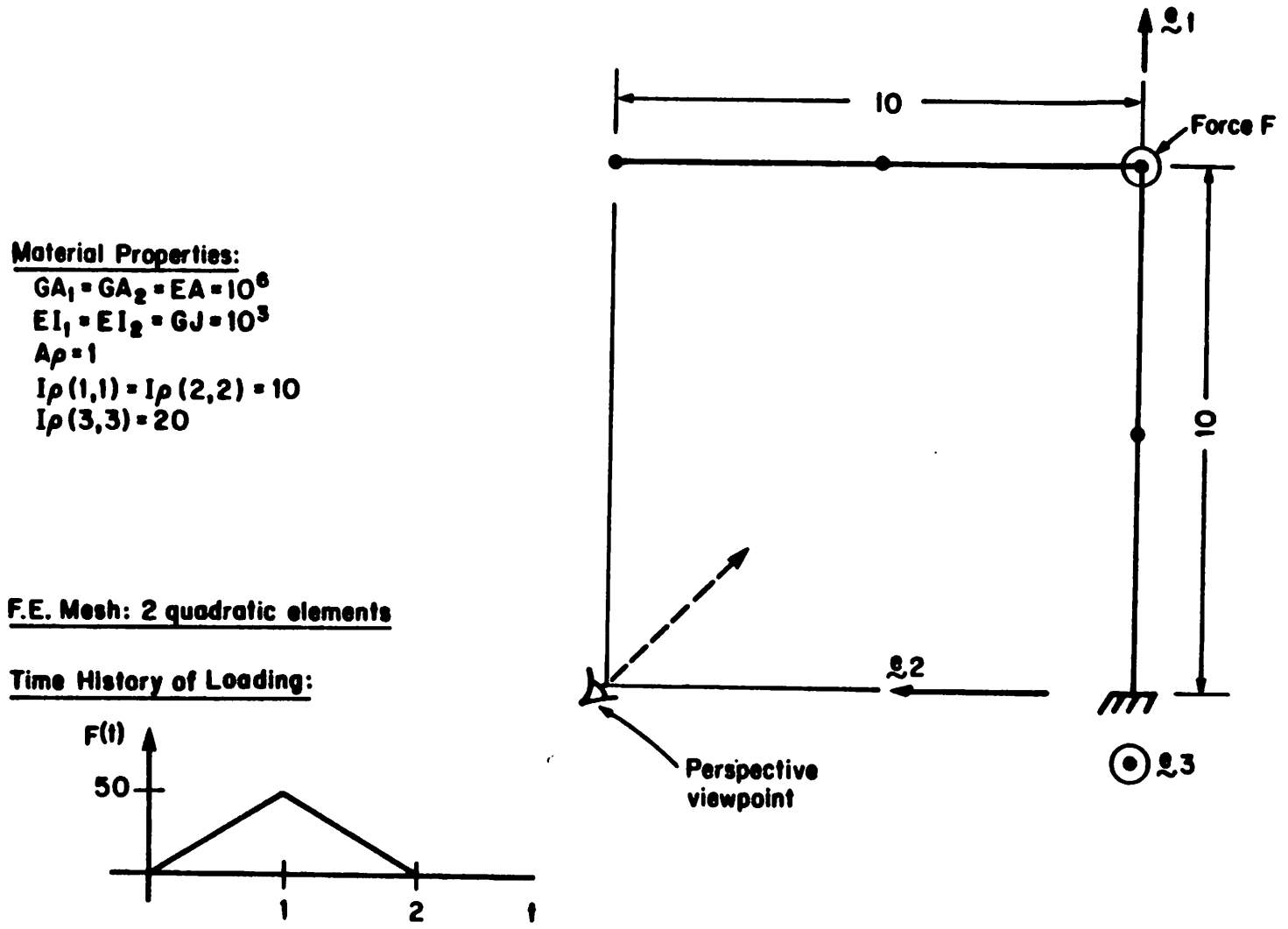

Figure 5.5.1a. *Right angle cantilever beam subject to out-of-plane loading.* Problem data.

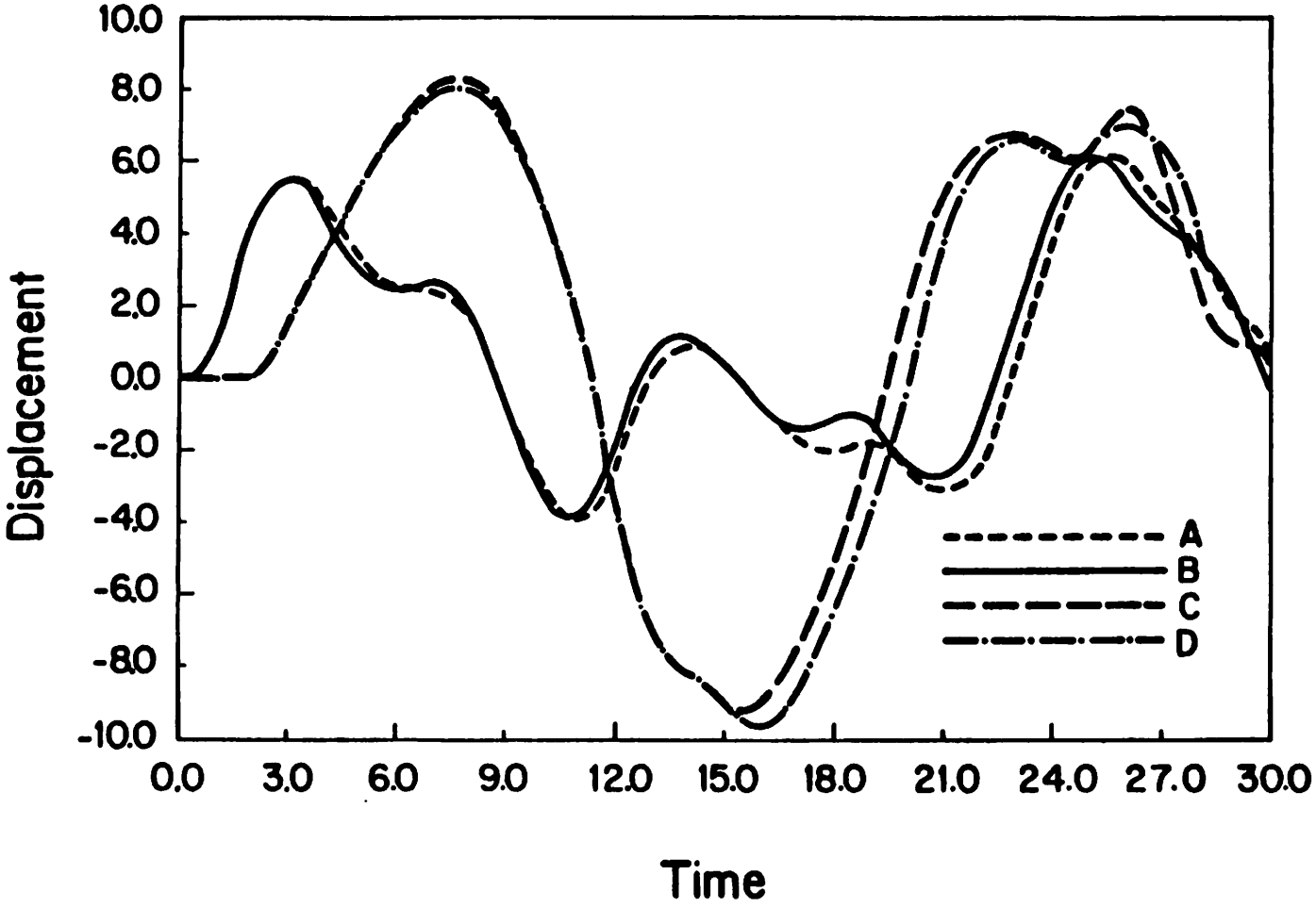

Figure 5.5.1b. ***Right angle cantilever beam subject to out-of-plane loading.*** Time histories of elbow displacements; Line A: 2 elements, line B: 10 elements. Time histories of tip displcement; Line C: 2 elements, line D: 10 quadratic elements.

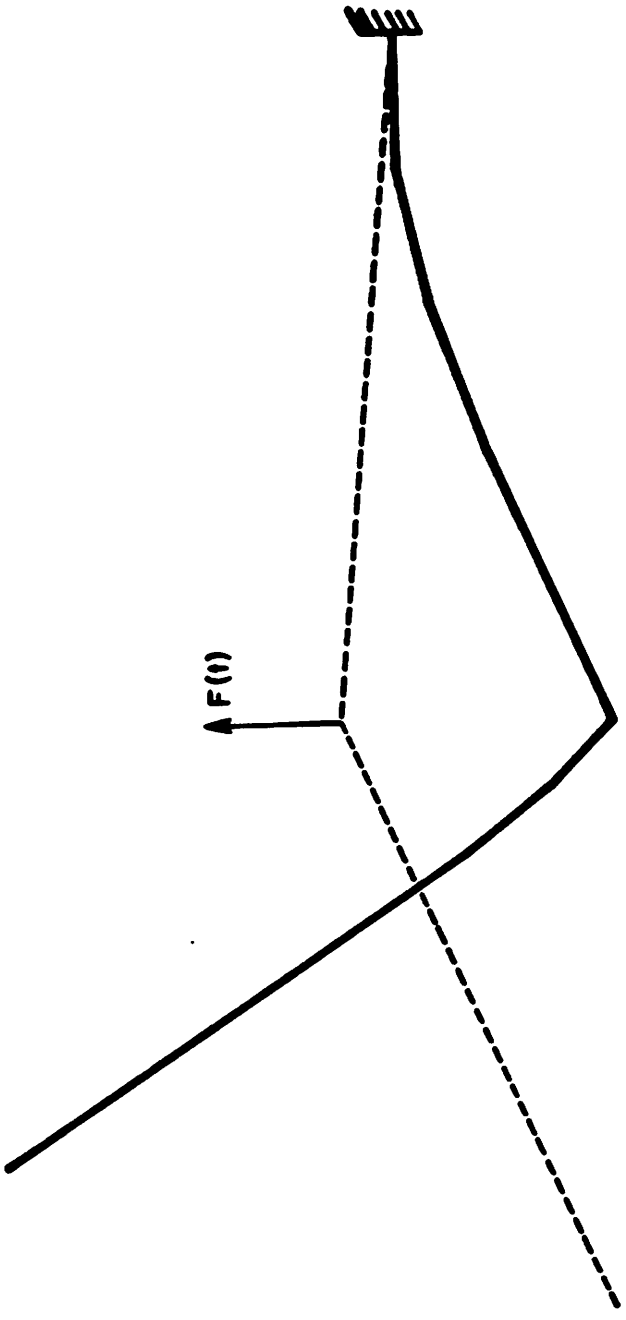

Figure 5.5.1c. *Right angle cantilever beam subject to out-of-plane loading.* Perspective view of deformed shape.

Material Properties:

$GA_1 = GA_2 = 5 \times 10^6$
$EA = 10^7$
$EI_1 = EI_2 = GJ = 833333$
$A\rho = 1$
$I\rho(1,1) = I\rho(2,2) = 10$
$I\rho(3,3) = 20$

F.E. Mesh: 8 linear elements

Time History of Follower Force: F(t) = 100 t

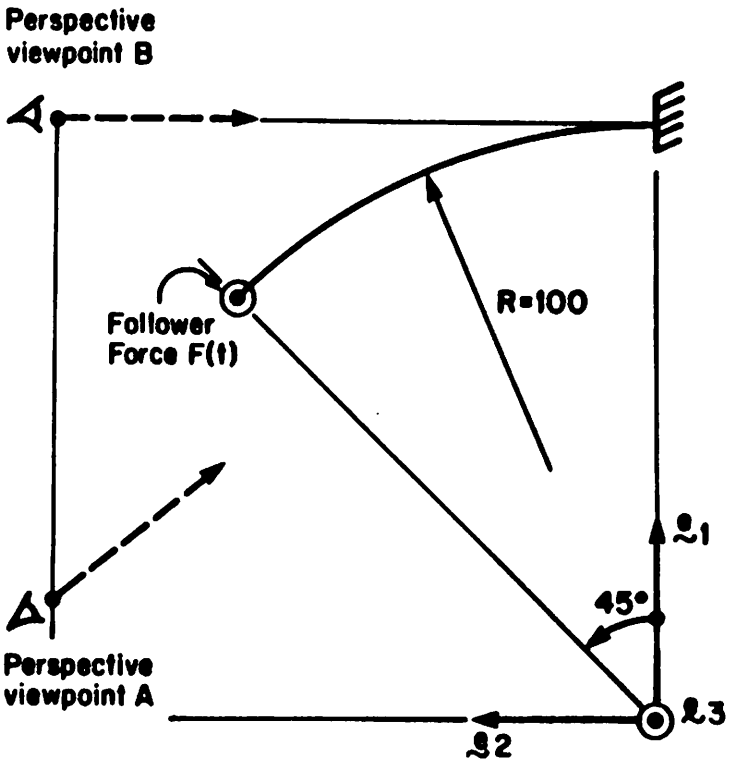

Figure 5.5.2a. *Fluttering of a 45-degree bend under follower load.* Problem data.

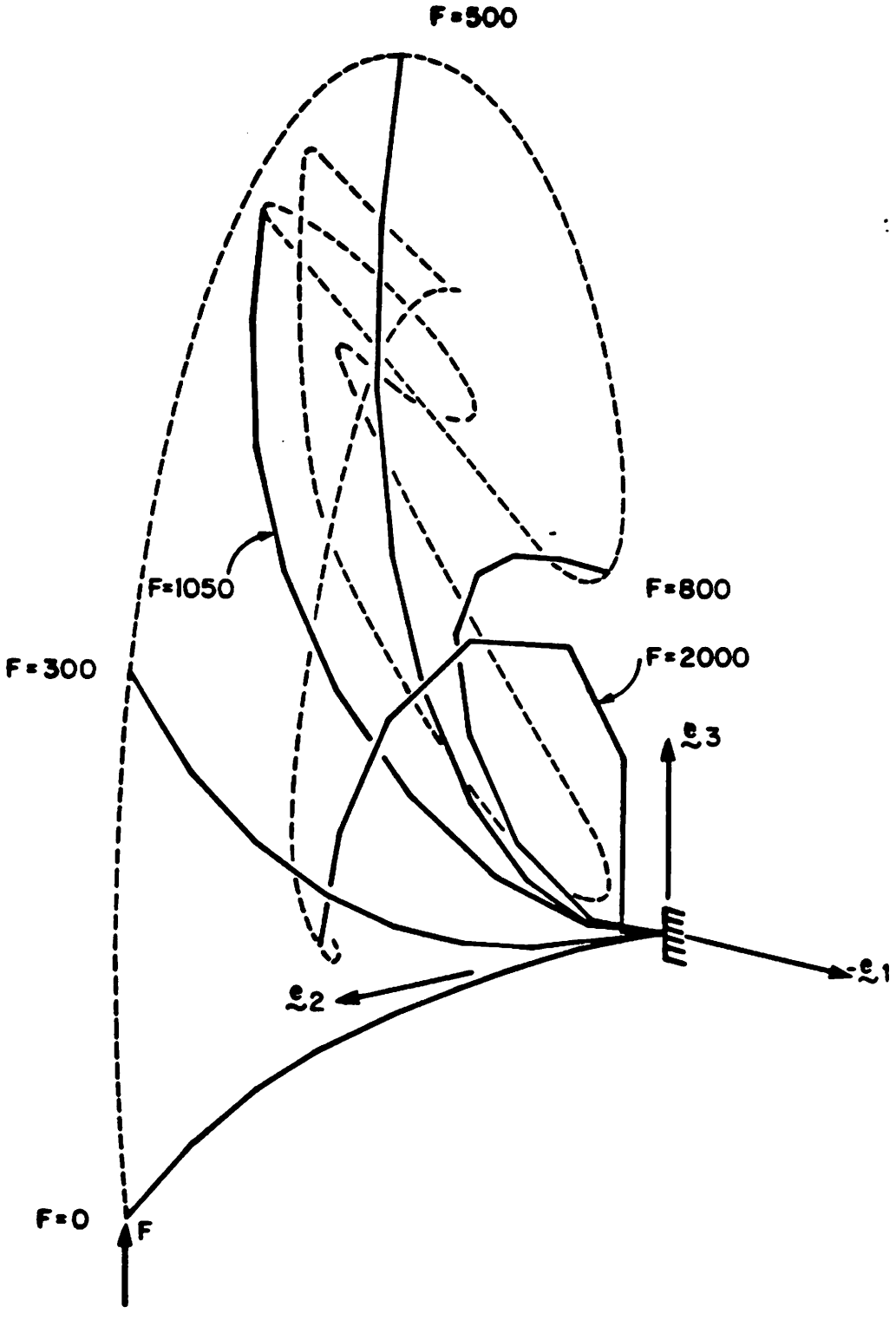

Figure 5.5.2b. *Fluttering of a 45-degree bend under follower load.* Perspective view of deformed shape from viewpoint A.

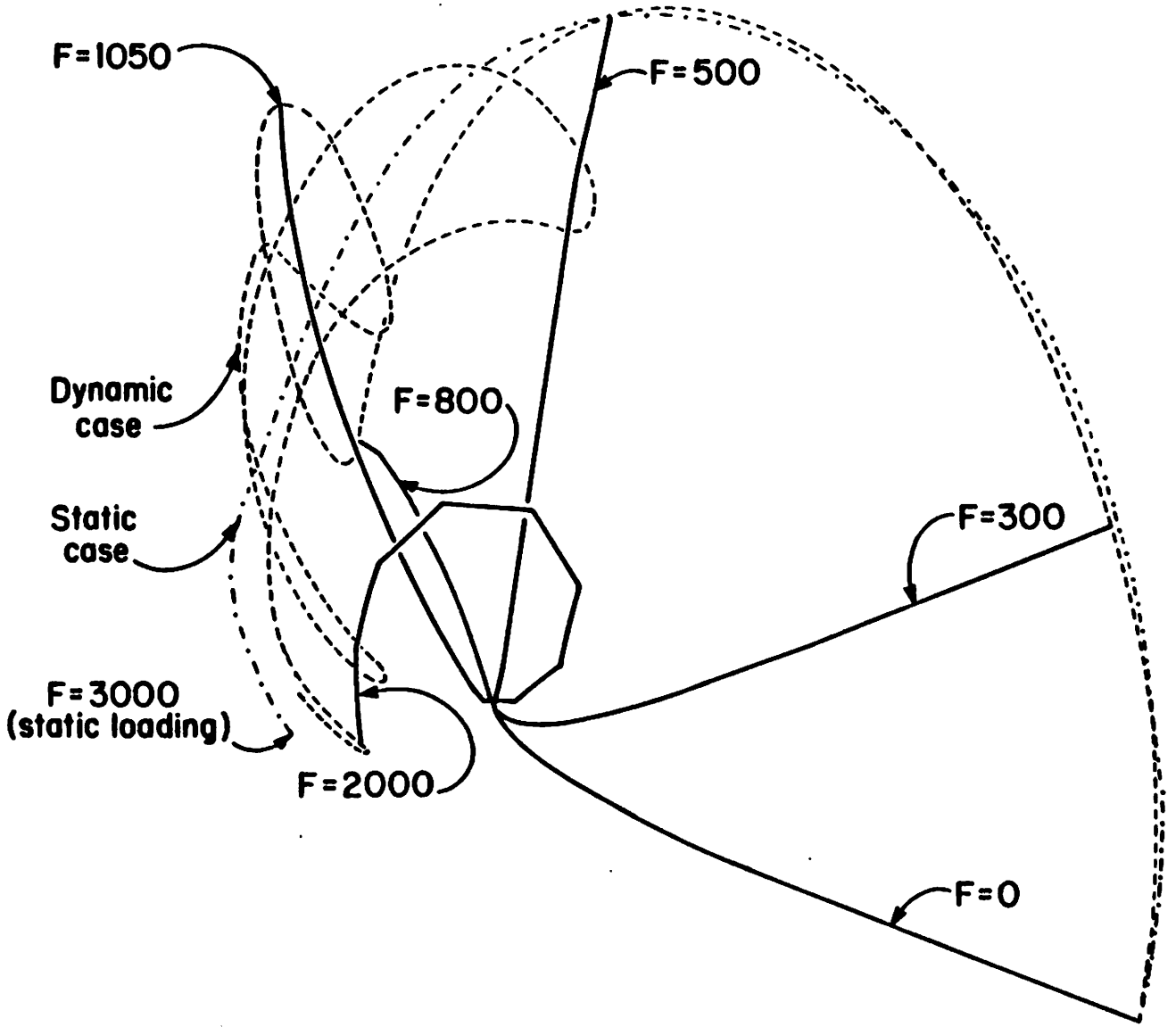

Figure 5.5.2c. *Fluttering of a 45-degree bend under follower load.* Perspective view of deformed shape from viewpoint B.

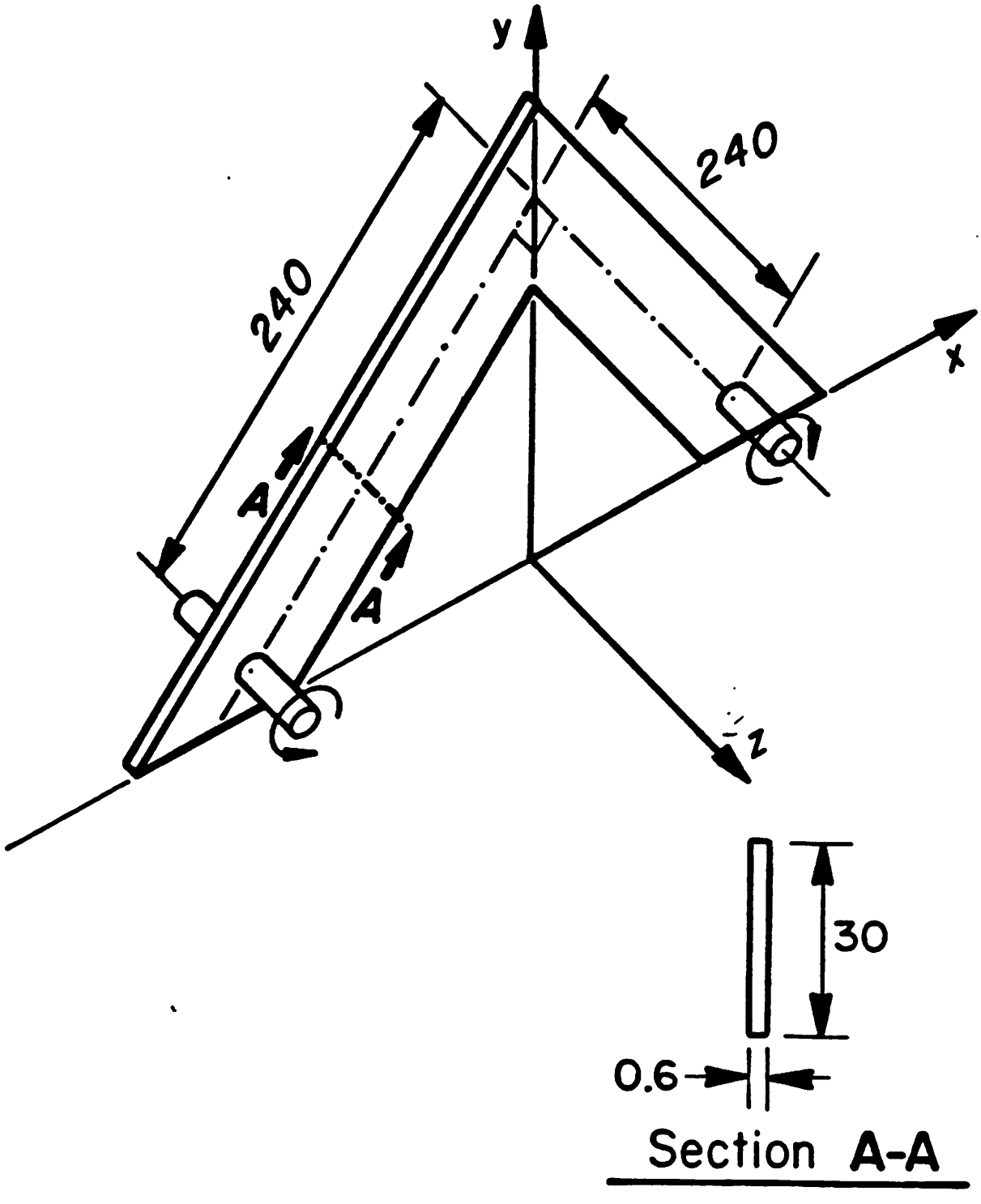

Figure 5.5.3a. *Out-of-plane dynamic snap-through of a right-angle frame.* Problem data.

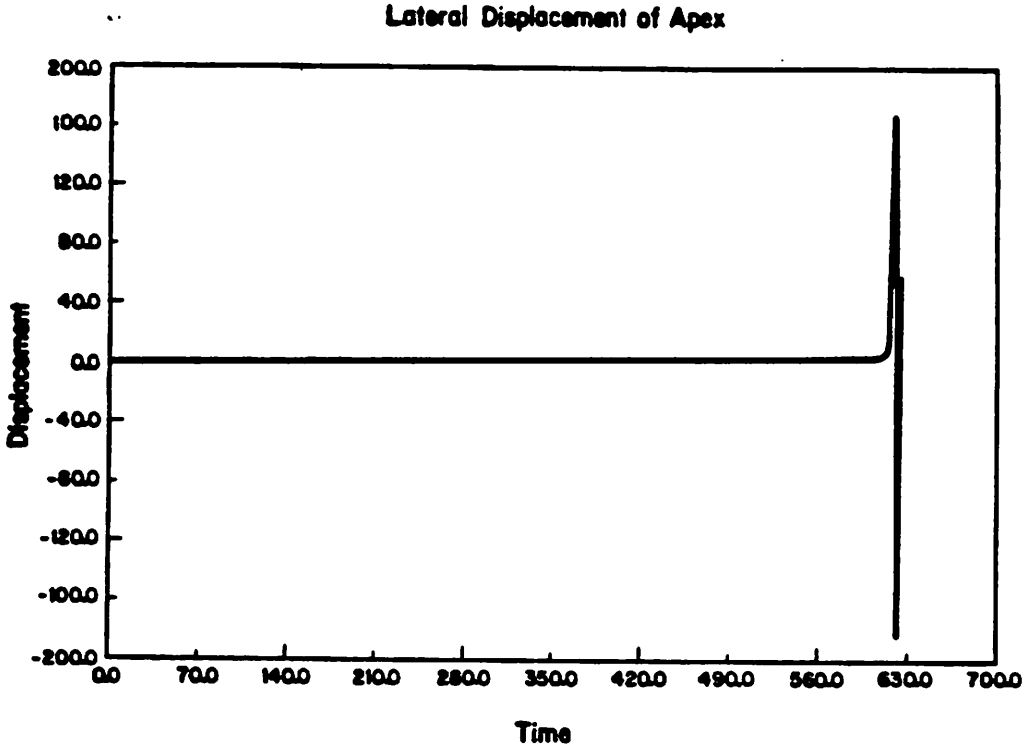

Figure 5.5.3b. *Out-of-plane dynamic snap-through of a right-angle frame.* Time history of lateral apex displacement.

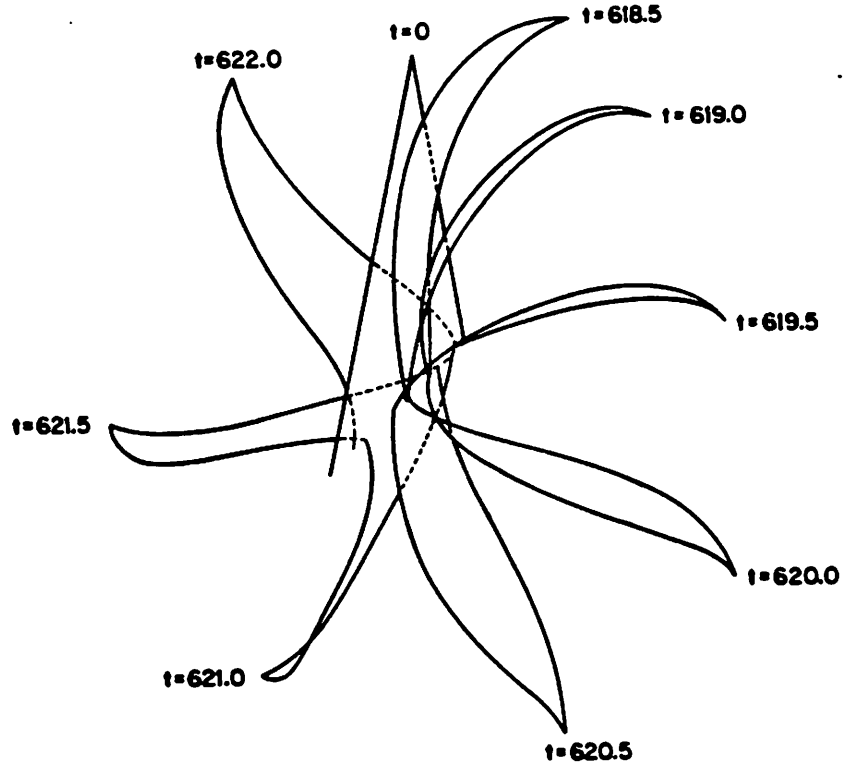

Figure 5.5.3c. *Out-of-plane dynamic snap-through of a right-angle frame.* Perspective view of deformed shapes.

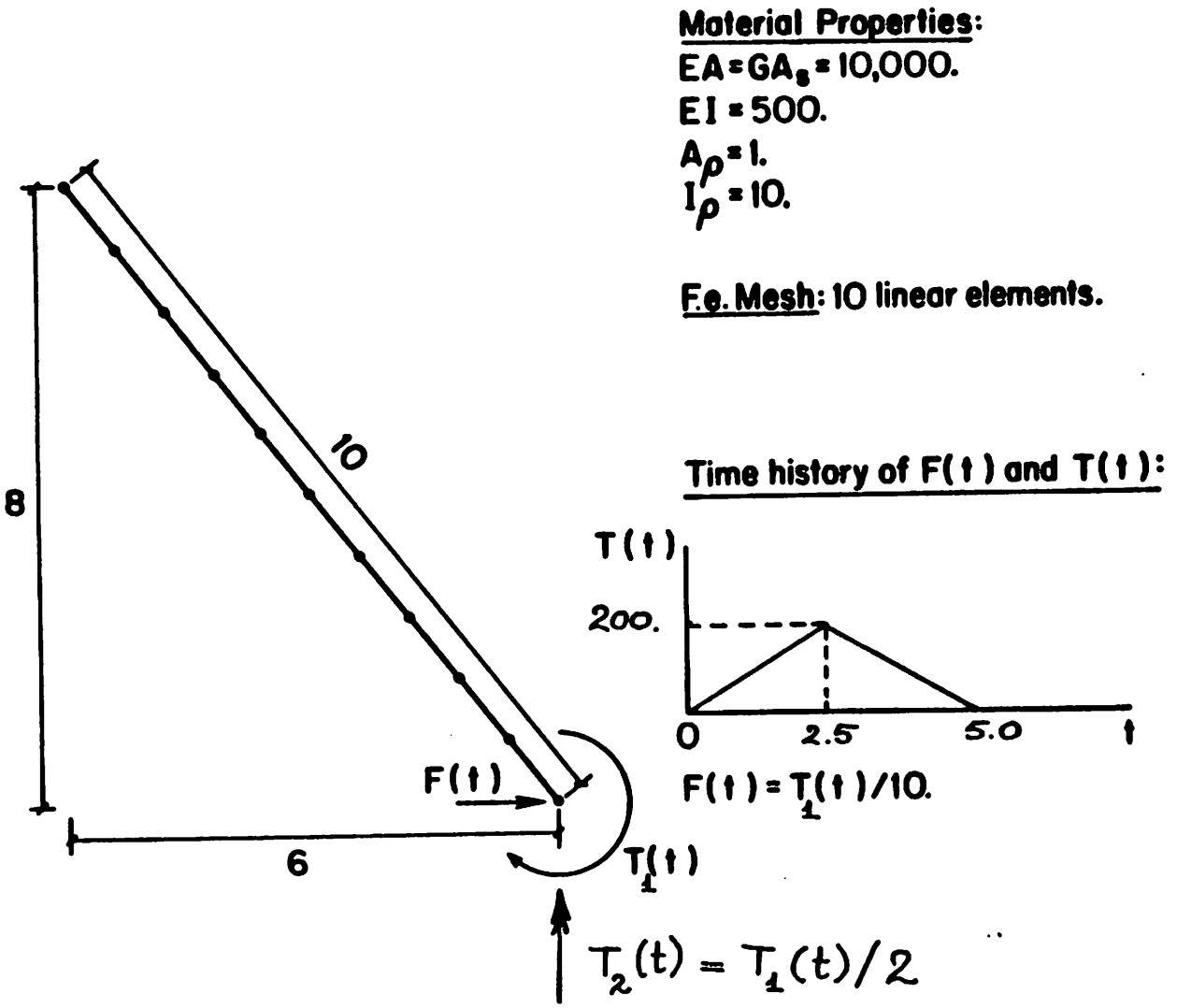

Figure 5.5.4a. *Free-free flexible beam undergoing large overall motions.* Problem data.

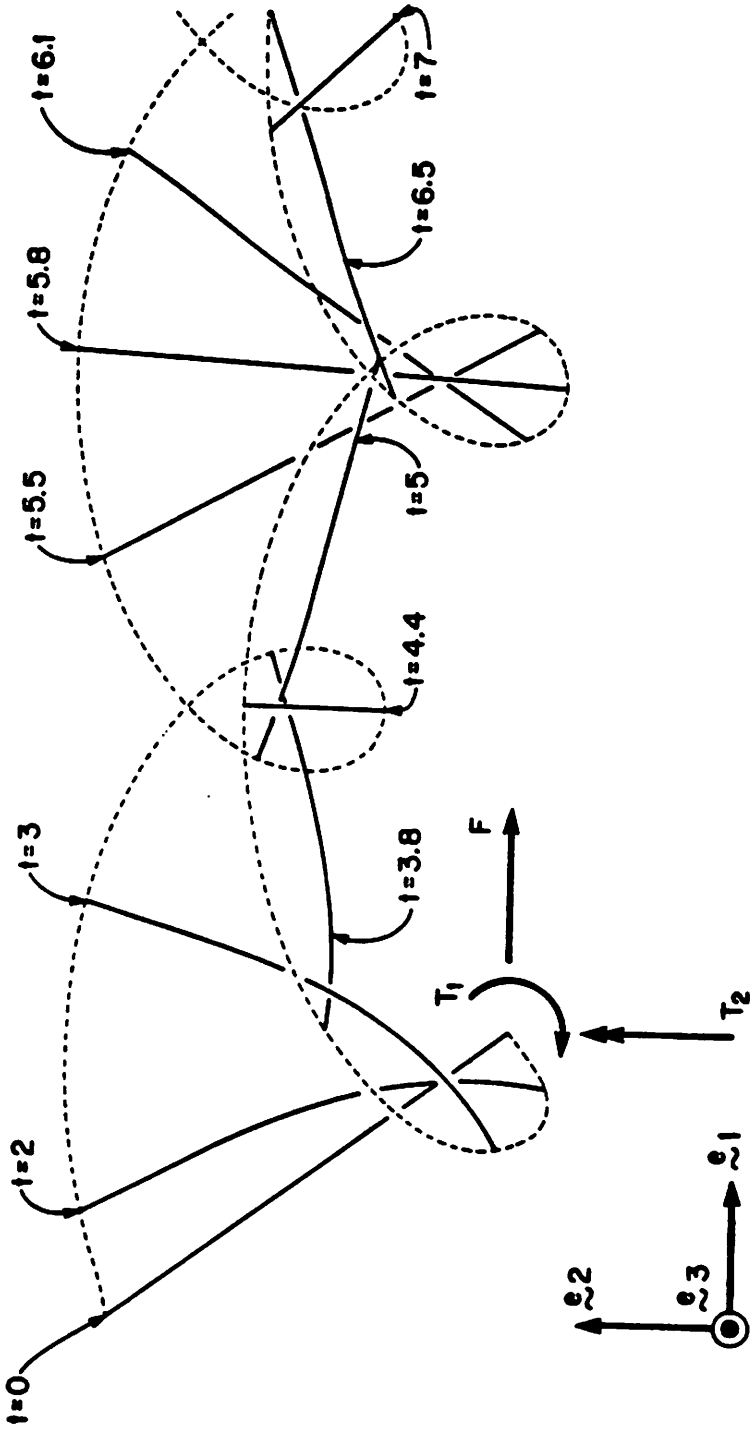

Figure 5.5.4b. *Free-free flexible beam undergoing large overall motions.* Early tumbling stage.

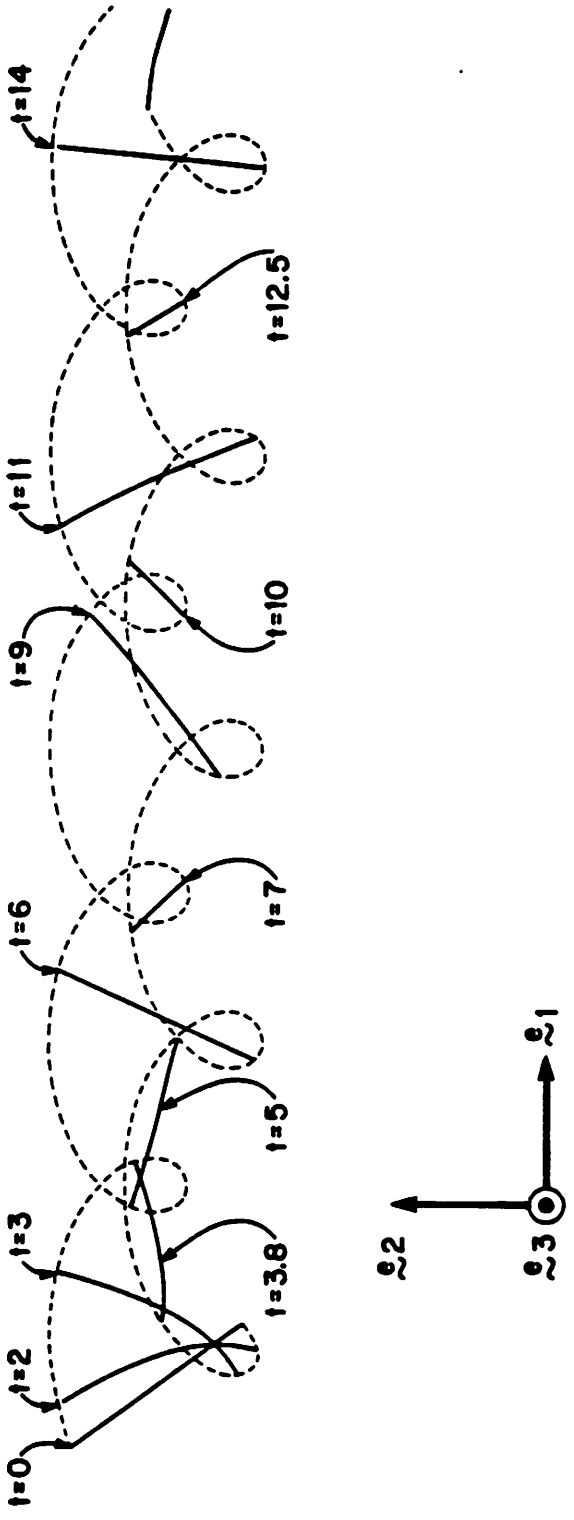

Figure 5.5.4c. *Free-free flexible beam undergoing large overall motions.* Entire sequence of motion.

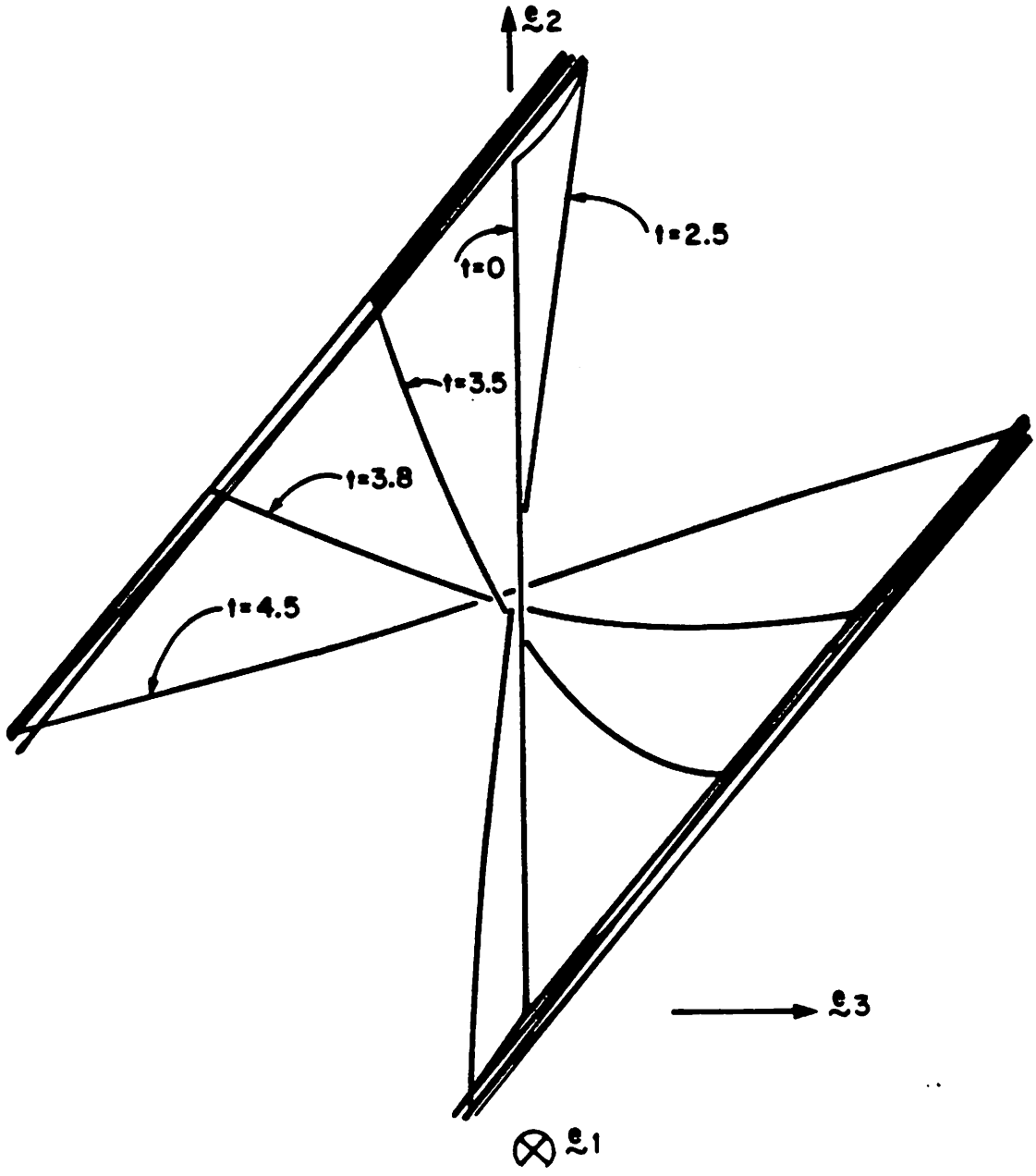

Figure 5.5.4d. *Free-free flexible beam undergoing large overall motions.* Side view of deformed shapes.

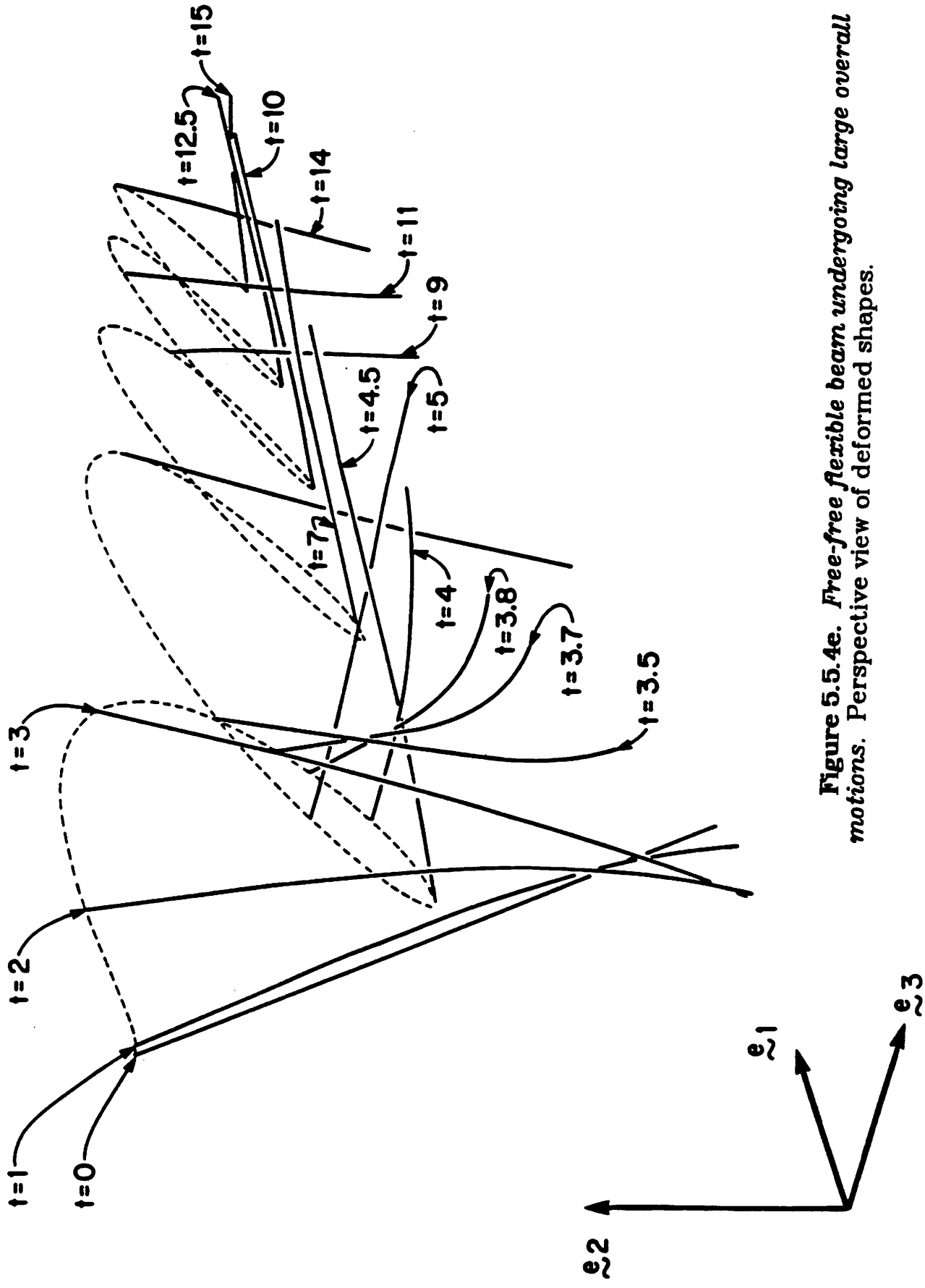

Figure 5.5.4e. *Free-free flexible beam undergoing large overall motions.* Perspective view of deformed shapes.

CHAPTER 6

THE DYNAMICS OF FLEXIBLE EARTH-ORBITING SATELLITES AND MULTIBODY SYSTEMS

6.1. Introduction

In previous chapters, we presented a methodology to analyze the dynamic response of flexible structures undergoing large overall motions based on a finite-strain approach. Restricting our attention to one-dimensional structural elements, we demonstrated the generality of the proposed methodology, employing a finite-strain rod model, through several examples of flexible beams subjected to complex motions and a wide range of structural deformations. These analyses were performed using efficient algorithms which were developed from concepts in differential geometry.

In this concluding chapter, we shall present an important application of the methodology developed throughout this dissertation: an application to the dynamics of flexible earth-orbiting satellites and of multibody systems. Recall that our formulation essentially makes use of the property of invariance under superposed rigid body motion of fully nonlinear structural theories. This property enables us to refer the dynamics of the satellite directly to the inertial frame. In addition, geometric instability effects are automatically accounted for in the formulation. To avoid numerical ill-conditioning, the deformation map is additively decomposed into the far field, which describes the orbit of the satellite, and the near field, which describes the structural deformations as seen by an observer in a close neighborhood of the satellite (Vu-Quoc & Simo [1986]). The dynamics of the far field and of the near field are treated separately by introducing a rotationally-fixed floating frame which in fact can be conveniently chosen to be a parallel translate of the inertial frame with origin placed at the

instantaneous center of mass of the satellite. Constraints to determine the orientation of the floating frame that typically arise in standard treatments are thus entirely by-passed. The proposed formulation can accommodate an unrestricted class of maneuvers under the action of follower actuator forces and gravity force, and is particularly well suited for the dynamics of flexible multibody systems undergoing a broad range of structural deformations.

6.2. Dynamics of flexible satellites

The configuration of earth-orbiting satellites has evolved markedly from rigid vehicles (spinners, dual spinners), hybrid rigid-elastic systems (dual spinners with flexible appendages), towards future generation of flexible large space structures (space antennae, solar power satellites); see Kline [1979]. The size of space antennae may vary from 50 to 300 meters, even to one kilometer in diameter; the projected solar power satellite measures 5 kilometers in width by 10 kilometers in length. Spacecrafts of this size, constructed using light weight materials, are therefore highly flexible. These structures can no longer be prefabricated on earth, but must be assembled directly in space.

It was recognized that flexibility significantly influences the behavior of satellites early in the start of the space program,† thus posing serious difficulty in the stabilization of their attitude. In fact, Likins [1971] identified the influence of spacecraft flexibility to the spacecraft attitude control problem.

Even though the proposed methodology is applicable to a large class of structural elements, —rods, plates, shells, 3-D continua —we shall limit our discussion to the case of a flexible satellites composed of beam elements. In

† For example, the instability of Explorer I, the first U.S. satellite, was caused by the flexibility of its small wire turnstile antennae.

Section 6.2.1, we introduce the concept of a rotationally-fixed floating frame that permits additive decomposition of the deformation map into the far field (Section 6.2.2) and the near field (Section 6.2.3). A computational procedure to solve for the dynamics of the far field and of the near field, coupled through the presence of gravity force, is proposed in Section 6.3.

6.2.1. Rotationally-fixed floating frame

Some traditional floating frames. Current approaches to the dynamics of flexible structures in orbit are largely based on the assumption of small deformation, and rely on the use of a floating reference frame to describe the structural displacements; that is, a frame that floats with the structure and such that, relative to this frame, infinitesimal structural deformations are observed. To prevent the rigid body motions relative to the floating frame, one imposes constraints on the displacement field of the entire body. There are typically five types of floating reference frames: (1) a locally attached frame, (2) a principal axis frame, (3) Tisserand's frame, (4) Buckens' frame, and (5) a rigid body mode frame (Canavin & Likins [1977]). When the structure has a central rigid body with attached flexible appendages, the frame is attached to the rigid body (the locally attached frame) and no constraint equation is needed. For structures with distributed flexibility, other types of floating frame should be used. In these frames, the origin is fixed at the center of mass of the deformed structure, i.e., one seeks to annihilate the linear momentum relative to the floating frame. Its orientation is then defined by adding constraints concerning the relative angular momentum. When small structural deformation is assumed, the Buckens frame is the most widely used since one can either use the free-free elastic modes to eliminate these (holonomic) constraints from the equations of motion (Canavin & Likins [1977]), or apply the Gram-Schmidt orthogonalization

procedure on an independent set of basis functions to eliminate the Buckens constraints (Benson & Hallquist [1985]).

For the type of highly flexible large space structures described above, what would guarantee that the deformations remain small? Clearly, traditional approaches employing the small strain assumption would yield only a first order approximation to the fully nonlinear theory. The methodology proposed in previous chapters represents a departure from traditional approaches in that, by employing fully nonlinear structural theories, we refer the dynamics of the structure directly to the inertial frame, and thus completely by-pass the use of a floating reference frame. The inertia term for the translation part then becomes linear simply as mass times acceleration; the rotational part has the structure of the equations of motion of a rigid body. Moreover, the role of nonlinear theories in the dynamic analysis of rotating flexible structures, where linear theories are inadequate to capture certain phenomena, has been explored in Chapter 3.

Rotationally-fixed floating frame. Mathematically, the system of partial differential equations summarized in Box 5.1 completely describes the dynamics of a flexible satellite constituted of beam elements. However, when gravitational force is accounted for, it is computationally unwarranted to refer the dynamics of flexible satellites directly to the inertial frame using finite precision mathematics. The reason clearly stems from the large difference in magnitude of structural deformations and the distance from the center of the earth to the satellite. Owing to the property of invariance with respect to superposed rigid body motion of the rod model, we can refer the dynamics of the satellite to a parallel translate of the inertial frame. As a result, when this floating frame is placed in the neighborhood of the satellite, the structural deformations, will be properly described.

Let us introduce the frame $\{Z;\mathbf{a}_1, \mathbf{a}_2, \mathbf{a}_3\}$, as shown in Figure 6.2.1, with base point $Z \in \mathbb{R}^3$ whose position relative to origin O of the inertial frame is given by the position vector

$$\mathbf{Z}(t) = Z_i(t)\, \mathbf{e}_i\,, \tag{6.1}$$

and such that the orthonormal basis vectors $\{\mathbf{a}_i\}$ have constant components relative to the inertial basis $\{\mathbf{e}_i\}$. This frame is thus rotationally fixed with respect to the inertial frame, and will be henceforth referred to as the *rotationally-fixed floating frame*. For convenience, we choose $\mathbf{a}_k = \mathbf{e}_k = \mathbf{E}_k$, which makes $\{Z;\mathbf{e}_1, \mathbf{e}_2, \mathbf{e}_3\}$ simply a parallel translate of the inertial frame $\{O;\mathbf{e}_1, \mathbf{e}_2, \mathbf{e}_3\}$. Let $\boldsymbol{\phi}_o^Z:[0, L]\to\mathbb{R}^3$ denote the deformation map of the line of centroids of the beam relative to this frame. The position vector of the centroid $\mathbf{x}_o$ defined in (4.1b) can now be restated in terms of $\boldsymbol{\phi}_o^Z$ as follows

$$\mathbf{x}_o = \boldsymbol{\phi}_o(S,t) = \mathbf{Z}(t) + \boldsymbol{\phi}_o^Z(S,t) = [Z_i(t) + \phi_{oi}^Z(S,t)]\, \mathbf{e}_i \tag{6.2}$$

Note that the relation (4.1c) for the rotation field remains identically the same for the rotationally-fixed floating frame. We shall refer to the map $t\to\mathbf{Z}(t)$ as the *far-field* dynamics which will be used later to describe the position of the satellite relative to the inertial frame. By the dynamics of the *near field*, we refer to the map $t\to\boldsymbol{\phi}_o^Z(S,t)$ which describes the structural deformation.

6.2.2. Loading conditions and far-field dynamics

Loading conditions. Three types of loading are considered. The simplest loading is the spatially fixed type with (possibly time varying) components relative to the inertial basis vectors given by $\mathbf{n}^f(t) = n_i^f(t)\, \mathbf{e}_i$. Most relevant to flexible satellites is loading which is dependent on the deformation of the structures such as actuator control forces — coming, for example, from gas jets or ion thrusters — used for the pointing maneuver and vibration suppression. The

actuator control force considered herein falls into the category of follower loading of the circulatory type —that is, loading which is not derivable from a potential and not explicitly dependent on time —defined as follows

$$\mathbb{n}^a(t) := N^{\gamma}(t)\, t_i(t)\,. \tag{6.3a}$$

The applied load in (6.3a) thus follows the change in orientation of the cross section, represented by the basis $\{t_i\}$, and may have time varying magnitude. By virtue of (4.1c), relation (6.3a) can be rewritten as

$$\mathbb{n}^a(A) = \Lambda_{iJ}\, N^{\gamma}\, e_i\,, \tag{6.3b}$$

thus explicating the dependence of the actuator loading on the configuration. Finally, gravity loading derived from a spherical potential applied to a material point of mass A_ρ located at a distance ϕ_o from the source, here the origin O, of the form

$$\mathbb{n}^g(\phi_o) = -\frac{A_\rho\, \mu\, \phi_o}{\|\phi_o\|^3} \tag{6.4}$$

is also configuration dependent. In (6.4), μ denotes the gravitational constant. For the rod model, using (6.4) implies the reasonable assumption that the mass of the rod is concentrated on the line of centroids. Even though more complex models of the gravitation field could be considered, our purpose here is to show how the formulation could accommodate configuration dependent loading. For this reason, within the confines of this chapter, we shall consider only the following type of loading

$$\mathbb{n} = \mathbb{n}^f + \mathbb{n}^a(A) + \mathbb{n}^g(\phi_o) \tag{6.5}$$

Far-field dynamics. To determine the far field dynamics $t \to \mathbb{Z}(t)$, we shall employ the following equation which defines the motion of the center of mass of the satellite,

$$\ddot{\mathbf{Z}}(t) = \mathbf{f}(\mathbf{Z}, \mathbf{A}) := \frac{\mu \mathbf{p}}{\|\mathbf{Z}\|^2} + \frac{1}{M} \int_{[0,L]} [\bar{\mathbf{n}}^f + \bar{\mathbf{n}}^a(\mathbf{A})]\, dS\,, \tag{6.6a}$$

where $\mathbf{p}$ is the unit vector defined as $\mathbf{p} := \frac{\mathbf{Z}}{\|\mathbf{Z}\|}$ and M the total mass of the satellite,

$$M := \int_{[0,L]} A_\rho(S)\, dS \tag{6.6b}$$

The first term on the right-hand side of (6.6a) gives the acceleration due to the gravitational field, whereas the second term represents the acceleration produced by the spatially fixed and actuator follower forces applied to the satellite.

6.2.3. Near-field dynamics and weak formulation

Near-field dynamics. In treating the dynamics of the near field one can always assume that the far field $t \to \mathbf{Z}(t)$ is known. The equations of motion for the near field are in fact valid for any known function $\mathbf{Z}(t)$. Noting that $\frac{\partial \boldsymbol{\phi}_o}{\partial S} = \frac{\partial \boldsymbol{\phi}_o^Z}{\partial S}$ and using the decomposition (6.2), i.e., $\boldsymbol{\phi}_o(S,t) = \mathbf{Z}(t) + \boldsymbol{\phi}_o^Z(S,t)$, we obtain

$$\begin{aligned} \frac{\partial \mathbf{n}}{\partial S} + [\,\bar{\mathbf{n}}^f + \bar{\mathbf{n}}^a(\mathbf{A}) + \bar{\mathbf{n}}^g(\mathbf{Z}, \boldsymbol{\phi}_o^Z) - A_\rho \ddot{\mathbf{Z}}] &= A_\rho \ddot{\boldsymbol{\phi}}_o^Z \\ \frac{\partial \mathbf{m}}{\partial S} + \frac{\partial \boldsymbol{\phi}_o^Z}{\partial S} \times \mathbf{n} + \bar{\mathbf{m}} &= \mathbf{I}_\rho \dot{\mathbf{w}} + \mathbf{w} \times [\mathbf{I}_\rho \mathbf{w}] \end{aligned} \tag{6.7a}$$

The strain measure $\boldsymbol{\Gamma}$ is now evaluated by

$$\boldsymbol{\Gamma} = \mathbf{A}^T \frac{\partial \boldsymbol{\phi}_o^Z}{\partial S} - \mathbf{E}_3 \tag{6.7b}$$

It is noted that equations concerning the dynamics of the rotation field of the rod and its curvature in Box 5.1 remain identically the same in the above formulation.

In all applications of interest, the origin Z of the rotationally-fixed floating frame, with position vector $\mathbf{Z}(t)$, is located in a small neighborhood of the center of mass. Thus, in the present situation, we have $\varepsilon := \dfrac{\|\boldsymbol{\phi}_o^Z\|}{\|\mathbf{Z}\|} \ll 1$. To avoid numerical ill-conditioning of the gravitational force field $\bar{\mathbf{n}}^g(\mathbf{Z}, \boldsymbol{\phi}_o^Z)$, one employs the following standard Taylor series expansion that retains terms up to order $O(\varepsilon^2)$

$$\bar{\mathbf{n}}^g(\mathbf{Z}, \boldsymbol{\phi}_o^Z) = -A_\rho \mu \frac{\boldsymbol{\phi}_o^Z + \mathbf{Z}}{\|\boldsymbol{\phi}_o^Z + \mathbf{Z}\|^3} = -\frac{A_\rho \mu \boldsymbol{\phi}_o^Z}{\|\mathbf{Z}\|^3}\left[1 - \frac{3\,\mathbf{p}\cdot\boldsymbol{\phi}_o^Z}{\|\mathbf{Z}\|}\right]$$

$$-\frac{A_\rho \mu \mathbf{p}}{\|\mathbf{Z}\|^2}\left[1 - \frac{3\,\mathbf{p}\cdot\boldsymbol{\phi}_o^Z}{\|\mathbf{Z}\|} - \frac{3}{2}\frac{\|\boldsymbol{\phi}_o^Z\|^2}{\|\mathbf{Z}\|^2} + \frac{15}{2}\frac{(\mathbf{Z}\cdot\boldsymbol{\phi}_o^Z)^2}{\|\mathbf{Z}\|^4}\right] + O(\varepsilon^3)\,. \qquad (6.8)$$

The complete system of partial differential equations describing the dynamics of the far field and of the near field is summarized in Box 6.1.

Remark 6.1. It should be noted that the far-field dynamics and the near-field dynamics are coupled through the presence of the follower actuator force $\bar{\mathbf{n}}^a(\mathbf{A})$, dependent on the rotation field $\mathbf{A}$ of the rod, in equation (6.6) and the presence of the forcing term $A_\rho \ddot{\mathbf{Z}}$ as well as the gravity force $\bar{\mathbf{n}}^g(\mathbf{Z}, \boldsymbol{\phi}_o^Z)$, which depends on the far field $\mathbf{Z}(t)$, in equation (6.7). ∎

Dynamic weak form of the near field. The weak formulation of the local equations (6.7) governing the dynamics of the near field is the cornerstone of the finite element numerical solution procedure discussed in the next section. Consider a configuration of the satellite defined by $\boldsymbol{\phi}_o(S, t) = \mathbf{Z}(t) + \boldsymbol{\phi}_o^Z(S, t)$ and $\mathbf{A}(S, t)$. We shall denote by $S \to \boldsymbol{\eta}(S) := (\boldsymbol{\eta}_o(S), \boldsymbol{\psi}(S))$ an *admissible variation* of the configuration $\boldsymbol{\phi} := (\boldsymbol{\phi}_o^Z, \mathbf{A})$. Physically, $S \to \boldsymbol{\eta}_o(S)$ represents a superposed infinitesimal displacement field, and $S \to \boldsymbol{\psi}(S)$ a superposed infinitesimal rotation field onto the satellite. By multiplying (6.7) by $\boldsymbol{\eta}(S)$ and integrating

BOX 6.1. *The far-field and the near-field dynamics*

Far field

$$\ddot{\mathbf{Z}}(t) = \frac{\mu \mathbf{Z}}{\|\mathbf{Z}\|^3} + \frac{1}{M}\int_{[0,L]} [\bar{\mathbf{n}}^I + \bar{\mathbf{n}}^a(\mathbf{A})]\, dS$$

Near field

$$\frac{\partial \mathbf{A}(S,t)}{\partial S} = \tilde{\boldsymbol{\omega}}(S,t)\,\mathbf{A}(S,t)\,, \qquad \frac{\partial \mathbf{A}(S,t)}{\partial t} = \tilde{\mathbf{w}}(S,t)\,\mathbf{A}(S,t)$$

$$\boldsymbol{\Gamma} = \mathbf{A}^T \frac{\partial \boldsymbol{\phi}_o^Z(S,t)}{\partial S} - \mathbf{E}_3\,, \qquad \boldsymbol{\Omega} = \mathbf{A}^T \boldsymbol{\omega}$$

$$\mathbf{n} = \mathbf{A}\,\frac{\partial \psi(S, \boldsymbol{\Gamma}, \boldsymbol{\Omega})}{\partial \boldsymbol{\Gamma}}, \qquad \mathbf{m} = \mathbf{A}\,\frac{\partial \psi(S, \boldsymbol{\Gamma}, \boldsymbol{\Omega})}{\partial \boldsymbol{\Omega}}$$

$$\frac{\partial \mathbf{n}}{\partial S} + [\,\bar{\mathbf{n}} - A_\rho \ddot{\mathbf{Z}}] = A_\rho\, \ddot{\boldsymbol{\phi}}_o^Z$$

$$\frac{\partial \mathbf{m}}{\partial S} + \frac{\partial \boldsymbol{\phi}_o^Z}{\partial S} \times \mathbf{n} + \bar{\mathbf{m}} = \mathbf{I}_\rho\, \dot{\mathbf{w}} + \mathbf{w} \times [\mathbf{I}_\rho\, \mathbf{w}]$$

over $[0, L]$ we obtain, after integration by parts, the following dynamic weak form

$$G_{dyn}(\boldsymbol{\phi}, \boldsymbol{\eta}) := \int_{[0,L]} \{A_\rho\, \ddot{\boldsymbol{\phi}}_o^Z \cdot \boldsymbol{\eta}_o + [\mathbf{I}_\rho\, \dot{\mathbf{w}} + \mathbf{w} \times (\mathbf{I}_\rho\, \mathbf{w})] \cdot \boldsymbol{\psi}\} dS - G(\boldsymbol{\phi}, \boldsymbol{\eta}) \quad (6.9a)$$

Here, $G(\boldsymbol{\phi}, \boldsymbol{\eta})$ denotes the static weak form of equilibrium given by

$$G(\boldsymbol{\phi}, \boldsymbol{\eta}) := \int_{[0,L]} \{\mathbf{n} \cdot [\frac{\partial \boldsymbol{\eta}_o}{\partial S} - \boldsymbol{\psi} \times \frac{\partial \boldsymbol{\phi}_o^Z}{\partial S}] + \mathbf{m} \cdot \frac{\partial \boldsymbol{\psi}}{\partial S}\} dS - G_{ext}(\boldsymbol{\phi}, \boldsymbol{\eta}) \quad (6.9b)$$

where $G_{ext}(\phi, \eta)$ is the weak form of the externally applied loading; that is

$$G_{ext}(\phi, \eta) := \int_{[0,L]} \{[\mathbf{n}^f + \mathbf{n}^g(\mathbf{Z}, \phi_o^Z) + \mathbf{n}^a(\mathbf{A}) - A_\rho \ddot{\mathbf{Z}}] \cdot \eta_o + \mathbf{m} \cdot \psi\} dS \ . \quad (6.10)$$

It is noted that in (6.10), the far field $\mathbf{Z}(t)$ is assumed to be known, and the acceleration term $A_\rho \ddot{\mathbf{Z}}$ is regarded as an additional forcing term.

6.3. Computational solution strategy

In this section, we shall discuss in detail the numerical integration procedure to solve the system of equations in Box 6.1. The proposed treatment relies on an essential property of our formulation: The motion of the rotationally-fixed floating frame relative to the satellite (the map $t \to \mathbf{Z}(t)$), in strict mathematical consideration, has absolutely no influence on the mechanical behavior of the satellite (the deformation map $t \to \phi_o^Z(S,t)$). Its role in the formulation can be thought of simply as a "zooming device," and serves the sole practical purpose of avoiding numerical ill-conditioning resulting from the large difference in magnitude between the structural deformation and the distance from the satellite to the center of the earth. This ill-conditioning of course arises only when gravitational force is taken into account in the formulation.

Conceptually, the coupled problem to be solved may be stated as

Find $\mathbf{Z}(t)$, $\phi_o^Z(S, t)$, *and* $\mathbf{A}(S, t)$ *such that:*

$$\ddot{\mathbf{Z}} = \mathbf{f}(\mathbf{Z}, \mathbf{A}), \text{ and}$$

$$G_{dyn}(\phi, \eta) = 0, \text{ for any } \eta \text{ admissible},$$

where $\phi := (\phi_0, \mathbf{A})$, and $\phi_0 = \mathbf{Z} + \phi_o^Z$. The single-step solution procedure can be summarized as follows:

Assume that at time $t = t_n$, the solution is known, i.e., we have solved for $\{\mathbf{Z}(t_n), \boldsymbol{\phi}_o^Z(S,t_n), \mathbf{A}(S,t_n)\}$. Find the solution at time $t_{n+1} = t_n + h$ denoted by $\{\mathbf{Z}(t_{n+1}), \boldsymbol{\phi}_o^Z(S,t_{n+1}), \mathbf{A}(S,t_{n+1})\}$, where h represents the time step size, based only on the known solution at time t_n.

We propose a single-step explicit/implicit transient algorithm to solve the above coupled far-field/near-field satellite dynamics problem. Consider the time interval of interest $[0, T]$ to be discretized into subintervals such that $[0, T] = \bigcup_{n\geq 0} [t_n, t_{n+1}]$, where $t_{n+1} := t_n + h$, and h is the time-step size. The following steps are performed over the interval $[t_n, t_{n+1}]$:

(i) Solve the initial value problem $\ddot{\mathbf{Z}} = f(\mathbf{Z}, \mathbf{A})$, with initial condition $\mathbf{Z}(t_n) = \mathbf{Z}_n$, by *assuming that* $\mathbf{A}$ *remains unchanged within this time interval, i.e.,* $\mathbf{A}(S,t) = \mathbf{A}(S, t_n)$, *for* $t \in [t_n, t_{n+1}]$. The numerical integration is performed by an *explicit* integration method.

(ii) Solve the *nonlinear structural dynamics problem* $G_{dyn}(\boldsymbol{\phi}, \eta) = 0$ by a generalized Newmark *implicit* time-stepping algorithm and the spatial Galerkin finite element method. This discretization procedure results in a system of nonlinear algebraic equations that can be solved by Newton's method.

We shall first discuss in Section 6.3.1 the temporal discretization in steps (i) and (ii), followed by the spatial Galerkin finite element discretization of the weak form for the near-field in Section 6.3.2.

6.3.1. Temporal discretization

In line with standard usage, we employ the subscript n to denote the temporal discrete approximate of a time-varying quantity at time t_n; thus for the far field $\mathbf{Z}_n \cong \mathbf{Z}(t_n)$, for the near field $\mathbf{d}_n(S) \cong \boldsymbol{\phi}_o^Z(S,t_n)$, $\mathbf{v}_n(S) \cong \dot{\boldsymbol{\phi}}_0^Z(S,t_n)$,

$\mathbf{a}_n(S) \cong \ddot{\boldsymbol{\phi}}_o^Z(S,t_n)$, and for the rotation field $\mathbf{A}_n(S) \cong \mathbf{A}(S,t_n)$, $\mathbf{w}_n(S) \cong \mathbf{w}(S,t_n)$, $\dot{\mathbf{w}}_n(S) \cong \dot{\mathbf{w}}(S,t_n)$. Also denote the configuration at time t_n as $\boldsymbol{\phi}_n(S)$ $:= (\mathbf{d}_n(S), \mathbf{A}_n(S))$.

Far-field dynamics: Explicit scheme. The ordinary differential equation (ODE) describing the motion of the center of mass of the satellite given in (6.8) is easily solved by employing any of the classical explicit single-step algorithms for ODE's (e.g., Gear [1971]) if the function $\mathbf{f}(\mathbf{Z}, \mathbf{A})$ is explicitly known. However, the dynamics of the rotation field $t \to \mathbf{A}(S,t)$ for $t \geq t_n$ is not known until we have solved the equations of motion (6.7). Hence, to solve for $\mathbf{Z}_{n+1}$, with known solution $\{\mathbf{Z}_n, \mathbf{A}_n(S)\}$, we *assume that* $\mathbf{A}(S,t) \equiv \mathbf{A}_n(S)$, *for all time* t *in the interval* $[t_n, t_{n+1}]$. In the implementation, we employ the explicit Runge-Kutta 4th order method.

Remark 6.2. In fact, a wide choice of numerical algorithms for ODE's — explicit or implicit, single-step or multi-step — could be considered to solve for the far field with the above assumption. We note that in general, due to structural vibration, the time step size of the whole numerical integration scheme is rather governed by the near-field dynamics. ■

Remark 6.3. Numerical integration of the far-field dynamics is only necessary when external forces from other than the (spherical) gravitational field are applied on the satellite. In the absence of these applied forces, one can use well-known analytical solutions in orbital mechanics (the two-body problem) to obtain directly the solution for the far field $\mathbf{Z}(t)$. ■

Remark 6.4. Because of the assumption that the follower load remains constant in the interval $[t_n, t_{n+1}]$ for the integration of the far-field, the origin Z of the rotationally-fixed floating frame will not exactly follow the path of the center of mass of the satellite, and could gradually drift away from the latter. We note

that the assumption of piecewise constant applied follower loading used in the integration of the far field is closely related to the rectangular integration rule. This assumption can therefore be viewed as a convenient interpolation of the follower actuator load; the role of this interpolation is to allow a decoupling in the numerical treatment of the coupled far field/near field problem. However, first due to the small time step size to accommodate structural vibration as noted in Remark 6.2, the drift of origin Z from the center of mass would be insignificant. Second, since one could always arbitrarily re-position the floating frame relative to the satellite as will be shown later, the drift of Z from the center of mass is therefore inconsequential as far as the structural response of the satellite is concerned. ■

Near-field dynamics: Implicit scheme. The basic problem concerning the discrete time-stepping algorithm for the near field may be formulated as follows. With $\mathbf{Z}_{n+1}$ known from solving the far-field dynamics as described above, and given the configuration $\boldsymbol{\phi}_n := (\mathbf{d}_n, \mathbf{A}_n) \in \mathbb{R}^3 \times SO(3)$ at time t_n, its associated linear and angular velocities, $(\mathbf{v}_n, \mathbf{w}_n)$, and linear and angular accelerations $(\mathbf{a}_n, \boldsymbol{\alpha}_n)$, obtain the configuration $\boldsymbol{\phi}_{n+1} := (\mathbf{d}_{n+1}, \mathbf{A}_{n+1}) \in \mathbb{R}^3 \times SO(3)$ at time t_{n+1}, the associated linear and angular velocities $(\mathbf{v}_{n+1}, \mathbf{w}_{n+1})$, and the linear and angular acceleration $(\mathbf{a}_{n+1}, \boldsymbol{\alpha}_{n+1})$. To this end, we employ the generalized implicit Newmark algorithm summarized in Box 5.2.

Remark 6.5. The accuracy of the implicit integration scheme for the near field is independent of the accuracy of the integration scheme for the far field in the sense that we shall always obtain the structural displacement and rotation fields of the rod up to second order accuracy (see the analysis in Chapter 5) regardless of the choice of integration scheme for the far field. ■

We shall now proceed to the spatial discretization procedure of $G_{dyn}(\boldsymbol{\phi}_{n+1}, \boldsymbol{\eta})$.

6.3.2. Linearization and spatial discretization

We recall that as a result of introducing the generalized Newmark time stepping algorithm in Box 5.2, the weak form $G_{dyn}(\boldsymbol{\phi}_{n+1}, \boldsymbol{\eta}) = 0$ governing the dynamics of the near field becomes a nonlinear functional depending on $\boldsymbol{\phi}_{n+1}(S) := (\mathbf{d}_{n+1}(S), \mathbf{A}_{n+1}(S))$. In what follows, we shall be concerned with the spatial discretization of this nonlinear functional by a Galerkin procedure.

Tangent gravity load stiffness operator. The solution of the nonlinear variational problem $G_{dyn}(\boldsymbol{\phi}_{n+1}, \boldsymbol{\eta}) = 0$ by Newton's method — step (ii) of the solution strategy outlined above — involves the solution of a sequence of linearized problems, denoted by $L[\, G(\boldsymbol{\phi}_{n+1}^{(i)}, \boldsymbol{\eta})\,] = 0$ where the superscript (i) designates the iteration number. These linear problems are obtained by consistent linearization of $G_{dyn}(\boldsymbol{\phi}, \boldsymbol{\eta}) = 0$, at the current configuration $S \to \boldsymbol{\phi}_{n+1}^{(i)}(S) := (\mathbf{d}_{n+1}^{(i)}(S), \mathbf{A}_{n+1}^{(i)}(S))$, in the direction of an incremental field $S \to \Delta\boldsymbol{\phi}_{n+1}^{(i)}(S) := (\Delta\mathbf{u}_{n+1}^{(i)}(S), \Delta\boldsymbol{\theta}_{n+1}^{(i)}(S))$ according to the directional derivative formula

$$L[\, G_{dyn}(\boldsymbol{\phi}_{n+1}^{(i)}, \boldsymbol{\eta})\,] := G_{dyn}(\boldsymbol{\phi}_{n+1}^{(i)}, \boldsymbol{\eta}) + \frac{d}{d\varepsilon}\bigg|_{\varepsilon=0} G_{dyn}(\boldsymbol{\phi}_{n+1}^{(i)} + \varepsilon\, \Delta\boldsymbol{\phi}_{n+1}^{(i)}, \boldsymbol{\eta}) = 0 \quad (6.11)$$

A detailed account of the linearization process for the static weak form $G(\boldsymbol{\phi}_{n+1}^{(i)}, \boldsymbol{\eta})$ defined in (6.9b) that includes consideration of follower loading is contained in Chapter 4. Extension of this methodology to the dynamic problem governed by the weak form $G_{dyn}(\boldsymbol{\phi}_{n+1}^{(i)}, \boldsymbol{\eta})$ in (6.9a) is given in Chapter 5. Thus, within the present context, it only remains to address the linearization of the contribution to $G_{ext}(\boldsymbol{\phi}_{n+1}^{(i)}, \boldsymbol{\eta})$ defined by (6.10) of the gravity force field. This contribution will be denoted by $G_{ext}^{g}(\boldsymbol{\phi}_{n+1}^{(i)}, \boldsymbol{\eta})$ in what follows. By making use of

the Taylor series expansion (6.8) in (6.10), use of the directional derivative formula yields the expression

$$\frac{d}{d\varepsilon}\bigg|_{\varepsilon=0} G_{\text{grav}}(\phi_{n+1}^{(i)}+\varepsilon\Delta\phi_{n+1}^{(i)},\eta) = -\int_{[0,L]} \frac{A_\rho\,\mu\,\eta_0}{\|\mathbf{Z}_{n+1}\|^3}\cdot\left[3\left[1-\frac{5\,\mathbf{p}_{n+1}\cdot\mathbf{d}_{n+1}^{(i)}}{\|\mathbf{Z}_{n+1}\|}\right]\mathbf{p}_{n+1}\otimes\mathbf{p}_{n+1}\right.$$

$$\left.+\frac{3}{\|\mathbf{Z}_{n+1}\|}\mathbf{p}_{n+1}\otimes\mathbf{d}_{n+1}^{(i)}+\left[1-\frac{3\,\mathbf{p}_{n+1}\cdot\mathbf{d}_{n+1}^{(i)}}{\|\mathbf{Z}_{n+1}\|}\right]\mathbf{1}_3\right]\Delta\mathbf{u}_{n+1}^{(i)}\,dS \qquad (6.12)$$

Note that the above tangent gravity load stiffness operator is non-symmetric and concerns only the translational degrees of freedom. This result will be used in the computation of the load stiffness matrix upon introducing the spatial discretization.

Galerkin finite element discretization. Following the same procedure as in Section 4.6.1, we begin by introducing a partition of the interval $[0, L]$ into non-overlapping subintervals according to $[0, L] = \bigcup_{k=1}^{N-1} [S_k, S_{k+1}]$, where $0 = S_1 < S_2 < \cdots < S_N = L$. Consider the following approximation for the translational field

$$\mathbf{d}_{n+1}(S) \cong \sum_{I=1}^{N} N_I(S)\,\mathbf{d}_{n+1,I}\,, \quad \text{where} \quad \mathbf{d}_{n+1,I} \cong \mathbf{d}_{n+1}(S_I)\,. \qquad (6.13a)$$

Here, $N_I(S)$ is a set of global functions which are either prescribed or constructed from local finite element approximations in the standard manner. An interpolation for the rotation field $S \to \mathbf{A}_{n+1}(S)$ is constructed by noting that $\mathbf{A}_{n+1}(S) = \exp[\overset{\vee}{\chi}_{n+1}(S)]$, where $\overset{\vee}{\chi}(S)$ is the skew-symmetric matrix associated with the rotation vector χ. We then consider the approximation for the rotation field

$$\chi_{n+1}(S) \cong \sum_{I=1}^{N} N_I(S)\,\chi_{n+1,I}\,, \quad \text{where} \quad \chi_{n+1,I} \cong \chi_{n+1}(S_I)\,,$$
$$\text{and} \quad \mathbf{A}_{n+1}(S) \cong \exp[\chi_{n+1}(S)]\,. \qquad (6.13b)$$

Note that the approximation scheme for the rotation field preserves exactly the orthogonality property of $\mathbf{A}$. By substitution of the interpolation in (6.13a-b) into the the weak form $G_{dyn}(\boldsymbol{\phi}_{n+1}, \boldsymbol{\eta}) = 0$, and assuming that the admissible variations $\boldsymbol{\eta} := (\boldsymbol{\eta}_o, \boldsymbol{\psi})$ are approximated in the same manner according to

$$\boldsymbol{\eta}(S) \cong \sum_{I=1}^{N} N_I(S)\, \boldsymbol{\eta}_I \quad \text{with } \boldsymbol{\eta}_I \cong \boldsymbol{\eta}(S_I)\,, \tag{6.13c}$$

after application of standard results in variational calculus, we arrive at a system of nonlinear algebraic equations whose linearized form is given by

$$\mathbf{P}_I(\boldsymbol{\phi}_{n+1}^{(i)}) + \sum_{J=1}^{N} \mathbf{K}_{IJ}(\mathbf{A}_n, \boldsymbol{\phi}_{n+1}^{(i)})\, \Delta\boldsymbol{\phi}_{n+1,J}^{(i)} = \mathbf{0}\,, \tag{6.14a}$$

for $I=1,\ldots,N$. In (6.14a), $\mathbf{P}_I$ represents the residual force, and $\mathbf{K}_{IJ}$ the dynamic tangent stiffness matrix obtained from

$$\mathbf{K}_{IJ}(\mathbf{A}_n, \boldsymbol{\phi}_{n+1}^{(i)}) = \mathbf{M}_{IJ}(\mathbf{A}_n, \mathbf{A}_{n+1}^{(i)}) + \mathbf{S}_{IJ}(\boldsymbol{\phi}_{n+1}^{(i)}) + \mathbf{G}_{IJ}(\boldsymbol{\phi}_{n+1}^{(i)}) + \mathbf{L}_{IJ}^{\mathcal{S}}(\mathbf{A}_{n+1}^{(i)}) + \mathbf{L}_{IJ}^{\mathcal{G}}(\mathbf{Z}_{n+1}, \mathbf{d}_{n+1}^{(i)})\,. \tag{6.14b}$$

Expressions for the tangent inertia matrix $\mathbf{M}_{IJ}$, the material tangent stiffness matrix $\mathbf{S}_{IJ}$, the tangent geometric stiffness matrix $\mathbf{G}_{IJ}$, and the tangent follower load stiffness $\mathbf{L}_{IJ}^{\mathcal{S}}$ have been obtained in Chapters 4 and 5 —see equations (5.23), (4.61), (4.62), and (4.63), respectively. The expression for the tangent gravity load stiffness results from the introduction of the approximations (6.13a,c) into (6.12),

$$\mathbf{L}_{IJ}^{\mathcal{G}}(\mathbf{Z}_{n+1}, \mathbf{d}_{n+1}^{(i)}) = -\int_{[0,L]} \frac{A_\rho\, \mu}{\|\mathbf{Z}_{n+1}\|^3} \left[3\left(1 - \frac{5\,\mathbf{p}_{n+1}\cdot\mathbf{d}_{n+1}^{(i)}(S)}{\|\mathbf{Z}_{n+1}\|}\right) \mathbf{p}_{n+1}\otimes\mathbf{p}_{n+1} + \frac{3}{\|\mathbf{Z}_{n+1}\|}\mathbf{p}_{n+1}\otimes\mathbf{d}_{n+1}^{(i)}(S) + \left(1 - \frac{3\,\mathbf{p}_{n+1}\cdot\mathbf{d}_{n+1}^{(i)}(S)}{\|\mathbf{Z}_{n+1}\|}\right)\mathbf{1}_3 \right] N_I(S)\, N_J(S)\, dS \tag{6.14c}$$

The incremental displacement and rotation $\Delta\boldsymbol{\phi}_{n+1}^{(i)}$ can be obtained easily by solving (6.14a). The update procedure to obtain the solution $\boldsymbol{\phi}_{n+1}^{(i+1)}$ at iteration $(i+1)$

such that the solution always remains in the configuration manifold is, however, non-trivial; we refer to Chapters 4 and 5 for the detailed discussion.

6.3.3. Re-positioning of the rotationally-fixed floating frame

One of the salient features of our formulation is that the rotationally-fixed floating frame could be arbitrarily re-positioned and its velocity in the inertial frame reset at any time. Thus in case of a drift of the origin Z of the floating frame from the center of mass, one could easily re-position the floating frame to the center of mass by first computing the current position of the center of mass relative to Z, denoted by $\mathbf{r}$,

$$\mathbf{r}(t) = \frac{1}{M} \int_{[0,L]} A_\rho(S)\, \boldsymbol{\phi}_o^Z(S,t)\, dS \tag{6.15a}$$

with velocity and acceleration relative to the floating frame given by,

$$\dot{\mathbf{r}}(t) = \frac{1}{M} \int_{[0,L]} A_\rho(S)\, \dot{\boldsymbol{\phi}}_o^Z(S,t)\, dS\,, \tag{6.15b}$$

$$\ddot{\mathbf{r}}(t) = \frac{1}{M} \int_{[0,L]} A_\rho(S)\, \ddot{\boldsymbol{\phi}}_o^Z(S,t)\, dS\,. \tag{6.15b}$$

Only when $\|\mathbf{Z}\|$ and $\|\mathbf{r}\|$ are of comparable magnitude to threaten the loss of precision on the structural deformation due to round-off error that the re-positioning procedure need be performed. In this case, suppose that we wish to re-position the floating frame at time $t = \bar{t}$, we simply restart the integration of the far-field dynamics with initial conditions reset as follows:

$$\begin{aligned} \mathbf{Z}(\bar{t}) &\leftarrow [\, \mathbf{Z}(\bar{t}) + \mathbf{r}(\bar{t}) \,] \\ \dot{\mathbf{Z}}(\bar{t}) &\leftarrow [\, \dot{\mathbf{Z}}(\bar{t}) + \dot{\mathbf{r}}(\bar{t}) \,] \end{aligned} \tag{6.16a}$$

Also the near-field dynamics is reset according to

$$\begin{aligned} \boldsymbol{\phi}_o^Z(\bar{t}) &\leftarrow [\, \boldsymbol{\phi}_o^Z(\bar{t}) - \mathbf{r}(\bar{t}) \,] \\ \dot{\boldsymbol{\phi}}_o^Z(\bar{t}) &\leftarrow [\, \dot{\boldsymbol{\phi}}_o^Z(\bar{t}) - \dot{\mathbf{r}}(\bar{t}) \,] \\ \ddot{\boldsymbol{\phi}}_o^Z(\bar{t}) &\leftarrow [\, \ddot{\boldsymbol{\phi}}_o^Z(\bar{t}) - \ddot{\mathbf{r}}(\bar{t}) \,] \end{aligned} \tag{6.16b}$$

It is clear that the above re-positioning procedure leaves strictly unchanged the value at time $\bar{t}$ of $\boldsymbol{\phi}_o(\bar{t}) = \mathbf{Z}(\bar{t}) + \boldsymbol{\phi}_o^Z(\bar{t})$, and hence the values of the velocity $\dot{\boldsymbol{\phi}}_o(\bar{t})$, and acceleration $\ddot{\boldsymbol{\phi}}_o(\bar{t})$. Further, this re-positioning procedure is most conveniently employed when a single-step integration algorithm for ODE's is used to solve for the far field.

6.3.4. Numerical examples

We shall give two numerical examples of application of the concept rotationally-fixed floating frame in the dynamics of flexible rods undergoing large overall motions with and without the effects of gravitational force. All figures of the deformed shapes reported herein are given at the same scale as the geometry of the structure. There is no artificial magnification of the structural deformation for visualization purpose.

Example 6.3.1. Free-free flexible beam undergoing large overall motions (revisited). Consider a free-free flexible beam initially placed at an inclined position and subjected to applied force and torques at the lower free end as in Example 5.5.4. Since the gravitational field is not considered in this example, and since only spatially fixed loading is applied on the beam, the dynamics of the far field and the dynamics of the near field are completely decoupled:

$$\ddot{\mathbf{Z}} = \frac{1}{M}\int_{[0,L]} \mathbf{n}'(S)\,dS\,, \tag{6.17}$$

$$\frac{\partial \mathbf{n}}{\partial S} + [\,\mathbf{n}' - A_\rho \ddot{\mathbf{Z}}] = A_\rho \ddot{\boldsymbol{\phi}}_o^Z\,. \tag{6.18}$$

Substitution of (6.17) into (6.18) yields the equation of motion for the near field

$$\frac{\partial \mathbf{n}}{\partial S} + [\,\mathbf{n}' - \frac{A_\rho}{M}\int_{[0,L]} \mathbf{n}'(S)\,dS\,] = A_\rho \ddot{\boldsymbol{\phi}}_o^Z\,. \tag{6.19}$$

Thus, in this example, one does not need to solve for the far field if only the near-field dynamics is of prime interest. The result is shown in Figure 6.3.1 with a clear physical meaning: The motion given in Figure 5.5.4*a* as perceived by an inertial observer is now seen by an observer, attached to the rotationally-fixed floating frame and moving with the center of mass. A time step size of $h = 0.1$ is used in both analyses (with and without the rotationally-fixed floating frame). A justification of the time step size chosen was given in Example 5.5.4.

Example 6.3.2. Satellite dynamics: Libration and orbit transfer. To illustrate the proposed methodology for solving the coupled far-field/near-field problem in the presence of gravitational force, we consider in this example a beam of length $100\sqrt{2}$ completely contained in the plane $\{\mathbf{e}_1, \mathbf{e}_2\}$ and placed at 45° with respect to axis $\mathbf{e}_1$. The center of mass of the beam is initially located at a distance of 7×10^6 from the center of the earth, i.e., $\mathbf{Z}(0) = 7\times10^6\,\mathbf{e}_1$. For the center of mass to describe a circular orbit, an initial velocity of $\dot{\mathbf{Z}} = 7544.1557\,\mathbf{e}_2$ is chosen; the gravitational constant being $\mu = 3.984\times10^{14}$. We are interested here in capturing the well known librational motion, due to the effect of gravity gradient, of orbiting satellite when the geometric configuration of the latter departs from spherical symmetry. Hence, for simplicity we choose the initial conditions for the near field to be $\boldsymbol{\phi}_o^Z(S,0) = \dot{\boldsymbol{\phi}}_o^Z(S,0) = \ddot{\boldsymbol{\phi}}_o^Z(S,0) \equiv 0$. For the rotation field of the beam, $\mathbf{A}(S,0) = 1_3$, $\mathbf{w}(S,0) = \boldsymbol{\alpha}(S,0) \equiv 0$. Let λ be the (libration) angle between the beam and the unit vector $\mathbf{p} := \dfrac{\mathbf{Z}}{\|\mathbf{Z}\|}$ known as the local vertical, see Figure 6.3.2*a*. The dynamics of libration of a uniform bar on circular orbit ($\|\mathbf{Z}\| = constant$) is governed by the differential equation

$$\ddot{\lambda} = \frac{3\,\mu \sin 2\lambda}{2\,\|\mathbf{Z}\|^3} \tag{6.20}$$

The initial conditions for (6.20) that correspond to the above chosen initial conditions for the far field and the near field are given by $\lambda(0) = \frac{\pi}{4}$ and $\dot{\lambda}(0) = -\frac{\|\dot{\mathbf{z}}(0)\|}{\|\mathbf{z}(0)\|}$. Figure 6.3.2*b* shows the evolution of the libration angle λ as obtained from the proposed approach to finite deformation satellite dynamics and from using the 4th order Runge-Kutta method to integrate (6.20); both curves are obtained with a time step size of $h = 100$ which in fact covers a complete circular orbit in about 60 steps — the orbital period for the above initial conditions of the far field is 5830 sec. With a smaller time step size, for example $h = 10$, we can exactly achieve the result as obtained from solving (6.20). In addition to the second order accuracy of the algorithm summarized in Box 5.2 as compared to the fourth order accuracy in the integration of (6.20), we note that the need for a smaller step size stems from the fact that the semi-discrete equations (ODE's) of the PDE's in Box 6.1 are actually much stiffer than (6.20).

Next, to demonstrate how a combination of loading given by (6.15) could be applied on the satellite, we consider an orbit transfer from the current circular orbit to a higher circular orbit by passing through an intermediate elliptic orbit. This orbit transfer is achieved by activating the satellite thrusters under the form of impulsive loading in two stages. First, when the satellite completes the first revolution in the low circular orbit, impulse loading with resultant in the direction of axis $\mathbf{e}_2$ is applied to induce an increase in magnitude of the velocity $\dot{\mathbf{z}}$, and thus put the satellite into a transitory elliptic orbit as depicted in Figure 6.3.2*c*. The time history of the libration angle (in degree) is given in Figure 6.3.2*d*. Next, when the satellite reaches the apogee of this transitory orbit, impulsive thruster force, with resultant in the negative direction of axis $\mathbf{e}_2$, is again applied to put the satellite on a higher circular orbit with the radius defined as the distance from O, the center of the earth, to the apogee of the

elliptic orbit. Since the satellite tumbles on the transitory orbit, as can be seen from Figure 6.3.2*d*, an impulsive couple is also applied at the same time to stop the tumbling; it therefore subsequently induces the satellite into a librational motion in the higher circular orbit. The radius of the higher orbit is about 1.643×10^7 with an amplitude of libration about 70° over a half librational period of about 9610sec. This result can be easily verified using (6.20).

6.4. Dynamics of multibody systems

A robot manipulator arm consisting of human-like links connected by joints is an example of a multibody system. Today's commercial robots are designed to be rigid because of the limitation of currently available analytical tools — mainly in the active control design of these mechanical systems (Dubowsky [1985]). As a result, they are heavy and slow. Future robots will be light weight, thus very flexible, and operating at high speed. Robot arms also play an important role in space technology: for instance, the Canadarm on the Space Shuttle assists in launching and retrieving satellites. † Future space stations assembled from several modules with different degree of flexibility — habitation module, solar array, radiator, universal interface — provide another example of multibody systems. In the construction phase of these space stations, the versatile robot manipulator arm will find its role increased even more. In the envisioned Automated Space Manufacturing Facility, robotics are essential for efficient manufacturing, repair, and for building new generations of equipment.

There exists a vast body of literature on multibody dynamics starting with the pioneering work by Hooker & Margulies [1965] and Roberson & Wittenburg

† The Canadarm also helped closing balky hatches and knocking off a block of ice that accumulated on the liquid-waste vent of the Space Shuttle.

[1967]. Most of the research in this area was focused on systems of rigid bodies; attention has been, however, directed to the study of flexible multibody systems. An overview of several approaches to the dynamics of n-body systems can be found in Jerkovsky [1977]. An extensive reference list is contained in Huston [1981]. Ho & Herber [1985] classify multibody systems into several categories in the order of increasing difficulty in the formulation as follows: (1) two-rigid-body system, (2) all-rigid topological tree multibody system,‡ (3) cluster of flexible appendages around a central rigid body, (4) topological tree multibody system with rigid interconnected bodies and flexible terminal bodies, (5) all-flexible chain system, and (6) all-flexible topological tree multibody system. There are basically two points of view to treat the dynamics of multibody systems (Hughes [1979]): (i) the formalism developed by Roberson & Wittenburg [1967] known as the Augmented Body Approach, and (ii) the Direct Path Method propounded by Ho [1977]. In these approaches, one first transforms the individual body dynamics into a common set of dynamic variables, then eliminates the interacting forces and couples at the connecting hinges. Treatment of the flexible chain system (5) may be found for example in Hughes [1979] with some restriction in the speed of motion of the angles at the joints, while treatment of the more complex topological tree multibody system is explored in Huston [1981]. In general, with the presence of closed-loops, additional non-holonomic constraints have to be included in the equations of motion (e.g., Kane & Levinson [1983]), and thus require special care in the numerical integration procedure.

It is emphasized that as a direct by-product of our formulation, one can easily analyze flexible multibody configurations of classes (5) and (6) of the Ho-

‡ That is a set of $(n+1)$ bodies interconnected by n points, each of which is common to two bodies. The tree topology thus implies the absence of closed loops.

Herber classification, and even with the presence of closed loops. This is achieved without alteration of the formulation and without any additional constraints since hinge conditions are accounted for in a straightforward manner using the spatial Galerkin finite element discretization of the equations of motion.

We shall first consider the case of a flexible beam attached to a rigid block in Section 6.4.1, and show how the present approach could be easily applied to analyze this system. Also, we will discuss how to treat systems constutituted from a rigid body with several attached flexible appendages including closed-loop links —this class of multibody systems in fact encompasses class (3) of the Ho-Herber classification as a subset. In Section 6.4.2, we shall present several examples that involve flexible chains undergoing large overall motions. Further, owing to the full nonlinearity of our formulation, should the chain be made more flexible, large deformations in these links would be obtained. Also, no limitation on the speed of evolution of the system is imposed.

6.4.1. Rigid body with attached flexible appendages

For simplicity in the exposition and without loss of generality, consider the free plane motion of a flexible beam attached to a rigid block of mass A_ρ^R and inertia I_ρ^R with respect to the connection point. We then use the same notation as in Section 2.3 of Chapter 2. The kinetic energy of the system is given by expression (2.24) augmented by the kinetic energy of the rigid block,

$$K = \frac{1}{2}\int_{[0,L]} [A_\rho \|\dot{\boldsymbol{\phi}}_o\|^2 + I_\rho \dot{\vartheta}^2]\, dX_1 + A_\rho^R \|\dot{\boldsymbol{\phi}}_o(0,t)\|^2 + I_\rho^R \dot{\vartheta}^2(0,t)\,. \qquad (6.21)$$

The expression for the potential energy remains the same as in (2.28),

$$\Pi = \frac{1}{2}\int_{[0,L]} [EA\,\Gamma_1^2 + GA_s\,\Gamma_2^2 + EI\,(\vartheta')^2]\, dS - \int_{[0,L]} [\,\bar{\mathbf{n}}\cdot\boldsymbol{\phi}_o + \bar{m}\,\vartheta\,]\, dX_1 \quad (6.22)$$

where the expression for the strain measures Γ_1 and Γ_2 in terms of the displacement components (u_1, u_2) and rotation ϑ is given in (2.27b). Application of Hamilton's principle yields the following system of PDE's

$$\begin{aligned} n_1' + \bar{n}_1 &= A_\rho \ddot{u}_1 \\ n_2' + \bar{n}_2 &= A_\rho \ddot{u}_2 \\ m' + [(1+u_1')n_2 - u_2' n_1] + \bar{m} &= I\ddot{\vartheta} \end{aligned} \tag{6.23a}$$

with boundary conditions

$$\begin{aligned} n_1(0,t) &= A_\rho^R \ddot{u}_1(0,t), \quad n_1(L,t) = 0 \\ n_2(0,t) &= A_\rho^R \ddot{u}_2(0,t), \quad n_2(L,t) = 0 \\ m(0,t) &= I_\rho^R \ddot{\vartheta}(0,t), \quad m(L,t) = 0 \end{aligned} \tag{6.23b}$$

where (n_1, n_2) represent the internal forces and m the internal moment defined in (2.33).

Weak form. The weak form of the above set of PDE's and boundary conditions is obtained from expression (2.42) augmented by the terms corresponding to the boundary conditions

$$G_{dyn}(\boldsymbol{\phi}, \eta) = \int_{[0,L]} \eta \cdot \mathbf{I}\ddot{\boldsymbol{\phi}}\, dX_1 + \eta(0) \cdot \mathbf{I}^R \ddot{\boldsymbol{\phi}}(0,t) - \eta(0) \cdot \begin{Bmatrix} n_1(0,t) \\ n_2(0,t) \\ m(0,t) \end{Bmatrix} + G(\boldsymbol{\phi}, \eta) = 0, \tag{6.24}$$

for all admissible variations $\eta \in (H^1(0,L))^3$. All quantities such as $\mathbf{I}$, $\boldsymbol{\phi}$, $G(\boldsymbol{\phi}, \eta)$ have been defined in (2.41) and (2.43) of Section 2.4.1, except $\mathbf{I}^R := Diag[A_\rho^R, A_\rho^R, I_\rho^R]$. Upon integrating by parts the first term in $G(\boldsymbol{\phi}, \eta)$ of (2.43), and from the cancellation of the boundary terms, the dynamic weak form in (6.24) becomes

$$G_{dyn}(\boldsymbol{\phi}, \eta) = \int_{[0,L]} \eta \cdot \mathbf{I}\ddot{\boldsymbol{\phi}}\, dX_1 + \eta(0) \cdot \mathbf{I}^R \ddot{\boldsymbol{\phi}}(0,t) + G(\boldsymbol{\phi}, \eta), \tag{6.25}$$

where $G(\phi, \eta)$ is now given in (2.45). The temporal and spatial discretization of the above weak form, as discussed in Section 2.4, leads to the same mass matrix as in (2.64) with the exception that

$$\mathbf{M}_{11} = \frac{1}{h^2\beta}\{ \int_{[0,L]} \mathbf{I}[N_1(X_1)]^2 dX_1 + \mathbf{I}^R \} \tag{6.26}$$

as a result of the choice of the global shape functions $N_I(X)$ such that $N_I(X_J) = \delta_{IJ}$.† The other tangent matrices are the same as given in Section 2.4.3. It thus follows that the case of a flexible beam attached to a rigid block and subject to large overall motions can be accomodated easily within the proposed methodology.

Satellites often have the configuration of a cluster of flexible beams (e.g., antennae) attached to a central rigid block (e.g., main body of the satellite). In this case, one can choose, as a basic structural component, the rigid block and one of the attached flexible beams; thus the model for this basic component has been discussed previously. The remaining flexible beams are then tied to the basic component by means of algebraic constraint equations expressing that the distance between the points of connection of the beams to the rigid body remains constant at all time. We are thus led to a constrained nonlinear problem. Further, treatment of the three-dimensional case is identically the same.

6.4.2. Numerical examples of flexible hinge-connected multibody systems

As a direct application of the proposed methodology, one can treat the dynamics of flexible beams interconnected by hinges without alteration in the formulation. This is possible since the hinge conditions can be easily accounted for in the finite element formulation by simply identifying the displacement

† δ_{IJ} denotes the Kronecker delta.

degrees of freedom of the hinged ends, leaving free the rotational degrees of freedom. The case of a closed-loop chain attached to a rigid body presents in principle no difficulty, except that the treatment must include possible algebraic constraints.

Example 6.4.1. Multi-component robot arm. The robot arm considered in Example 2.5.1 is in this example stiffer by a factor of 100, and now consists of two flexible components connected together by a hinge at mid-length. The two-component robot arm is subjected to the same prescribe rotation $\psi(t) = \vartheta(0, t)$ as in Example 2.5.1. The problem data are summarized in Figure 6.4.1*a*. The sequence of motions is shown in Figures 6.4.1*b* and 6.4.1*c*. Note that while the first component vibrates about the stop angle $\psi(t) = 1.5\,rad$ for $t \geq 2.5$, the second one undergoes a complete revolution about the connecting hinge at mid-length.

Example 6.4.2. Articulated beam in free flight. A two-body system consisting of two flexible links connected by a hinge, is initially at an inclined position. The system is set into motion by applying a force and a torque at one end of the lower link, as shown in Figure 6.4.2. The applied loads are subsequently removed at time $t = 0.5$, so that subsequently the articulated beam undergoes free flight. The lower link, indicated by the letter A in the figure, then moves in the same clockwise direction as the applied torque, whereas the upper link, indicated by the letter B, moves in the opposite counter-clockwise direction.

Example 6.4.3. Closed-loop chain in free-flight. To demonstrate the capability of the present approach to model the dynamics of flexible multibody systems, we consider a closed-loop chain constituted of 4 flexible links interconnected by hinges as shown in Figure 6.4.3*a*. One of the links is 500 times stiffer than the other three: Link AB in Figure 6.4.3*a* has a bending stiffness of $EI = 10^5$, while the remaining links have a bending stiffness of $EI = 200$. The

other material properties are chosen to be identical for the four links, and are listed in Figure 6.4.3*a*. Initially, the closed-loop chain forms a square of length 10 for each side. The whole system has no prescribed displacement boundary condition. To create a forward motion, a force is applied at end A of the stiff link AB; the overall tumbling motion of the chain is induced by a torque applied at the same end as shown together with the time history of their magnitude in Figure 6.4.3*a*. Figure 6.4.3*b* depicts the entire sequence of motion with three close-ups given in Figures 6.4.3*c*–*e*. A time step size of $h = 0.1$ is used throughout the analysis.

6.5. Conclusion

We have presented a methodology to treat the dynamics of flexible structures performing large complex motions. The essence of the proposed approach is largely based on the use of fully nonlinear strain measures. These strain measures together with the stress resultants and constitutive laws are required to satisfy the property of invariance with respect to superposed isometries (rigid body motions). This property allows the dynamics of flexible structures be referred directly to the inertial frame, and thus simplifies considerably the inertia operator in the equations of motion.

In addition to the above advantage, the centrifugal stiffening effect in rotating structures is properly accounted for when using nonlinear theory. Further, the proposed methodology is suitable to treat the dynamics of flexible structures subjected to large overall motions and undergoing a wide range of structural deformations.

We have focused our attention only on one-dimensional structural elements, i.e., flexible rods. Since the rotation field in the rod is represented by orthogonal, generally non-commutative transformations, the deformation map takes

values in the nonlinear differentiable manifold $\mathbb{R}^3 \times SO(3)$, instead of the linear space $\mathbb{R}^3 \times \mathbb{R}^3$ usually encountered in nonlinear structural dynamics. Concepts from modern differential geometry proved to be useful in the numerical treatment of the nonlinear PDE's governing the motion of the rod. An efficient computational algorithm has been developed; its convergence and accuracy is also established. Quadratic rate of convergence of the Newton iterative procedure in the integration algorithm results from the exact linearization process. Moreover, the update procedure is stable in the sense that the solution be required to remain in the configuration manifold, and that the property of invariance with respect to superposed isometries be preserved.

The dynamics of earth-orbiting flexible satellites is completely described by the same system of equations of motion for the fully nonlinear rod model. However, to avoid numerical ill-conditioning due to the large difference in magnitude between the distance from the earth to the satellite and the structural deformations, we introduce an additive decomposition of the displacement field of the rod into the far field and the near field. This decomposition led to the concept of rotationally-fixed floating frame to treat satellite dynamics. To integrate the coupled far-field/near-field problem, an algorithm has been proposed such that, for the near-field dynamics, all of the properties concerning convergence and accuracy mentioned above are preserved. In other words, the accuracy of the integration of the near-field dynamics is unspoiled by the integration of the coupled far-field dynamics. Further, the proposed methodology can be applied to the dynamics of flexible multibody systems (rigid body with flexible appendages, all flexible chain system, flexible closed-loop chain) without alteration in the formulation.

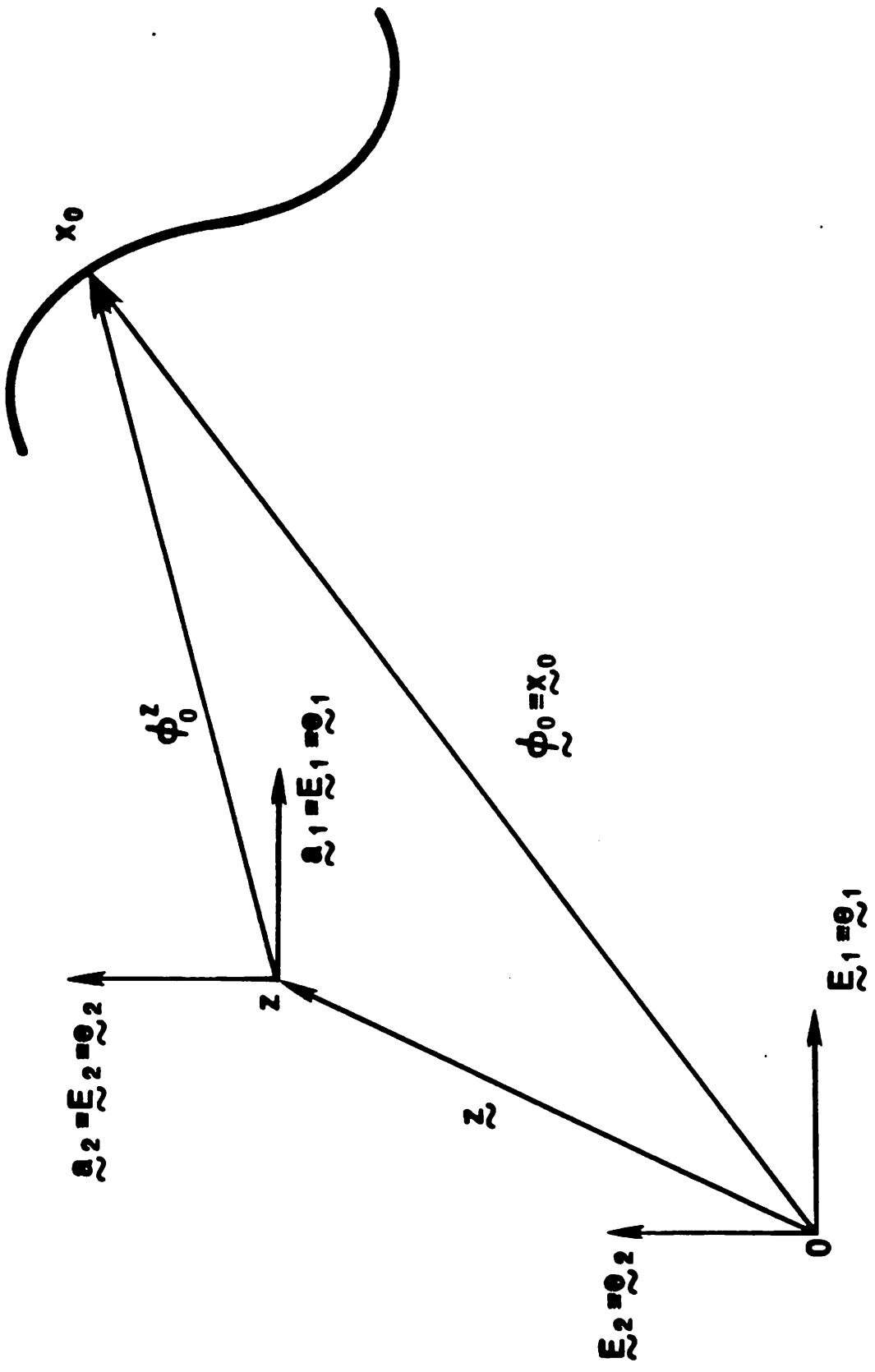

Figure 6.2.1. Rotationally-fixed floating frame: parallel translate of inertial frame.

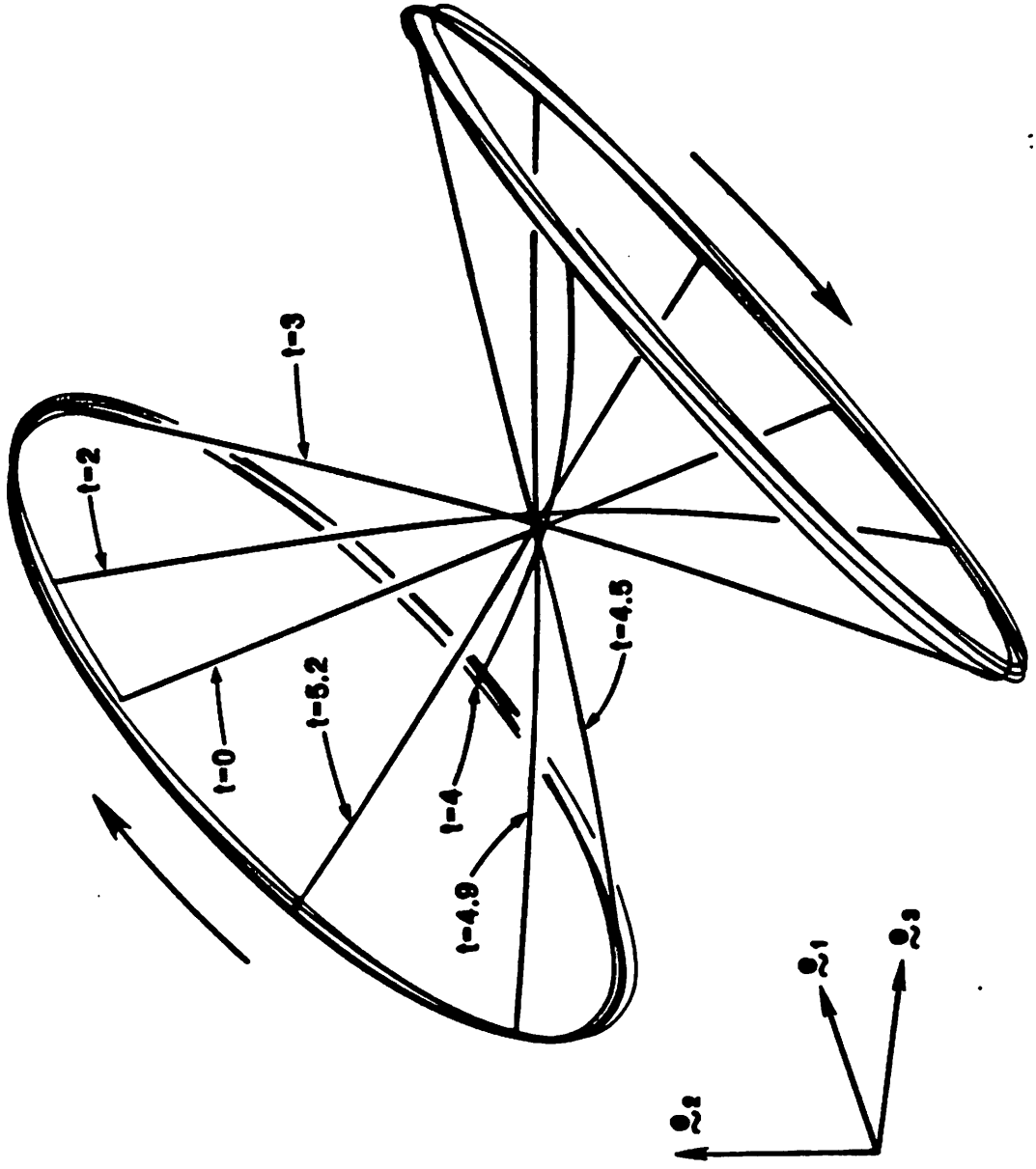

Figure 6.3.1. *Free-free flexible beam undergoing large overall motions.* Perspective of deformed shapes as seen by an observer attached to the rotationally-fixed floating frame.

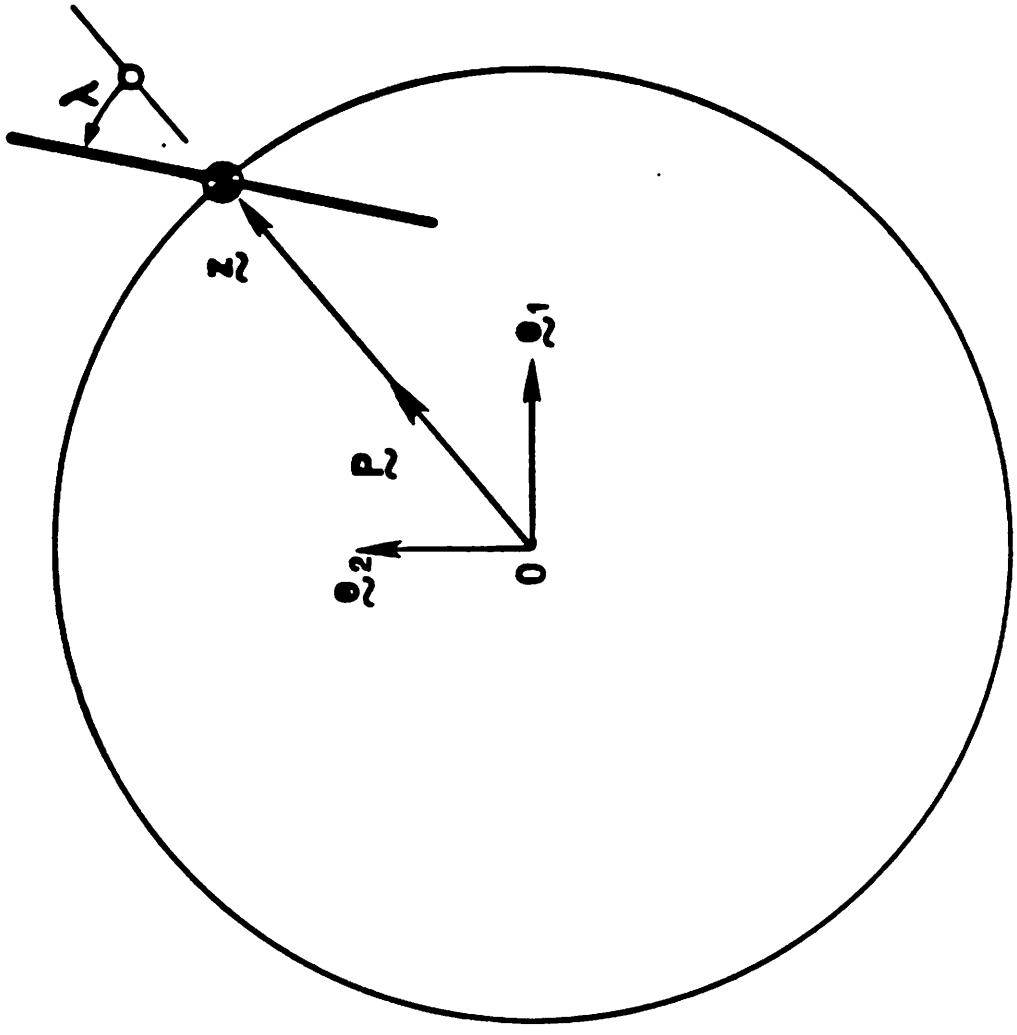

Figure 6.3.2a *Satellite dymamics: Libration and orbit transfer.* **Libration angle** λ, *local vertical* **p**.

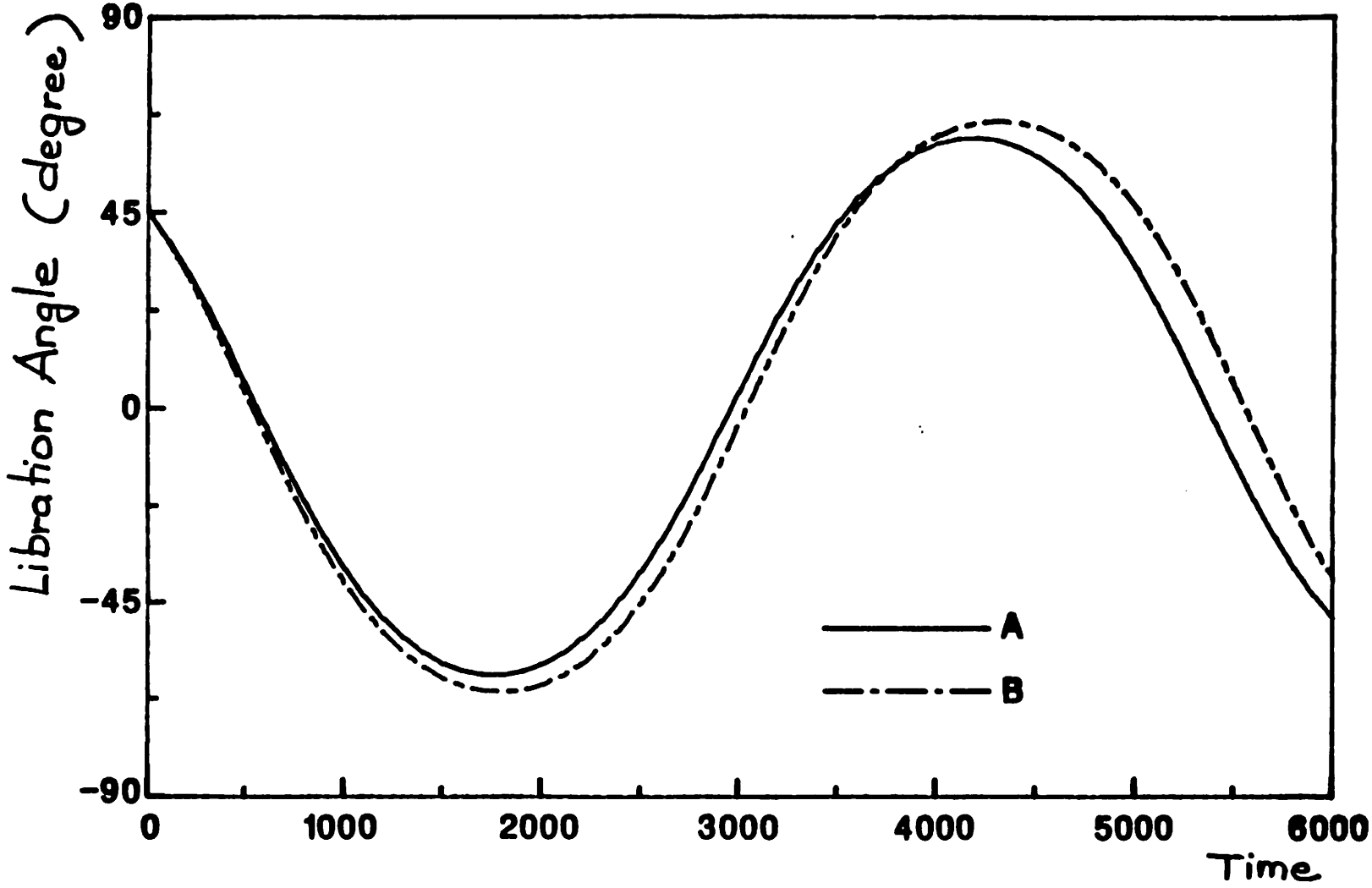

Figure 6.3.2b. *Satellite dynamics: Libration and orbit transfer.* **Time history of libration angle** λ *on lower circular orbit. Line A: present formulation; line B: "exact" solution.*

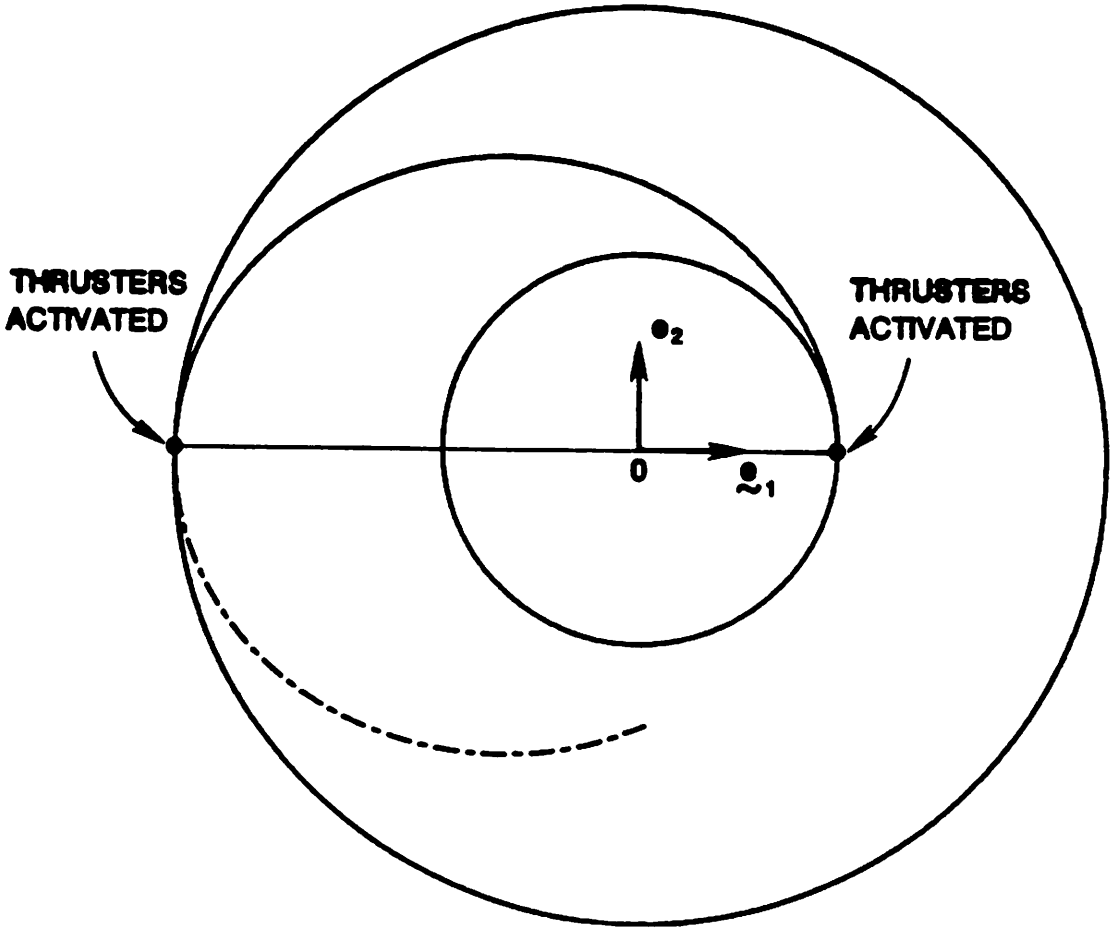

Figure 6.3.2c. *Satellite dynamics: Libration and orbit transfer.* **Transfer from lower circular orbit to higher orbit through a transitory elliptic orbit.**

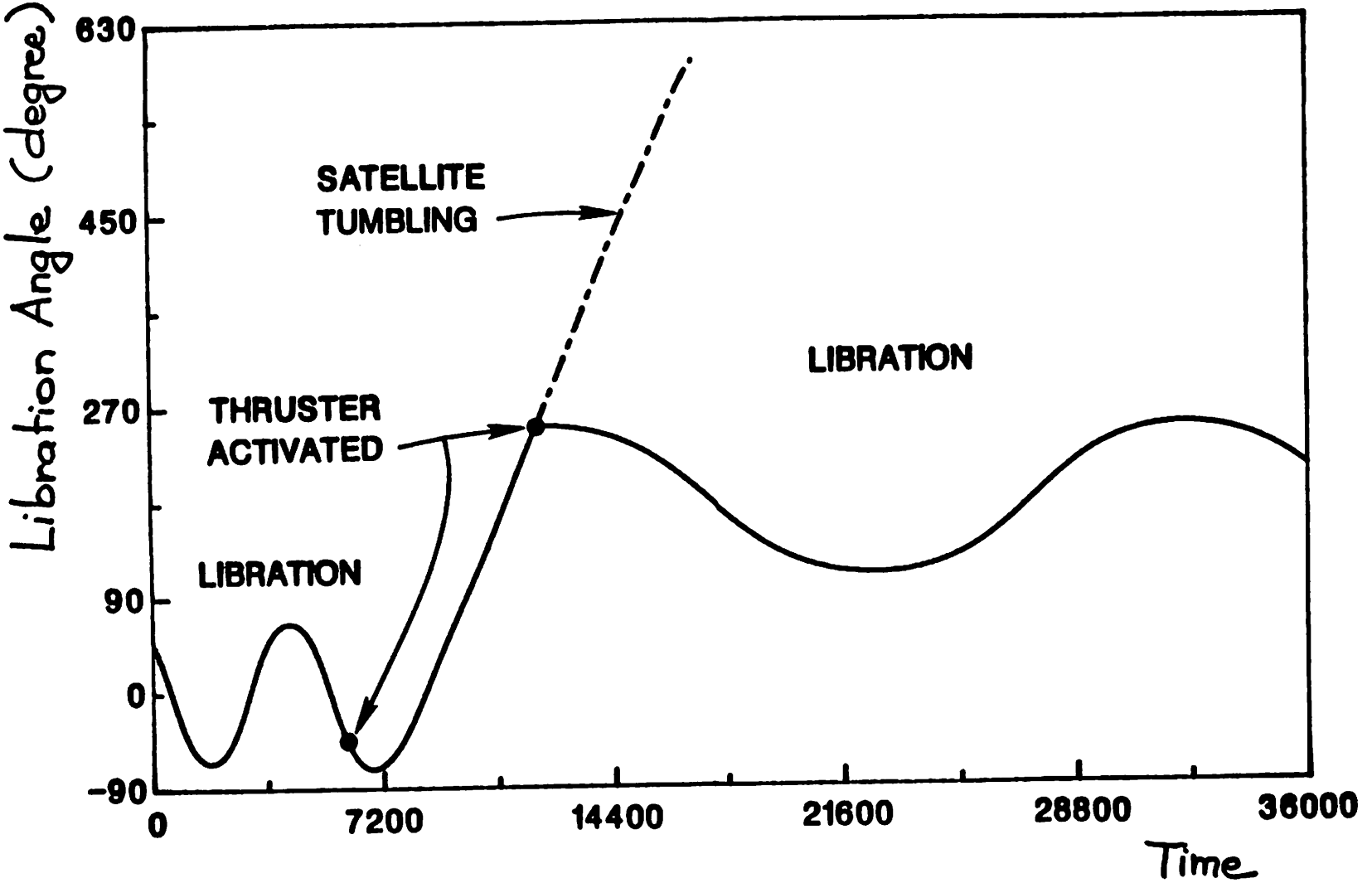

Figure 6.3.2d. *Satellite dynamics: Libration and orbit transfer.* **Entire time history of the libration angle.**

Material Properties:

$EA = GA_s = 1{,}000{,}000.$

$EI = 100{,}000.$

$A_\rho = 1.$

$I_\rho = 1.$

F.e. Mesh: 4 quadratic elements.

Time history of $\psi(t)$:

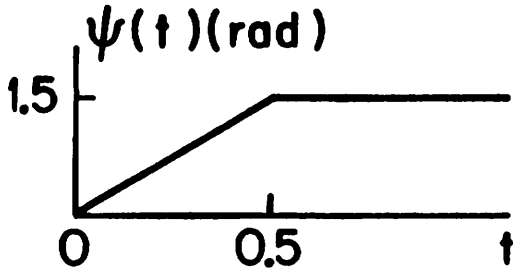

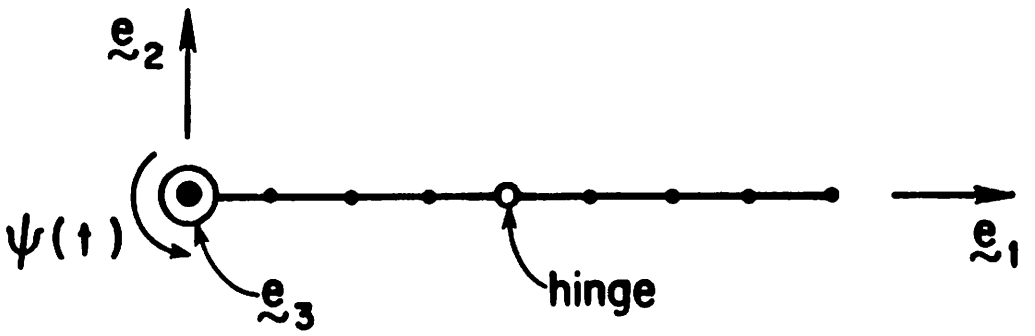

Figure 6.4.1a. *Multi-component robot arm.* Problem data.

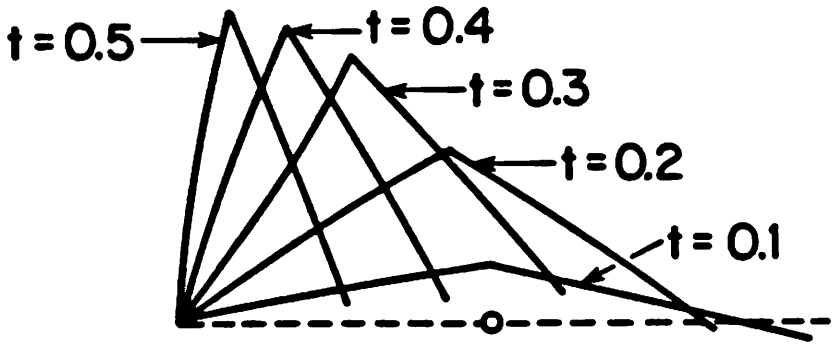

Figure 6.4.1b. *Multi-component robot arm.* Repositioning sequence to stop angle $\psi = 1.5rad$. Time step size $h = 0.1$.

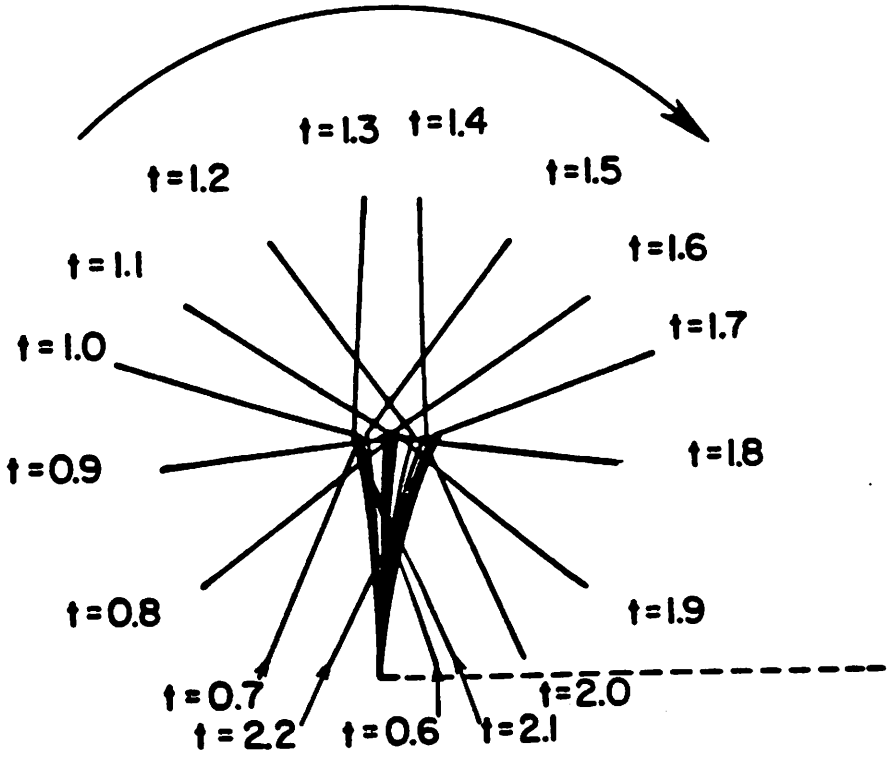

Figure 6.4.1c. *Multi-component robot arm.* Vibration of robot arm about stop angle, and revolution of flexible appendage about connecting hinge. Time step size $h = 0.01$, plot after each 10 time increments.

Material Properties:

$EA = GA_s = 1{,}000{,}000.$

$EI = 10{,}000.$

$A\rho = 1.$

$I\rho = 1.$ for link A

$I\rho = 10.$ for link B

F.e. Mesh: 4 quadratic elements.

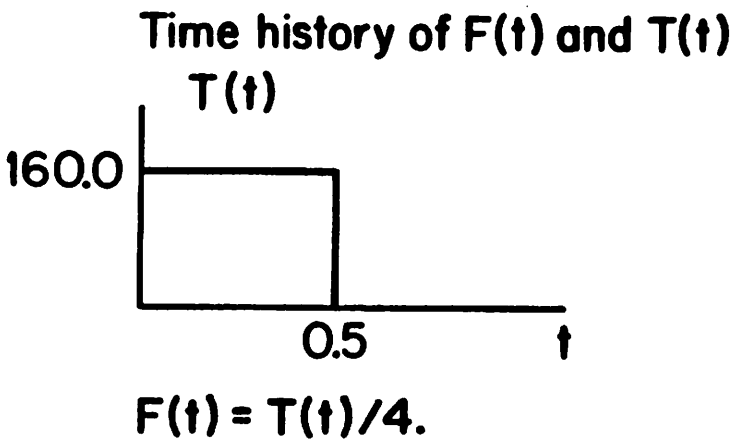

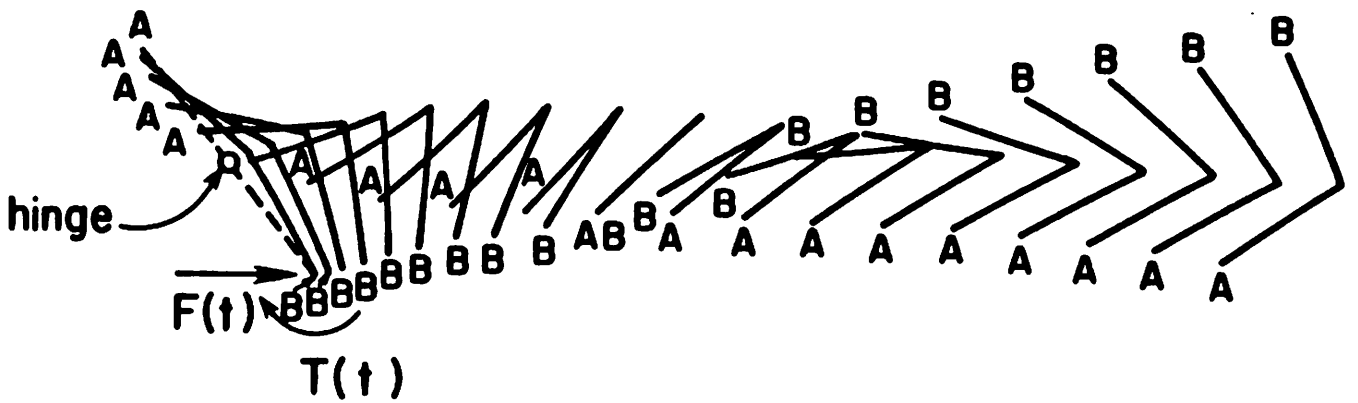

Figure 6.4.2. *Articulated beam in free flight.* Time step size $h = 0.05$, plot after each 5 time increments.

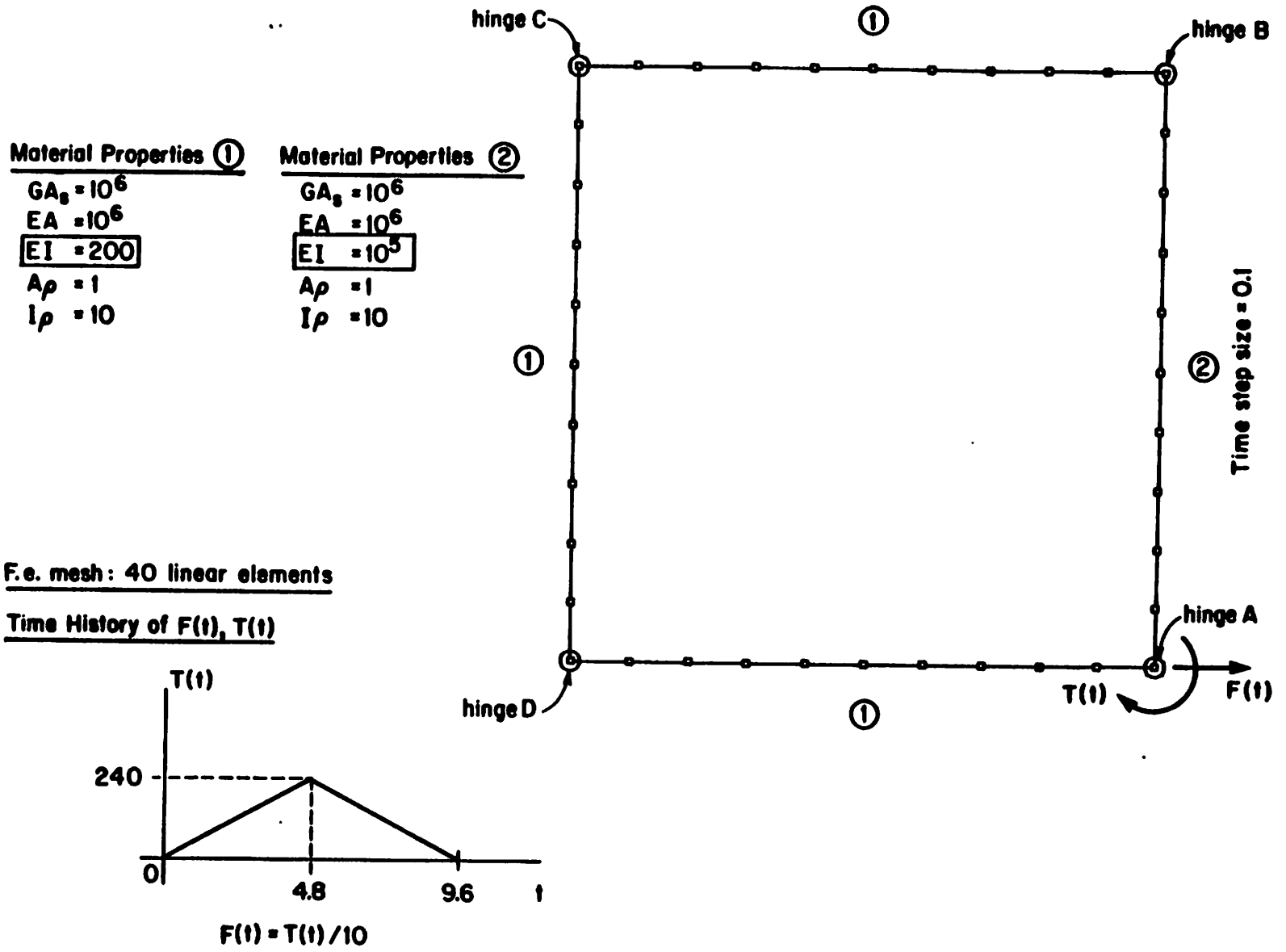

Figure 6.4.3a. *Closed-loop chain in free flight.* Problem data.

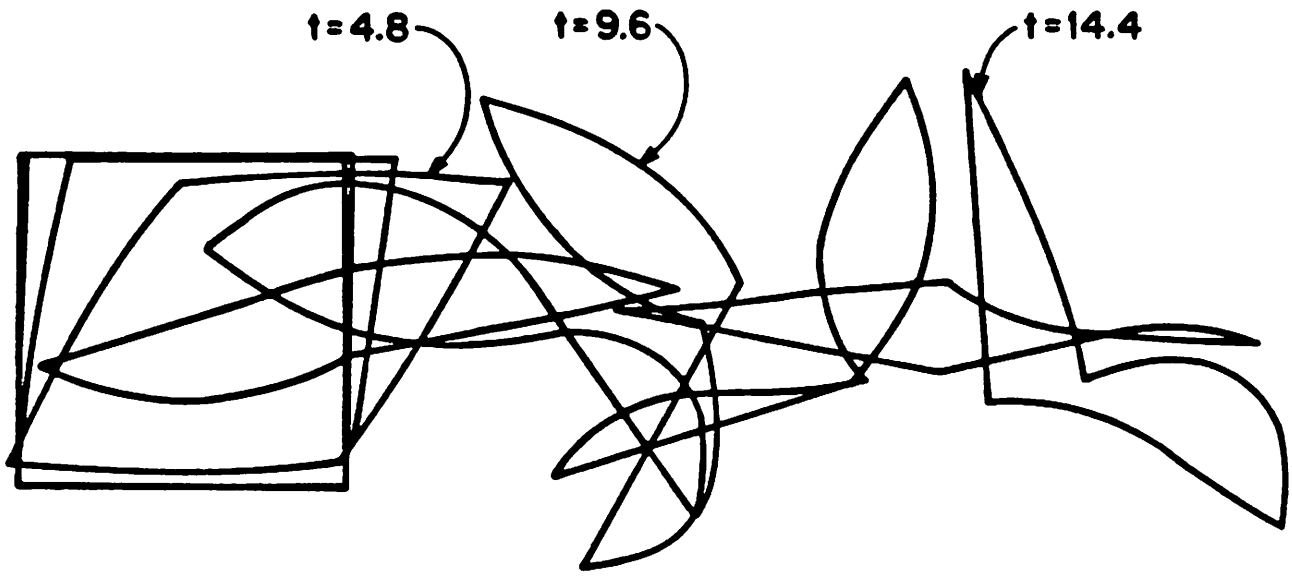

Figure 6.4.3b. *Closed-loop chain in free flight.* Entire sequence of motion.

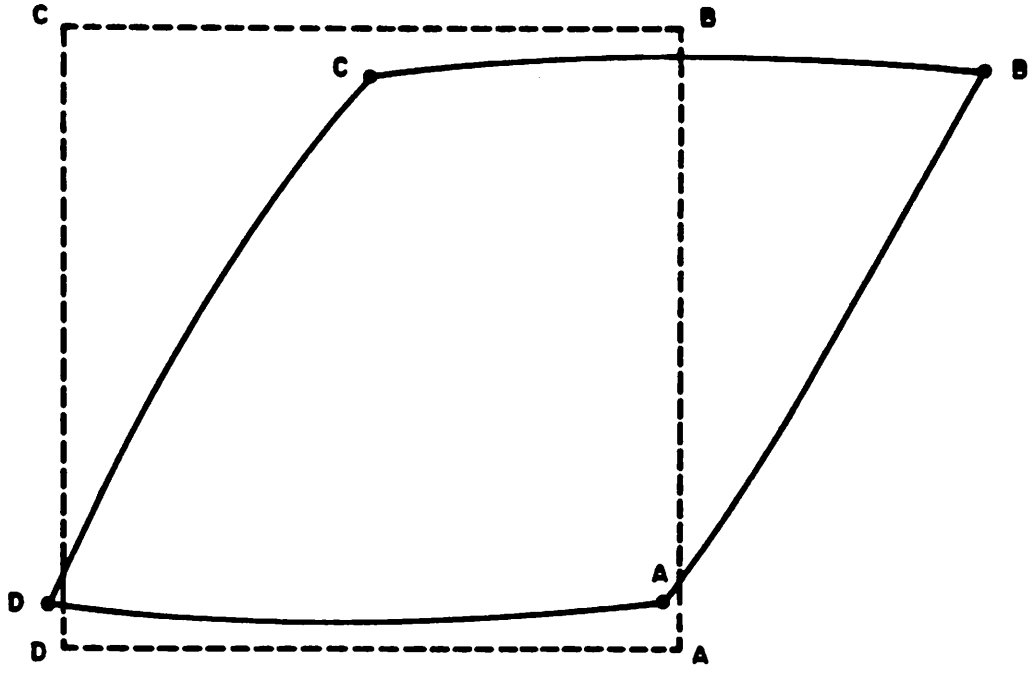

Figure 6.4.3c. *Closed-loop chain in free flight.* Deformed shape at time $t = 4.8$.

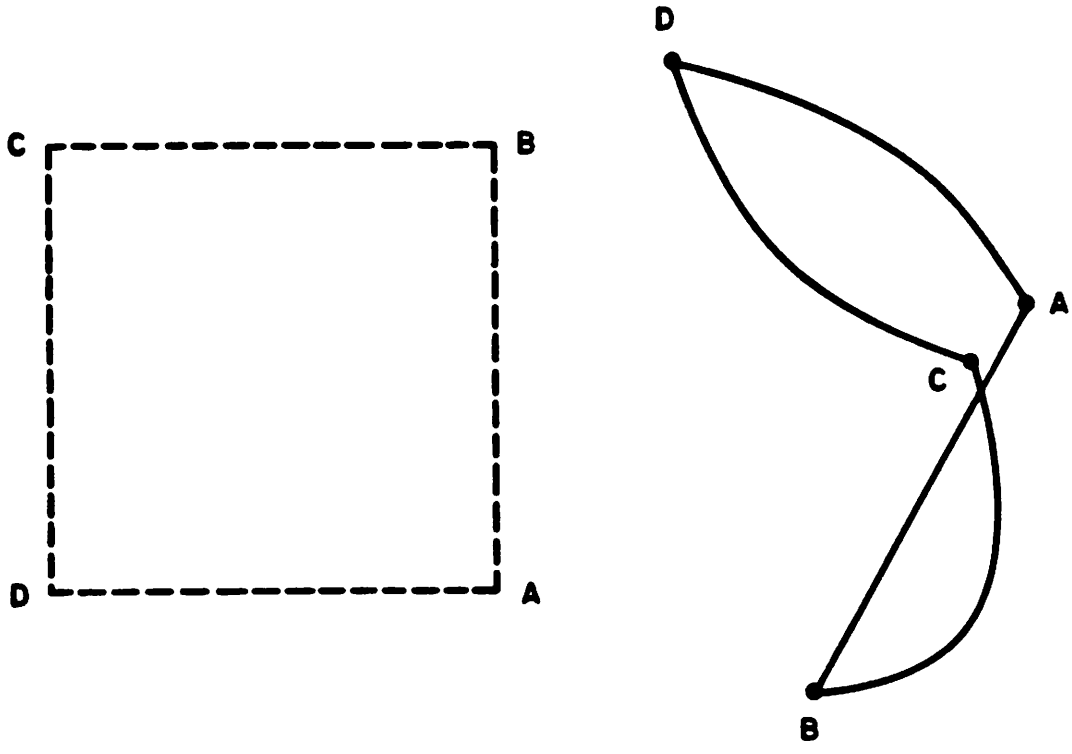

Figure 6.4.3d. *Closed-loop chain in free flight.* Deformed shape at time $t = 9.6$.

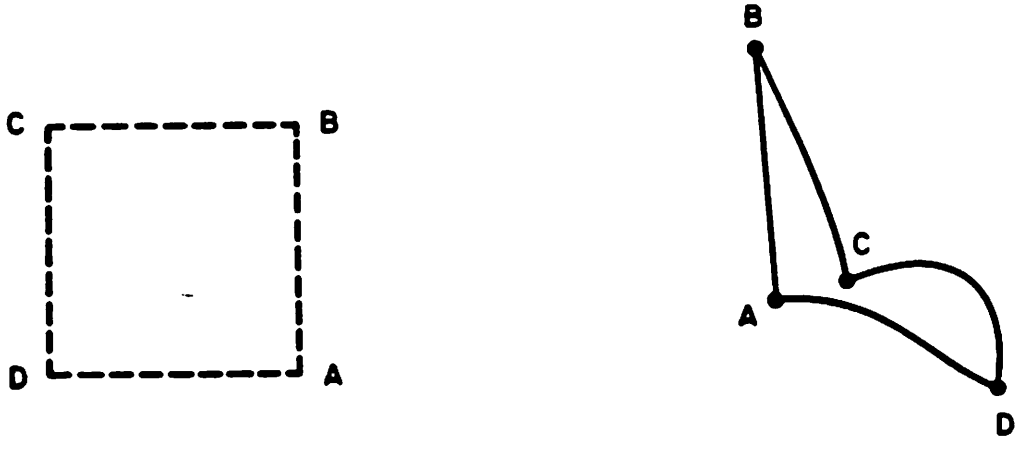

Figure 6.4.3e. *Closed-loop chain in free flight.* Deformed shape at time $t = 14.4$.

REFERENCES

Antman, S.S. [1972], "The theory of rods," *Handbuch der Physik*, Vol. VIa/2, Springer-Verlag, Berlin.

Antman, S.S. [1974], "Kirchhoff problem for nonlinearly elastic rods," *Quat. J. Appl. Math.* ***XXXII***(3), 221-240.

Antman, S.S., and K. B. Jordan [1975], "Qualitative aspects of the spatial deformation of non-linearly elastic rods," *Proc. Royal Society of Edinburg*, ***73A***(5), 85-105.

Argyris J.H., H. Balmer, J. St. Doltsinis, P.C. Dunne, M. Haase, M. Kleiber, G.A. Malejannakis, J.P. Mlejenek, M. Muller and D.W. Scharpf [1979], "Finite Element Method — The natural approach," *Comp. Meth. Appl. Mech. Engrg.*, **17/18**, 1-106.

Argyris. J.H. and Sp. Symeonides [1981], "Nonlinear finite element analysis of elastic systems under nonconservative loading — Natural formulation. Part I. Quasitatic problems,: *Comp. Meth. Appl. Mech. Engrg*. **26**, 75-123.

Argyris. J.H. and Sp. Symeonides [1981], "A sequel to: Nonlinear finite element analysis of elastic systems under nonconservative loading — Natural formulation. Part I. Quasitatic problems," *Comp. Meth. Appl. Mech. Engrg*. 26, 377-383.

Argyris, J.H. [1982], "An excursion into large rotations," *Comp. Meth. Appl. Mech. Engrg.*, 32, 85-155.

Arnold, D.N. [1981], "Discretization by finite elements of a model parameter dependent problem," *Numerische Mathematiks*, **37**, 405-421.

Arnold, V.I. [1980], *Mathematical Methods of Classical Mechanics*, Springer-Verlag, New York.

Ashley, H. [1967], "Observation on the dynamic behavior of flexible bodies in orbit," *AIAA J.*, 5(3), 460-469.

Bathe, K.J., and S. Bolourchi [1979], "Large displacement analysis of three dimensional beam structures," *Int. J. Num. Meth. Engng.*, 14, 961-986.

Belytschko T., and T.J.R. Hughes [1983], *Computational Methods for Transient Analysis*, Elsevier Science Publishers.

Belytschko, T., H. Stolarski and N. Carpenter [1984], "A triangular plate element with one-point quadrature," Comp. Meth. Appl. Mech. Engng., **15**, 63-81.

Benson, D.J., and J.O. Hallquist [1985], "A simple rigid body algorithm for structural dynamics program. Part I," *Proc. of the Int. Conf. on Numerical Methods in Engineering Theory and Applications, Swansea*, Ed. by J. Middleton & G.N. Pande, A.A. Balkema Publishers, Netherlands.

Bishop, R.L., and S.I. Goldberg [1980], *Tensor Analysis on Manifolds*, Dover, New

York.

Bufler, H. [1984], "Pressure loaded structures under large deformations," *ZAMM (Z. Angew. Math. u. Mech.)*, 64(7), 287-295, *Int. J. Num. Meth. Engrg.*, 20 787-802.

Burns, J. and E.M. Cliff [1985], "On finite element models for control of flexible structures," *SIAM Spring Meeting*, Pittsburg, Pennsylvania, June 24-26.

Burns, J., E.M. Cliff, and R.K. Powers [1985], "Computational method for the control of distributed parameter systems," *The 24th IEEE Conf. on Decision and Control*, Ft. Lauderdale, Florida, December 11-13.

Canavin, J.R. and P.W. Likins [1977], "Floating reference frames for flexible spacecrafts," *J. of Spacecraft*, 14(12), 724-732.

Chadwick, P. [1976], *Continuum Mechanics*, Halsted Press, John Wiley & Sons, New York.

Chorin, A.J., T.J.R. Hughes, M.F. McCracken, and J.E. Marsden [1978], "Product formulas and numerical algorithms," *Communications on Pure and Applied Mathematics*, 31, 205-256.

Ciarlet, P. G. [1978], *The Finite Element Method for Elliptic Problems* , North Holland Publishers Co.

DaDeppo, D. A., and R. Schmidt [1975], "Instability of Clamped-Hinged Circular Arches Subjected to a Point Load," *Trans. Am. Soc. Mech. Eng.*, ASME, 97(3).

Dahlquist, G. [1963], "A special stability problem for linear multistep methods," *BIT*, 3, 27-43.

de Veubeke, B.F. [1976], "The dynamics of flexible bodies," *J. Eng. Science.*, 14, 895-913.

Dubowsky, S. [1985], "Active control of mechanical systems: The state-of-the-art for robotic manipulator," *Proc. of the 26th Structures, Structural Dynamics, and Material Conference*, Part 2, Orlando, Florida.

Erdman, A.G., and G.N. Sandor [1972], "Kineto-elastodynamics — A review of the state of the art and trends," *Mechanisms and Machine Theory*, 7, 19-33.

Fung, Y.C. [1965], *Foundations of Solid Mechanics*, Prentice-Hall, Englewood Cliffs, New Jersey.

Gear, C.W. [1971a], *Numerical Initial Value Problems in Ordinary Differential Equations*, Prentice-Hall, Englewood Cliffs, New Jersey.

Gear, C.W. [1971b], "Simultaneous numerical solution of differential-algebraic equations," *IEEE Transaction on Circuit Theory*, *CT*−18(1), 89-95.

Gear, C.W. and L.R. Petzold [1984], "ODE methods for the solution of

differential/algebraic systems," *SIAM J. Numerical Analysis*, 21(4), 716-728.

Goldstein, H. [1980], *Classical Mechanics*, Second edition, Addison Wesley, Reading, Massachusetts.

Goudreau G.L., and R.L. Taylor [1973], "Evaluation of numerical methods in elastodynamics," *Comp. Meth. Appl. Mech. Engrg.*, 2, 69-97.

Grotte, P.B., J.C. McMunn, and R. Gluck [1971], "Equations of motion of flexible spacecraft," *J. of Spacecraft and Rockets*, 8(6), 561-567.

Hilber, H.M. [1976], *Analysis and Design of Numerical Integration Methods in Structural Dynamics*, Earthquake Engineering Research Center, EERC Report No. 76-29, University of California, Berkeley.

Hilber, H.M. [1978], "Collocation, dissipation and 'overshoot' for time integration schemes in structural dynamics," *Earthq. Engng. and Struct. Dyn.*, 6, 99-117.

Hughes, T.J.R. [1976], "Stability, convergence and growth and decay of energy of the average acceleration method in nonlinear structural dynamics," *Computers & Structures*, 6, 313-324.

Hughes T.J.R., and J. Winget [1980], "Finite rotation effects in numerical integration of rate constitutive equations arising in large-deformation analysis," *Int. J. Num. Meth. Engng.*, 15(9), 1413-1418.

Hughes, T.J.R. [1984] "Numerical implementation of constitutive models: Rate independent deviatoric plasticity," in *Theoretical Foundations for Large Scale Computations*, S. Nemat-Nasser, R. Asaro and G. Hegemier Edts. Mechanics of elastic and inelastic solids 6, Martinus Nijhoff Publishers.

Hughes, T.J.R. and T.E. Tezduyar [1981], "Finite elements based upon Mindlin plate theory with particular reference to the four node bilinear isoparametric element," *J. Appl. Mech* 48, 587-596.

Kane, T.R., and D.A. Levinson [1981], "Simulation of large motions of nonuniform beams in orbit: Part II — The unrestrained beam," *The J. of the Astronautical Sciences*, 29(3), 213-244.

Kane T.R., and D.A. Levinson [1983], "Multibody dynamics," *J. of Applied Mechanics*, 50, 1071-1078.

Kane, T.R., P.W. Likins, D.A. Levinson [1983], *Spacecraft Dynamics*, McGraw-Hill Book Co., New York.

Kane, T.R., R.R. Ryan, and A.K. Banerjee [1985], "Dynamics of a beam attached to a moving base," *AAS/AIAA Astrodynamics Specialist Conference*, paper AAS 85-390, Vail, Colorado, August 12-15. (To appear in *J. of Guidance, Dynamics, and Control*, 1986.)

Karger A., and J. Novak [1985], *Space Kinematics and Lie Group*, Gordon and

Breach Science Publishers, New York.

Kline, R.L. [1979], "Construction of large space structures," *The J. of the Astronautical Sciences*, 27(4), 401-418.

Kumar, V.K., and P.M. Bainum [1980], "Dynamics of a flexible body in orbit," *J. of Guidance and Control*, 3(1), 90-91.

Laskin, R.A., P.W. Likins, and R.W. Longman [1983], "Dynamical equations of a free-free beam subject to large overall motions," *The J. of the Astronautical Sciences*, 31(4), 507-528.

Levinson, D.A., and T.R. Kane [1981], "Simulation of large motions of nonuniform beams in orbit: Part I — The cantilever beam," *The J. of the Astronautical Sciences*, 29(3), 245-276.

Likins, P.W. [1974a], *Analytical Dynamics and Nonrigid Spacecraft Simulation*, Jet Propulsion Laboratory, Technical Report 32-1593, California Institute of Technology.

Likins, P.W. [1974b], *Dynamic Analysis of A System of Hinge Connected Rigid Bodies with Nonrigid Appendages*, NASA Technical Report 32-1576.

Love, A.E.H. [1944], *The Mathematical Theory of Elasticity*, Dover Publications, New York.

Lowrie J.W. [1979], "Autonomous Attitude Determination Systems," in *Advances in The Astronautical Sciences* series, *Guidance and Control 1979*, 53-92, An American Astronautical Society Publication.

Malkus, D.S. and T.J.R. Hughes [1978], "Mixed Finite Element Methods-Reduced and Selective Integration Techniques: A Unification of Concepts," *Comp. Meth. Appl. Mech. Engng.*, 15, 63-81.

Marsden J.E. and T.J.R Hughes [1983], *Mathematical Foundations of Elasticity*, Prentice-Hall Englewood Cliffs, New Jersey.

Naghdi, P.M. [1980], "Finite deformations of elastic rods and shells," *Proc. IUTAM Symposium on Finite Elasticity*, Lehigh University.

Mital N.K., and A.I. King [1979], "Computation of rigid-body rotation in three-dimensional space from body-fixed linear acceleration measurements," *J. Applied Mechanics*, 46, 925-930.

Misner, C., K. Thorne, and J. Wheeler [1973], *Gravitation*, W.H. Freeman & Co, Publishers, Inc., San Francisco.

Newmark, N.M. [1959], "A method of computation for structural dynamics," *J. of the Engineering Mechanics Division, ASCE*, 67-94.

Noor, A.K., and J.M. Peters [1981], "Mixed models and selective/reduced integration displacement models for nonlinear analysis of curved beams," *Int. J. Num. Meth. Engng.*, 17, 615-631.

Noor, A.K., J.M. Peters, and C.M. Andersen [1984], "Mixed models and reduction techniques for large-rotation nonlinear problems," *Comp. Meth. Appl. Mech. Engng.*, **44**, 67-89.

Nordgren, R.P. [1974] "On Computation of the Motion of Elastic Rods," *J. Applied Mechanics*, 777-780.

Park, K.C. [1975], "Evaluating time integration methods for nonlinear dynamics analysis," in *FEM Analysis of Transient Nonlinear Behavior*, edited by Belytschko, Osias, and Marcal, Applied Mechanics Symposia series (ASME, New York, 1975).

Parker, D.F. [1979], "The role of Saint Venant's solutions in rods and beam theories," *J. Applied Mechanics*, 46, 861-866.

Petzold, L.R. [1982], "Differential/algebraic equations are not ODE's," *SIAM J. Sci. Stat. Comput.*, 3(3), 367-384.

Reddy, J.N., and I.R. Singh [1981], "Large deflection and large amplitude free vibrations of straight and curved beams," *Int. J. Num. Meth. Engng.*, 17, 829-852.

Reissner, E. [1972], "On a one-dimensional finite strain beam theory: The Plane Problem," *J. Appl. Math. Phys.* **23**, 795-804.

Reissner, E. [1973], "On a one-dimensional large-displacement finite-strain beam theory," *Studies in Applied Mathematics*, 52, 87-95.

Reissner, E. [1981], "On finite deformations of space-curved beams," *ZAMP*, 32, 734-744.

Reissner, E. [1982], "Some remarks on the problem of column buckling," *Ingenieur-Archiv*, 52, 115-119, Springer.

Richtmyer, D., and K.W. Morton [1967], *Difference Methods for Initial Value Problems*, Second edition, Interscience, New York.

Riks, E. [1972], "The application of Newton's method to the problem of elastic stability," *J. Appl. Mech.*, **39**, 1060-1066.

Sander,G., M. Geradin, C. Nyssen, and M. Hogge [1979], "Accuracy versus computational efficiency in nonlinear dynamics," *Comp. Meth. Appl. Mech. Engng.*, **17/18**, 315-340.

Shweizerhof, K. & E. Ramm [1984], "Displacement dependent pressure loads in nonlinear finite element analysis," *Comp. Struct.*, **18**.

Simo, J.C. [1982], *A Consistent Formulation of Nonlinear Theories of Elastic Beams and Plates*, Structural Engineering and Structural Mechanics Report No. UCB/SESM-82/06, November.

Simo, J.C., K.H. Hjelmstad & R.L. Taylor, [1984], "Numerical formulations for the elasto-viscoplastic response of beams accounting for the effect of shear,"

Comp. Meth. Appl. Mech. Engn., 42, 301-330.

Simo, J.C. [1985], "A finite strain beam formulation. Part I: The three dimensional dynamic problem," *Comp. Meth. Appl. Mech. Engrg.*, 49, 55-70.

Simo, J.C., and L. Vu-Quoc [1985a], *On The Dynamics of Flexible Beams Under Large Overall Motions — The Plane Case*, Electronics Research Laboratory Memorandum UCB/ERL M85/63, University of California, Berkeley, August.

Simo, J.C., and L. Vu-Quoc [1985b], "Three-dimensional finite-strain rod model. Part II: Computational aspects," Electronics Research Laboratory Memorandum UCB/ERL M85/31, University of California, Berkeley, April.

Simo, J.C., and L. Vu-Quoc [1986a], *The Role of Nonlinear Theories in the Dynamics Analysis of Rotating Structures*, Electronics Research Laboratory Memorandum UCB/ERL M86/10, University of California, Berkeley, January.

Simo, J.C., and L. Vu-Quoc [1986b], *On The Dynamics of Finite-Strain Rods Undergoing Large Motions — The Three Dimensional Case*, Electronics Research Laboratory Memorandum No. UCB/ERL M86/11, University of California, Berkeley, January.

Simo, J.C., P. Wriggers, K. Shweizerhof, and R.L. Taylor [1984], "Finite deformation post-buckling analysis involving inelasticity and contact constraints," *ASME Anual Winter Meeting*, New Orleans, November.

Song, J.O., and E.J. Haug [1980], "Dynamic analysis of planar flexible mechanism," *Comp. Meth. Appl. Mech. Engrg.*, 24, 359-381.

Sunada W., and S. Dubowsky [1980], "The application of finite element method to the dynamic analysis of flexible spatial and co-planar linkage systems," *J. of Mechanical Design*, 103, 643-651.

Spivak, M. [1979], *A Comprehensive Introduction to Differential Geometry, Volume One*," Publish or Perish, Inc, Berkeley.

Spurrier, R.A. [1978], "Comment on 'Singularity-Free Extraction of a Quaternion from a Direction-Cosine Matrix,'" *Journal of Spacecraft*, 15(4), 255, July-August.

Stanley, G. [1985], *Continuum Based Shell Elements*, Ph.D dissertation, Applied Mechanics Division, Stanford University.

Stolarski, H. and T. Belytschko, "On the equivalence of mode decomposition and mixed finite elements," *Comp. Meth. Appl. Mech. Engrg.*, (To appear).

Strang, G., and G. Fix [1973], *An Analysis of the Finite Element Method*, Prentice-Hall, New York.

Taylor, R.L. [1985], Private communication.

Truesdell, C., and W. Noll [1965], "The nonlinear field theories of mechanics," in

Handbuch der Physics, Vol. III/3, Springer Verlag, Berlin.

Vu-Quoc, L., and J.C. Simo [1986], *On The Dynamics of Earth-Orbiting Satellites with Multibody Components*, Electronics Research Laboratory Memorandum UCB/ERL M86/29, University of California, Berkeley, April.

Wempner, G.A. [1972], "Discrete approximations related to non-linear theories of solids," *Int. J. Solids Structures*, **7**, 1581-1599.

Whittaker, E.T. [1937], *Analytical Dynamics*, Cambridge, London.

Ziegler, H. [1977], *Principles of Structural Stability*, Birkhauser, Basel, 2nd ed.

Zienkiewicz, O. C., [1977], *The Finite Element Method* , Third Edition, McGraw-Hill, New York.